FUNCTIONAL CHARACTERIZATION OF PPAR TARGETS HILPDA AND SLC25A47

MONTSERRAT A. DE LA ROSA RODRIGUEZ

Propositions

1. Although lipid droplets appear the same, distinct coating patterns by lipid droplet-associated proteins raise awareness of their heterogeneous functions within the cell.
(this thesis)

2. Controlling fatty acid flux requires strict regulation of lipid droplet-triglyceride lipolysis coupled with re-esterification and storage.
(this thesis)

3. Consumer nudging is a better public policy strategy to tackle obesity in México than restrictive regulations, like taxation on high sugar products or complex food labeling.

4. An academic policy that provides space and opportunity for motherhood is a better strategy to increase the footprint of women in science rather than gender-preferential grants.

5. The best diet for weight loss is the one the patient can adhere to alongside psychological and behavioral therapy.

6. "Freedom from want" and "Freedom from fear" are outcomes of social wellness and equal education opportunities.

7. Sustainable consumption and lifestyle should be included in the syllabus of all primary schools.

Propositions belonging to the PhD thesis entitled:
Functional Characterization of PPAR targets HILPDA and SLC25A47

Montserrat A. De la Rosa Rodríguez
Wageningen, 14 September 2021

Functional Characterization of PPAR

targets HILPDA and SLC25A47

Montserrat A. de la Rosa Rodriguez

Thesis committee

Promotor
Prof. Dr Sander Kersten
Professor of Nutrition, Metabolism and Genomics
Chair Division of Human Nutrition & Health
Wageningen University & Research

Co-promotor
Dr Jan Willem Borst
Assistant Professor, Biochemistry
Wageningen University & Research

Other members
Prof. Dr MKC Hesselink – Maastricht University
Prof. Dr N Zelcer – University of Amsterdam
Dr MA Hink – University of Amsterdam
Prof. Dr J Keijer – Wageningen University and Research

This research was conducted under the auspices of the Graduate School VLAG (Advanced studies in Food Technology, Agrobiotechnology, Nutrition and Health Sciences).

Functional Characterization of PPAR targets HILPDA and SLC25A47

Montserrat A. de la Rosa Rodriguez

Thesis

submitted in fulfilment of the requirements for the degree of doctor
at Wageningen University
by the authority of the Rector Magnificus,
Prof. Dr A.P.J. Mol,
in the presence of the
Thesis Committee appointed by the Academic Board
to be defended in public
on Tuesday September 14, 2021
at 11 a.m. in the Aula.

Montserrat A. de la Rosa Rodriguez

Functional Characterization of PPAR targets HILPDA and SLC25A47
252 pages

PhD thesis, Wageningen University, Wageningen, NL (2021)
With references and summary in English

ISBN: 978-94-6395-922-3
DOI: https://doi.org/10.18174/551028

A mis pequeños grandes amores,
Dudu & Lila

&

A mi amado esposo Eduardo,
norte e sul

Contents

Abstract

Background

Peroxisomal proliferator activator receptor alpha (PPARα) is a ligand-activated transcription factor that plays a major role in the regulation of lipid metabolism. Gene expression studies performed on PPARα null mice have shed light into a variety of genes regulated by PPARα. However, less is known about the effect of PPARα activation in human liver in vivo. Inasmuch as the function of the vast majority of PPARα target genes has been characterized, still a few remain unknown or poorly characterized.

Objectives

This thesis sought to improve our current knowledge on the transcriptional regulation by peroxisome proliferator-activated receptors alpha (PPAR)-α activation in human liver in vivo, and to expand our understanding on the physiological and molecular function of two PPARα target genes: Hilpda and Slc25a47.

Methods

To study the effects of PPARα activation in human liver in vivo, we used a novel chimeric mouse model carrying human liver cells. We treated chimeric mice containing hepatocyte humanized livers with an oral dose of 300 mg/kg fenofibrate daily for 4 days. Livers were collected and analysed by hematoxilin and eosin staining, qPCR, and transcriptomics. Transcriptomics data were compared with existing datasets on fenofibrate treatment in normal mice and other human model systems. Next, we characterized the physiological and molecular function of HILDPA in adipose tissue macrophages in the context of obesity-induced inflammation and in hepatocytes during non-alcoholic steatohepatitis. To this end we used a HILPDA tissue-specific knockout mice model in macrophages and hepatocytes generated by using LysM-Cre and Alb-Cre transgenic mice, respectively. Ultimately, to characterize the physiological function of SLC25A47 we performed adeno-associated virus mediated liver overexpression and studied the effect of Slc25a47 under 11 weeks high fat diet or fed and fasted conditions. Subsequently, we used a Slc25a47 knockout mice model and performed indirect calorimetry measurements under fed and fasted conditions. We next characterized the effect of Slc25a47 deletion in mice under 20 weeks high-fat and low-fat diet. Ultimately, we studied the effect of Slc25a47 in mitochondria respiration on transiently transfected Hepa 1-6 cells and mice livers overexpressing Slc25a47.

Results

In the chimeric humanized mice liver, human hepatocytes exhibited excessive lipid accumulation. Fenofibrate increased the size of the mouse but not human hepatocytes and tended to reduce steatosis in the human hepatocytes. Quantitative PCR indicated that induction of PPARα targets by fenofibrate was less pronounced in the human hepatocytes than in the residual mouse hepatocytes. Comparison with other transcriptomics datasets indicated that hepatocyte humanized livers recapitulate the principal effects of PPARα activation on lipid metabolism. In contrast, pathways connected to DNA synthesis were downregulated by fenofibrate in chimeric mice with hepatocyte humanized livers yet upregulated by fenofibrate in normal mouse livers.

In diet-induced obese mice, HILPDA deficiency in macrophages markedly reduced lipid accumulation in macrophages yet it did not alter any measured inflammatory or metabolic parameters. Mechanistically, HILPDA inhibited ATGL-mediated lipolysis in macrophages. Treatment with the ATGL inhibitor Atglistatin rescued lipid accumulation inside lipid droplets in HILPDA-deficient macrophages. Similarly, in diet-induced NASH mice, HILPDA hepatocyte deficiency modestly yet significantly reduced liver triglyceride accumulation and plasma ALT levels. However, expression of macrophage/inflammatory markers and fibrosis were not different between HILPDA knockout and floxed mice. In hepatoma cell lines, fatty acids increased Hilpda expression and protein levels. Hilpda overexpression in turn induced triglyceride accumulation inside lipid droplets. Mechanistically, HILPDA interacts and increases DGAT1 protein level and activity as indicated by FRET-FLIM analysis, western blot and Dgat1 activity assay.

In the liver, Slc25a47 overexpression in fed and fasted mice had no significant effects on liver triglyceride levels, plasma glucose, triglyceride, cholesterol, glycerol, non-esterified fatty acids nor on β-hydroxybutyrate levels. Similarly, after feeding mice a high fat diet for 8 weeks, there were no effect of Slc25a47 overexpression on any of the beforementioned parameters. However, transcriptome analysis at the pathway level showed that several gene sets related to cholesterol synthesis were significantly enriched among the upregulated genes, suggesting that SLC25A47 might stimulate cholesterol synthesis. Indirect calorimetry performed in wildtype and Slc25a47 knockout mice in the fed and fasted state showed no difference in energy expenditure, activity level nor respiratory exchange ratio between genotypes. After 20 weeks of low or high-fat diet, WT and Slc25a47-/- mice showed no significant differences in body weight gain, food intake, liver or white adipose tissue weight, on either diet. By contrast, glucose tolerance was significantly improved in the Slc25a47-/- mice compared to the WT mice. Similarly, no significant differences were observed between WT and Slc25a47-/- mice in hepatic triglyceride, plasma glucose, cholesterol, triglycerides, glycerol and non-esterified fatty

acids in either condition. At the molecular level, we did not observe any change in mitochondria respiration in livers of mice overexpressing Slc25a47, nor in transiently transfected Hepa 1-6 cells as measured by high-resolution respirometry with Oroboros.

General conclusion

The research contained in this thesis has broadened our understanding on the physiological role of PPARα and the modulation of lipid metabolism through its target genes.

Chapter 1

General Introduction

Introduction

Lipids are small hydrophobic molecules with diverse cellular functions. They are utilized as energy source, structural components for biological membranes, signaling molecules in diverse cellular pathways, and regulators of gene expression. Abnormal metabolism of lipids in different tissues has been associated with a wide range of degenerative and infectious diseases. Cytoplasmic lipid accumulation is a characteristic sign of non-alcoholic fatty liver disease (NAFLD) and viral hepatitis C infection and strongly correlates with disease severity and development (1–3). Similarly, in atherosclerosis, macrophages in the atherosclerotic plaque accumulate excess lipids and eventually become inflammatory lipid-laden foam cells promoting atherosclerosis disease progression (4,5). In type 2 diabetes, accumulation of large lipid droplets in the subsarcolemmal regions of oxidative type 2 muscle fibers has been shown to negatively correlate with insulin sensitivity (6). In neurodegenerative diseases, like Alzheimer and Parkinson's disease, lipid accumulation and altered lipid composition is connected to impaired cell function and neural activity (7,8). In cancer, excessive lipid and cholesterol accumulation as lipid droplets in tumor cells has been considered as an indicator of cancer aggressiveness (9–12).

In order to therapeutically address lipid dysregulation-associated diseases, a comprehensive understanding of the physiological function of lipid accumulation, the proteins involved in lipid metabolism, and their molecular mechanisms is required.

Peroxisome proliferator-activated receptors (PPARs)

Peroxisome proliferator-activated receptors (PPARs) are the master regulators of lipid metabolism. They are nuclear receptors that exert the dual function of transcription factors and receptors by regulating gene expression according to the cellular environment. PPARs serve as receptors for diverse molecules of natural origin, such as fatty acids and its derivatives, or synthetic compounds like fibrate drugs, plasticizers, and insecticides (13,14). Following ligand- activation, PPARs forms a heterodimer with the nuclear receptor RXR and together bind to specific DNA-sequences, known as PPAR response elements (PPRE) around its target genes. These PPRE are a direct repeat of the consensus six nucleotides AGGTCA separated by a single nucleotide. Binding of ligand leads to the dissociation of co-repressor proteins and the association of co- activator proteins, which facilitates the assembly of the transcription initiation complex (15,16). Through activation of gene expression, PPARs regulate diverse biological pathways such as glucose metabolism, biotransformation, amino

acid metabolism, inflammation, but most importantly lipid metabolism(15,17). The PPAR subfamily of nuclear receptors is composed by three subtypes PPARα, PPARγ, PPARδ with different expression patterns.

PPARα is most highly expressed in liver and brown adipose tissue. Also, PPARα can be found in heart, small intestine, and kidney. In liver, PPARα regulates lipid metabolism, especially during fasting. PPARα activates fatty acid uptake and oxidation, triglyceride storage and utilization, ketogenesis, and glucose metabolism. Liver PPARα null mice have a severe fasting-induced phenotype characterized by elevated plasma fatty acids, hepatic steatosis, hypoketonemia, and hypoglycemia. PPARδ is ubiquitously expressed in different tissues and cell types. PPARδ has been best characterized in skeletal muscle where it is known to mediate the effects of fatty acids on gene expression and stimulate fatty acid transport, β-oxidation and mitochondrial respiration(18). PPARγ is mainly expressed in adipose tissue, colon, and macrophages. In adipose tissue, PPARγ serves as the master regulator of adipogenesis. In non-adipose tissue like liver, heart, and skeletal muscle, induction of PPARγ results in triglyceride accumulation inside lipid droplets. The overall physiological function of the different PPARs is related to the function of their distinct target genes(16). Although the function of many PPARs target genes have been elucidated, the physiological role of lots of other PPAR target genes remains unknown. In this thesis, we characterized the physiological and molecular function of the PPARα target genes *Hilpda* and *Slc25a47* with a focus on liver and adipose tissue macrophages.

An overview of fatty acid fluxes and regulation by PPARs

Liver

The liver is the primary regulator of systemic lipid homeostasis. Through the uptake, synthesis, packaging, and secretion of fatty acids (as triglycerides in lipoproteins), the liver regulates systemic lipid availability. In healthy populations, liver fatty acid content as triglyceride is less than 5% of the wet liver weight (19). Fatty acids in the liver originate from the diet, LPL-mediated fatty acid spillover in adipose tissue and muscle, adipose tissue lipolysis, *de novo* lipogenesis, and from endogenous intracellular triglycerides stored in lipid droplets (20).

Diet-derived fatty acids are packed as triglycerides in chylomicrons within the enterocyte, then released into the lymphatic system and finally reach the bloodstream via the thoracic duct (21). Fatty acids in chylomicrons are taken up by the peripheral tissues after triglyceride hydrolysis catalysed by lipoprotein lipase (LPL). The remaining particles known

as chylomicron remnants are removed from the circulation by the liver via receptor-mediated endocytosis and posterior lysosomal degradation (22,23). Additionally, a fraction of the chylomicron triglycerides hydrolysed by LPL are not successfully taken-up by peripheral tissues and thus enter the systemic non-esterified-FA pool (NEFA). These "spillover" derived fatty acids are then taken-up by the liver (24,25). Besides via spillover, the NEFA pool is fed by fatty acids released by adipose tissue. Especially under fasting conditions, triglycerides stored in adipose tissue are hydrolysed into free fatty acids and released into the blood plasma bound to albumin, followed by their uptake in the liver (26). Finally, liver fatty acids can come from *de novo* lipogenesis, which describes the synthesis of fatty acids from acetyl-CoA subunits that are produced by different pathways within the cell, including glycolysis. This process requires multiple enzymes and begins with the production of malonyl-CoA from acetyl-CoA by acetyl-CoA carboxylase (ACC) (27).

In the fasted state, fatty acids are mainly directed toward oxidative pathways. The acetyl-CoA produced from β-oxidation can continue in the tricarboxylic acid cycle or can be used to generate ketones. FAs are also esterified to triglycerides and stored in lipid droplets. The LD-derived triglycerides can then be hydrolyzed to release fatty acids and re-esterified for VLDL synthesis and export to peripheral tissues. In the fed state, dietary fatty acids or *de novo* synthesised fatty acids are directed towards esterification and storage as lipid droplets (28). In addition, fatty acids can serve as signaling molecules for instance by binding to PPARα (Figure 1).

In the liver, lipid metabolism is regulated through several transcription factors, including PPAR, PXR, CAR, LXR, and FXR (29,30). PPARs directly bind fatty acids and its derivatives. thereby acting as metabolic sensors. Binding of fatty acids to PPARα induces the expression of genes involved in fatty acid uptake, transport, activation, and oxidation, including peroxisomal, microsomal and mitochondrial oxidation. Additionally, PPARα induces the expression several enzymes in the triglyceride biosynthesis pathway as well as lipid droplet-associated proteins (Reviewed in 13,14) (Figure 2). Although PPARγ is not abundantly expressed in liver, under obesogenic conditions PPARγ induces genes involved in *de novo* lipogenesis and triglyceride storage (33).

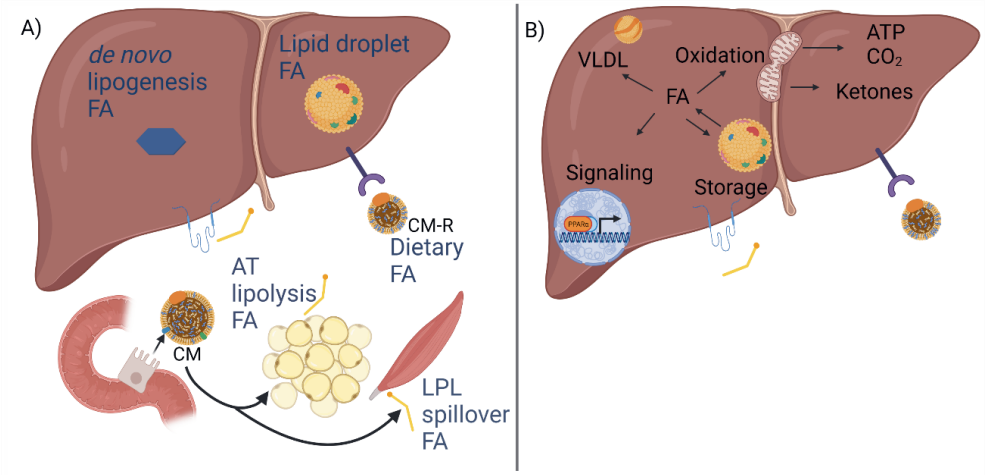

Figure 1. Hepatic lipid flux. A) Origin of fatty acids in the liver. Liver fatty acids can be derived from the diet as chylomicron remnants, LPL spillover from adipose tissue and muscle, adipose tissue lipolysis, *de novo* lipogenesis, and from endogenous intracellular triglycerides stored inside lipid droplets. B) Metabolic fate of fatty acids in the liver. Liver fatty acids can be stored inside lipid droplets, used for VLDL production, fatty acid oxidation for energy and ketone body production, and as signalling molecules. CM:Chylomicron; AT: Adipose tissue; FA: Fatty acid; LPL: Lipoprotein lipase; CM-R: Chylomicron remnant; LD: Lipid droplet.

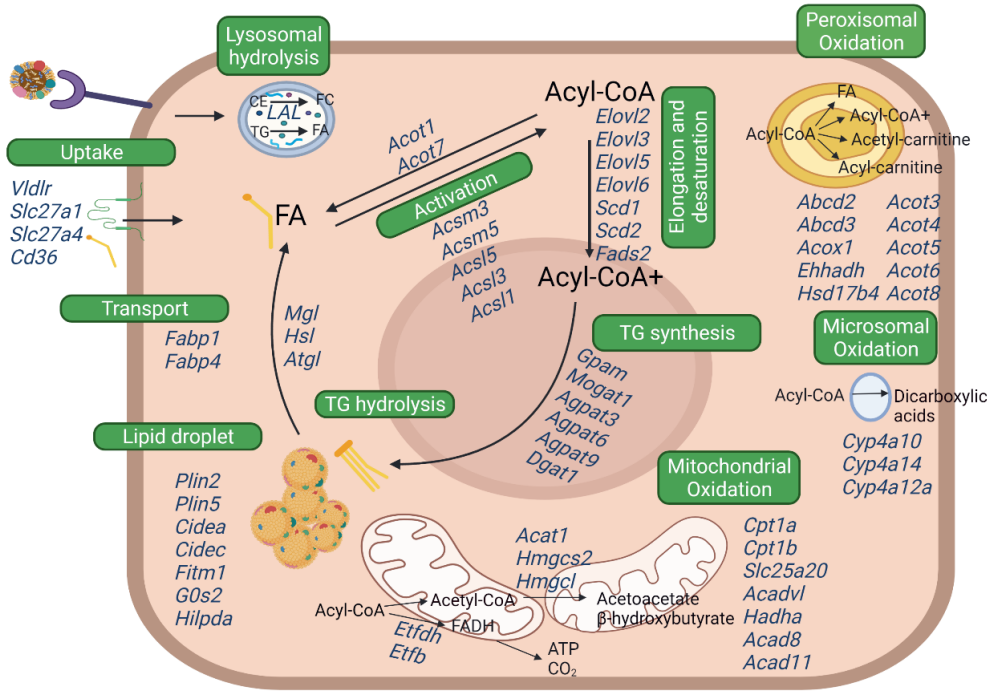

Figure 2. Overview of several PPARα regulated genes involved in fatty acid metabolism. Based on PPARα knockout mouse models treated with agonist WY14643, fenofibrate or fasted. Adapted from (31).

Adipose tissue macrophages

Adipose tissue macrophages (ATM) are important for the maintenance of healthy adipose tissue by promoting adipose tissue remodeling, insulin sensitivity, clearance of dead adipocytes, and lipid buffering from adipocyte lipolysis or dead adipocytes (34–37). ATM can be classified according to their origin into two major subtypes: tissue-resident macrophages and `recruited' monocyte-derived macrophages (38). In the lean state, ATM constitute about 8% of the cells from adipose tissue, whilst during obesity they can increase up to 50% (39,40). The increased number of ATM during obesity can be attributed to recruitment of macrophages from circulating monocytes as well as local proliferation of recruited macrophages (38). Simplistic classification of ATM according to their phenotype distinguishes two main different populations: M1, classically activated macrophages, and M2, alternatively activated macrophages. The ATM phenotype is dependent on the tissue environment mediated by diverse stimuli including cytokines, growth factors, and fatty acids. Classically activated M1 macrophages are induced by Th1 mediators including LPS, TNF-α, IFNγ. M1 macrophages are characterized by the overproduction of proinflammatory cytokines and recognized by cell surface markers CD11c, CD64, CCR2. To meet metabolic demands, M1 macrophages rely on glycolysis. In contrast, alternatively activated M2 are stimulated by Th2 mediators, including IL-4 and IL-13. M2 macrophages are associated with anti-inflammatory properties including tissue remodeling, inflammation resolution, immunosuppressive properties, and high phagocytic capacity. To meet metabolic demands, M2 macrophages rely on oxidative phosphorylation. M2 macrophages are further classified in 3 subsets M2a, M2b, and M2, according to the stimuli presented and their functional state (Figure 3) (Detail reviews on macrophage activation in 9–11). Activation of ATM by glucose, insulin, and palmitate representing "metabolic activation" leads to the recognition of a third type of activated ATM that neither resembles M1 nor M2 activation. Metabolically activated macrophages (MMe) can secrete proinflammatory cytokines, yet they do not share the cell surface markers of M1 macrophages. Moreover, depending on their intracellular signaling, they can span through the spectrum between "M1-like" and "M2-like" macrophages (44). Recently, studies using single-cell transcriptomics and RNA sequencing has led to the detection of additional more distinct ATM populations with unique morphology, tissue localization, and transcriptomes, which for the sake of simplicity will not be discussed here (45,46).

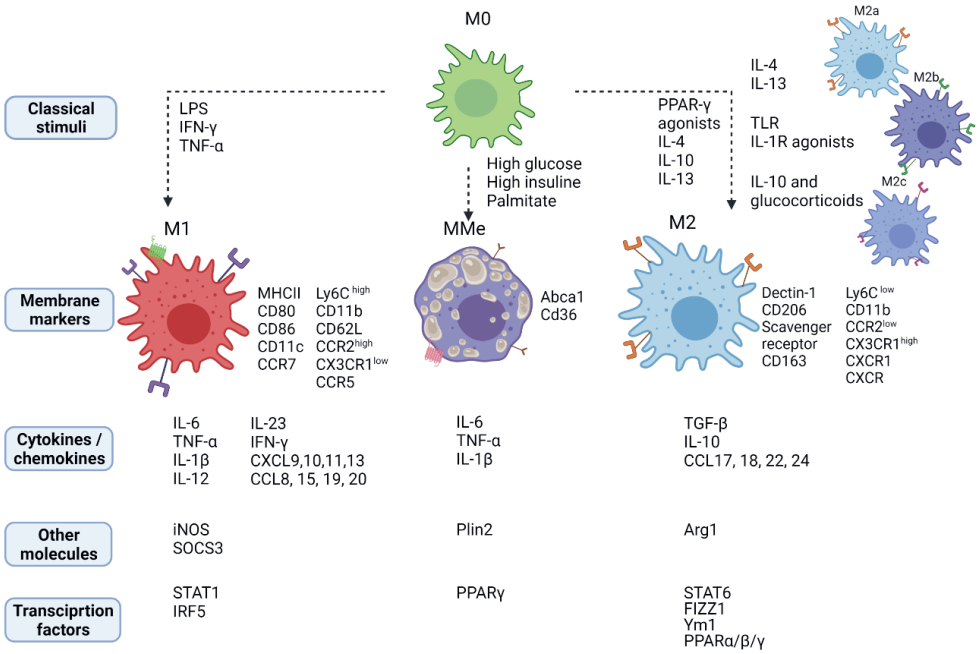

Figure 3. Simplified overview of ATM classification. Depending on the stimuli, 'M0' macrophages differentiate into several subsets. 'M1' originate from the stimulation with lipopolysaccharide (LPS), interferon (IFN)-γ or tumor necrosis factor α (TNF-α). 'MMe' Metabolic activated macrophages are induced by high glucose, high insulin, and palmitate. 'M2' macrophages originate from the stimulation with PPAR-γ agonists/IL-4/IL-10/IL-13 and are classified into 3 subsets: 'M2a', induced by IL-4 or IL-13; 'M2b' induced by TLR and IL-1R agonists; and 'M2c' induced by glucocorticoids or IL-10.

As mentioned earlier, ATMs have an important role in buffering lipids from adipose tissue. Lipid buffering by ATMs can be achieved by the following mechanisms: 1) uptake of circulating fatty acids or lipoproteins, 2) uptake of adipocyte-released free fatty acids or exosomes, and 3) digestion and uptake of dying adipocytes.

Free fatty acids released from LPL-mediated hydrolysis of chylomicrons and VLDLs on the adipose tissue and ATMs can be taken up by ATMs through fatty acid transporters, including CD36 and FABPT1 (47–51). Additionally, VLDLs can be internalized into ATMs via VLDLR and delivered to lysosomes through endocytic pathway for subsequent hydrolysis of cholesterol esters and triglycerides into free cholesterol and fatty acids (52,53). Similarly, free fatty acids released from adipocyte lipolysis can be taken up by macrophages through the beforementioned fatty acid transporters. Additionally, adipocytes release exosome-sized lipid-filled vesicles which can be internalized by the AMTs through macropinocytosis and

processed via endolysosomal pathway (54). Finally, ATMs within crown-like structures surround the apoptotic adipocytes and partially engulf them through a process called exophagy. During exophagy, the ATMs form an extracellular acidic hydrolytic compartment at contact points with the adipocyte. This extracellular compartment contains lysosomal enzymes delivered to the adipocyte via exocytosis. The enzymes partly digest the apoptotic adipocyte, thus allowing the macrophage to internalize pieces of the adipocyte (Figure 4) (55).

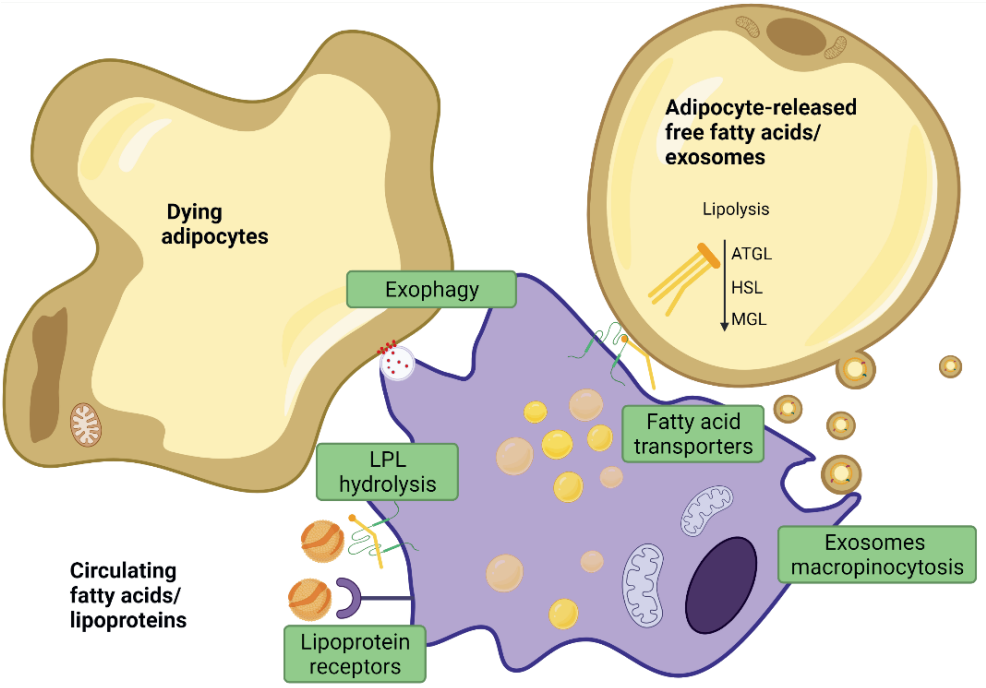

Figure 4. Overview of fatty acid uptake by adipose tissue macrophages. Circulating fatty acids and lipoproteins can be taken-up by adipose tissue macrophages through fatty acid receptors and VLDLR, respectively. Free fatty acids released from adipocyte lipolysis can be taken up by fatty acid transporters. Adipocyte-released exosome-sized lipid-filled vesicles can be internalized through micropinocytosis. Apoptotic adipocytes can be digested and partially by macrophages through a process called exophagy.

As in other cell-types, lipids are used in macrophages as energy source, components for membrane synthesis, signaling molecules, and regulators of gene expression. Interestingly, macrophages lipid metabolism is correlated with macrophage activation and function. In the classical view, M2 macrophages rely on fatty acid oxidation and oxidative phosphorylation and this metabolic signature is associated with their anti-inflammatory properties. By contrast, M1 macrophages rely on glycolytic metabolism and display increased fatty acid synthesis, which is associated with the secretion of proinflammatory

cytokines (for in depth review on macrophage lipid metabolism Ref. (56–59)). However, the classical view has been questioned since recent evidence has shown that glucose uptake, glycolysis and fatty acid synthesis are essential for M2 activation (60). Even though the precise mechanisms of lipid metabolism and macrophage activation still needs clarification, the relation between lipid metabolism and macrophage function is evident.

From the PPAR isoforms, PPARγ is the most abundantly expressed in macrophages. Functionally, PPARγ enhances the differentiation of monocytes into M2 activated macrophages, as well as inhibiting pro-inflammatory gene expression including TNF-α, CCL-3, MCP-1, IL6, mainly by interfering with the action of other transcription factors such as NF-κB, through a mechanism known as transrepression (60,61).PPARδ is also highly expressed in macrophages, where it is involved in the regulation of lipid metabolism, inflammation and the phagocytosis of apoptotic cells (62).In contrast, PPARα is only weakly expressed in macrophages. Nevertheless, its activation has been shown to mediate inflammation response through β-oxidation and through inhibiting the production of proinflammatory molecules (63,64).

The lipid droplet

Fatty acids are stored intracellularly as triglycerides inside lipid droplets (LD). Lipid droplets are mainly composed by a neutral lipid core of triglycerides and sterol esters surrounded by a monolayer of phospholipids into which regulatory proteins are embedded. The synthesis of triglycerides and its subsequent storage inside LD provides a mechanism for protecting the cells from lipotoxicity of fatty acids and regulating glycerolipid availability for lipid-mediated signaling (65,66).

Triglyceride synthesis is mediated through the glycerol-3-phosphate pathway, also know as the “Kennedy pathway”. The glycerol 3-phosphate pathway is the stepwise esterification of fatty acids to a glycerol-3-phosphate backbone by the action of several enzymes, including glycerol-3-phosphate acyltransferases (GPAT/GPAM), 1-acylglycerol-3-phosphate acyltransferase (AGPAT/LPAAT), lipin phosphatidic acid phosphatase (PAP/LPIN), and diacylglycerol acyltransferases (DGAT) (67). Although triglyceride synthesis mainly occurs in the endoplasmic reticulum (ER), different isoforms of these enzymes are also present in the LDs, mitochondria membrane, and the nucleus. An interesting feature of the DGAT enzymes is that they are not isoforms yet catalyze the same reaction. DGAT1 is a multiple transmembrane protein and member of the membrane-bound O-acyltransferase gene family. It localizes exclusively to the ER, and mainly esterifies exogenous fatty acids to diacylglycerol. In contrast, DGAT2 possess only a hydrophobic sequence that is embedded

in the ER bilayer, localizes to the ER and lipid droplet, and preferentially catalyzes triglyceride synthesis from endogenously synthesized fatty acids (68,69). Excellent reviews exist about the isoforms of the enzymes involved in the glycerol-3-phosphate pathway (67,70)). The first step in triglyceride synthesis is catalyzed by GPAT, which synthesizes lysophosphatidate (LPA) from glycerol-3-phosphate and fatty acyl-CoA. Thereafter, AGPAT mediates the conversion of LPA to phosphatidate (PA). Subsequently, PA is dephosphorylated by Lipin PAP to diacylglycerol. Finally, DGAT catalyzes the ultimate step in triglyceride synthesis.

According to the lipid droplet biogenesis model proposed by Walther et al. (71), after triglyceride synthesis occurs, a lens of neutral lipids begins to accumulate within the ER bilayer. When sufficient triglyceride has accumulated within the lipid lens, it buds into the cytosol as an initial LD (iLD). Finally, the iLD expands through the acquisition of specialized lipid-droplet associated proteins and becomes an expanding LD (eLD) characterized by localized triglyceride synthesis (71). The eLD is very dynamic and can expand or shrink regulated by the lipid-droplet associated proteins to meet cellular demands.

Lipid droplet-associated proteins play crucial role in the synthesis, breakdown and maintenance of LD. Proteomics studies suggest that hundreds of proteins are physically connected to LD. However, the nature of the interaction and the role of most of these proteins in LD biology remains unclear. The best characterized LD-associated proteins are the perilipins, represented by PLIN1 through PLIN5. Consistent with the role of PPARs as master regulators of adipose and hepatic lipid metabolism, many LD-associated proteins are under transcriptional control of PPARs, including the perilipins. Indeed, a disproportionate number of target genes of PPARs encode LD-associated proteins.

PPARα target genes: HILPDA and SLC25A47

Hypoxia inducible lipid droplet associated (HILPDA)

HILPDA is a LD-associated protein that was shown to promote lipid storage in different types of cells and tissues (72–74). The human HILPDA gene covers a genomic region of 2.6 kb on chromosome 7 and consists of two exons and one intron. The human HILPDA cDNA gives rises to a 63 amino acids protein in mouse and 64 amino acids in human. In humans, high HILPDA mRNA expression is reported in various diverse immune cells, adipocytes, esophagus, blood vessels, dendritic cells, and various epithelial cells. Similarly, in mice, the highest Hilpda mRNA expression is also observed in various types of immune cells as well as cultured hepatocytes. At the protein level, high HILPDA levels are found in murine white and brown adipose tissue, heart, and lung (75).

Hilpda is regulated by diverse stimuli in different cell types. As the names suggests, Hilpda is highly upregulated by hypoxia in different cell lines (76). In addition, an increase in Hilpda mRNA levels has consistently been detected in numerous cancers including renal, ovarian, and colorectal adenoma and carcinoma (77–79). Likewise, treatment with fatty acids have also been shown to increase Hilpda mRNA and protein expression level in macrophages, hepatocytes, human colon cancer cell line, and mouse embryonic fibroblasts. Interestingly, the relative increase in HILPDA protein by fatty acids is greater than the increase in Hilpda mRNA, which supports the notion that fatty acids protect HILPDA from degradation (80). Meanwhile, in adipocytes and adipose tissue, stimuli that increase Hilpda mRNA and protein levels are several β-adrenergic agonists, forskolin and fasting (81). In bone marrow-derived macrophages, HILPDA protein is highly induced by lipopolysaccharide.

Transcriptional control of Hilpda is mediated by diverse transcription factors dependent on the environmental stimuli. In renal cell carcinoma cell lines Hilpda expression is under positive transcriptional control of the β-catenin/Wnt pathway mediated by TCF/LEF transcription factor (82). In oxygen deficient conditions, Hilpda induction is under control of the transcription factor HIF1-α in several carcinoma cell lines (76). In human and mouse hepatocytes, Hilpda mRNA is upregulated by PPARα when treated with PPARα agonist. However, during fasting, hepatic Hilpda mRNA induction is not mediated by PPARα but possibly PPARγ (73). In human and mouse adipocytes, Hilpda mRNA is upregulated by PPARγ (81).

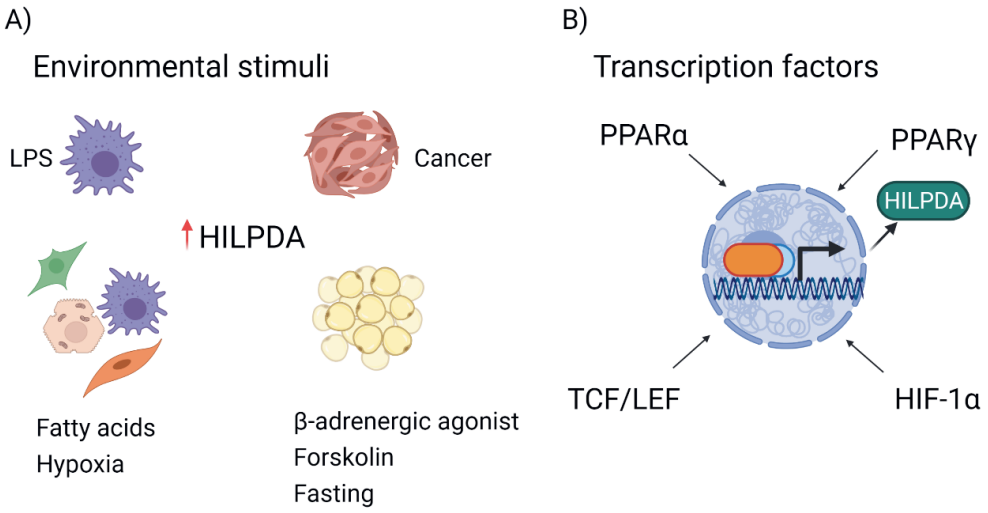

Figure 5. Regulation of Hilpda by environmental stimuli and transcription factors. A) Environmental stimuli that upregulate HILPDA at the protein level include LPS in macrophages; β-adrenergic agonists and forskolin in adipocytes; cancer, hypoxia and fatty acids in diverse cell types. B) Hilpda transcription can be regulated by PPARα, PPARγ, TCF/LEF/ and HIF1-α.

In hepatocytes, *in vitro* and *in vivo* Hilpda overexpression led to significantly increased intracellular lipid accumulation (73,74). Conversely, hepatocyte-specific HILPDA deletion resulted in lower liver triglycerides liver in mouse fed chow, but this decrease was not observed when mice were fed a high-fat diet (74). In adipocytes, HILPDA deficiency significantly reduced weight of the epididymal fat depot in mice fed a high fat diet (83). However, in adipose tissue explants and primary hepatocytes, HILPDA deficiency did not altered basal or isoproterenol-induced NEFA and glycerol release (83,84). Thus, further research is needed to clarify the function on HILPDA in adipose tissue lipolysis. In atherosclerosis prone Apoe−/− mice, macrophage HILPDA-deficiency (Tie2-driven) was associated with reduced aortic plaque area and plaque lipid content (77). Mechanistically, it was recently shown that HILPDA can interact and inhibit ATGL (79,85). The interaction and inhibition by HILPDA is dependent on the conserved hydrophobic domain of HILPDA (residues 7-11), and the catalytic patatin-like domain (residues 10–178) of ATGL (86).

Solute Carrier Family 25 Member 47 (SLC25A47)

SLC25A47 belongs to the SLC25 (solute-carrier-protein 25) family of transporters also known as mitochondrial carrier family (MC). MCs transport diverse types of solutes from

the mitochondrial matrix to the cytosol and vice versa. They can be ubiquitously expressed or tissue-specific, reflecting tissue-specific functions (87). A few examples of other SLC25 family members are the citrate carrier (SLC25A1), and uncoupling protein 1 (UCP1) (SLC25A7). Citrate carriers transport citrate from the mitochondria matrix into the cytosol in exchange of a dicarboxylate, mainly malate (88). It was recently shown that pharmacological inhibition of the citrate carrier reduced inflammatory macrophage infiltration into liver and adipose tissue, reverted NASH, and prevented steatohepatitis in high-fat diet fed mice (89). Whereas UCP1 is specifically expressed in brown/brite adipose tissue and gives this depot its thermogenic characteristic. UCP1 facilitates the leak of protons (generated by NADH) across the mitochondrial inner membrane, dissipating the electrochemical proton gradient needed for ATP production by ATP-synthase. Consequently, the energy derived from the oxidation of respiratory substrate is released as heat(90). The ablation of UCP1 has been associated with increased weight gain, body fat %, and fat depot size in mice fed a high-fat diet at thermoneutral conditions(91).

SLC25A47 was first identified by Tan and colleagues screening for the most significant downregulated genes in hepatocellular carcinoma. Hence, it was formerly named Hepatocellular Downregulated Mitochondrial Carrier Protein (HDMCP). Tan and colleges observed that transient overexpression of SLC25A47 in cancer cells results in the reduction of mitochondrial membrane potential, accompanied by a significant decrease of cellular ATP (92). Later, studies in yeast cells confirmed the function of SLC25A47 as an uncoupler of mitochondrial respiration. Additionally, in the same studies, knockdown of SLC25A47 in hepatic cell lines resulted on increased lipid content. Follow-up in vivo studies characterizing the physiological function of SLC25A47 are lacking.

Outline of this thesis

The research on this thesis aims to 1) Augment our knowledge on the transcriptional regulation by peroxisome proliferator-activated receptors (PPAR)-α activation on human liver in vivo. 2) Characterize the physiological and molecular function of the PPARα target HILDPA in adipose tissue macrophages (ATM) in the context of obesity induced inflammation and in hepatocytes during non-alcoholic steatohepatitis. 3) Elucidate the physiological function of the PPARα target SLC25A47 in liver lipid metabolism and energy expenditure.

The role of PPARα in gene regulation in mouse liver is very well characterized, however less is known about the effect of PPARα activation in human liver. In **Chapter 2**, we aim to better characterize the impact of PPARα activation on gene regulation in human liver by treating

chimeric mice carrying human liver cells with the PPARα agonist fenofibrate. Interestingly induction of PPARα targets by fenofibrate was less pronounced in the human hepatocytes than in the residual mouse hepatocytes. Fenofibrate upregulated interferon/cytokine signaling-related pathways in hepatocyte humanized liver but downregulated these pathways in normal mouse liver. Overall, the results support the major role of PPARα in regulating hepatic lipid metabolism and highlights the more modest effect of PPARα activation on gene regulation in human liver compared to mouse. In **Chapter 3**, we provide an overview of the regulation of lipid droplet-associated proteins by PPARα, PPARδ, and PPARγ in adipose tissue, liver, macrophages, and skeletal muscle. In **Chapter 4**, we explore the role of the lipid droplet-associated protein HILPDA in adipose tissue macrophages. Intriguingly, mice with myeloid-specific deficiency of HILPDA protein exhibited a pronounced reduction in intracellular lipid droplets. The decreased lipid storage in HILPDA-deficient macrophages could be restored by inhibition of adipose triglyceride lipase (ATGL). In diet-induced obese mice, HILPDA deficiency did not alter inflammatory or metabolic parameters. These data questions the contribution of lipid-laden adipose tissue macrophages on obesity-induced inflammation. In **Chapter 5**, we explore the physiological and mechanism of action of HILPDA in the context of non-alcoholic steatohepatitis (NASH). Hepatocyte-specific deficiency of HILPDA modestly but significantly reduced hepatic triglycerides in mice with NASH. Mechanistically, HILPDA overexpression increased lipid storage concomitant with an increase in DGAT activity and DGAT1 protein levels. Furthermore, our data indicated HILPDA colocalizes and physically interacts with DGAT1. Overall, these findings suggest a novel mechanism in hepatocytes that links elevated fatty acid levels to stimulation of triglyceride synthesis and storage. In **Chapter 6**, we present the contemporary knowledge of HILPDA on lipid droplet regulation. In **Chapter 7**, we characterize the physiological and molecular role of the PPARα target gene Slc25a47 in relation to energy expenditure and liver lipid metabolism. Finally, in **Chapter 8** we discuss the findings of this thesis.

References

1. Ipsen DH, Lykkesfeldt J, Tveden-Nyborg P. Molecular mechanisms of hepatic lipid accumulation in non-alcoholic fatty liver disease. Vol. 75, Cellular and Molecular Life Sciences. Birkhauser Verlag AG; 2018. p. 3313–27.
2. Syed GH, Amako Y, Siddiqui A. Hepatitis C virus hijacks host lipid metabolism. Vol. 21, Trends in Endocrinology and Metabolism. Elsevier Current Trends; 2010. p. 33–40.
3. Rubbia-Brandt L, Quadri R, Abid K, Giostra E, Malé PJ, Mentha G, et al. Hepatocyte steatosis is a cytopathic effect of hepatitis C virus genotype 3. J Hepatol. 2000 Jul 1;33(1):106–15.
4. Amengual J, Barrett TJ. Monocytes and macrophages in atherogenesis. Current Opinion in Lipidology Lippincott Williams and Wilkins; Oct 1, 2019 p. 401–8.
5. Pagler TA, Wang M, Mondal M, Murphy AJ, Westerterp M, Moore KJ, et al. Deletion of ABCA1 and ABCG1 impairs macrophage migration because of increased Rac1 signaling. Circ Res. 2011 Jan 21;108(2):194–200.
6. Daemen S, Gemmink A, Brouwers B, Meex RCR, Huntjens PR, Schaart G, et al. Distinct lipid droplet characteristics and distribution unmask the apparent contradiction of the athlete's paradox. Mol Metab. 2018 Nov 1;17:71–81.
7. Hamilton LK, Dufresne M, Joppé SE, Petryszyn S, Aumont A, Calon F, et al. Aberrant Lipid Metabolism in the Forebrain Niche Suppresses Adult Neural Stem Cell Proliferation in an Animal Model of Alzheimer's Disease. Cell Stem Cell. 2015 Oct 1;17(4):397–411.
8. Fanning S, Haque A, Imberdis T, Baru V, Barrasa MI, Nuber S, et al. Lipidomic Analysis of α-Synuclein Neurotoxicity Identifies Stearoyl CoA Desaturase as a Target for Parkinson Treatment. Mol Cell. 2019 Mar 7;73(5):1001-1014.e8.
9. Li Z, Guan M, Lin Y, Cui X, Zhang Y, Zhao Z, et al. Aberrant lipid metabolism in hepatocellular carcinoma revealed by liver lipidomics. Int J Mol Sci. 2017 Dec 1;18(12):2550.
10. de Gonzalo-Calvo D, López-Vilaró L, Nasarre L, Perez-Olabarria M, Vázquez T, Escuin D, et al. Intratumor cholesteryl ester accumulation is associated with human breast cancer proliferation and aggressive potential: A molecular and clinicopathological study. BMC Cancer. 2015 Dec 12;15(1):1–14.
11. Yue S, Li J, Lee SY, Lee HJ, Shao T, Song B, et al. Cholesteryl ester accumulation induced by PTEN loss and PI3K/AKT activation underlies human prostate cancer aggressiveness. Cell Metab. 2014 Mar 4;19(3):393–406.
12. Guri Y, Colombi M, Dazert E, Hindupur SK, Roszik J, Moes S, et al. mTORC2 Promotes Tumorigenesis via Lipid Synthesis. Cancer Cell. 2017 Dec 11;32(6):807-823.e12.
13. Georgiadi A, Kersten S. Mechanisms of gene regulation by fatty acids. Adv Nutr. 2012 Mar 1;3(2):127–34.
14. Takeuchi S, Matsuda T, Kobayashi S, Takahashi T, Kojima H. In vitro screening of 200 pesticides for agonistic activity via mouse peroxisome proliferator-activated receptor (PPAR)α and PPARγ and quantitative analysis of in vivo induction pathway. Toxicol Appl Pharmacol. 2006 Dec 15;217(3):235–44.
15. Varga T, Czimmerer Z, Nagy L. PPARs are a unique set of fatty acid regulated transcription factors controlling both lipid metabolism and inflammation. Biochim Biophys Acta. 2011 Aug;1812(8):1007–22.
16. Kersten S. Integrated physiology and systems biology of PPARα. Mol Metab. 2014 Jul;3(4):354–71.
17. Mandard S, Muller M, Kersten S. Peroxisome proliferator-activated receptor a target genes. Cell Mol Life Sci. 2004 Feb 1;61(4):393–416.
18. Luquet S, Gaudel C, Holst D, Lopez-Soriano J, Jehl-Pietri C, Fredenrich A, et al. Roles of PPAR delta in lipid absorption and metabolism: A new target for the treatment of type 2 diabetes. In: Biochimica et Biophysica Acta - Molecular Basis of Disease. Elsevier; 2005. p. 313–7.
19. Browning JD, Szczepaniak LS, Dobbins R, Nuremberg P, Horton JD, Cohen JC, et al. Prevalence of hepatic steatosis in an urban population in the United States: Impact of ethnicity. Hepatology. 2004 Dec

1;40(6):1387–95.

20. Donnelly KL, Smith CI, Schwarzenberg SJ, Jessurun J, Boldt MD, Parks EJ. Sources of fatty acids stored in liver and secreted via lipoproteins in patients with nonalcoholic fatty liver disease. J Clin Invest. 2005;115(5):1343–51.

21. Goodman BE. Staying Current Insights into digestion and absorption of major nutrients in humans Goodman BE. Insights into digestion and absorption of major nutrients in humans. Adv Physiol Educ. 2010;34:44–53.

22. May P, Herz J, Bock HH. Review Molecular mechanisms of lipoprotein receptor signalling. C Cell Mol Life Sci. 2005;62:2325–38.

23. Havel RJ. Receptor and non-receptor mediated uptake of chylomicron remnants by the liver. In: Atherosclerosis. Elsevier Ireland Ltd; 1998. p. S1–7.

24. Piché ME, Parry SA, Karpe F, Hodson L. Chylomicron-derived fatty acid spillover in adipose tissue: A signature of metabolic health? J Clin Endocrinol Metab. 2018;103(1):25–34.

25. Barrows BR, Parks EJ. Contributions of different fatty acid sources to very low-density lipoprotein-triacylglycerol in the fasted and fed states. J Clin Endocrinol Metab. 2006 Apr 1;91(4):1446–52.

26. Finn PF, Dice JF. Proteolytic and lipolytic responses to starvation. Vol. 22, Nutrition. Elsevier; 2006. p. 830–44.

27. Sanders FWB, Griffin JL. De novo lipogenesis in the liver in health and disease: More than just a shunting yard for glucose. Biol Rev. 2016 May 1;91(2):452–68.

28. Hodson L, Fielding BA. Clinical Lipidology Trafficking and partitioning of fatty acids: the transition from fasted to fed state. 2017;

29. Karpen SJ. Nuclear receptor regulation of hepatic function. Vol. 36, Journal of Hepatology. Elsevier; 2002. p. 832–50.

30. Yu S, Matsusue K, Kashireddy P, Cao W-Q, Yeldandi V, Yeldandi A V, et al. Adipocyte-specific gene expression and adipogenic steatosis in the mouse liver due to peroxisome proliferator-activated receptor gamma1 (PPARgamma1) overexpression. J Biol Chem. 2003 Jan 3;278(1):498–505.

31. Kersten S. Integrated physiology and systems biology of PPARα. Vol. 3, Molecular Metabolism. Elsevier GmbH; 2014. p. 354–71.

32. Wang Y, Nakajima T, Gonzalez FJ, Tanaka N. Molecular Sciences PPARs as Metabolic Regulators in the Liver: Lessons from Liver-Specific PPAR-Null Mice. 2020;

33. Zhang YL, Hernandez-Ono A, Siri P, Weisberg S, Conlon D, Graham MJ, et al. Aberrant hepatic expression of PPARγ2 stimulates hepatic lipogenesis in a mouse model of obesity, insulin resistance, dyslipidemia, and hepatic steatosis. J Biol Chem. 2006 Dec 8;281(49):37603–15.

34. Lumeng CN, Bodzin JL, Saltiel AR. Obesity induces a phenotypic switch in adipose tissue macrophage polarization. J Clin Invest. 2007 Jan 4;117(1):175–84.

35. Pang C, Gao Z, Yin J, Zhang J, Jia W, Ye J. Macrophage infiltration into adipose tissue may promote angiogenesis for adipose tissue remodeling in obesity. Am J Physiol - Endocrinol Metab. 2008 Aug;295(2):313–22.

36. Kosteli A, Sugaru E, Haemmerle G, Martin JF, Lei J, Zechner R, et al. Weight loss and lipolysis promote a dynamic immune response in murine adipose tissue. J Clin Invest. 2010 Oct 1;120(10):3466–79.

37. Cinti S, Mitchell G, Barbatelli G, Murano I, Ceresi E, Faloia E, et al. Adipocyte death defines macrophage localization and function in adipose tissue of obese mice and humans. J Lipid Res. 2005 Nov 1;46(11):2347–55.

38. Daemen S, Schilling JD. The Interplay Between Tissue Niche and Macrophage Cellular Metabolism in Obesity. Vol. 10, Frontiers in Immunology. Frontiers Media S.A.; 2020. p. 3133.

39. Boutens L, Stienstra R. Adipose tissue macrophages: going off track during obesity. Diabetologia. 2016 May

3;59(5):879–94.

40. Weisberg SP, McCann D, Desai M, Rosenbaum M, Leibel RL, Ferrante AW. Obesity is associated with macrophage accumulation in adipose tissue. J Clin Invest. 2003 Dec 15;112(12):1796–808.

41. Viola A, Munari F, Sánchez-Rodríguez R, Scolaro T, Castegna A. The metabolic signature of macrophage responses. Vol. 10, Frontiers in Immunology. Frontiers Media S.A.; 2019.

42. Koo S jie, Garg NJ. Metabolic programming of macrophage functions and pathogens control. Vol. 24, Redox Biology. Elsevier B.V.; 2019. p. 101198.

43. Russo L, Lumeng CN. Properties and functions of adipose tissue macrophages in obesity. Vol. 155, Immunology. Blackwell Publishing Ltd; 2018. p. 407–17.

44. Kratz M, Coats BR, Hisert KB, Hagman D, Mutskov V, Peris E, et al. Metabolic dysfunction drives a mechanistically distinct proinflammatory phenotype in adipose tissue macrophages. Cell Metab. 2014 Oct 7;20(4):614–25.

45. Hill DA, Lim HW, Kim YH, Ho WY, Foong YH, Nelson VL, et al. Distinct macrophage populations direct inflammatory versus physiological changes in adipose tissue. Proc Natl Acad Sci U S A. 2018 May 29;115(22):E5096–105.

46. Miranda DA, Kim J-H, Nguyen LN, Cheng W, Tan BC, Goh VJ, et al. Fat storage-inducing transmembrane protein 2 is required for normal fat storage in adipose tissue. J Biol Chem. 2014 Apr 4;289(14):9560–72.

47. Aouadi M, Vangala P, Yawe JC, Tencerova M, Nicoloro SM, Cohen JL, et al. Lipid storage by adipose tissue macrophages regulates systemic glucose tolerance. Am J Physiol - Endocrinol Metab. 2014 Aug 15;307(4):374–83.

48. Ye G, Gao H, Wang Z, Lin Y, Liao X, Zhang H, et al. PPARα and PPARγ activation attenuates total free fatty acid and triglyceride accumulation in macrophages via the inhibition of Fatp1 expression. Cell Death Dis. 2019 Jan 15;10(2):1–14.

49. Johnson AR, Qin Y, Cozzo AJ, Freemerman AJ, Huang MJ, Zhao L, et al. Metabolic reprogramming through fatty acid transport protein 1 (FATP1) regulates macrophage inflammatory potential and adipose inflammation. Mol Metab. 2016 Jul 1;5(7):506–26.

50. Huang YL, Morales-Rosado J, Ray J, Myers TG, Kho T, Lu M, et al. Toll-like receptor agonists promote prolonged triglyceride storage in macrophages. J Biol Chem. 2014 Jan 31;289(5):3001–12.

51. Abumrad NA, El-Maghrabi MR, Amri EZ, Lopez E, Grimaldi PA. Cloning of a rat adipocyte membrane protein implicated in binding or transport of long-chain fatty acids that is induced during preadipocyte differentiation. Homology with human CD36. J Biol Chem. 1993 Aug 25;268(24):17665–8.

52. Shin KC, Hwang I, Choe SS, Park J, Ji Y, Kim JI, et al. Macrophage VLDLR mediates obesity-induced insulin resistance with adipose tissue inflammation. Nat Commun. 2017 Dec 1;8(1):1–14.

53. Dubland JA, Francis GA. Lysosomal acid lipase: At the crossroads of normal and atherogenic cholesterol metabolism. Vol. 3, Frontiers in Cell and Developmental Biology. Frontiers Media S.A.; 2015. p. 3.

54. Flaherty SE, Grijalva A, Xu X, Ables E, Nomani A, Ferrante AW. A lipase-independent pathway of lipid release and immune modulation by adipocytes. Science (80-). 2019 Mar 1;363(6430):989–93.

55. Haka AS, Barbosa-Lorenzi VC, Lee HJ, Falcone DJ, Hudis CA, Dannenberg AJ, et al. Exocytosis of macrophage lysosomes leads to digestion of apoptotic adipocytes and foam cell formation. J Lipid Res. 2016 Jun 1;57(6):980–92.

56. Yan J, Horng T. Lipid Metabolism in Regulation of Macrophage Functions. Vol. 30, Trends in Cell Biology. Elsevier Ltd; 2020. p. 979–89.

57. O'Neill LAJ, Kishton RJ, Rathmell J. A guide to immunometabolism for immunologists. Vol. 16, Nature Reviews Immunology. Nature Publishing Group; 2016. p. 553–65.

58. Batista-Gonzalez A, Vidal R, Criollo A, Carreño LJ. New Insights on the Role of Lipid Metabolism in the Metabolic Reprogramming of Macrophages. Vol. 10, Frontiers in Immunology. Frontiers Media S.A.; 2020.

p. 2993.

59. Remmerie A, Scott CL. Macrophages and lipid metabolism. Cell Immunol. 2018 Aug 1;330:27–42.

60. Huang SCC, Smith AM, Everts B, Colonna M, Pearce EL, Schilling JD, et al. Metabolic Reprogramming Mediated by the mTORC2-IRF4 Signaling Axis Is Essential for Macrophage Alternative Activation. Immunity. 2016 Oct 18;45(4):817–30.

61. Odegaard JI, Ricardo-Gonzalez RR, Goforth MH, Morel CR, Subramanian V, Mukundan L, et al. Macrophage-specific PPARγ controls alternative activation and improves insulin resistance. Nature. 2007 Jun 28;447(7148):1116–20.

62. Chinetti-Gbaguidi G, Staels B. PPARβ in macrophages and atherosclerosis. Vol. 136, Biochimie. Elsevier B.V.; 2017. p. 59–64.

63. Devchand PR, Keller H, Peters JM, Vazquez M, Gonzalez FJ, Wahli W. The PPARα-leukotriene B4 pathway to inflammation control. Nature. 1996 Nov 7;384(6604):39–43.

64. Shu H, Wong B, Zhou G, Li Y, Berger J, Woods JW, et al. Activation of PPARα or γ reduces secretion of matrix metalloproteinase 9 but not interleukin 8 from human monocytic THP-1 cells. Biochem Biophys Res Commun. 2000 Jan 7;267(1):345–9.

65. Listenberger LL, Han X, Lewis SE, Cases S, Farese R V., Ory DS, et al. Triglyceride accumulation protects against fatty acid-induced lipotoxicity. Proc Natl Acad Sci U S A. 2003 Mar 18;100(6):3077–82.

66. Topham MK, Prescott SM. Mammalian diacylglycerol kinases, a family of lipid kinases with signaling functions. Vol. 274, Journal of Biological Chemistry. Elsevier; 1999. p. 11447–50.

67. Coleman RA, Mashek DG. Mammalian triacylglycerol metabolism: Synthesis, lipolysis, and signaling. Vol. 111, Chemical Reviews. American Chemical Society; 2011. p. 6359–86.

68. Villanueva CJ, Monetti M, Shih M, Zhou P, Watkins SM, Bhanot S, et al. Specific role for acyl CoA:diacylglycerol acyltransferase 1 (Dgat1) in hepatic steatosis due to exogenous fatty acids. Hepatology. 2009 Aug 1;50(2):434–42.

69. Wurie HR, Buckett L, Zammit VA. Diacylglycerol acyltransferase 2 acts upstream of diacylglycerol acyltransferase 1 and utilizes nascent diglycerides and de novo synthesized fatty acids in HepG2 cells.

70. Wang H, Airola M V., Reue K. How lipid droplets "TAG" along: Glycerolipid synthetic enzymes and lipid storage. Biochim Biophys Acta - Mol Cell Biol Lipids. 2017;

71. Walther TC, Chung J, Farese R V. Lipid droplet biogenesis. Vol. 33, Annual Review of Cell and Developmental Biology. Annual Reviews Inc.; 2017. p. 491–510.

72. Maier A, Wu H, Cordasic N, Oefner P, Dietel B, Thiele C, et al. Hypoxia-inducible protein 2 Hig2/Hilpda mediates neutral lipid accumulation in macrophages and contributes to atherosclerosis in apolipoprotein E-deficient mice. FASEB J. 2017 Nov 1;31(11):4971–84.

73. Mattijssen F, Georgiadi A, Andasarie T, Szalowska E, Zota A, Krones-Herzig A, et al. Hypoxia-inducible lipid droplet-associated (HILPDA) is a novel peroxisome proliferator-activated receptor (PPAR) target involved in hepatic triglyceride secretion. J Biol Chem. 2014 Jul 11;289(28):19279–93.

74. DiStefano MT, Danai L V, Roth Flach RJ, Chawla A, Pedersen DJ, Guilherme A, et al. The Lipid Droplet Protein Hypoxia-inducible Gene 2 Promotes Hepatic Triglyceride Deposition by Inhibiting Lipolysis. J Biol Chem. 2015 Jun 12;290(24):15175–84.

75. de la Rosa Rodriguez MA, Kersten S. Regulation of lipid droplet homeostasis by hypoxia inducible lipid droplet associated HILPDA. Biochim Biophys acta Mol cell Biol lipids. 2020 Sep 1;1865(9):158738.

76. Gimm T, Wiese M, Teschemacher B, Deggerich A, Schödel J, Knaup KX, et al. Hypoxia-inducible protein 2 is a novel lipid droplet protein and a specific target gene of hypoxia-inducible factor-1. FASEB J. 2010 Nov 12;24(11):4443–58.

77. Maier A, Wu H, Cordasic N, Oefner P, Dietel B, Thiele C, et al. Hypoxia-inducible protein 2 Hig2/Hilpda mediates neutral lipid accumulation in macrophages and contributes to atherosclerosis in apolipoprotein

E–deficient mice. FASEB J. 2017 Jul 31;fj.201700235R.

78. Vandekopple MJ, Wu J, Auer EN, Giaccia AJ, Denko NC, Papandreou I. HILPDA regulates lipid metabolism, lipid droplet abundance, and response to microenvironmental stress in solid tumors. 2019;

79. Zhang X, Saarinen AM, Hitosugi T, Wang Z, Wang L, Ho TH, et al. Inhibition of intracellular lipolysis promotes human cancer cell adaptation to hypoxia. Elife. 2017 Dec 19;6.

80. Gimm T, Wiese M, Teschemacher B, Deggerich A, Schodel J, Knaup KX, et al. Hypoxia-inducible protein 2 is a novel lipid droplet protein and a specific target gene of hypoxia-inducible factor-1. FASEB J. 2010 Nov 1;24(11):4443–58.

81. Dijk W, Mattijssen F, de la Rosa Rodriguez M, Loza Valdes A, Loft A, Mandrup S, et al. Hypoxia-Inducible Lipid Droplet–Associated Is Not a Direct Physiological Regulator of Lipolysis in Adipose Tissue. Endocrinology. 2017 May 1;158(5):1231–51.

82. Togashi A, Katagiri T, Ashida S, Fujioka T, Maruyama O, Wakumoto Y, et al. Hypoxia-Inducible Protein 2 (HIG2), a novel diagnostic marker for renal cell carcinoma and potential target for molecular therapy. Cancer Res. 2005 Jun 1;65(11):4817–26.

83. DiStefano MT, Roth Flach RJ, Senol-Cosar O, Danai L V., Virbasius J V., Nicoloro SM, et al. Adipocyte-specific Hypoxia-inducible gene 2 promotes fat deposition and diet-induced insulin resistance. Mol Metab. 2016 Dec;5(12):1149–61.

84. Dijk W, Mattijssen F, de la Rosa Rodriguez M, Loza Valdes A, Loft A, Mandrup S, et al. Hypoxia-Inducible Lipid Droplet?Associated Is Not a Direct Physiological Regulator of Lipolysis in Adipose Tissue. Endocrinology. 2017 May 1;158(5):1231–51.

85. Padmanabha Das KM, Wechselberger L, Liziczai M, De La Rosa Rodriguez M, Grabner GF, Heier C, et al. Hypoxia-inducible lipid droplet-associated protein inhibits adipose triglyceride lipase. J Lipid Res. 2018;59(3).

86. Zhang X, Saarinen AM, Hitosugi T, Wang Z, Wang L, Ho TH, et al. Inhibition of intracellular lipolysis promotes human cancer cell adaptation to hypoxia. Elife. 2017 Dec 19;6:e31132.

87. Palmieri F. The mitochondrial transporter family SLC25: identification, properties and physiopathology. Mol Aspects Med. 2013 Jan;34(2–3):465–84.

88. Majd H, King MS, Smith AC, Kunji ERS. Pathogenic mutations of the human mitochondrial citrate carrier SLC25A1 lead to impaired citrate export required for lipid, dolichol, ubiquinone and sterol synthesis. Biochim Biophys Acta - Bioenerg. 2018 Jan 1;1859(1):1–7.

89. Tan M, Mosaoa R, Graham GT, Kasprzyk-Pawelec A, Gadre S, Parasido E, et al. Inhibition of the mitochondrial citrate carrier, Slc25a1, reverts steatosis, glucose intolerance, and inflammation in preclinical models of NAFLD/NASH. Cell Death Differ. 2020 Jul 1;27(7):2143–57.

90. Crichton PG, Lee Y, Kunji ERS. The molecular features of uncoupling protein 1 support a conventional mitochondrial carrier-like mechanism. Vol. 134, Biochimie. Elsevier B.V.; 2017. p. 35–50.

91. Luijten IHN, Feldmann HM, von Essen G, Cannon B, Nedergaard J. In the absence of UCP1-mediated diet-induced thermogenesis, obesity is augmented even in the obesity-resistant 129S mouse strain. Am J Physiol - Endocrinol Metab. 2019 May 1;316(5):E729–40.

92. Tan MGK, Ooi LLPJ, Aw SE, Hui KM. Cloning and identification of hepatocellular carcinoma down-regulated mitochondrial carrier protein, a novel liver-specific uncoupling protein. J Biol Chem. 2004 Oct 22;279(43):45235–44.

Chapter 2

The whole transcriptome effects of the PPARα agonist fenofibrate on livers of hepatocyte humanized mice

Montserrat A. de la Rosa Rodriguez, Go Sugahara, Yuji Ishida, Chise Tateno, Sander Kersten

BMC Genomics, 19(1), 443 (2018)

Abstract

The role of PPARα in gene regulation in mouse liver is well characterized. However, less is known about the effect of PPARα activation in human liver. The aim of the present study was to better characterize the impact of PPARα activation on gene regulation in human liver by combining transcriptomics with the use of hepatocyte humanized livers. To that end, chimeric mice containing hepatocyte humanized livers were given an oral dose of 300 mg/kg fenofibrate daily for 4 days. Livers were collected and analysed by hematoxilin and eosin staining, qPCR, and transcriptomics. Transcriptomics data were compared with existing datasets on fenofibrate treatment in normal mice.

The human hepatocytes exhibited excessive lipid accumulation. Fenofibrate increased the size of the mouse but not human hepatocytes, and tended to reduce steatosis in the human hepatocytes. Quantitative PCR indicated that induction of PPARα targets by fenofibrate was less pronounced in the human hepatocytes than in the residual mouse hepatocytes. Transcriptomics analysis indicated that, after filtering, a total of 282 genes was significantly different between fenofibrate- and control-treated mice ($P<0.01$). 123 genes were significantly lower and 159 genes significantly higher in the fenofibrate-treated mice, including many established PPARα targets such as FABP1, HADHB, HADHA, VNN1, PLIN2, ACADVL and HMGCS2. According to gene set enrichment analysis, fenofibrate upregulated interferon/cytokine signaling-related pathways in hepatocyte humanized liver, but downregulated these pathways in normal mouse liver. Also, fenofibrate downregulated pathways related to DNA synthesis in hepatocyte humanized liver but not in normal mouse liver.

The results support the major role of PPARα in regulating hepatic lipid metabolism, and underscore the more modest effect of PPARα activation on gene regulation in human liver compared to mouse liver. The data suggest that PPARα may have a suppressive effect on DNA synthesis in human liver, and a stimulatory effect on interferon/cytokine signalling.

Keywords: PPARα, liver, fenofibrate, chimeric mouse.

Introduction

The Peroxisome Proliferator Activated Receptors (PPARs) are a group of nuclear receptors involved in the transcriptional regulation of a variety of biological processes, including lipid metabolism and inflammation [1-3]. PPARs regulate gene expression by acting as ligand-activated transcription factors. PPARs interact with DNA as part of a heterodimeric complex with the retinoid X receptor RXR [4-6]. The ligands for PPARs cover a broad range of synthetic and endogenous compounds ranging from environmental contaminants to specific drug classes, fatty acids, eicosanoids, and other lipid species [7]. Three different PPAR subtypes exist in mammals: PPARα, PPARδ, and PPARγ, each with a distinct tissue expression profile and set of functions.

PPARα is expressed in several tissues, particularly in liver, kidney, heart, skeletal muscle and intestine [8, 9]. Studies in mice using whole-body or liver-specific PPARα-/- mice have shown that PPARα is the master regulator of lipid metabolism in the liver during fasting [10-12]. Specifically, fasted PPARα-/- mice suffer from a host of metabolic abnormalities including hypoglycemia, hypoketonemia, elevated plasma non-esterified fatty acids, and a fatty liver. These metabolic defects are rooted in defective transcription of hundreds of genes involved in numerous metabolic pathways covering nearly every aspect of hepatic lipid metabolism [13].

Besides its role as key transcriptional regulator of lipid metabolism during fasting, PPARα is mainly known as the receptor for a diverse group of compounds known as peroxisome proliferators [14, 15]. The group of peroxisome proliferators include plasticizers, insecticides, herbicides, surfactants, organic solvents, and hypolipidemic fibrate drugs [16]. Safety concerns have been raised about these compounds due to their ability to promote hepatocarcinogenesis and the proliferation of peroxisomes in rodent species [17, 18]. Studies using human liver model systems have largely allayed these concerns by failing to find supportive evidence for a proliferative and pro-carcinogenic effect of PPARα ligands in human cells [19].

Whereas the effect of PPARα ligands on cell and peroxisome proliferation is clearly distinct between rodent and human liver cells, the effect of PPARα ligands on the expression of genes involved in lipid metabolism is generally well conserved between the different species. Indeed, numerous genes connected to lipid metabolism are commonly induced by PPARα ligands in mouse and human hepatocytes, including prototypical PPARα targets such as CPT1A, ACOX1, FABP1, and HMGCS2 [20]. A recent review on PPARα summarizes the conclusions that can be reached from the use of human liver model systems [19]. In particular, it was concluded that PPARα in human liver is able to effectively induce the expression of genes involved in numerous lipid metabolic pathways. In addition, similar to

what is observed in mouse liver, PPARα activation in human liver causes the down-regulation of a large number of genes involved in various immunity-related pathways [19, 21].

The specific model systems used to study PPARα in human liver vary from hepatoma cell lines such as HepG2 to human primary hepatocytes [20, 22-24], human precision cut liver slices [21], and mice expressing human PPARα [25, 26]. Each of these models have their specific advantages and disadvantages. An alternative model consist of chimeric mice carrying human liver cells. These mice are generated by transplanting human hepatocytes into albumin enhancer–driven urokinase-type plasminogen activator transgenic/severe combined immunodeficiency (uPA/SCID) mice, leading to replacement of the host hepatocytes at a repopulation rate exceeding 70% [27, 28]. An important advantage of the hepatocyte humanized livers is that the hepatocytes still replicate, in contrast to cultured human primary hepatocytes or liver slices. Recently, we used these PXB mice to study the in vivo effect of PPARα activation using fenofibrate on peroxisome proliferation and the growth of human hepatocytes in mice, leading to the conclusion that rodent data on PPARα-induced hepatocarcinogenesis cannot be accurately extrapolated to human data [2]. Here, we performed transcriptomics analysis on the effect of fenofibrate in chimeric mice with hepatocyte-humanized livers and compared the results with other relevant transcriptomics datasets.

Results

First, we compared the whole genome expression profile of the human liver biopsies with the whole genome expression profile of the hepatocyte-humanized livers, primary human hepatocytes, and human precision-cut liver slices. Scatter plot analysis of normalized expression values revealed that a substantial number of genes that showed expression in human liver tissue were minimally (or not) expressed in hepatocyte-humanized livers (Supplemental figure 1). For highly expressed genes, however, hepatocyte-humanized livers more closely resembled actual human liver tissue as compared to primary human hepatocytes and human precision-cut liver slices, as reflected by the smaller scatter at the high range. Importantly, mRNA expression levels of PPARα in hepatocyte humanized livers were similar to the levels measured in human liver biopsies (Figure 1A). These data support the notion that hepatocyte-humanized livers are a suitable model for human liver, with some restrictions.

To study the effect of PPARα activation on gene expression in hepatocyte-humanized livers, chimeric mice with hepatocyte-humanized livers were given fenofibrate or vehicle at a daily oral dose of 300 mg/kg for 4 days. Fenofibrate has a similar affinity for mouse and human PPARα[36]. Fenofibrate did not affect bodyweight or liver weight (Figure 1B). Also, blood albumin (Figure 1C), as well as plasma glucose, triglycerides and cholesterol levels were not significantly different between the fenofibrate and control-treated mice (Figure 1D). Histological examination of the H&E-stained livers showed clearly distinctive clusters of human and mouse hepatocytes. Human hepatocytes show a light eosin staining while mouse hepatocytes are highly eosinophilic (Figure 1E) [29]. In contrast to the mouse hepatocytes, the human hepatocytes exhibited excessive lipid accumulation (micro- and macrosteatosis). In agreement with our previous study [2], fenofibrate increased the size of the mouse hepatocytes but did not affect the morphology of the human hepatocytes. A tendency toward reduced steatosis by fenofibrate was observed in the sections of the liver populated by human hepatocytes (Figure 1E).

Figure 1

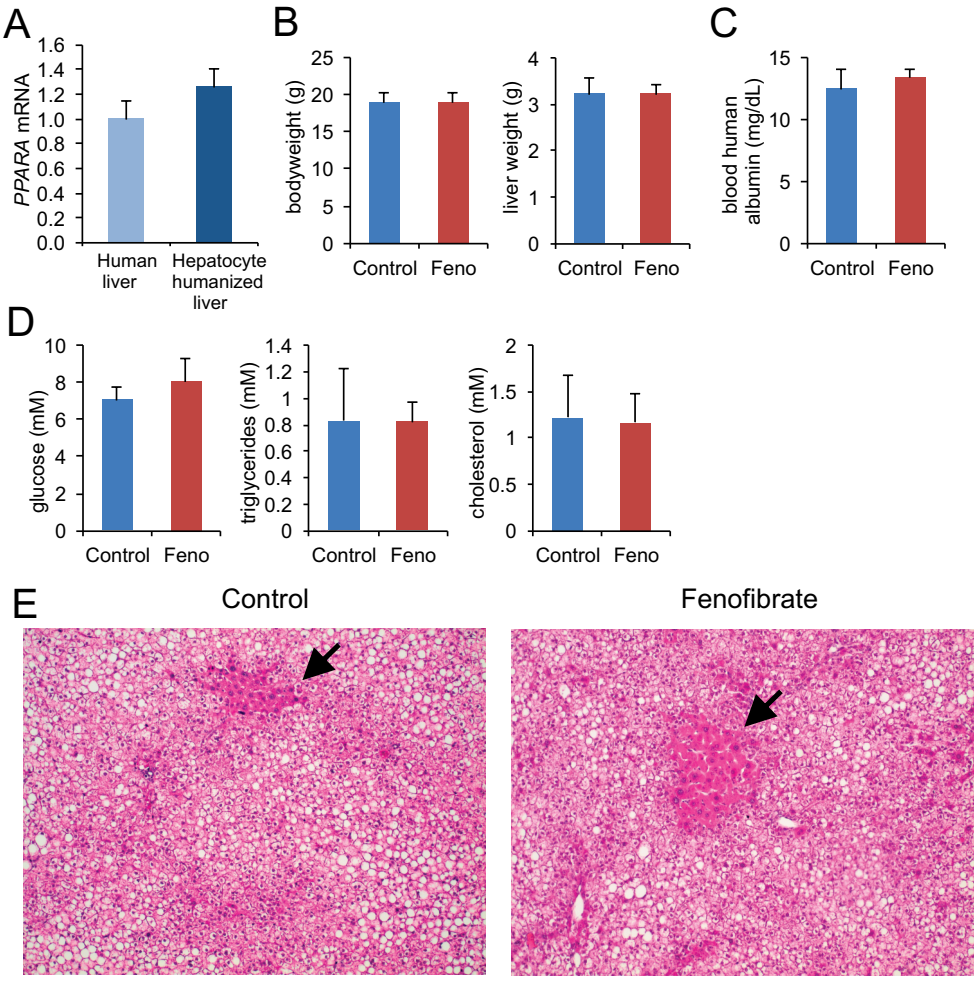

Figure 1. Fenofibrate does not cause any changes in basic parameters in hepatocyte humanized mice. Chimeric mice containing hepatocyte humanized livers were treated with 300 mg/kg fenofibrate daily for 4 days. Control mice received vehicle only. A) mRNA expression of PPARα in 15 human liver biopsies collected during bariatric surgery and in liver samples from 3 chimeric mice containing hepatocyte humanized livers. B) Bodyweight and liver weight. C) Blood human albumin concentration. D) Plasma concentration of glucose, triglycerides and cholesterol. Error bars represent SEM. E)Histological examination of livers of chimeric mice containing hepatocyte humanized livers that received control or fenofibrate treatment. Hematoxilin and eosin staining was carried out according to standard protocols. Images are at 200x magnification. A section containing mouse hepatocytes is indicated (arrow).

To determine whether fenofibrate treatment stimulated PPARα-dependent gene regulation in the mouse and human hepatocytes, we measured the expression of mouse and human PPARα target genes by qPCR in whole liver cDNA using species-specific primers. Fenofibrate treatment significantly increased the expression of known PPARα target genes in human and mouse hepatocytes (Figure 2A). The overall inductions in gene expression were more pronounced in the mouse hepatocytes than the human hepatocytes. This was also observed for the genes that were measured in both human and mouse hepatocytes, including Angptl4, Pdk4 and Cpt1a (Figure 2A). Consistent with the induction of ANGPTL4 mRNA, fenofibrate treatment also significantly increased levels of human ANGPTL4 in mouse plasma (Figure 2B).

Principle component analysis of the transcriptomics data showed that the livers of the fenofibrate-treated hepatocyte-humanized mice clearly separated from the livers of the control-treated hepatocyte-humanized mice (Figure 3A). The liver samples from the fenofibrate-treated mice showed less variation than the liver samples from the control-treated mice. A dendogram confirmed the separate clustering of the two sets of samples (Figure 3B). After filtering, a total of 282 genes was found to be significantly different between fenofibrate- and control-treated mice ($P<0.01$), of which 159 genes were significantly higher and 123 genes were significantly lower in the fenofibrate-treated mice. The top 20 of most highly induced and repressed genes by fenofibrate is shown in Figure 3C. The list of induced genes contains many established PPARα targets connected to lipid metabolism, including *FABP1, HADHB, HADHA, VNN1, PLIN2, ACADVL* and *HMGCS2*. The list of repressed genes is very diverse and does not reveal a common pathway. It includes cytokines (*CCL16*), coagulation factors (*F5*), structural proteins (*ACTG1*), transporters (*SLC16A4/SLC6A12*, and enzymes (*DAK, PPIF*).

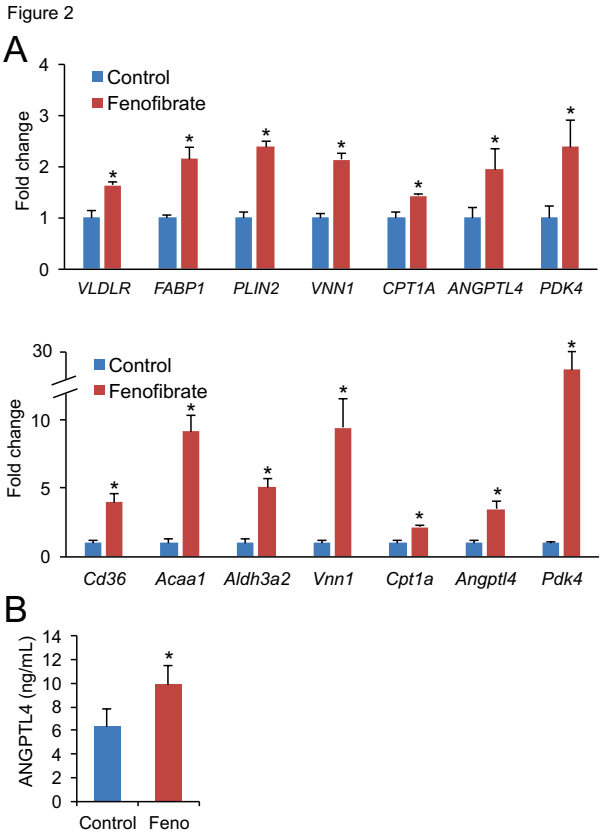

Figure 2. Parallel induction of mouse and human PPARα target genes by fenofibrate in hepatocyte humanized livers. A) qPCR was performed on cDNA generated from livers of control-treated and fenofibrate-treated mice containing hepatocyte humanized livers, using human primers (upper panel) or mouse primers (lower panel) (n= 3 per group). B) Concentration of ANGPTL4 in plasma of control-treated and fenofibrate-treated mice containing hepatocyte humanized livers, as determined by ELISA (n= 3 per group). Error bars represent SEM. Asterisks indicate statistically significant difference between control and fenofibrate-treated mice according to Student's t-test with cut-off of $P < 0.05$.

Figure 3

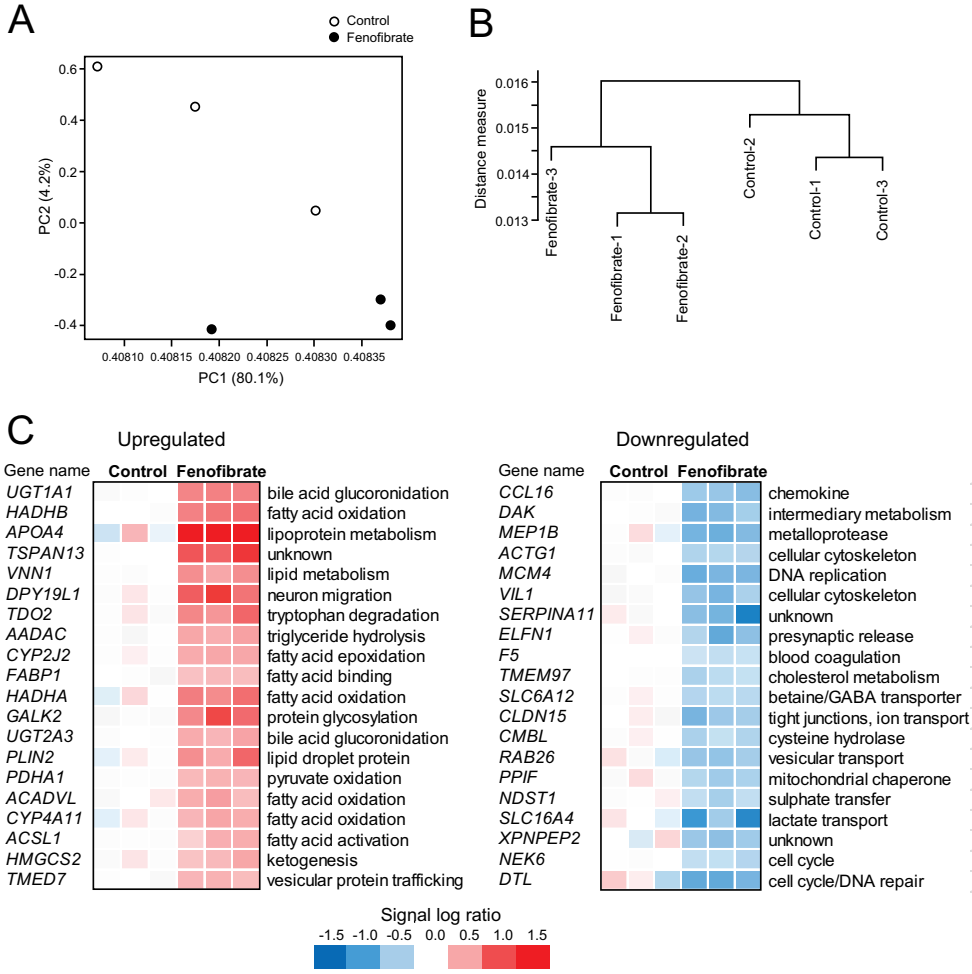

Figure 3. Distinct clustering of livers of control-treated and fenofibrate-treated chimeric mice. Transcriptomics was performed on livers of chimeric mice containing hepatocyte humanized livers. Mice were treated with 300 mg/kg fenofibrate daily for 4 days or vehicle (control) (n= 3 per group). A) Principle component analysis of transcriptomics data from the control and fenofibrate treated mice. The graph shows the clear separation of fenofibrate and control groups. B) Hierarchical clustering of transcriptomics data from the control and fenofibrate treated mice. The dendogram reveals the distinct clustering and separation of the fenofibrate and control groups. C) Top 20 of most highly upregulated and downregulated genes by fenofibrate in hepatocyte humanized livers. Transcriptomics was performed on livers of chimeric mice containing hepatocyte humanized livers. Mice were treated with 300 mg/kg fenofibrate daily for 4 days or vehicle (control). The top 20 most significantly upregulated and downregulated genes by fenofibrate were ranked according to statistical significance (IBMT P-value). The changes in gene expression are expressed relative to the mean of the control group as a signal log ratio.

Previously, we performed transcriptomics analysis on mouse livers harvested either 6 hours after a single oral dose of fenofibrate (4 mg/mouse) or harvested from mice dosed daily with fenofibrate for 14 days by mixing it in the feed (0.03 wt/wt, equivalent to approximately 1 mg/mouse/day). To compare the effect of fenofibrate between normal mouse liver and chimeric humanized liver, we performed a comparative analysis of the three transcriptomics datasets. Volcano plot showed that the two week dosing with fenofibrate in normal mice had a much bigger impact on liver gene expression as compared to the fenofibrate treatment in the hepatocyte-humanized mice, which is not surprising given the longer duration of the treatment (Figure 6). Surprisingly, the single treatment of normal mice with 4 mg of fenofibrate also had a more pronounced effect on liver gene expression as compared to the 4-day treatment of the hepatocyte-humanized mice with 6 mg of fenofibrate per day (Figure 4). These data suggest that in vivo, human liver cells are less sensitive to the effect of fenofibrate as compared to mouse liver cells, confirming the results of the qPCR on the hepatocyte humanized livers. Unfortunately, no transcriptomics dataset was available from normal mice treated with fenofibrate at the same dose and for the same duration as the chimeric hepatocyte-humanized mice.

Figure 4

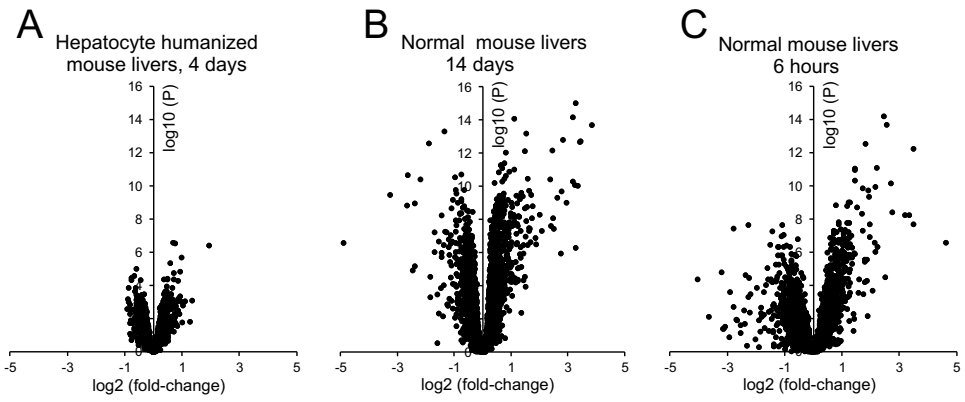

Figure 4. Comparative analysis of the effect of fenofibrate in normal mouse liver and hepatocyte humanized liver. Transcriptomics was performed on livers of chimeric mice containing hepatocyte humanized livers. Mice were treated with 300 mg/kg fenofibrate daily for 4 days or vehicle (control) (n= 3 per group). Volcano plots in which 2log(fold-change) is plotted against -10log-(P-value) for A) Treatment of chimeric mice containing hepatocyte humanized livers with 300 mg/kg fenofibrate daily for 4 days as compared to control; B) Treatment of wildtype mice with fenofibrate for 14 days via the feed (0.03 wt/wt, equivalent to approximately 1 mg/mouse/day) as compared to control; C) Treatment of wildtype mice with fenofibrate for 6 hours via a single oral gavage of 4 mg/mouse as compared to control.

To further compare the effects of fenofibrate between normal mouse liver and hepatocyte-humanized liver, we performed gene set enrichment analysis (GSEA). As expected, pathways covering PPARα signaling and fatty acid oxidation featured prominently among the most significantly induced pathways in both normal mouse liver and hepatocyte-humanized liver (Figure 5A, red). The induction by fenofibrate of genes that are part of the fatty acid degradation pathway is illustrated in Figure 5C. Surprisingly, certain immune-related pathways such as interferon signaling were strongly upregulated in hepatocyte-humanized liver, but were markedly downregulated in normal mouse liver (Figure 5A,B, green). The differential regulation of interferon signaling by fenofibrate in normal mouse liver and hepatocyte-humanized liver is illustrated for specific genes in Figure 5C. With respect to down-regulated pathways, it was observed that many of the most significantly downregulated pathways by fenofibrate in hepatocyte-humanized liver were related to DNA synthesis and telomere extension (Figure 5B, orange), which was not observed in normal mouse liver. Indeed, in normal mouse liver, fenofibrate significantly upregulated pathways related to cell cycle and DNA replication, although they were not in the top 20 pathways. In addition, pathways related to cholesterol biosynthesis were downregulated by fenofibrate in hepatocyte-humanized liver, which also was not seen in normal mouse liver (Figure 5B, grey). Overall, GSEA shows that the effects of fenofibrate in normal mouse liver and hepatocyte-humanized liver are quite distinct, especially in relation to DNA synthesis pathways and interferon signaling pathways.

We previously studied the effect of PPARα activation in human primary hepatocytes and human precision cut liver slices. The studies were not carried out with fenofibrate but with Wy14,643, another PPARα agonist, precluding a whole genome comparison with the study in chimeric mice carrying hepatocyte-humanized livers. Nevertheless, we took the top 40 most highly induced genes by fenofibrate in hepatocyte-humanized livers and compared the fenofibrate-induced gene expression changes with the Wy-14,643-induced expression changes in human primary hepatocytes and human precision cut liver slices (Figure 6). The most apparent difference was the regulation of several interferon-sensitive genes, including IFI6, IFITM1, PSMB9 and ISG15, which were upregulated by fenofibrate in the hepatocyte-humanized mouse livers but downregulated by Wy-14,643 in human primary hepatocytes and human precision cut liver slices. Other genes, nearly all representing genes involved in lipid metabolism, were consistently induced by PPARα activation in the three model systems, with in general the highest fold-inductions observed in human primary hepatocytes.

Figure 5

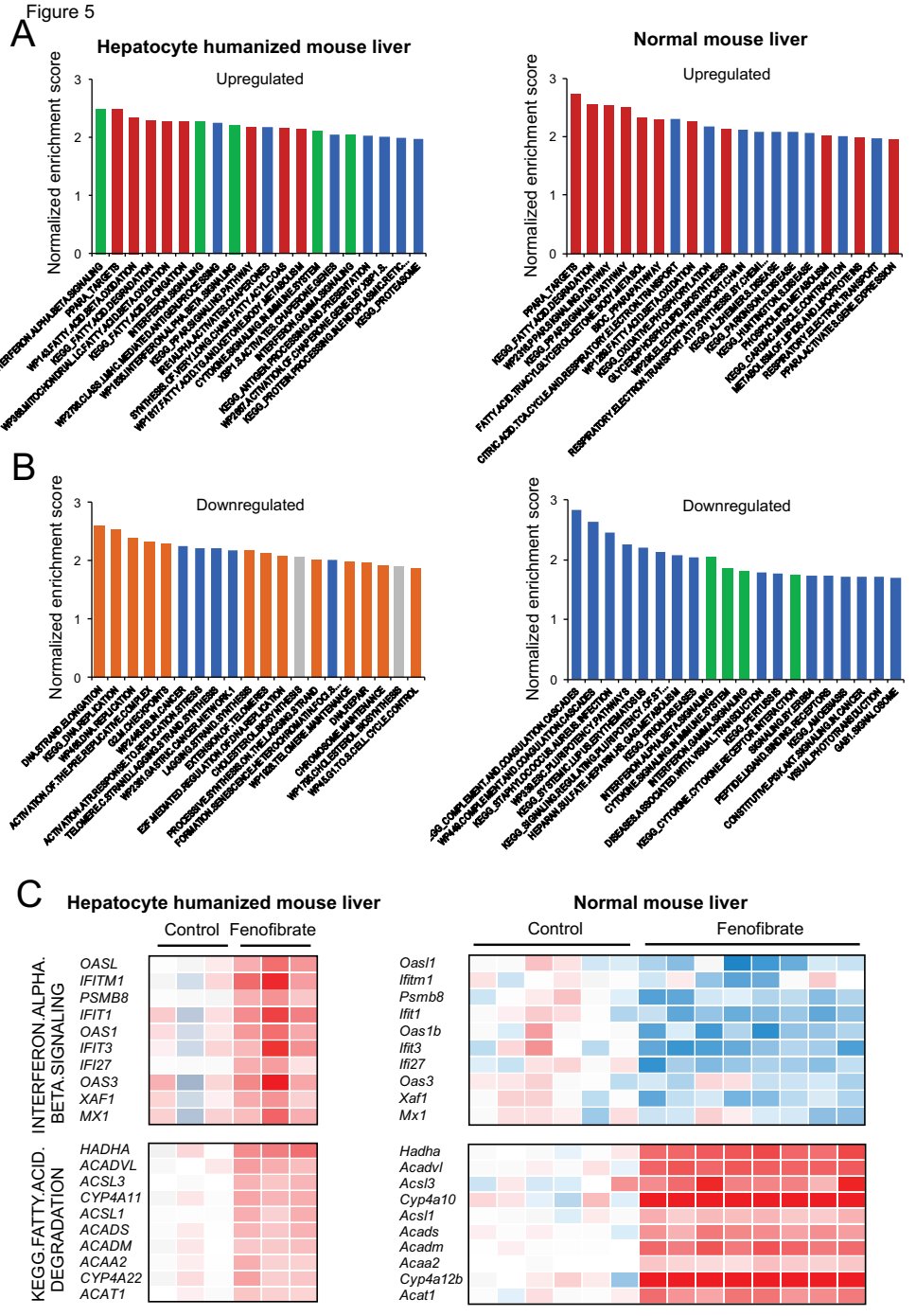
A
Hepatocyte humanized mouse liver
Upregulated
Normalized enrichment score
Normal mouse liver
Upregulated
Normalized enrichment score
B
Downregulated
Normalized enrichment score
Downregulated
Normalized enrichment score
C
Hepatocyte humanized mouse liver
Control
Fenofibrate
INTERFERON.ALPHA.BETA.SIGNALING
OASL
IFITM1
PSMB8
IFIT1
OAS1
IFIT3
IFI27
OAS3
XAF1
MX1
KEGG.FATTY.ACID.DEGRADATION
HADHA
ACADVL
ACSL3
CYP4A11
ACSL1
ACADS
ACADM
ACAA2
CYP4A22
ACAT1
Normal mouse liver
Control
Fenofibrate
Oasl1
Ifitm1
Psmb8
Ifit1
Oas1b
Ifit3
Ifi27
Oas3
Xaf1
Mx1
Hadha
Acadvl
Acsl3
Cyp4a10
Acsl1
Acads
Acadm
Acaa2
Cyp4a12b
Acat1

Figure 5. Comparative pathway analysis of the effect of fenofibrate in normal mouse liver and hepatocyte-humanized liver. Gene set enrichment analysis was performed on the effect of treatment of chimeric mice containing hepatocyte humanized livers with 300 mg/kg fenofibrate daily for 4 days, and on the effect of treatment of wildtype mice with fenofibrate for 14 days via the feed (0.03 wt/wt, equivalent to approximately 1 mg/mouse/day). The top 20 most highly upregulated and downregulated gene sets are shown, ranked according to normalized enrichment score. A) The top 20 most highly upregulated gene sets in hepatocyte humanized livers (left panel) and normal mouse livers (right panel). B) The top 20 most highly downregulated gene sets in hepatocyte humanized livers (left panel) and normal mouse livers (right panel). Gene sets related to cytokine/interferon signalling are shown in green, gene sets related to PPAR signalling and fatty acid oxidation are in red, gene sets related to cholesterol synthesis are in grey, gene sets related to DNA synthesis in orange. C) Heat map of the fenofibrate-induced gene expression changes in normal mouse liver (n=8 per group) and hepatocyte humanized liver (n=3 per group). The most highly ranked genes in the gene sets INTERFERON.ALPHA.BETA.SIGNALING (top panel) and KEGG.FATTY.ACID.DEGRADATION (bottom panel) are shown.

Figure 6

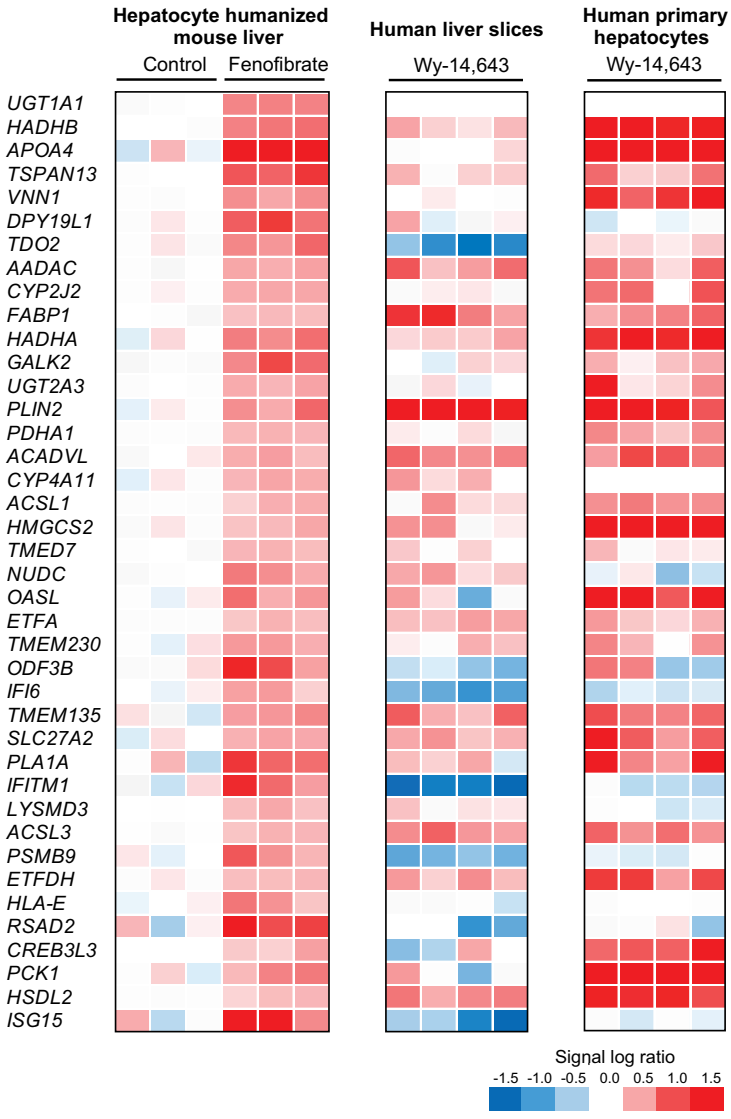

Figure 6. Comparative analysis of fenofibrate-induced genes between different experiments. Transcriptomics was performed on livers of chimeric mice containing hepatocyte humanized livers. Mice were treated with 300 mg/kg fenofibrate daily for 4 days or vehicle (control). A) The top 40 most significantly induced genes by fenofibrate in hepatocyte humanized livers were ranked according to IBMT P-value. In parallel, the expression profiles of the same genes in two independent microarray datasets are shown. The first dataset is derived from human precision cut liver slices treated with the PPARα agonist Wy-14,643 (100 µM) for 24 hours (n=4, GSE17251)[21]. The second dataset is derived from human primary hepatocytes treated with the PPARα agonist GW7647 (1 uM) for 24 hours (n=4, GSE53399) [49].

Discussion

We previously showed that chimeric mice with hepatocyte humanized livers represent an appropriate model to investigate the pharmacological effects of fibrates on human liver [2]. By harbouring clusters of mouse and human hepatocytes, the hepatocyte humanized livers are also an ideal tool to study the parallel effects of a particular treatment on mouse and human hepatocytes. Here, to gain more insight into the whole genome effects of fenofibrate in this model system, we performed transcriptomics on chimeric mice with hepatocyte-humanized livers treated with fenofibrate. The main observations were: 1) The hepatocyte humanized livers recapitulate the principal effects of PPARα activation on lipid metabolism revealed by other model systems of human liver. 2) The effects of PPARα activation on gene expression in chimeric mice with hepatocyte humanized livers were modest compared to normal mouse livers, which is unlikely due to different treatment protocols. 3) Pathways connected to DNA synthesis were downregulated by fenofibrate in chimeric mice with hepatocyte humanized livers, yet are upregulated by fenofibrate in normal mouse livers. 4) Pathways connected to interferon/cytokine signalling were upregulated by fenofibrate in chimeric mice with hepatocyte-humanized livers, yet are downregulated by fenofibrate in normal mouse livers. 5) Chimeric mice with hepatocyte humanized livers can be used to study the effect of activation of PPARα and other nuclear receptors on secretion of hepatokines into plasma.

Studies using human liver model systems, including HepG2 cells, human primary hepatocytes, human precision cut liver slices, and PPARα-humanized mice, have yielded detailed information about the effects of PPARα activation on gene regulation in human liver. The results have been summarized in a recent review [19], highlighting the pivotal role of PPARα in governing various metabolic processes and pathways in human liver. Our transcriptomics study in chimeric mice with hepatocyte humanized livers confirms the important role of PPARα in the regulation of lipid metabolism in human liver. Many of the most highly induced genes are well-known targets of PPARα involved in lipid metabolism, including FABP1, ANGPTL4, PDK4, HADHA, HADHA, PLIN2, and ACADVL. The position of the fenofibrate-induced genes in cellular lipid metabolism is illustrated in Figure 7. Other genes that were highly induced by PPARα activation in the hepatocyte-humanized mouse livers include TSPAN13, DPY19L1, TDO2. Whether any of these genes are actual PPAR target genes remains to be determined.

Chronic treatment of rodents with peroxisome proliferators causes hepato-carcinogenesis, while short-term treatment promotes hepatocyte and peroxisome proliferation [15-17, 37]. These effects are dependent on induction of several genes involved in DNA synthesis, cell proliferation, and peroxisomal biogenesis and are known to be mediated by PPARα [38]. The pro-carcinogenic effects of peroxisome proliferators led to concerns about their

potential hepato-carcinogenicity in humans and triggered numerous studies aimed at investigating the effect of PPARα in human liver model systems. Collectively, these studies have dispelled the notion that peroxisome proliferators are hepato-carcinogenic in humans and have also yielded a wealth of information about the role of PPARα in human liver [19, 39]. In this study, we found that PPARα activation in chimeric mice with hepatocyte humanized livers causes the downregulation of genes and pathways connected to DNA synthesis, further strengthening the notion that the effect of PPARα activation on DNA synthesis, cell proliferation and hepato-carcinogenesis are distinct between mouse liver and human liver. Our data thus further mitigate concerns about the hepato-carcinogenic effect of peroxisome proliferators in humans.

One of the major discrepancies between the effect of PPARα activation in hepatocyte humanized livers and normal mouse livers is the regulation of immune-related pathways, specifically interferon signaling. Whereas PPARα activation causes the downregulation of interferon signaling in mouse liver, it leads to upregulation of interferon signaling in hepatocyte humanized liver. Intriguingly, PPARα activation caused the downregulation of interferon signaling in human precision cut liver slices. Whether the upregulation of interferon signaling by PPARα activation in hepatocyte humanized livers is an artefact of the interaction between human hepatocytes and mouse Kupffer cells, is related to the immune-deficiency in the SCID host mice, or in fact most accurately reflects the response to PPARα activation in human liver remains to be established.

The fold-changes in gene expression in response to fenofibrate treatment were generally lower in chimeric mice with hepatocyte humanized livers compared to normal mouse livers. Unfortunately, differences in the duration of treatment and to a lesser extent dosage preclude a very accurate in vivo comparison of the effect of fenofibrate on gene expression between hepatocyte-humanized livers and normal mouse livers. Alternatively, the residual presence of mouse hepatocytes in the hepatocyte humanized mouse livers allowed for direct evaluation of the effect of fenofibrate on human and mouse hepatocytes. The results showed that the fold-changes in expression of the same genes is more pronounced in mouse as compared to human hepatocytes, verifying the notion that human hepatocytes are less sensitive to PPARα activation.

An important advantage of the hepatocyte humanized livers is that the level of expression of PPARα itself is similar to the expression level in actual human liver. This is in contrast which primary human hepatocytes and precision cut liver slices, which were shown to express PPARα at substantially lower levels [19]. Hence, the relatively modest changes in gene expression by fenofibrate in hepatocyte humanized mice cannot be attributed to a reduced expression of PPARα in comparison with human liver.

Evidence has been provided that PPARα activation alters the expression of a number of apolipoproteins that may account for the plasma triglyceride-lowering and HDL raising effects of PPARα agonists in human patients [40]. For instance, fenofibrate was found to induce APOA1 expression in primary human hepatocytes and elevate plasma APOA1 levels in humans subjects [41, 42]. Similarly, APOA5 was identified as a direct PPARα target and was shown to be induced by PPARα activators in primary human and cynomolgus hepatocytes [43, 44]. Consistent with these findings, administration of the PPARα agonist LY570977 to cynomolgus monkeys increased serum APOA5 concentration by 2-fold [45]. PPARα activation has also been shown to regulate APOC3. Specifically, fenofibrate lowered APOC3 mRNA in primary human hepatocytes, concomitant with reduced secretion of APOC3 in the culture medium [46]. Interestingly, in the hepatocyte humanized mouse livers we did not see any significant changes in the expression of APOA1 and APOC3 mRNA. By contrast, fenofibrate increased mRNA levels of APOA4 (fold-change = 3.9, $P<0.0001$), and APOA5 (fold-change is 1.4, $P<0.05$). Our data, together with data obtained using other model systems for human liver, question the regulation of APOA1 and APOC3 mRNA by PPARα activation in human liver.

The use of chimeric mice with hepatocyte humanized livers in principle allows for study of the secretion of human liver proteins into the blood. Indeed, we were able to detect human ANGPTL4 in blood plasma of mice with hepatocyte humanized livers. Furthermore, in agreement with the induction of ANGPTL4 mRNA by PPARα, treatment of the mice with fenofibrate significantly increased plasma ANGPTL4 levels. These data are consistent with the increase in plasma ANGPTL4 levels in subjects treated with fenofibrate [30, 47]. Intriguingly, the absolute levels of ANGPTL4 in plasma of the mice with hepatocyte humanized livers was similar to the levels observed in human subjects, suggesting that liver is the primary source of ANGPTL4 in plasma. Overall, these data suggest that chimeric mice with hepatocyte humanized livers are a suitable model to study the secretion of human liver proteins into the blood.

In our study, the livers of the hepatocyte humanized mice were very fatty, which was observed specifically in the liver sections populated by human hepatocytes. It has been demonstrated that the elevated lipid storage is likely due to a deficiency of the human growth hormone [48]. Whether the difference in lipid storage between mouse and human hepatocytes is in any way connected to differences in PPARα expression or function remains unclear. The excess lipid storage in the hepatocyte humanized livers is a limitation for the study of lipid metabolism.

In conclusion, using transcriptomics, we show that chimeric mice containing hepatocyte humanized livers are an excellent tool to study the in vivo function of PPARα in human liver. The results confirm the major role of PPARα in the regulation of hepatic lipid metabolism,

yet also demonstrate the more modest effect of PPARα activation on target gene induction in human hepatocytes as compared to mouse hepatocytes. The data suggest that PPARα may have a suppressive effect on DNA synthesis in human liver, and a stimulatory effect on interferon/cytokine signalling.

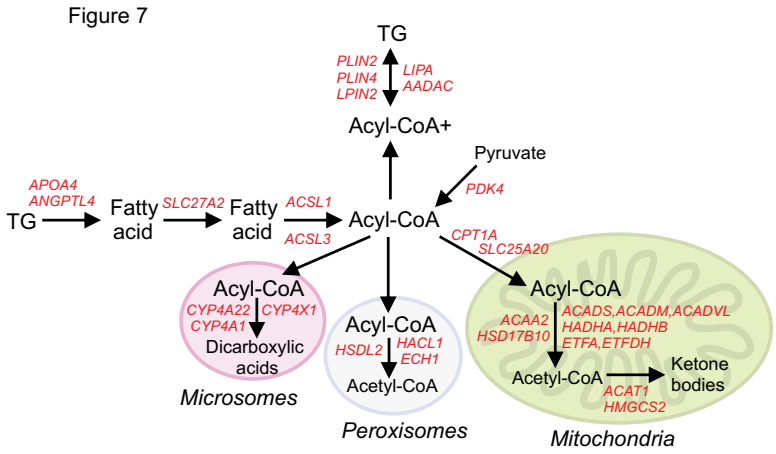

Figure 7. Role of fenofibrate-induced genes in cellular lipid metabolism. Genes significantly induced by fenofibrate (IBMT P-value > 0.02) and with known roles in cellular lipid metabolism were selected. Their roles in specific pathways of cellular lipid metabolism is illustrated.

Methods

Animals

The animal study was carried out in PXB mouse (Genotype: cDNA-uPA+/wt/SCID, uPA+/wt; B6;129SvEv-Plau, SCID; C.B-17/Icr-scid/scid Jcl) at PhoenixBio Co. Ltd. A full description of the generation of these mice can be found elsewhere [29]. Briefly, cryopreserved human hepatocytes from a 2-year-old Hispanic girl were purchased from BD Biosciences (Woburn, MA, USA). After thawing, the hepatocytes were transplanted into hemizygous 2- to 4-week-old cDNA-uPA/SCID mice via the spleen under anesthesia. Six male mice between 12-18 weeks of age were used for the study.

Fenofibrate was dissolved in 0.5% hydroxypropyl methylcellulose (Shinestu Kagaku Kogyo, Japan) and administered orally to the mice at a dose of 300 mg/kg once per day for 4 days with a disposable plastic sonde (Fuchigami Kikai Co., Kyoto, Japan). Three mice received fenofibrate and three mice received the control treatment with vehicle only.

The experiment was terminated 24 hours after the final dosing with fenofibrate. Mice were anesthetized using isoflurane and a minimum of 300 µL of blood was collected via cardiac puncture into sodium heparinized syringes. The mice were euthanized by exsanguination. Blood was used for measurement of human albumin or centrifuged to obtain plasma. Plasma was subsequently frozen at -80°C. Liver tissue was collected and either frozen at -80°C or fixed in formaldehyde and further processed for histology. All experimental procedures were conducted in accordance with the guidelines provided by Proper Conduct of Animal Experiments (June 1, 2006; Science Council of Japan) and approved by the Animal Care and use Committee of PhoenixBio Co., Ltd

Plasma measurements

Plasma concentrations of glucose (Sopachem, Ochten, the Netherlands), triglycerides (TG), and cholesterol (Instruchemie, Delfzijl, the Netherlands) were determined following the manufacturers' instructions. The plasma concentration of ANGPTL4 was determined as previously described [30].

RNA isolation and qPCR

Total RNA of human and mouse tissue was isolated using TRIzol reagent (Invitrogen). RNA was reverse transcribed using the iScript cDNA Synthesis Kit (Bio-Rad Laboratories BV, Veenendaal, The Netherlands). Messenger RNA levels of selected genes were determined by reverse transcription quantitative PCR using SensiMix (Bioline; GC Biotech, Alphen aan den Rijn, The Netherlands) on a CFX384 real-time PCR detection system (Bio-Rad Laboratories, Veenendaal, the Netherlands). The housekeeping gene 36b4 was used for normalization. Sequences of the primers used are listed in Supplementary table 1. Mouse primers and human primers are specific for mouse and human, respectively. Primer pairs contain at least 4 mismatches with the opposite organism. Primer specificity was assessed using NCBI primer-BLAST. Gene set enrichment analysis (GSEA) was used to identify gene sets that were enriched among the upregulated or downregulated genes [32]. Genes were ranked based on the IBMT-statistic and subsequently analyzed for over- or underrepresentation in predefined gene sets derived from Gene Ontology, KEGG, National Cancer Institute, PFAM, Biocarta, Reactome and WikiPathways pathway databases. Only gene sets consisting of more than 15 and fewer than 500 genes were taken into account. Statistical significance of GSEA results was determined using 1,000 permutations.

Microarray analysis

For microarray hybridization, the isolated RNA was further purified using RNeasy Minikit columns (Qiagen). RNA concentrations were measured on a nanodrop ND-1000 UV-Vis spectrophotometer (Isogen, Maarssen, The Netherlands) and analyzed on an Agilent 2100 bioanalyzer (Agilent Technologies, Amsterdam, The Netherlands) with 6000 Nano Chips, according to the manufacturer's protocol. RNA was judged suitable for array hybridization only if samples exhibited intact bands corresponding to the 18S and 28S ribosomal RNA subunits, and displayed no chromosomal peaks or RNA degradation products.

Purified RNA (100 ng) was labeled with the Ambion WT expression kit (Invitrogen) and hybridized to Affymetrix Human Gene 1.1 ST arrays, provided in plate format (Affymetrix, Santa Clara, CA). Hybridization, washing and scanning of the array plates was performed on an Affymetrix GeneTitan instrument, according to the manufacturer's recommendations. Normalized expression estimates were obtained from the raw intensity values applying the robust multi-array analysis preprocessing algorithm available in the Bioconductor library AffyPLM with default settings [31, 32]. Probe sets were defined according to Dai et al. [33]. In this method probes are assigned to Entrez IDs as a unique gene identifier. In this study, probes were reorganized based on the Entrez Gene database, build 37, version 1 (remapped CDF v22). The entire geneset was condensed by applying an Inter Quartile Range filter of

0.25 and by excluding genes with mean expression level below 20. The P values were calculated using an Intensity-Based Moderated T-statistic (IBMT) [34]. Genes were defined as significantly changed when P <0.01. The microarray data were submitted to the Gene Expression Omnibus (accession number pending).

Gene set enrichment analysis (GSEA) was used to identify gene sets that were enriched among the upregulated or downregulated genes [35]. Genes were ranked based on the IBMT-statistic and subsequently analyzed for over- or underrepresentation in predefined gene sets derived from Gene Ontology, KEGG, National Cancer Institute, PFAM, Biocarta, Reactome and WikiPathways pathway databases. Only gene sets consisting of more than 15 and fewer than 500 genes were taken into account. Statistical significance of GSEA results was determined using 1,000 permutations.

Statistical analysis

Data are presented as mean ± SEM. Differences between the fenofibrate and control groups were analysed using two-tailed Student's t-test. P < 0.05 was considered as statistically significant.

Declarations

Ethics approval and consent to participate

This study was performed with approval of PhoenixBio Research Ethics Committee of Human Tissue. All experimental procedures were conducted in accordance with the guidelines provided by Proper Conduct of Animal Experiments (June 1, 2006; Science Council of Japan) and approved by the Animal Care and use Committee of PhoenixBio Co., Ltd.

Consent for publication

"Not applicable"

Availability of data and material

The microarray data have been submitted to Gene Expression Omnibus (accession number-GSE107041)

Competing interests

The authors have nothing to disclose. Go Sugahara, Yuji Ishida and Chise Tateno are employees of PhoenixBio Co., Ltd.

Funding

This work was supported by a grant from the Netherlands Organisation for Scientific Research (NWO-ALW) and by Consejo Nacional de Ciencia y Tecnología (Mexico).

Authors' contributions

MR made substantial contributions to the conception and draft of the manuscript, performed the histological examination, qPCR, and plasma measurements.
GS performed the animal study.
YI performed the animal study and contributed to the writing of the manuscript.
CT designed the animal study and contributed to the writing of the manuscript
SK conceived the idea, analyzed the microarray data, and drafted the manuscript.
All authors read and approved the final manuscript

References

1. Gross B, Pawlak M, Lefebvre P, Staels B: PPARs in obesity-induced T2DM, dyslipidaemia and NAFLD. *Nat Rev Endocrinol* 2016.
2. Tateno C, Yamamoto T, Utoh R, Yamasaki C, Ishida Y, Myoken Y, Oofusa K, Okada M, Tsutsui N, Yoshizato K: Chimeric mice with hepatocyte-humanized liver as an appropriate model to study human peroxisome proliferator-activated receptor-alpha. *Toxicologic pathology* 2015, 43(2):233-248.
3. Varga T, Czimmerer Z, Nagy L: PPARs are a unique set of fatty acid regulated transcription factors controlling both lipid metabolism and inflammation. *Biochim Biophys Acta* 2011, 1812(8):1007-1022.
4. Gearing KL, Gottlicher M, Teboul M, Widmark E, Gustafsson JA: Interaction of the peroxisome-proliferator-activated receptor and retinoid X receptor. *Proc Natl Acad Sci U S A* 1993, 90(4):1440-1444.
5. Issemann I, Prince RA, Tugwood JD, Green S: The retinoid X receptor enhances the function of the peroxisome proliferator activated receptor. *Biochimie* 1993, 75(3-4):251-256.
6. Keller H, Dreyer C, Medin J, Mahfoudi A, Ozato K, Wahli W: Fatty acids and retinoids control lipid metabolism through activation of peroxisome proliferator-activated receptor-retinoid X receptor heterodimers. *Proc Natl Acad Sci U S A* 1993, 90(6):2160-2164.
7. Georgiadi A, Kersten S: Mechanisms of gene regulation by Fatty acids. *Advances in nutrition* 2012, 3(2):127-134.
8. Bookout AL, Jeong Y, Downes M, Yu RT, Evans RM, Mangelsdorf DJ: Anatomical profiling of nuclear receptor expression reveals a hierarchical transcriptional network. *Cell* 2006, 126(4):789-799.
9. Escher P, Braissant O, Basu-Modak S, Michalik L, Wahli W, Desvergne B: Rat PPARs: quantitative analysis in adult rat tissues and regulation in fasting and refeeding. *Endocrinology* 2001, 142(10):4195-4202.
10. Kersten S, Seydoux J, Peters JM, Gonzalez FJ, Desvergne B, Wahli W: Peroxisome proliferator-activated receptor alpha mediates the adaptive response to fasting. *J Clin Invest* 1999, 103(11):1489-1498.
11. Leone TC, Weinheimer CJ, Kelly DP: A critical role for the peroxisome proliferator-activated receptor alpha (PPARalpha) in the cellular fasting response: the PPARalpha-null mouse as a model of fatty acid oxidation disorders. *Proc Natl Acad Sci U S A* 1999, 96(13):7473-7478.
12. Regnier M, Polizzi A, Lippi Y, Fouche E, Michel G, Lukowicz C, Smati S, Marrot A, Lasserre F, Naylies C *et al*: Insights into the role of hepatocyte PPARalpha activity in response to fasting. *Mol Cell Endocrinol* 2017.
13. Kersten S: Integrated physiology and systems biology of PPARalpha. *Molecular metabolism* 2014, 3(4):354-371.
14. Issemann I, Green S: Activation of a member of the steroid hormone receptor superfamily by peroxisome proliferators. *Nature* 1990, 347(6294):645-650.
15. Lee SS, Pineau T, Drago J, Lee EJ, Owens JW, Kroetz DL, Fernandez-Salguero PM, Westphal H, Gonzalez FJ: Targeted disruption of the alpha isoform of the peroxisome proliferator-activated receptor gene in mice results in abolishment of the pleiotropic effects of peroxisome proliferators. *Mol Cell Biol* 1995, 15(6):3012-3022.
16. Reddy JK, Lalwai ND: Carcinogenesis by hepatic peroxisome proliferators: evaluation of the risk of hypolipidemic drugs and industrial plasticizers to humans. *Crit Rev Toxicol* 1983, 12(1):1-58.
17. Corton JC, Lapinskas PJ, Gonzalez FJ: Central role of PPARalpha in the mechanism of action of hepatocarcinogenic peroxisome proliferators. *Mutat Res* 2000, 448(2):139-151.
18. Gonzalez FJ: The peroxisome proliferator-activated receptor alpha (PPARalpha): role in hepatocarcinogenesis. *Mol Cell Endocrinol* 2002, 193(1-2):71-79.
19. Kersten S, Stienstra R: The role and regulation of the peroxisome proliferator activated receptor alpha in human liver. *Biochimie* 2017, 136:75-84.

20. Rakhshandehroo M, Hooiveld G, Muller M, Kersten S: Comparative analysis of gene regulation by the transcription factor PPARalpha between mouse and human. *PLoS One* 2009, 4(8):e6796.

21. Janssen AW, Betzel B, Stoopen G, Berends FJ, Janssen IM, Peijnenburg AA, Kersten S: The impact of PPARalpha activation on whole genome gene expression in human precision cut liver slices. *BMC genomics* 2015, 16(1):760.

22. Mukherjee R, Jow L, Noonan D, McDonnell DP: Human and rat peroxisome proliferator activated receptors (PPARs) demonstrate similar tissue distribution but different responsiveness to PPAR activators. *The Journal of steroid biochemistry and molecular biology* 1994, 51(3-4):157-166.

23. van der Meer DL, Degenhardt T, Vaisanen S, de Groot PJ, Heinaniemi M, de Vries SC, Muller M, Carlberg C, Kersten S: Profiling of promoter occupancy by PPARalpha in human hepatoma cells via ChIP-chip analysis. *Nucleic Acids Res* 2010, 38(9):2839-2850.

24. Kandel BA, Thomas M, Winter S, Damm G, Seehofer D, Burk O, Schwab M, Zanger UM: Genomewide comparison of the inducible transcriptomes of nuclear receptors CAR, PXR and PPARalpha in primary human hepatocytes. *Biochim Biophys Acta* 2016, 1859(9):1218-1227.

25. Morimura K, Cheung C, Ward JM, Reddy JK, Gonzalez FJ: Differential susceptibility of mice humanized for peroxisome proliferator-activated receptor alpha to Wy-14,643-induced liver tumorigenesis. *Carcinogenesis* 2006, 27(5):1074-1080.

26. Yang Q, Nagano T, Shah Y, Cheung C, Ito S, Gonzalez FJ: The PPAR alpha-humanized mouse: a model to investigate species differences in liver toxicity mediated by PPAR alpha. *Toxicol Sci* 2008, 101(1):132-139.

27. Mercer DF, Schiller DE, Elliott JF, Douglas DN, Hao C, Rinfret A, Addison WR, Fischer KP, Churchill TA, Lakey JR *et al*: Hepatitis C virus replication in mice with chimeric human livers. *Nat Med* 2001, 7(8):927-933.

28. Tateno C, Yoshizane Y, Saito N, Kataoka M, Utoh R, Yamasaki C, Tachibana A, Soeno Y, Asahina K, Hino H *et al*: Near completely humanized liver in mice shows human-type metabolic responses to drugs. *Am J Pathol* 2004, 165(3):901-912.

29. Tateno C, Kawase Y, Tobita Y, Hamamura S, Ohshita H, Yokomichi H, Sanada H, Kakuni M, Shiota A, Kojima Y *et al*: Generation of Novel Chimeric Mice with Humanized Livers by Using Hemizygous cDNA-uPA/SCID Mice. *PLoS One* 2015, 10(11):e0142145.

30. Kersten S, Lichtenstein L, Steenbergen E, Mudde K, Hendriks HF, Hesselink MK, Schrauwen P, Muller M: Caloric restriction and exercise increase plasma ANGPTL4 levels in humans via elevated free fatty acids. *Arterioscler Thromb Vasc Biol* 2009, 29(6):969-974.

31. Bolstad BM, Irizarry RA, Astrand M, Speed TP: A comparison of normalization methods for high density oligonucleotide array data based on variance and bias. *Bioinformatics* 2003, 19(2):185-193.

32. Irizarry RA, Bolstad BM, Collin F, Cope LM, Hobbs B, Speed TP: Summaries of Affymetrix GeneChip probe level data. *Nucleic Acids Res* 2003, 31(4):e15.

33. Dai M, Wang P, Boyd AD, Kostov G, Athey B, Jones EG, Bunney WE, Myers RM, Speed TP, Akil H *et al*: Evolving gene/transcript definitions significantly alter the interpretation of GeneChip data. *Nucleic Acids Res* 2005, 33(20):e175.

34. Sartor MA, Tomlinson CR, Wesselkamper SC, Sivaganesan S, Leikauf GD, Medvedovic M: Intensity-based hierarchical Bayes method improves testing for differentially expressed genes in microarray experiments. *BMC Bioinformatics* 2006, 7:538.

35. Subramanian A, Tamayo P, Mootha VK, Mukherjee S, Ebert BL, Gillette MA, Paulovich A, Pomeroy SL, Golub TR, Lander ES *et al*: Gene set enrichment analysis: a knowledge-based approach for interpreting genome-wide expression profiles. *Proc Natl Acad Sci U S A* 2005, 102(43):15545-15550.

36. Willson TM, Brown PJ, Sternbach DD, Henke BR: The PPARs: from orphan receptors to drug discovery. *J Med Chem* 2000, 43(4):527-550.

37. Gonzalez FJ, Peters JM, Cattley RC: Mechanism of action of the nongenotoxic peroxisome proliferators: role of the peroxisome proliferator-activator receptor alpha. *J Natl Cancer Inst* 1998, 90(22):1702-1709.

38. Peters JM, Aoyama T, Cattley RC, Nobumitsu U, Hashimoto T, Gonzalez FJ: Role of peroxisome proliferator-activated receptor alpha in altered cell cycle regulation in mouse liver. *Carcinogenesis JID - 8008055* 1998, 19(11):1989-1994.

39. Corton JC, Cunningham ML, Hummer BT, Lau C, Meek B, Peters JM, Popp JA, Rhomberg L, Seed J, Klaunig JE: Mode of action framework analysis for receptor-mediated toxicity: The peroxisome proliferator-activated receptor alpha (PPARalpha) as a case study. *Crit Rev Toxicol* 2014, 44(1):1-49.

40. Duval C, Muller M, Kersten S: PPARalpha and dyslipidemia. *Biochim Biophys Acta* 2007, 1771(8):961-971.

41. Berthou L, Duverger N, Emmanuel F, Langouet S, Auwerx J, Guillouzo A, Fruchart JC, Rubin E, Denefle P, Staels B *et al*: Opposite regulation of human versus mouse apolipoprotein A-I by fibrates in human apolipoprotein A-I transgenic mice. *J Clin Invest* 1996, 97(11):2408-2416.

42. Duez H, Lefebvre B, Poulain P, Torra IP, Percevault F, Luc G, Peters JM, Gonzalez FJ, Gineste R, Helleboid S *et al*: Regulation of human apoA-I by gemfibrozil and fenofibrate through selective peroxisome proliferator-activated receptor alpha modulation. *Arterioscler Thromb Vasc Biol* 2005, 25(3):585-591.

43. Prieur X, Coste H, Rodriguez JC: The human apolipoprotein AV gene is regulated by peroxisome proliferator-activated receptor-alpha and contains a novel farnesoid X-activated receptor response element. *J Biol Chem* 2003, 278(28):25468-25480.

44. Vu-Dac N, Gervois P, Jakel H, Nowak M, Bauge E, Dehondt H, Staels B, Pennacchio LA, Rubin EM, Fruchart-Najib J *et al*: Apolipoprotein A5, a crucial determinant of plasma triglyceride levels, is highly responsive to peroxisome proliferator-activated receptor alpha activators. *J Biol Chem* 2003, 278(20):17982-17985.

45. Schultze AE, Alborn WE, Newton RK, Konrad RJ: Administration of a PPARalpha agonist increases serum apolipoprotein A-V levels and the apolipoprotein A-V/apolipoprotein C-III ratio. *J Lipid Res* 2005, 46(8):1591-1595.

46. Staels B, Vu-Dac N, Kosykh VA, Saladin R, Fruchart JC, Dallongeville J, Auwerx J: Fibrates downregulate apolipoprotein C-III expression independent of induction of peroxisomal acyl coenzyme A oxidase. A potential mechanism for the hypolipidemic action of fibrates. *J Clin Invest* 1995, 95(2):705-712.

47. Rakhshandehroo M, Stienstra R, de Wit NJ, Bragt MC, Haluzik M, Mensink RP, Muller M, Kersten S: Plasma mannose-binding lectin is stimulated by PPARalpha in humans. *Am J Physiol Endocrinol Metab* 2012, 302(5):E595-602.

48. Tateno C, Kataoka M, Utoh R, Tachibana A, Itamoto T, Asahara T, Miya F, Tsunoda T, Yoshizato K: Growth hormone-dependent pathogenesis of human hepatic steatosis in a novel mouse model bearing a human hepatocyte-repopulated liver. *Endocrinology* 2011, 152(4):1479-1491.

49. McMullen PD, Bhattacharya S, Woods CG, Sun B, Yarborough K, Ross SM, Miller ME, McBride MT, Lecluyse EL, Clewell RA *et al*: A map of the PPARalpha transcription regulatory network for primary human hepatocytes. *Chemico-biological interactions* 2013, 209C:14-24.

50. Ahrens M, Ammerpohl O, von Schonfels W, Kolarova J, Bens S, Itzel T, Teufel A, Herrmann A, Brosch M, Hinrichsen H *et al*: DNA methylation analysis in nonalcoholic fatty liver disease suggests distinct disease-specific and remodeling signatures after bariatric surgery. *Cell Metab* 2013, 18(2):296-302.

Supplemental Material

Supplementary table 1: Sequences of primers used in qPCR analysis

Name	*Forward*	*Reverse*
36B4/36b4	*CGGGAAGGCTGTGGTGCTG*	*GTGAACACAAAGCCCACATTCC*
VNN1	*AGTGGCATCTATGCACCCAAT*	*GGAATCCAGTTGCGAGAGGA*
FGF21	*AGTGGAGCGATCCATACAGG*	*ACTCCAGTCCTCTCCTGCAA*
PPARα	*CAGAACAAGGAGGCGGAGGTC*	*TTCAGGTCCAAGTTTGCGAAGC*
ANGPTL4	*CGTACCCTTCTCCACTTGGG*	*GCTCTTGGCGCAGTTCTTG*
CPT1α	*TCCAGTTGGCTTATCGTGGTG*	*CTAACGAGGGGTCGATCTTGG*
PDK4	*TGGAGCATTTCTCGCGCTAC*	*ACAGGCAATTCTTGTCGCAAA*
VLDLR	*GGTGAAAATGATTGTGACAGTGG*	*GTGAACTCGTCGGGACTACA*
PLIN2	*ATGGCAGAGAACGGTGTGAAG*	*CAACTGCAATTTGCGGCTC*
FABP1	*ATGAGTTTCTCCGGCAAGTACC*	*CTCTTCCGGCAGACCGATTG*
Cd36	*GAGCAACTGGTGGATGGTTT*	*GCAGAATCAAGGGAGAGCAC*
Acaa1	*AAGGCAGGTTGTCACGCTACT*	*CCTCAGTTCCCAGGGTATTCAAAG*
Aldh3a2	*CCTGAGCAAAAGTGAACTCAATG*	*GCTCCAATAATCAGTACGACTCC*
Pparα	*TATTCGGCTGAAGCTGGTGTAC*	*CTGGCATTTGTTCCGGTTCT*
Cpt1α	*CTCCGCCTGAGCCATGAAG*	*CACCAGTGATGATGCCATTCT*
Plin2	*CTTGTGTCCTCCGCTTATGTC*	*GCAGAGGTCACGGTCTTCAC*
Pdk4	*TCTACAAACTCTGACAGGGCTTT*	*CCGCTTAGTGAACACTCCTTC*
Ucp2	*GTGGTGGTCGGAGATACCAG*	*CATAGGTCACCAGCTCAGCA*
Vnn1	*CTTTCCTCGCGGCTGTTTAC*	*CCTCCAGGTATGGGTAGATCGT*

Supplementary figure 1

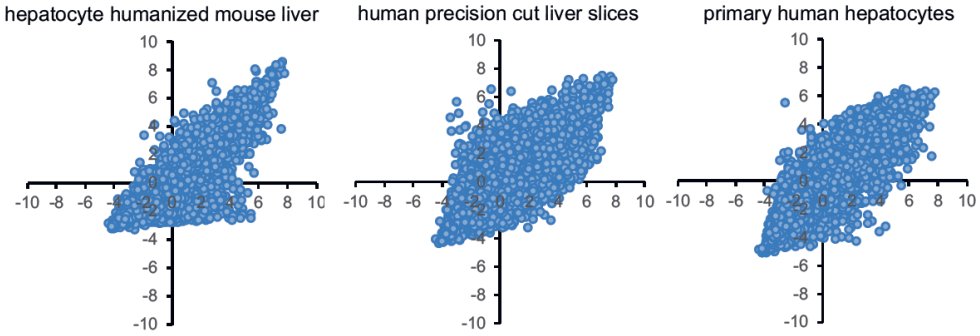

Supplemental figure 1. Comparative transcriptomics analysis of different human liver model systems. Transcriptomics was carried out on human liver biopsies (GSE48452) [50], hepatocyte humanized livers, primary human hepatocytes (GSE76148) [24], and human precision-cut liver slices (GSE17251) [21]. Scatter plot analysis of normalized expression values comparing the whole genome expression profile of the human liver biopsies (x-axis) with the whole genome expression profile of the hepatocyte-humanized livers (left panel), human precision-cut liver slices (middle panel), and primary human hepatocytes (right panel) (all y-axis).

Chapter 3

Regulation of Lipid Droplet-Associated Proteins by Peroxisome Proliferator-Activated Receptors

Montserrat A. de la Rosa Rodriguez, Sander Kersten

BBA-Molecular and Cell Biology of Lipids, 1862(10), 1212-1220 (2017)

Highlights

- Most cell types carry lipid droplets and lipid droplet-associated proteins.
- PPARs are master regulators of lipid metabolism in various cell types.
- The three PPARs differ in their ligand specificity and in their expression profile across tissues.
- PPARs play a key role in the regulation of the expression of LD-associated proteins.
- The expression level of LD-associated proteins and the regulation by PPARs is cell type specific.

Abstract

Excess fatty acids are stored in cells as triglycerides in specialized organelles called lipid droplets (LD). LD can be found in nearly all cell types and may expand during certain (patho)physiological conditions. The synthesis and breakdown of triglycerides and their deposition in LD is governed by a diverse set of enzymes and LD-associated proteins. These proteins serve structural roles in and around LD and regulate the activity of key lipogenic and lipolytic enzymes. The LD-associated proteins are subject to multiple regulatory mechanisms at the protein and gene expression level. A group of transcription factors that govern the expression of many LD-associated proteins are the Peroxisome Proliferator-Activated Receptors (PPARs). PPARs are lipid-activated transcription factors that play a key role in the regulation of lipid metabolism in liver (PPARα), adipose tissue (PPARγ), and skeletal muscle (PPARδ). This review provides an overview of the regulation of LD-associated protein by PPARα, PPARδ, and PPARγ in adipose tissue, liver, macrophages, and skeletal muscle. It is concluded that many LD-associated proteins, including members of the PLIN family, CIDEC, CIDEA, HILPDA, FITM1, FITM2, and G0S2 are under direct transcriptional control of PPARs. Upregulation of LD-associated proteins by PPARs provides a mechanism to link uptake of lipids to regulation of lipid storage capacity.

Keywords: PPARs; lipid droplet; lipid droplet-associated proteins; perilipins

Lipid droplets

Fatty acids represent an important cellular fuel. Via the successive processes of β-oxidation, the TCA cycle, and oxidative phosphorylation, part of the energy in fatty acids is converted into ATP, with the remainder of the energy lost as heat. Fatty acids enter cells via several fatty acid transporters, and once taken up are bound by fatty acid-binding proteins that guide the fatty acids to their different metabolic fates. Apart from oxidation, an important metabolic fate of fatty acids is storage. Indeed, most cell types have the ability to stockpile excess fatty acids by converting them into triglycerides. The triglycerides are synthesized in the endoplasmic reticulum and are stored in specialized organelles called lipid droplets (LD) [1]. The ability to store excess fatty acids as triglycerides in LD can be considered as a protective mechanism that allows cells to cope with fluctuations in fatty acid supply without risking lipotoxicity. With the exception of adipocytes, most cell types have minuscule LD that together take up only a very small portion of the total cell volume. However, in certain pathological conditions, LD may expand and occupy considerable space in the cell, potentially interfering with important cellular functions [2]. One example is the accumulation of lipids in macrophages in atherosclerotic plaques, leading to activation of macrophages and giving rise to the characteristic foam cells. Another example involves the massive growth of LD in hepatocytes as part of alcoholic and non-alcoholic fatty liver disease. In comparison with most other organelles, LD are very dynamic and can quickly expand or shrink depending on cellular demands, driven by fluctuations in the rate of triglyceride synthesis and degradation. The synthesis of triglycerides, their deposition in LD, and the subsequent breakdown of triglycerides into fatty acids is governed by a complex set of enzymes and LD-associated proteins. These LD-associated proteins serve structural roles in LD and regulate the activity of key lipogenic and lipolytic enzymes. An important group of LD-associated proteins are the five members of the perilipin family, PLIN1-PLIN5 [3]. Other LD-associated proteins that have been discovered in recent years include CIDEA, CIDEB, CIDEC, FITM1, FITM2, G0S2, ABHD5, and HILPDA. The function of these proteins is covered by other reviews in this special issue.

Peroxisome Proliferator-Activated Receptors

LD-associated proteins are themselves subject to multiple regulatory mechanisms at the protein and gene expression level. A group of transcription factors that play a key role in the transcriptional regulation of LD-associated proteins, as well as in the regulation of the lipogenic and lipolytic enzymes involved in LD remodeling, are the Peroxisome Proliferator-

Activated Receptors (PPARs) [4]. PPARs are ligand-activated transcription factors that belong to the family of nuclear hormone receptors. Similar to other nuclear receptors, they consist of an A/B domain involved in transcriptional activation, a C domain responsible for DNA binding, a D domain that serves as a hinge, and an E domain that binds the ligands and connects with the transcriptional machinery [5]. PPARs activate DNA transcription by binding to a relatively conserved DNA sequence in the vicinity of target genes. Analogous to several other nuclear receptors, PPARs bind to DNA mostly as a heterodimer with the Retinoid X Receptor RXR. PPARs activate gene transcription by promoting the release of co-repressor proteins and by stimulating the binding of co-activator proteins, processes that are triggered by the binding of ligand to either the PPAR or RXR moiety [6]. The ligands for PPARs encompass a range of exogenous and endogenous lipids, including various fatty acids, as well as a large number of synthetic compounds. Changes in the intracellular concentration of these lipids can influence PPAR-dependent gene regulation [7].

The group of PPARs consists of three distinct subtypes that differ in their expression profile across tissues and in their ligand specificity: PPARα, PPARδ, and PPARγ. PPARα is most highly expressed in liver and, at least in mice, in brown adipose tissue. Other tissues where PPARα is present and functional include the heart, the small intestine, and the kidney [8]. In the liver, PPARα functions at the master regulator of lipid metabolism, especially during fasting, by activating processes such as fatty acid oxidation and ketogenesis, fatty acid uptake, and triglyceride metabolism and storage [9]. In this capacity, PPARα regulates the expression of numerous genes involved in nearly every aspect of hepatic lipid metabolism, including many genes encoding LD-associated proteins and lipogenic and lipolytic enzymes. Consequently, the loss of PPARα in mouse liver leads to a severe fasting-induced phenotype consisting of hypoglycemia, hypoketonemia, elevated plasma non-esterified fatty acids, and hepatic steatosis [10][11].

PPARδ (also referred to as PPARβ) is expressed in most cells and tissues, which has made the identification of the (tissue-specific) functions of PPARδ particularly challenging. PPARδ is probably best known for its role in skeletal muscle, where it mediates the effects of fatty acids on gene expression and stimulates fatty acid oxidation and oxidative capacity [12][13][14]. In addition, PPARδ has been implicated in processes such as cell differentiation and wound healing [15].

In contrast to PPARα and PPARδ , PPARγ is only expressed in a limited number of tissues, including the adipose tissue, the colon, and macrophages. Based on the clever work of Drs. Tontonoz, Spiegelman, and others, it is evident that PPARγ serves as the master regulator of adipogenesis [16][17]. Indeed, during adipocyte differentiation, activation of PPARγ is responsible for the induction of hundreds of genes involved in nearly every aspect of adipocyte function. In mice, loss of PPARγ fails to yield viable offspring [18], while in

humans, homozygosity for loss-of-function mutations in PPARγ leads to a form of lipodystrophy [19]. Induction of PPARγ in non-adipose tissues, such as liver, heart, and skeletal muscle, can promote local, ectopic fat accumulation and is an important mechanism in the pathophysiology of non-alcoholic fatty liver disease, type 2 diabetes, and other metabolic diseases.

Many reviews have been written about PPARs and about LD-associated proteins. In this review, these two topics are combined by focusing on the role of the three PPARs in the transcriptional regulation of LD-associated proteins.

Peroxisome Proliferator-Activated Receptors

Two main types of adipocytes can be distinguished: white adipocytes and brown adipocytes. More recently, a third type of adipocyte, named brite (brown in white) or beige adipocyte, has been described. Beige adipocytes are similar to white adipocytes in their basic features but acquire a brown-like phenotype during β-adrenergic stimulation, cold acclimation, or other stimuli [20]. Whereas white adipocytes are responsible for storage of excess energy, the function of brown adipocytes is to produce heat via the process of uncoupling, thereby contributing to non-shivering thermogenesis [21]. Morphologically, white adipocytes generally contain only one LD (unilocular) with an approximate diameter of 100 µm that occupies most of the cell volume [22]. In comparison, brown adipocytes contain many LD (multilocular) with a diameter from several hundred nm to about 20 µm [23]. The difference in LD morphology between white and brown adipocytes may be related to differences in the turnover rate of the stored lipids. Brown adipocytes have a higher LD surface area that facilitates access by the lipases, allowing for more efficient release of lipids. In contrast, the single LD in white adipocytes assures a maximal efficiency of lipid storage [23]. LD in white and brown adipocytes also differ in the expression level and regulation of LD-associated proteins. At the mRNA level, most members of the *Plin* family, *Cide* family, *Pnpla2, Abhd5*, and *G0s2* are more highly expressed in brown than in white adipocytes. The differences in expression is most pronounced for *Cidea* and *Plin5* [24]. By contrast, PLIN3 and PLIN4 protein appear to be more abundant in white adipose tissue (WAT), whereas the level of PLIN1 protein is comparable in white and brown adipocytes [25]. Interestingly, upon cold exposure, the gene expression level of *Cidea* and *Plin5* increases dramatically in inguinal white adipocytes, suggesting the involvement of *Cidea* and Plin5 in the browning process [26].

As indicated before, PPARγ is highly abundant in adipose tissue and serves as the master regulator of adipogenesis. By contrast, PPARα is not required for adipogenesis [27], while conflicting data have been reported on the role of PPARδ [27]. It was shown that PPARδ-/- adipocytes exhibit impaired lipid accumulation and reduced expression of adipose differentiation markers, including *Fabp4, Cd36, Plin1*, and *Plin2* [28]. Apart from these data, little is known about the regulation of LD-associated proteins by PPARδ. The expression of PPARα is much higher in brown adipose tissue (BAT) as compared to WAT. Nevertheless, loss of PPARα seems to have comparatively little effect on gene expression in BAT, including on expression of LD-associated proteins (our unpublished observation).

Several LD-associated proteins have shown to be regulated by PPARγ in adipocytes. In fact, many represent direct target genes of PPARγ, as elaborated below. Using publicly available datasets of ChIP-seq experiments performed on differentiated 3T3-L1 adipocytes, a recent study found PPARγ binding sites in the vicinity of *Plin1, Plin2, Plin4, Plin5, Abhd5, Pnpla2, G0s2, Cidea* and *Cidec*, whereas Plin3 and Cideb didn't show enrichment for PPARγ [24].

G0/G1 switch 2 (G0S2)

G0S2 is an inhibitor of PNPLA2 (adipose triglyceride lipase) [29]. Homozygous *G0s2*-/- mice are lean, resistant to diet-induced weight gain, glucose tolerant, and insulin sensitive. Lipase activity is increased in WAT of *G0s2*-/- mice. Furthermore, *G0s2*-/- mice have increased cold tolerance and expression of thermoregulatory and oxidation genes in WAT [30]. Levels of G0S2 protein increase during differentiation of human SGBS adipocytes, concurrent with an increase in PPARγ. Transactivation, gel shift, and chromatin immunoprecipitation assays have confirmed that *G0s2* is a direct PPARγ target. A functional PPAR response element was identified in the *G0s2* promoter at approximately 1500 nucleotides upstream of the transcriptional start site [31].

Perilipin 1 and 4 (PLIN1 and PLIN4)

Plin1 and *Plin4* are expressed at high levels in murine WAT. *Plin1*-/- mice are lipodystrophic, as shown by markedly reduced body fat. Moreover, the mice have increased basal lipolysis, ectopic lipid accumulation in cardiomyocytes, cardiac hypertrophy, and heart failure [32]. By contrast, inactivation of *Plin4* does not affect body weight or adipose mass. Furthermore, inactivation of *Plin4* has no effect on adipose tissue differentiation nor growth in vivo [33]. Both *Plin1* and *Plin4* were identified as PPARγ target by transactivation and gel shift assays. Their promoters contain three and one conserved PPAR response elements, respectively.

The expression of *Plin4* and *Plin1* in adipocytes is highly correlated to the expression and activation of PPARγ [34] [35].

Perilipin 2 (PLIN2)

PLIN2, also known as adipose differentiation related protein or adipophilin, is associated with the surface of LD. *Plin2* was originally identified by screening for genes that are upregulated during adipocyte differentiation [36]. Expression of *Plin2* increases during 3T3-L1 adipocyte differentiation in parallel with PPARγ. In addition, *Plin2* mRNA is upregulated in WAT of mice treated with rosiglitazone for 7 days [37]. These data indicate that *Plin2* is probably a target gene of PPARγ in adipocytes.

Perilipin 5 (PLIN5)

Basal *Plin5* expression in WAT is relatively low. Expression of *Plin5* in mouse WAT was found to be induced by the PPARγ agonist rosiglitazone, together with gene markers of fatty acid oxidation, oxidative phosphorylation, and the TCA cycle. Accordingly, induction of *Plin5* by PPARγ likely reflects increased browning. Whether *Plin5* is a direct target of PPARγ during browning is likely although formal proof is missing [25][38]. In support of direct regulation of PLIN5 by PPARs in human adipocytes, treatment of human MADS adipocytes with PPARγ and PPARα agonists was found to increase PLIN5 protein levels [39].

Cell death-inducing DFFA-like effector c (CIDEC)

Cidec (also referred to as FSP27) is expressed at high levels in both WAT and BAT. Loss of *Cidec* in cultured white adipocytes leads to the formation of multilocular lipid droplets, increased lipolysis, and decreased triglyceride storage, while overexpression of *Cidec* in COS cells increases lipid droplet size [40][41]. Consistent with these findings, *Cidec*-/- mice exhibit multilocular lipid droplets in white adipocytes. Moreover, *Cidec*-/- mice are protected from diet-induced obesity and insulin resistance and have an increased metabolic rate, probably due to elevated mitochondrial biogenesis in WAT. Expression of *Cidec* mRNA in adipocytes was found to go up upon treatment with PPARγ agonists and markedly go down upon silencing of PPARγ [40][42][43]. Chromatin immunoprecipitation assay, gel shift, and transactivation assay confirmed the binding of PPARγ2 to the promoter of *Cidec* about 200 nucleotides upstream of the transcriptional start site, indicating that *Cidec* is a direct PPARγ target gene [42]. Silencing of PPARγ in adipocytes also led to reduced expression of *Cidea*, suggesting *Cidea* is a transcriptional target of PPARγ as well [40].

Hypoxia inducible lipid droplet associated (HILPDA)

HILPDA, also referred to as HIG-2, is a recently identified LD-associated protein that was suggested to be involved in the regulation of lipolysis [44][45][46]. Silencing of *Hilpda* in adipocytes did not significantly alter the release of non-esterified fatty acids. In addition, adipocyte-specific *Hilpda*-/- animals displayed no detectable changes in adipocyte lipolysis after various physiological or pharmacological stimuli [47][48]. Interestingly, adipocyte-specific *Hilpda*-/- mice showed a reduction in epididymal fat pad weight and improved glucose tolerance after high fat feeding, which could be ascribed to brown/beige adipocyte-specific *Hilpda* deficiency [48].

HILPDA is among the 20 most significantly upregulated genes by rosiglitazone in differentiated human SGBS and MADS adipocytes. Rosiglitazone also markedly induces *Hilpda* mRNA and protein in mature 3T3-L1 adipocytes. In both mouse and human adipocytes, a prominent PPARγ superenhancer is located near the *HILPDA* gene containing several conserved PPARγ binding sites. These collective data suggest that *HILPDA* is a direct target of PPARγ in murine and human adipocytes.

Liver

The liver contains several cell types, with most of the liver mass consisting of hepatocytes. Fatty acids in the liver can originate from several different sources: they can be supplied by the diet in the fed state, they can be produced via *de novo lipogenesis* from glucose, or they can be derived from the adipose tissue and enter the liver as free fatty acids. After synthesis or uptake, fatty acids can be esterified into triglycerides and secreted as part of very low-density lipoprotein or stored in LD in hepatocytes. Next to adipose tissue, the liver has the second greatest capacity to store lipids. The size of the LD in hepatocytes can range from a diameter of less than 1 µm to 10 µm in case of steatosis [49][22][50]. The LD in hepatocytes can be further classified by their location and protein composition into cytosolic LD, apoB-free LD in the lumen of the endoplasmic reticulum (ER), and the apoB-containing LD (VLDL) [51].

All three PPARs are expressed in the liver. PPARα is the master regulator of lipid metabolism in the liver during fasting [9]. PPARα-/- mice have enhanced steatosis and enlarged LD, especially during fasting [10]. Heatmaps generated from publicly available microarray datasets reveal a PPARα-dependent regulation of several LD-associated proteins during fasting in mouse liver, and upon treatment with the PPARα agonist Wy-14,643 in mouse liver and primary mouse hepatocytes (Fig. 1). Recent data from hepatocyte-specific

PPARα-/- mice further support the regulation of several LD-associated proteins by PPARα in mouse hepatocytes, including *Cidec, G0s2, Fitm1, Fitm2*, and *Plin5* [52]. PPARδ in the liver has been connected with a number of biological functions, including regulation of lipoprotein metabolism and various pathways related to glucose utilization, but the role of PPARδ in liver is still not fully clear [53]. PPARγ is known to exist in two isoforms, PPARγ1 and PPARγ2, but only PPARγ1 is expressed in liver. Feeding mice a high fat diet leads to induction of liver PPARγ [54][55], which in turn causes the upregulation of genes involved in lipogenesis, thus contributing to hepatic steatosis. Consistent with this notion, liver specific PPARγ-/- mice have reduced hepatic steatosis on a leptin-deficient and lipoatrophic background [54][56], whereas mice overexpressing PPARγ1 in liver have enhanced steatosis [57]. Treatment of liver slices and primary hepatocytes with the PPARγ agonist rosiglitazone alone or in combination with oleic acid increased triglyceride accumulation, which was abolished in liver slices and primary hepatocytes from liver-specific PPARγ-/- mice [58]. It should be noted, however, that PPARγ mRNA expression does not seem to be elevated in human steatosis or non-alcoholic steatohepatitis ([59], our unpublished observations).

Cell death-inducing DFFA-like effector a (CIDEA)

Overexpression of *Cidea* in mice increases hepatic lipid accumulation and leads to larger LD, whereas *Cidea*-/- mice have decreased lipid accumulation, smaller LD, and reduced hepatic steatosis under conditions of high fat feeding or an ob/ob background [60]. It has been shown that *Cidea* is highly expressed in fatty liver of ob/ob mice and that its expression is markedly lowered by loss of PPARγ [61]. Consistent with these data, adenoviral-mediated overexpression of PPARγ1 in mouse liver causes a massive increase in *Cidea* expression [62]. Furthermore, adenoviral-mediated overexpression of PPARγ in primary mouse hepatocytes upregulates *Cidea* expression [62]. With respect to a potential role of PPARα, activation of PPARα using Wy-14,643 causes a massive increase in *Cidea* mRNA, which is completely abolished in PPARα-/- mice [62]. Molecular experiments subsequently demonstrated that *Cidea* is a direct PPARγ and PPARα target gene in liver, as shown by transactivation, gel-shift, and chromatin immunoprecipitation assays [62].

Cell death-inducing DFFA-like effector c (CIDEC)

Cidec is highly expressed in adipose tissue but undetectable in normal liver. Its hepatic expression in mice is increased by fasting and under conditions of hepatic steatosis [63]. There is also evidence that CIDEC expression may be increased in human steatosis. Adenoviral-mediated overexpression of *Cidec* in hepatocytes in vitro or in vivo leads to elevated liver triglyceride levels, whereas knockdown of *Cidec* by adenoviral shRNA has the

opposite effect. Evidence abounds indicating that *Cidec* is a direct target of PPARα and PPARγ in mouse and human liver. Adenoviral-mediated overexpression of PPARγ1 in PPARα-/- mice induced hepatic steatosis and greatly increased expression of *Cidec* [57]. Also, rosiglitazone treatment markedly upregulated the expression of *Cidec* in livers of ob/ob mice, which was abolished in ob/ob mice with liver-specific PPARγ deletion. Importantly, treatment of non-obese mice with rosiglitazone failed to induce hepatic Cidec expression [61]. In agreement with these data, *Cidec* was identified as a direct target gene of PPARγ by gel shift assay and chromatin immunoprecipation. The PPAR response element was located about 200 nucleotides upstream of the transcriptional start site [61].

As indicated above, expression of *Cidec* is increased by fasting. In contrast to many other genes involved in lipid metabolism, this increase does not seem to be mediated by PPARα. Interestingly, adenoviral-mediated silencing of hepatic *Cidec* attenuated the induction of liver steatosis by fasting. Interestingly, *Cidec* is highly induced by synthetic PPARα agonists in primary mouse hepatocytes and in mouse liver in a PPARα-dependent manner, as well as in primary human hepatocytes [52][64] [65]. *Cidec* was confirmed as a direct target of PPARα by transactivation assay and chromatin immuno-precipitation using extracts from mouse primary hepatocytes [64]. Recently, an alternative *Cidec* isoform was identified referred to as FSP27β. Fsp27β does not appear to be regulated by PPARs but rather by the transcription factor cyclic-AMP-responsive-element-binding protein H (CREBH, CREB3L3) [66].

Cell death-inducing DFFA-like effector b (CIDEB)

Cideb is expressed at high levels in liver, intestine, and kidney [67][68][69]. CIDEB is an important regulator of lipid and cholesterol homeostasis in the liver. *Cideb-/-* mice exhibit lower levels of plasma cholesterol and LDL when fed with either a normal diet or a high cholesterol diet, concurrent with lower rates of cholesterol biosynthesis in liver and reduced expression levels of sterol response element-binding protein 2 and its downstream target genes [70]. Currently, there is no evidence that *Cideb* is under transcriptional control of PPARα.

Hypoxia inducible lipid droplet associated (HILPDA)

HILPDA is a LD-associated protein that is involved in lipid metabolism. Overexpression of *Hilpda* in mice via adeno-associated virus increases liver triglyceride levels and reduces hepatic triglyceride secretion. *Hilpda* was found to be induced in mouse precision cut liver slices treated with the PPARα agonist Wy-14,643. Similarly, oral dosing of Wy-14.643

markedly induced *Hilpda* mRNA and HILDPA protein levels in livers of wild-type mice but not PPARα-/- mice. *Hilpda* regulation by PPARα was further confirmed by transactivation and chromatin immunoprecipitation assays, indicating that *Hilpda* is a direct PPARα target in liver [71].

G0/G1 switch 2 (G0S2)

G0s2 was identified as a putative target gene of PPARα by comparing liver mRNAs of wild-type and PPARα-/- mice using microarrays. Hepatic expression of G0s2 is up-regulated by fasting and by the PPARα agonist Wy-14,643 and fenofibrate in a PPARα-dependent manner [31] [52]. Wy-14,643 also markedly induces G0s2 mRNA in primary mouse hepatocytes [31]. Transactivation, gel shift and chromatin immunoprecipitation assays indicated that G0s2 is a direct PPAR target gene with a functional PPRE in its promoter [31][72][29]. Intriguingly, the expression of G0s2 in liver is elevated in PPARα-/- mice compared to wildtype mice in the fed state, suggesting the involvement of other regulatory mechanisms. Recently, a role of LXR in the regulation of hepatic G0s2 expression was proposed [73].

Perilipin 2 (PLIN2)

Plin2 is expressed at high levels in mouse and human liver. The abundance of PLIN2 is related to the amount of lipid found within cells [74]. Plin2 is a direct target of PPARα and possibly PPARγ in mouse liver. Expression of Plin2 mRNA in mouse liver is markedly induced by synthetic PPARα agonists in a PPARα-dependent manner. Plin2 mRNA is also induced in mouse liver during fasting. However, this increase is independent of PPARα. Transactivation and gel shift assays showed that Plin2 is a direct target of PPARα via a PPAR response element that is conserved between mice and humans [75][76]. In line with these data, expression of PLIN2 is upregulated by synthetic PPARα agonist in human hepatoma cells, human primary hepatocytes, and human precision cut liver slices [75][76][77][78]. Interestingly, although overexpression of PPARγ2 increased the protein level of PLIN2—concurrent with enhanced lipid accumulation—no induction of Plin2 mRNA was observed, suggesting that Plin2 is not a direct target of PPARγ in the liver [79].

Perilipin 5 (PLIN5)

PLIN5, also known as LSDA5, LSDP5, MLDP, OXPAT, is highly abundant in oxidative tissues, including liver. Overexpression of *Plin5* in vitro promotes fatty acid–induced triglyceride accumulation, fatty acid oxidation, and mRNAs associated with oxidative metabolism. By contrast, adenoviral-mediated *Plin5* knockdown in AML12 cells and in primary mouse

hepatocytes decreased the triglyceride content of LD, stimulated lipolysis, and increased the mitochondrial content and fatty-acid β-oxidation [25][80][81]. Similarly, Plin5-/- mice are characterized by reduced hepatic lipid content, smaller-sized LD, and increased mitochondrial proliferation, yet enhanced lipotoxic injury [82]. Expression of *Plin5* mRNA and PLIN5 protein in mouse liver is markedly induced by synthetic PPARα agonists in a PPARα-dependent manner [83]. *Plin5* mRNA is also induced in mouse liver during fasting, yet this induction is only partially abolished in PPARα-/-mice [84]. In contrast to PLIN2, there is no evidence that PLIN5 is regulated by PPARα in human liver.

Perilipin 1 (PLIN1)

PLIN1 is a marker of adipocyte differentiation and normally absent from liver [85][25]. However, it has been reported that hepatic *Plin1* expression goes up under conditions of chronic steatosis. *PLIN1* mRNA became detectable in hepatic HuH7 cells after chronic treatment with a preadipocyte-adipocyte differentiation medium. Treatment of adipogenic HuH7 cells with PPARα and γ antagonists showed a clear reduction of *PLIN1* protein with PPARα but not with PPARγ antagonist [86]. Overall, more research is needed to better understand the regulation of *Plin1* by PPARs in adipogenic/steatotic hepatocytes.

Perilipin 4 (PLIN4)

Plin4 is very weakly expressed in liver under normal conditions [25] [34]. However, *Plin4* can be induced in hepatocytes upon PPARγ1 overexpression, indicating that *Plin4* may play a role in adipogenic transformation of hepatocytes [57]. Furthermore, *Plin4* expression is also induced by PPARα activation in mouse liver. More research is needed to unravel the potential role and regulation of *Plin4* in the liver.

Fat storage-inducing transmembrane protein 1 and 2 (FITM1, FITM2)

FITM1 and FITM2 do not have homology to known proteins or protein domains found in any species, indicating that FITM genes comprise a unique gene family. They were identified by screening for novel genes that are regulated by PPARα using liver tissue from mice treated with the PPARα agonist fenofibrate [87]. Adenoviral-mediated overexpression of *Fitm2* in mice increased liver triglycerides and LD. The pattern of regulation of *Fitm1* and *Fitm2* as shown in figure 1 and in hepatocyte-specific PPARα -/- mice indicates that *Fitm1* and *Fitm2* likely represent direct PPARα target genes [52].

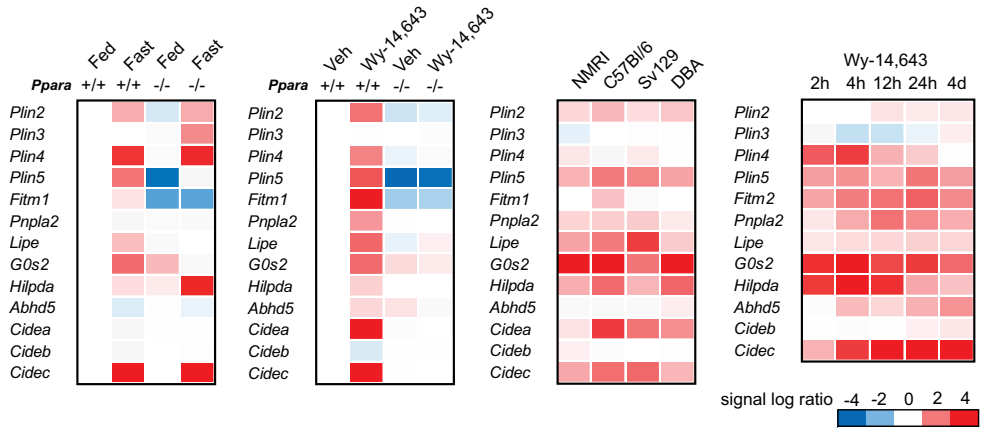

Figure 1: Heatmap of regulation of LD-associated proteins by PPARs in liver. The heatmaps were generated based on publicly available microarray datasets. GSE17863: livers of wildtype and PPARα-/- mice subjected to 24h of fasting; GSE8295: livers of wildtype and PPARα-/- mice treated with Wy-14,643 for 5 days; GSE17250: primary mouse hepatocytes treated with Wy-14,643 for 24h; GSE47844: livers of wildtype mice treated with Wy-14,643 for different duration.

Macrophages

In macrophages, the lowest expressing PPAR is PPARα. Despite its relatively low expression, PPARα activation has been shown to reduce foam cell formation in vitro, possibly by stimulating cholesterol efflux [88][89]. In addition, PPARα activation has been shown to have an anti-inflammatory effect. Both *Pparδ* and *Pparγ* are expressed at high levels in macrophages. Many studies have examined the role of PPARδ and PPARγ in macrophage function and in particular in the inflammatory properties of macrophages. Overall, macrophage PPARδ is involved in the regulation of lipid metabolism, inflammation, and the phagocytosis of apoptotic cells. An excellent overview of the role of PPARδ in macrophages is presented in a recent review by Staels and colleagues [90]. Inasmuch as both the genetic deletion of PPARδ and the activation of PPARδ using synthetic agonists have anti-inflammatory effects, the role of macrophage PPARδ in inflammation remains somewhat ambiguous [90].

Many of the functional properties of PPARδ in macrophages have also been assigned to PPARγ, including the regulation of inflammation and lipid metabolism. The expression of *Pparγ* increases markedly during the differentiation of monocytes into macrophages. However, unlike in adipocytes, PPARγ is dispensable for macrophage differentiation [91][92]. In differentiated macrophages, PPARγ has been demonstrated to repress

inflammatory gene expression by interfering with the action of other transcription factors such as NF-κB, a process known as transrepression. PPARγ has also been suggested to steer macrophages towards an anti-inflammatory, alternatively activated M2 phenotype [93].

A number of LD-associated proteins and enzymes are known to be present in macrophages, including PLIN2, PLIN3 and PNPLA2. A number of other LD-associated protein have low expression at baseline but may be induced in response to lipid uptake and foam cell formation. Wang and colleagues found that expression of PLIN2 in human monocyte-derived macrophages is induced by oxLDL, which is known to activate PPARs [94]. Similarly, Li and colleagues found that conversion of THP-1 macrophages into foam cells by oxLDL is accompanied by increased expression of *Cideb, Cidec, Plin2, Plin3*, and *Plin5*, whereas *Plin4* is down-regulated [95]. Similar to its role in other cell types, PLIN2 promotes lipid droplet formation in isolated macrophages upon incubation with oxLDL, and in vivo in atherosclerosis-prone *Apoe*-/- mice [96][97].

With respect to regulation of PLIN2 by fatty acids, it was shown that that very low density lipoproteins, and to a lesser extent LDL and aggregated LDL, markedly increase *PLIN2* protein levels in differentiated primary human monocytes [98]. Furthermore, total lipoprotein hydrolysis products generated by lipoprotein lipase markedly increased *PLIN2* expression in THP-1 macrophages [99]. In line with these data, triglyceride-rich lipoproteins induced levels of PLIN2 and PLIN3 proteins in mouse bone marrow-derived and human THP-1 macrophages in a fatty-acid-dependent manner [100]. Antagonists for PPARα and PPARγ abolished the stimulatory effect of triglyceride-rich lipoproteins, suggesting that the induction of PLIN2 and PLIN3 is mediated by PPARα and PPARγ.

In support of direct regulation of *Plin2* by PPARs, treatment of RAW 264.7 mouse macrophages with natural and synthetic agonists of PPARγ upregulated *Plin2* mRNA, suggesting *Plin2* is a target of PPARγ in macrophages [101]. Furthermore, activation of PPARδ using synthetic agonist promotes lipid accumulation in primary human macrophages and THP-1 macrophages, concomitant with induction of *CD36* and *PLIN2* mRNA, suggesting a possible role of these genes in PPARδ -induced lipid accumulation [102]. Lee and colleagues observed that activation of PPARδ using a synthetic agonist or triglyceride-rich lipoproteins increased PLIN2 protein levels in peritoneal macrophages, which was abolished in PPARδ -/- macrophages. A similar but smaller effect was observed for PNPLA2 [103]. In our hands we see strong induction of *Plin2* mRNA in RAW 264.7 and THP-1 macrophages by PPARδ activation, and to a lesser extent by PPARγ activation (our unpublished data).

Skeletal muscle

All three PPAR subtypes are expressed in skeletal muscle. The relative abundance of the PPAR subtypes depends on the species and on the type of muscle material. While *PPARδ* is the most abundant PPAR subtype in primary human myocytes, mouse skeletal muscle and mouse C2C12 myotubes, *PPARα* is the most abundant PPAR subtype in human muscle biopsies. Little is known about the role of PPARα in skeletal muscle. Studies in mice lacking PPARα have provided evidence for a functional redundancy between muscle PPARα and PPARδ [104]. Transcriptomics analysis of human subjects treated with fenofibrate showed relatively minor changes in muscle gene expression (our unpublished observations).

The role of PPARδ in muscle has been more extensively investigated, showing that PPARδ is an important regulator of lipid metabolism in mouse muscle [105]. Specifically, muscle-specific overexpression of PPARδ in mice leads to a shift in muscle fiber characteristic toward more oxidative fibers and an increase in the oxidative capacity of skeletal muscle [12]. Through this mechanism, PPARδ causes the sparing of glucose and promotes endurance capacity in mice [13][14].

Muscle fibers are full of LD [106]. LD can be found adjacent to mitochondria and are concentrated in the subsarcolemmal region near the plasma membrane or in-between the myofibril. Studies have shown that the intramyocellular LD are enlarged in endurance athletes and likely represent an important fuel during endurance exercise [107]. As observed in other cell types, the LD in myocytes are surrounded by a set of LD proteins. All members of the perilipin family are known to be expressed in skeletal muscle, except for PLIN1. Other LD-associated proteins that are well expressed in skeletal muscle or in cultured myocytes include FITM1, FITM2, G0S2, and PNPLA2.

Protein and mRNA levels of PLIN2 in C2C12 myotubes were found to be markedly induced by oleic acid and other fatty acids [108][109][110]. Agonists for PPARα, PPARδ, and PPARγ similarly induced PLIN2 protein in C2C12 cells [109]. Analysis of transcriptomics datasets showed that PLIN2 is induced by the synthetic PPARδ agonist GW501516 in human primary myocytes [111], and in mouse skeletal muscle [13]. Apart from PLIN2, two other LD-associated proteins that may be regulated by PPARs in muscle are PLIN4 and PLIN5. Both genes were induced by PPARα, PPARδ, and/or PPARγ agonists in C2C12 myotubes. Induction of PLIN5 by PPARδ agonist was confirmed at the protein level [110]. Silencing of PPARδ in C2C12 myotubes attenuated the induction of *Plin4* and *Plin5* mRNA by fatty acids. Treatment of mice with PPARδ agonist hints at a positive effect on PLIN5 mRNA and protein in skeletal muscle. Nevertheless, PLIN5 protein levels in skeletal muscle do no seems to be altered in PPARδ-/- mice. Reporter studies have provided evidence that *Plin5* is a direct PPARδ target gene in muscle cells [110]. Finally, treatment of human primary myocytes with

PPARδ agonist was shown to markedly increase PLIN5 mRNA [112]. In heart, *Plin5* was found to be upregulated by the PPARα agonist Wy-14,643 in wildtype but not PPARα-/- mice [83]. Intriguingly, PLIN5 may in turn influence PPARα-dependent gene regulation. Specifically, it was observed that overexpression of *Plin5* in rat skeletal muscle via electroporation caused an increase in the expression of a cluster of genes under control of PPARα involved in fatty acid catabolism and mitochondrial oxidation [113]. The mechanism underlying the observed induction of PPARα activity by Plin5 overexpression is unclear but might be related to enhanced lipolysis. Activation of PPARα may explain the marked induction of muscle *Fgf21* expression and plasma FGF21 levels in mice overexpression Plin5 in skeletal muscle [114].

So far there is no evidence that any of the other LD-associated proteins are regulated by PPARs in skeletal muscle.

Concluding remarks

It is concluded that many LD-associated proteins, including members of the PLIN family, CIDEC, CIDEA, HILPDA, FITM1, FITM2, G0S2 are under direct transcriptional control of PPARs (Figure 2). Activation of lipid-droplet-associated proteins by PPARs provides a mechanism to link uptake of lipids to regulation of lipid storage capacity.

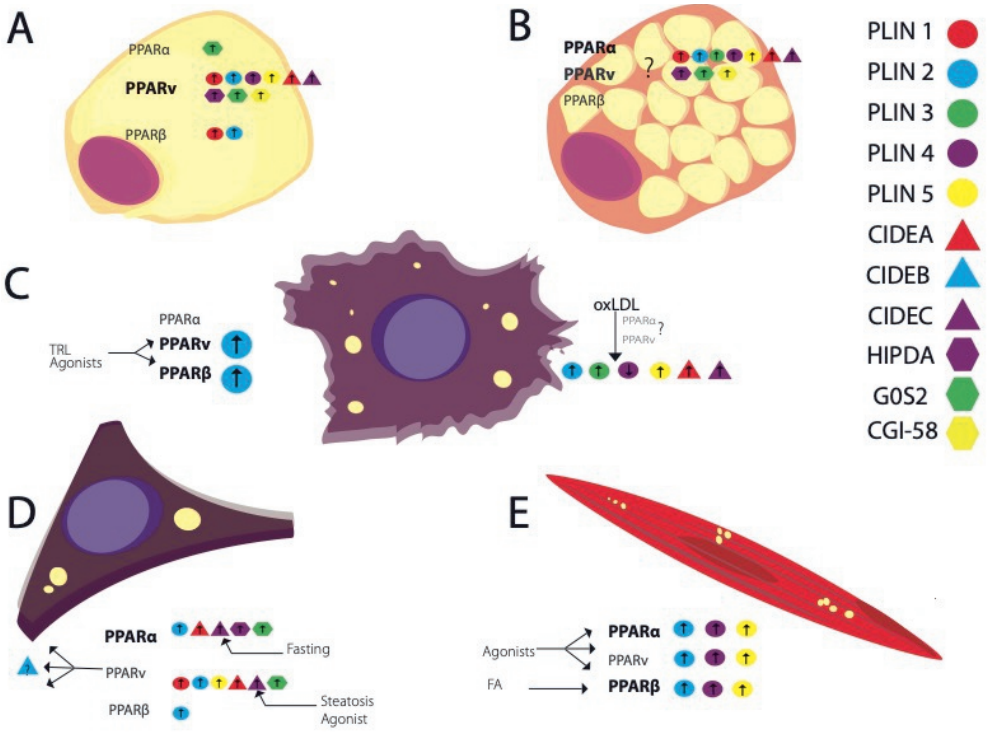

Figure 2: Overview of regulation of lipid droplet-associated proteins by PPARs. The picture illustrates the important role of PPARs in the transcriptional regulation of LD-associated proteins in several tissues. A particular LD-associated protein is shown if there is strong evidence that supports regulation of the corresponding gene by the indicated PPAR subtype. The font size of the PPAR subtypes provides a crude reflection of their relative expression in that particular tissue. Although few data are available on the regulation of LD-associated proteins by PPARs in BAT, it is expected that PPARs play an important role.

References

[1] D.A. Gross, D.L. Silver, Cytosolic lipid droplets: From mechanisms of fat storage to disease, Crit. Rev. Biochem. Mol. Biol. 49 (2014) 304–326. doi:10.3109/10409238.2014.931337.

[2] A.S. Greenberg, R.A. Coleman, F.B. Kraemer, J.L. McManaman, M.S. Obin, V. Puri, Q.-W. Yan, H. Miyoshi, D.G. Mashek, The role of lipid droplets in metabolic disease in rodents and humans., J. Clin. Invest. 121 (2011) 2102–10. doi:10.1172/JCI46069.

[3] H. Itabe, T. Yamaguchi, S. Nimura, N. Sasabe, Perilipins: a diversity of intracellular lipid droplet proteins., Lipids Health Dis. 16 (2017) 83. doi:10.1186/s12944-017-0473-y.

[4] T. Varga, Z. Czimmerer, L. Nagy, PPARs are a unique set of fatty acid regulated transcription factors controlling both lipid metabolism and inflammation., Biochim. Biophys. Acta. 1812 (2011) 1007–22. doi:10.1016/j.bbadis.2011.02.014.

[5] D.J. Mangelsdorf, C. Thummel, M. Beato, P. Herrlich, G. Schütz, K. Umesono, B. Blumberg, P. Kastner, M. Mark, P. Chambon, R.M. Evans, The nuclear receptor superfamily: The second decade, Cell. 83 (1995) 835–839. doi:10.1016/0092-8674(95)90199-X.

[6] B. Desvergne, W. Wahli, Peroxisome Proliferator-Activated Receptors: Nuclear Control of Metabolism 1, Endocr. Rev. 20 (1999) 649–688. doi:10.1210/edrv.20.5.0380.

[7] A. Georgiadi, S. Kersten, Mechanisms of gene regulation by fatty acids., Adv. Nutr. 3 (2012) 127–34. doi:10.3945/an.111.001602.

[8] S. Mandard, M. Muller, S. Kersten, Peroxisome proliferator-activated receptor a target genes, Cell. Mol. Life Sci. 61 (2004) 393–416. doi:10.1007/s00018-003-3216-3.

[9] S. Kersten, Integrated physiology and systems biology of PPARα, Mol. Metab. 3 (2014) 354–371. doi:10.1016/j.molmet.2014.02.002.

[10] S. Kersten, J. Seydoux, J.M. Peters, F.J. Gonzalez, B. Desvergne, W. Wahli, Peroxisome proliferator-activated receptor alpha mediates the adaptive response to fasting., J. Clin. Invest. 103 (1999) 1489–98. doi:10.1172/JCI6223.

[11] T.C. Leone, C.J. Weinheimer, D.P. Kelly, A critical role for the peroxisome proliferator-activated receptor (PPAR) in the cellular fasting response: The PPAR -null mouse as a model of fatty acid oxidation disorders, Proc. Natl. Acad. Sci. 96 (1999) 7473–7478. doi:10.1073/pnas.96.13.7473.

[12] S. Luquet, J. Lopez-Soriano, D. Holst, A. Fredenrich, J. Melki, M. Rassoulzadegan, P.A. Grimaldi, Peroxisome proliferator-activated receptor δ controls muscle development and oxydative capability, FASEB J. 17 (2003) 2299–301. doi:10.1096/fj.03-0269fje.

[13] V.A. Narkar, M. Downes, R.T. Yu, E. Embler, Y.-X. Wang, E. Banayo, M.M. Mihaylova, M.C. Nelson, Y. Zou, H. Juguilon, H. Kang, R.J. Shaw, R.M. Evans, AMPK and PPARδ Agonists Are Exercise Mimetics, Cell. 134 (2008) 405–415. doi:10.1016/j.cell.2008.06.051.

[14] W. Fan, W. Waizenegger, C.S. Lin, V. Sorrentino, M.-X. He, C.E. Wall, H. Li, C. Liddle, R.T. Yu, A.R. Atkins, J. Auwerx, M. Downes, R.M. Evans, PPARδ Promotes Running Endurance by Preserving Glucose, Cell Metab. 25 (2017) 1186–1193.e4. doi:10.1016/j.cmet.2017.04.006.

[15] N.S. Tan, M. Vázquez-Carrera, A. Montagner, M.K. Sng, H. Guillou, W. Wahli, Transcriptional control of physiological and pathological processes by the nuclear receptor PPARβ/δ, Prog. Lipid Res. 64 (2016) 98–122. doi:10.1016/j.plipres.2016.09.001.

[16] R.A. Graves, P. Tontonoz, B.M. Spiegelman, Analysis of a tissue-specific enhancer: ARF6 regulates adipogenic gene expression., Mol. Cell. Biol. 12 (1992) 1202–8. doi:10.1101/gad.8.10.1224.

[17] P. Tontonoz, E. Hu, B.M. Spiegelman, Stimulation of adipogenesis in fibroblasts by PPARγ2, a lipid-activated transcription factor, Cell. 79 (1994) 1147–1156. doi:10.1016/0092-8674(94)90006-X.

[18] Y. Barak, M.C. Nelson, E.S. Ong, Y.Z. Jones, P. Ruiz-Lozano, K.R. Chien, A. Koder, R.M. Evans, PPARγ Is Required for Placental, Cardiac, and Adipose Tissue Development, Mol. Cell. 4 (1999) 585–595. doi:10.1016/S1097-2765(00)80209-9.

[19] E.H. Jeninga, M. Gurnell, E. Kalkhoven, Functional implications of genetic variation in human PPARγ, Trends Endocrinol. Metab. 20 (2009) 380–387. doi:10.1016/j.tem.2009.04.005.

[20] K.A. Lo, L. Sun, Turning WAT into BAT: a review on regulators controlling the browning of white adipocytes., Biosci. Rep. 33 (2013). doi:10.1042/BSR20130046.

[21] E.D. Rosen, B.M. Spiegelman, Adipocytes as regulators of energy balance and glucose homeostasis, Nature. 444 (2006) 847–853. doi:10.1038/nature05483.

[22] M. Suzuki, Y. Shinohara, Y. Ohsaki, T. Fujimoto, Lipid droplets : size matters, (n.d.). doi:10.1093/jmicro/dfr016.

[23] J. Yu, S. Zhang, L. Cui, W. Wang, H. Na, X. Zhu, L. Li, G. Xu, F. Yang, M. Christian, P. Liu, Lipid droplet remodeling and interaction with mitochondria in mouse brown adipose tissue during cold treatment, Biochim. Biophys. Acta - Mol. Cell Res. 1853 (2015) 918–928. doi:10.1016/j.bbamcr.2015.01.020.

[24] M. Christian, Nuclear receptor-mediated regulation of lipid droplet-associated protein gene expression in adipose tissue, Horm. Mol. Biol. Clin. Investig. 14 (2013) 87. doi:10.1515/hmbci-2013-0028.

[25] N.E. Wolins, B.K. Quaynor, J.R. Skinner, A. Tzekov, M.A. Croce, M.C. Gropler, V. Varma, A. Yao-Borengasser, N. Rasouli, P.A. Kern, B.N. Finck, P.E. Bickel, OXPAT/PAT-1 Is a PPAR-Induced Lipid Droplet Protein That Promotes Fatty Acid Utilization, Diabetes. 55 (2006) 3418–3428. doi:10.2337/db06-0399.

[26] D. Barneda, A. Frontini, S. Cinti, M. Christian, Dynamic changes in lipid droplet-associated proteins in the “browning” of white adipose tissues, Biochim. Biophys. Acta - Mol. Cell Biol. Lipids. 1831 (2013) 924–933. doi:10.1016/j.bbalip.2013.01.015.

[27] R.P. Brun, P. Tontonoz, B.M. Forman, R. Ellis, J. Chen, R.M. Evans, B.M. Spiegelman, Differential activation of adipogenesis by multiple PPAR isoforms., Genes Dev. 10 (1996) 974–84. doi:10.1101/GAD.10.8.974.

[28] K. Matsusue, J.M. Peters, F.J. Gonzalez, PPAR / potentiates PPAR -stimulated adipocyte differentiation, FASEB J. 18 (2004) 1477–9. doi:10.1096/fj.04-1944fje.

[29] X. Yang, X. Lu, M. Lombès, G.B. Rha, Y.-I. Chi, T.M. Guerin, E.J. Smart, J. Liu, The G(0)/G(1) switch gene 2 regulates adipose lipolysis through association with adipose triglyceride lipase., Cell Metab. 11 (2010) 194–205. doi:10.1016/j.cmet.2010.02.003.

[30] W. El-Assaad, K. El-Kouhen, A.H. Mohammad, J. Yang, M. Morita, I. Gamache, O. Mamer, D. Avizonis, N. Hermance, S. Kersten, M.L. Tremblay, M.A. Kelliher, J.G. Teodoro, Deletion of the gene encoding G0/G1 switch protein 2 (G0s2) alleviates high-fat-diet-induced weight gain and insulin resistance, and promotes browning of white adipose tissue in mice, Diabetologia. 58 (2015) 149–157. doi:10.1007/s00125-014-3429-z.

[31] F. Zandbergen, S. Mandard, P. Escher, N.S. Tan, D. Patsouris, T. Jatkoe, S. Rojas-Caro, S. Madore, W. Wahli, S. Tafuri, M. Müller, S. Kersten, The G0/G1 switch gene 2 is a novel PPAR target gene., Biochem. J. 392 (2005) 313–24. doi:10.1042/BJ20050636.

[32] S. Liu, B. Geng, L. Zou, S. Wei, W. Wang, J. Deng, C. Xu, X. Zhao, Y. Lyu, X. Su, G. Xu, Development of hypertrophic cardiomyopathy in perilipin-1 null mice with adipose tissue dysfunction, Cardiovasc. Res. 105 (2015) 20–30. doi:10.1093/cvr/cvu214.

[33] W. Chen, B. Chang, X. Wu, L. Li, M. Sleeman, L. Chan, Inactivation of Plin4 downregulates Plin5 and reduces cardiac lipid accumulation in mice., Am. J. Physiol. Endocrinol. Metab. 304 (2013) E770-9. doi:10.1152/ajpendo.00523.2012.

[34] K.T. Dalen, K. Schoonjans, S.M. Ulven, M.S. Weedon-Fekjaer, T.G. Bentzen, H. Koutnikova, J. Auwerx, H.I. Nebb, Adipose Tissue Expression of the Lipid Droplet–Associating Proteins S3-12 and Perilipin Is Controlled by Peroxisome Proliferator–Activated Receptor-γ, Diabetes. 53 (2004). doi:10.2337/diabetes.53.5.1243.

[35] N. Arimura, T. Horiba, M. Imagawa, M. Shimizu, R. Sato, The peroxisome proliferator-activated receptor gamma regulates expression of the perilipin gene in adipocytes., J. Biol. Chem. 279 (2004) 10070–6. doi:10.1074/jbc.M308522200.

[36] H.P. Jiang, G. Serrero, Isolation and characterization of a full-length cDNA coding for an adipose differentiation-related protein., Proc. Natl. Acad. Sci. U. S. A. 89 (1992) 7856–60. doi:10.1073/pnas.89.17.7856.

[37] R. Stienstra, C. Duval, S. Keshtkar, J. van der Laak, S. Kersten, M. Müller, Peroxisome proliferator-activated receptor gamma activation promotes infiltration of alternatively activated macrophages into adipose tissue., J. Biol. Chem. 283 (2008) 22620–7. doi:10.1074/jbc.M710314200.

[38] Y. Takahashi, A. Shinoda, J. Inoue, R. Sato, The gene expression of the myocardial lipid droplet protein is highly regulated by PPARγ in adipocytes differentiated from MEFs or SVCs, Biochem. Biophys. Res. Commun. 399 (2010) 209–214. doi:10.1016/j.bbrc.2010.07.056.

[39] V. Barquissau, D. Beuzelin, D.F. Pisani, G.E. Beranger, A. Mairal, A. Montagner, B. Roussel, G. Tavernier, M.-A. Marques, C. Moro, H. Guillou, E.-Z. Amri, D. Langin, White-to-brite conversion in human adipocytes promotes metabolic reprogramming towards fatty acid anabolic and catabolic pathways., Mol. Metab. 5 (2016) 352–65. doi:10.1016/j.molmet.2016.03.002.

[40] V. Puri, S. Konda, S. Ranjit, M. Aouadi, A. Chawla, M. Chouinard, A. Chakladar, M.P. Czech, Fat-specific protein 27, a novel lipid droplet protein that enhances triglyceride storage., J. Biol. Chem. 282 (2007) 34213–8. doi:10.1074/jbc.M707404200.

[41] N. Nishino, Y. Tamori, S. Tateya, T. Kawaguchi, T. Shibakusa, W. Mizunoya, K. Inoue, R. Kitazawa, S. Kitazawa, Y. Matsuki, R. Hiramatsu, S. Masubuchi, A. Omachi, K. Kimura, M. Saito, T. Amo, S. Ohta, T. Yamaguchi, T. Osumi, J. Cheng, T. Fujimoto, H. Nakao, K. Nakao, A. Aiba, H. Okamura, T. Fushiki, M. Kasuga, FSP27 contributes to efficient energy storage in murine white adipocytes by promoting the formation of unilocular lipid droplets., J. Clin. Invest. 118 (2008) 2808–21. doi:10.1172/JCI34090.

[42] Y.-J. Kim, S.Y. Cho, C.H. Yun, Y.S. Moon, T.R. Lee, S.H. Kim, Transcriptional activation of Cidec by PPARγ2 in adipocyte, Biochem. Biophys. Res. Commun. 377 (2008) 297–302. doi:10.1016/j.bbrc.2008.09.129.

[43] J. Karbowska, Z. Kochan, Intermittent fasting up-regulates Fsp27/Cidec gene expression in white adipose tissue, Nutrition. 28 (2012) 294–299. doi:10.1016/j.nut.2011.06.009.

[44] T. Gimm, M. Wiese, B. Teschemacher, A. Deggerich, J. Schodel, K.X. Knaup, T. Hackenbeck, C. Hellerbrand, K. Amann, M.S. Wiesener, S. Honing, K.-U. Eckardt, C. Warnecke, Hypoxia-inducible protein 2 is a novel lipid droplet protein and a specific target gene of hypoxia-inducible factor-1, FASEB J. 24 (2010) 4443–4458. doi:10.1096/fj.10-159806.

[45] F. Mattijssen, A. Georgiadi, T. Andasarie, E. Szalowska, A. Zota, A. Krones-Herzig, C. Heier, D. Ratman, K. De Bosscher, L. Qi, R. Zechner, S. Herzig, S. Kersten, Hypoxia-inducible lipid droplet-associated (HILPDA) is a

novel peroxisome proliferator-activated receptor (PPAR) target involved in hepatic triglyceride secretion., J. Biol. Chem. 289 (2014) 19279–93. doi:10.1074/jbc.M114.570044.

[46] M.T. DiStefano, L. V Danai, R.J. Roth Flach, A. Chawla, D.J. Pedersen, A. Guilherme, M.P. Czech, The Lipid Droplet Protein Hypoxia-inducible Gene 2 Promotes Hepatic Triglyceride Deposition by Inhibiting Lipolysis., J. Biol. Chem. 290 (2015) 15175–84. doi:10.1074/jbc.M115.650184.

[47] W. Dijk, F. Mattijssen, M. de la Rosa Rodriguez, A. Loza Valdes, A. Loft, S. Mandrup, E. Kalkhoven, L. Qi, J.W. Borst, S. Kersten, Hypoxia-Inducible Lipid Droplet–Associated Is Not a Direct Physiological Regulator of Lipolysis in Adipose Tissue, Endocrinology. 158 (2017) 1231–1251. doi:10.1210/en.2016-1809.

[48] M.T. DiStefano, R.J. Roth Flach, O. Senol-Cosar, L. V. Danai, J. V. Virbasius, S.M. Nicoloro, J. Straubhaar, S. Dagdeviren, M. Wabitsch, O.T. Gupta, J.K. Kim, M.P. Czech, Adipocyte-specific Hypoxia-inducible gene 2 promotes fat deposition and diet-induced insulin resistance, Mol. Metab. 5 (2016) 1149–1161. doi:10.1016/j.molmet.2016.09.009.

[49] M. Bell, H. Wang, H. Chen, J.C. McLenithan, D.-W. Gong, R.-Z. Yang, D. Yu, S.K. Fried, M.J. Quon, C. Londos, C. Sztalryd, Consequences of Lipid Droplet Coat Protein Downregulation in Liver Cells, Diabetes. 57 (2008). doi:10.2337/db07-1383.

[50] N.L. Gluchowski, M. Becuwe, T.C. Walther, R. V. Farese, Lipid droplets and liver disease: from basic biology to clinical implications, Nat. Rev. Gastroenterol. Hepatol. 14 (2017) 343–355. doi:10.1038/nrgastro.2017.32.

[51] H. Wang, A.D. Quiroga, R. Lehner, Analysis of Lipid Droplets in Hepatocytes, in: Methods Cell Biol., 2013: pp. 107–127. doi:10.1016/B978-0-12-408051-5.00007-3.

[52] A. Montagner, A. Polizzi, E. Fouché, S. Ducheix, Y. Lippi, F. Lasserre, V. Barquissau, M. Régnier, C. Lukowicz, F. Benhamed, A. Iroz, J. Bertrand-Michel, T. Al Saati, P. Cano, L. Mselli-Lakhal, G. Mithieux, F. Rajas, S. Lagarrigue, T. Pineau, N. Loiseau, C. Postic, D. Langin, W. Wahli, H. Guillou, Liver PPARα is crucial for whole-body fatty acid homeostasis and is protective against NAFLD., Gut. 65 (2016) 1202–14. doi:10.1136/gutjnl-2015-310798.

[53] L.A. Bojic, M.W. Huff, Peroxisome proliferator-activated receptor δ: a multifaceted metabolic player., Curr. Opin. Lipidol. 24 (2013) 171–7. doi:10.1097/MOL.0b013e32835cc949.

[54] K. Matsusue, M. Haluzik, G. Lambert, S.-H. Yim, O. Gavrilova, J.M. Ward, B. Brewer, M.L. Reitman, F.J. Gonzalez, Liver-specific disruption of PPARgamma in leptin-deficient mice improves fatty liver but aggravates diabetic phenotypes., J. Clin. Invest. 111 (2003) 737–47. doi:10.1172/JCI17223.

[55] M. Inoue, T. Ohtake, W. Motomura, N. Takahashi, Y. Hosoki, S. Miyoshi, Y. Suzuki, H. Saito, Y. Kohgo, T. Okumura, Increased expression of PPARγ in high fat diet-induced liver steatosis in mice, Biochem. Biophys. Res. Commun. 336 (2005) 215–222. doi:10.1016/j.bbrc.2005.08.070.

[56] O. Gavrilova, M. Haluzik, K. Matsusue, J.J. Cutson, L. Johnson, K.R. Dietz, C.J. Nicol, C. Vinson, F.J. Gonzalez, M.L. Reitman, Liver peroxisome proliferator-activated receptor gamma contributes to hepatic steatosis, triglyceride clearance, and regulation of body fat mass., J. Biol. Chem. 278 (2003) 34268–76. doi:10.1074/jbc.M300043200.

[57] S. Yu, K. Matsusue, P. Kashireddy, W.-Q. Cao, V. Yeldandi, A. V Yeldandi, M.S. Rao, F.J. Gonzalez, J.K. Reddy, Adipocyte-specific gene expression and adipogenic steatosis in the mouse liver due to peroxisome proliferator-activated receptor gamma1 (PPARgamma1) overexpression., J. Biol. Chem. 278 (2003) 498–505. doi:10.1074/jbc.M210062200.

[58] E. Morán-Salvador, M. López-Parra, V. García-Alonso, E. Titos, M. Martínez-Clemente, A. González-Périz, C. López-Vicario, Y. Barak, V. Arroyo, J. Clària, Role for PPARγ in obesity-induced hepatic steatosis as

determined by hepatocyte- and macrophage-specific conditional knockouts., FASEB J. 25 (2011) 2538–50. doi:10.1096/fj.10-173716.

[59] R. Wang, X. Wang, L. Zhuang, Gene expression profiling reveals key genes and pathways related to the development of non-alcoholic fatty liver disease., Ann. Hepatol. 15 (n.d.) 190–9. doi:10.5604/16652681.1193709.

[60] L. Zhou, L. Xu, J. Ye, D. Li, W. Wang, X. Li, L. Wu, H. Wang, F. Guan, P. Li, Cidea promotes hepatic steatosis by sensing dietary fatty acids, Hepatology. 56 (2012) 95–107. doi:10.1002/hep.25611.

[61] K. Matsusue, T. Kusakabe, T. Noguchi, S. Takiguchi, T. Suzuki, S. Yamano, F.J. Gonzalez, Hepatic Steatosis in Leptin-Deficient Mice Is Promoted by the PPARγ Target Gene Fsp27, Cell Metab. 7 (2008) 302–311. doi:10.1016/j.cmet.2008.03.003.

[62] N. Viswakarma, S. Yu, S. Naik, P. Kashireddy, K. Matsumoto, J. Sarkar, S. Surapureddi, Y. Jia, M.S. Rao, J.K. Reddy, Transcriptional regulation of Cidea, mitochondrial cell death-inducing DNA fragmentation factor alpha-like effector A, in mouse liver by peroxisome proliferator-activated receptor alpha and gamma., J. Biol. Chem. 282 (2007) 18613–24. doi:10.1074/jbc.M701983200.

[63] C. Langhi, Á. Baldán, CIDEC/FSP27 is regulated by peroxisome proliferator-activated receptor alpha and plays a critical role in fasting- and diet-induced hepatosteatosis, Hepatology. (2015). doi:10.1002/hep.27607.

[64] C. Langhi, Á. Baldán, CIDEC/FSP27 is regulated by peroxisome proliferator-activated receptor alpha and plays a critical role in fasting- and diet-induced hepatosteatosis., Hepatology. 61 (2015) 1227–38. doi:10.1002/hep.27607.

[65] M. Rakhshandehroo, L.M. Sanderson, M. Matilainen, R. Stienstra, C. Carlberg, P.J. de Groot, M. Müller, S. Kersten, Comprehensive analysis of PPARalpha-dependent regulation of hepatic lipid metabolism by expression profiling., PPAR Res. 2007 (2007) 26839. doi:10.1155/2007/26839.

[66] X. Xu, J.-G. Park, J.-S. So, A.-H. Lee, Transcriptional activation of Fsp27 by the liver-enriched transcription factor CREBH promotes lipid droplet growth and hepatic steatosis., Hepatology. 61 (2015) 857–69. doi:10.1002/hep.27371.

[67] J.Z. Li, J. Ye, B. Xue, J. Qi, J. Zhang, Z. Zhou, Q. Li, Z. Wen, P. Li, Cideb Regulates Diet-Induced Obesity, Liver Steatosis, and Insulin Sensitivity by Controlling Lipogenesis and Fatty Acid Oxidation, Diabetes. 56 (2007). doi:10.2337/db07-0040.

[68] H. Li, Y. Song, L.J. Zhang, F.F. Li, Y. Gu, J. Zhang, W.P. Dong, L. Xue, L.Y. Zhang, F. Liu, J. Wang, L.N. Jiang, J. Ye, Q. Li, Cell death-inducing DFF45-like effector b (Cideb) is present in pancreatic beta-cells and involved in palmitate induced beta-cell apoptosis, Diabetes. Metab. Res. Rev. 28 (2012) 145–155. doi:10.1002/dmrr.1295.

[69] L. Da, D. Li, K.K. Yokoyama, T. Li, M. Zhao, Dual promoters control the cell-specific expression of the human cell death-inducing DFF45-like effector B gene, Biochem. J. 393 (2006) 779–788. doi:10.1042/BJ20051027.

[70] J.Z. Li, Y. Lei, Y. Wang, Y. Zhang, J. Ye, X. Xia, X. Pan, P. Li, Control of cholesterol biosynthesis, uptake and storage in hepatocytes by Cideb, Biochim. Biophys. Acta - Mol. Cell Biol. Lipids. 1801 (2010) 577–586. doi:10.1016/j.bbalip.2010.01.012.

[71] F. Mattijssen, A. Georgiadi, T. Andasarie, E. Szalowska, A. Zota, A. Krones-Herzig, C. Heier, D. Ratman, K. De Bosscher, L. Qi, R. Zechner, S. Herzig, S. Kersten, Hypoxia-inducible lipid droplet-associated (HILPDA) is a novel peroxisome proliferator-activated receptor (PPAR) target involved in hepatic triglyceride secretion., J. Biol. Chem. 289 (2014) 19279–93. doi:10.1074/jbc.M114.570044.

[72] Y. Wang, Y. Zhang, H. Qian, J. Lu, Z. Zhang, X. Min, M. Lang, H. Yang, N. Wang, P. Zhang, The G0/G1 Switch Gene 2 Is an Important Regulator of Hepatic Triglyceride Metabolism, PLoS One. 8 (2013) e72315. doi:10.1371/journal.pone.0072315.

[73] B.L. Heckmann, X. Zhang, A.M. Saarinen, G. Schoiswohl, E.E. Kershaw, R. Zechner, J. Liu, Liver X receptor α mediates hepatic triglyceride accumulation through upregulation of G0/G1 Switch Gene 2 expression, JCI Insight. 2 (2017) e88735. doi:10.1172/jci.insight.88735.

[74] Y. Imai, G.M. Varela, M.B. Jackson, M.J. Graham, R.M. Crooke, R.S. Ahima, Reduction of Hepatosteatosis and Lipid Levels by an Adipose Differentiation-Related Protein Antisense Oligonucleotide, Gastroenterology. 132 (2007) 1947–1954. doi:10.1053/j.gastro.2007.02.046.

[75] P. Targett-Adams, M.J. McElwee, E. Ehrenborg, M.C. Gustafsson, C.N. Palmer, J. McLauchlan, A PPAR response element regulates transcription of the gene for human adipose differentiation-related protein, Biochim. Biophys. Acta - Gene Struct. Expr. 1728 (2005) 95–104. doi:10.1016/j.bbaexp.2005.01.017.

[76] K.T. Dalen, PPAR activators and fasting induce the expression of adipose differentiation-related protein in liver, J. Lipid Res. 47 (2006) 931–943. doi:10.1194/jlr.M500459-JLR200.

[77] A.W.F. Janssen, B. Betzel, G. Stoopen, F.J. Berends, I.M. Janssen, A.A. Peijnenburg, S. Kersten, The impact of PPARα activation on whole genome gene expression in human precision cut liver slices, BMC Genomics. 16 (2015) 760. doi:10.1186/s12864-015-1969-3.

[78] M. Rakhshandehroo, G. Hooiveld, M. M?ller, S. Kersten, Comparative Analysis of Gene Regulation by the Transcription Factor PPARalpha between Mouse and Human, PLoS One. 4 (2009) e6796. doi:10.1371/journal.pone.0006796.

[79] S.E. Schadinger, N.L.R. Bucher, B.M. Schreiber, S.R. Farmer, PPARγ2 regulates lipogenesis and lipid accumulation in steatotic hepatocytes, Am. J. Physiol. - Endocrinol. Metab. 288 (2005). doi:10.1152/ajpendo.00513.2004.

[80] K.T. Dalen, T. Dahl, E. Holter, B. Arntsen, C. Londos, C. Sztalryd, H.I. Nebb, LSDP5 is a PAT protein specifically expressed in fatty acid oxidizing tissues, Biochim. Biophys. Acta - Mol. Cell Biol. Lipids. 1771 (2007) 210–227. doi:10.1016/j.bbalip.2006.11.011.

[81] H. Li, Y. Song, L.-J. Zhang, Y. Gu, F.-F. Li, S.-Y. Pan, L.-N. Jiang, F. Liu, J. Ye, Q. Li, LSDP5 Enhances Triglyceride Storage in Hepatocytes by Influencing Lipolysis and Fatty Acid β-Oxidation of Lipid Droplets, PLoS One. 7 (2012) e36712. doi:10.1371/journal.pone.0036712.

[82] C. Wang, Y. Zhao, X. Gao, L. Li, Y. Yuan, F. Liu, L. Zhang, J. Wu, P. Hu, X. Zhang, Y. Gu, Y. Xu, Z. Wang, Z. Li, H. Zhang, J. Ye, Perilipin 5 improves hepatic lipotoxicity by inhibiting lipolysis, Hepatology. 61 (2015) 870–882. doi:10.1002/hep.27409.

[83] T. Yamaguchi, S. Matsushita, K. Motojima, F. Hirose, T. Osumi, MLDP, a Novel PAT Family Protein Localized to Lipid Droplets and Enriched in the Heart, Is Regulated by Peroxisome Proliferator-activated Receptor α, J. Biol. Chem. 281 (2006) 14232–14240. doi:10.1074/jbc.M601682200.

[84] L.M. Sanderson, T. Degenhardt, A. Koppen, E. Kalkhoven, B. Desvergne, M. Müller, S. Kersten, Peroxisome proliferator-activated receptor beta/delta (PPARbeta/delta) but not PPARalpha serves as a plasma free fatty acid sensor in liver., Mol. Cell. Biol. 29 (2009) 6257–67. doi:10.1128/MCB.00370-09.

[85] K.T. Dalen, K. Schoonjans, S.M. Ulven, M.S. Weedon-Fekjaer, T.G. Bentzen, H. Koutnikova, J. Auwerx, H.I. Nebb, Adipose Tissue Expression of the Lipid Droplet-Associating Proteins S3-12 and Perilipin Is Controlled by Peroxisome Proliferator-Activated Receptor-, Diabetes. 53 (2004) 1243–1252. doi:10.2337/diabetes.53.5.1243.

[86] L.M. Pawella, M. Hashani, E. Eiteneuer, M. Renner, R. Bartenschlager, P. Schirmacher, B.K. Straub, Perilipin discerns chronic from acute hepatocellular steatosis, J. Hepatol. 60 (2014) 633–642. doi:10.1016/j.jhep.2013.11.007.

[87] B. Kadereit, P. Kumar, W.-J. Wang, D. Miranda, E.L. Snapp, N. Severina, I. Torregroza, T. Evans, D.L. Silver, Evolutionarily conserved gene family important for fat storage., Proc. Natl. Acad. Sci. U. S. A. 105 (2008) 94–9. doi:10.1073/pnas.0708579105.

[88] A.C. Li, C.J. Binder, A. Gutierrez, K.K. Brown, C.R. Plotkin, J.W. Pattison, A.F. Valledor, R.A. Davis, T.M. Willson, J.L. Witztum, W. Palinski, C.K. Glass, Differential inhibition of macrophage foam-cell formation and atherosclerosis in mice by PPARalpha, beta/delta, and gamma., J. Clin. Invest. 114 (2004) 1564–76. doi:10.1172/JCI18730.

[89] B. Staels, G. Chinetti, S. Lestavel, V. Bocher, A.T. Remaley, B. Neve, I.P. Torra, E. Teissier, A. Minnich, M. Jaye, N. Duverger, H.B. Brewer, J.-C. Fruchart, V. Clavey, PPAR-alpha and PPAR-gamma activators induce cholesterol removal from human macrophage foam cells through stimulation of the ABCA1 pathway., Nat. Med. 7 (2001) 53–58. doi:10.1038/83348.

[90] G. Chinetti-Gbaguidi, B. Staels, PPARβ in macrophages and atherosclerosis, Biochimie. 136 (2017) 59–64. doi:10.1016/j.biochi.2016.12.008.

[91] R.M. Evans, A. Chawla, Y. Barak, L. Nagy, D. Liao, P. Tontonoz, PPAR-gamma dependent and independent effects on macrophage-gene expression in lipid metabolism and inflammation., Nat. Med. 7 (2001) 48–52. doi:10.1038/83336.

[92] M.W. Freeman, K.J. Moore, E.D. Rosen, M.L. Fitzgerald, F. Randow, L.P. Andersson, D. Altshuler, D.S. Milstone, R.M. Mortensen, B.M. Spiegelman, The role of PPAR-gamma in macrophage differentiation and cholesterol uptake., Nat. Med. 7 (2001) 41–47. doi:10.1038/83328.

[93] P. Tontonoz, B.M. Spiegelman, Fat and Beyond: The Diverse Biology of PPARγ, Annu. Rev. Biochem. 77 (2008) 289–312. doi:10.1146/annurev.biochem.77.061307.091829.

[94] X. Wang, T.J. Reape, X. Li, K. Rayner, C.L. Webb, K.G. Burnand, P.G. Lysko, Induced expression of adipophilin mRNA in human macrophages stimulated with oxidized low-density lipoprotein and in atherosclerotic lesions., FEBS Lett. 462 (1999) 145–50. doi:10.1016/S0014-5793(99)01521-5.

[95] H. Li, Y. Song, F. Li, L. Zhang, Y. Gu, L. Zhang, L. Jiang, W. Dong, J. Ye, Q. Li, Identification of lipid droplet-associated proteins in the formation of macrophage-derived foam cells using microarrays., Int. J. Mol. Med. 26 (2010) 231–9. doi:10.3892/ijmm_00000457.

[96] A. Paul, B.H.-J. Chang, L. Li, V.K. Yechoor, L. Chan, Deficiency of Adipose Differentiation-Related Protein Impairs Foam Cell Formation and Protects Against Atherosclerosis, Circ. Res. 102 (2008) 1492–1501. doi:10.1161/CIRCRESAHA.107.168070.

[97] G. Larigauderie, C. Furman, M. Jaye, C. Lasselin, C. Copin, J.-C. Fruchart, G. Castro, M. Rouis, Adipophilin Enhances Lipid Accumulation and Prevents Lipid Efflux From THP-1 Macrophages: Potential Role in Atherogenesis, Arterioscler. Thromb. Vasc. Biol. 24 (2004) 504–510. doi:10.1161/01.ATV.0000115638.27381.97.

[98] J. Persson, E. Degerman, J. Nilsson, M.W. Lindholm, Perilipin and adipophilin expression in lipid loaded macrophages, Biochem. Biophys. Res. Commun. 363 (2007) 1020–1026. doi:10.1016/j.bbrc.2007.09.074.

[99] N. Thyagarajan, J.D. Marshall, A.T. Pickett, C. Schumacher, Y. Yang, S.L. Christian, R.J. Brown, Transcriptomic Analysis of THP-1 Macrophages Exposed to Lipoprotein Hydrolysis Products Generated by Lipoprotein Lipase, Lipids. 52 (2017) 189–205. doi:10.1007/s11745-017-4238-1.

[100] L.M. Varela, S. López, A. Ortega-Gómez, B. Bermúdez, I. Buers, H. Robenek, F.J.G. Muriana, R. Abia, Postprandial triglyceride-rich lipoproteins regulate perilipin-2 and perilipin-3 lipid-droplet-associated proteins in macrophages, J. Nutr. Biochem. 26 (2015) 327–336. doi:10.1016/j.jnutbio.2014.11.007.

[101] C.P. Hodgkinson, S. Ye, Microarray analysis of peroxisome proliferator-activated receptor-gamma induced changes in gene expression in macrophages., Biochem. Biophys. Res. Commun. 308 (2003) 505–10. doi:10.1016/S0006-291X(03)01416-5.

[102] H. Vosper, L. Patel, T.L. Graham, G.A. Khoudoli, A. Hill, C.H. Macphee, I. Pinto, S.A. Smith, K.E. Suckling, C.R. Wolf, C.N. Palmer, The peroxisome proliferator-activated receptor delta promotes lipid accumulation in human macrophages., J. Biol. Chem. 276 (2001) 44258–65. doi:10.1074/jbc.M108482200.

[103] C.-H. Lee, K. Kang, I.R. Mehl, R. Nofsinger, W.A. Alaynick, L.-W. Chong, J.M. Rosenfeld, R.M. Evans, Peroxisome proliferator-activated receptor γ promotes very low-density lipoprotein-derived fatty acid catabolism in the macrophage, Proc. Natl. Acad. Sci. 103 (2006) 2434–2439. doi:10.1073/pnas.0510815103.

[104] D.M. Muoio, P.S. MacLean, D.B. Lang, S. Li, J.A. Houmard, J.M. Way, D.A. Winegar, J.C. Corton, G.L. Dohm, W.E. Kraus, Fatty Acid Homeostasis and Induction of Lipid Regulatory Genes in Skeletal Muscles of Peroxisome Proliferator-activated Receptor (PPAR) Knock-out Mice: EVIDENCE FOR COMPENSATORY REGULATION BY PPAR, J. Biol. Chem. 277 (2002) 26089–26097. doi:10.1074/jbc.M203997200.

[105] R. Manickam, W. Wahli, Roles of Peroxisome Proliferator-Activated Receptor β/δ in skeletal muscle physiology, Biochimie. 136 (2017) 42–48. doi:10.1016/j.biochi.2016.11.010.

[106] M. Bosma, Lipid droplet dynamics in skeletal muscle, Exp. Cell Res. 340 (2016) 180–186. doi:10.1016/j.yexcr.2015.10.023.

[107] Z. Guo, B. Burguera, M.D. Jensen, Kinetics of intramuscular triglyceride fatty acids in exercising humans., J. Appl. Physiol. 89 (2000) 2057–64. http://www.ncbi.nlm.nih.gov/pubmed/11053362.

[108] M. Bosma, M.K.C. Hesselink, L.M. Sparks, S. Timmers, M.J. Ferraz, F. Mattijssen, D. van Beurden, G. Schaart, M.H. de Baets, F.K. Verheyen, S. Kersten, P. Schrauwen, Perilipin 2 Improves Insulin Sensitivity in Skeletal Muscle Despite Elevated Intramuscular Lipid Levels, Diabetes. 61 (2012) 2679–2690. doi:10.2337/db11-1402.

[109] J. de Wilde, E. Smit, F.J.M. Snepvangers, N.W.J. de Wit, R. Mohren, M.F.M. Hulshof, E.C.M. Mariman, Adipophilin protein expression in muscle - a possible protective role against insulin resistance, FEBS J. 277 (2010) 761–773. doi:10.1111/j.1742-4658.2009.07525.x.

[110] C. Bindesbøll, O. Berg, B. Arntsen, H.I. Nebb, K.T. Dalen, Fatty acids regulate perilipin5 in muscle by activating PPARδ., J. Lipid Res. 54 (2013) 1949–63. doi:10.1194/jlr.M038992.

[111] Y.Z. Feng, N. Nikolic, S.S. Bakke, M. V. Boekschoten, S. Kersten, E.T. Kase, A.C. Rustan, G.H. Thoresen, PPARδ activation in human myotubes increases mitochondrial fatty acid oxidative capacity and reduces glucose utilization by a switch in substrate preference, Arch. Physiol. Biochem. 120 (2014) 12–21. doi:10.3109/13813455.2013.829105.

[112] C. Laurens, V. Bourlier, A. Mairal, K. Louche, P.-M. Badin, E. Mouisel, A. Montagner, A. Marette, A. Tremblay, J.S. Weisnagel, H. Guillou, D. Langin, D.R. Joanisse, C. Moro, Perilipin 5 fine-tunes lipid oxidation to metabolic demand and protects against lipotoxicity in skeletal muscle., Sci. Rep. 6 (2016) 38310. doi:10.1038/srep38310.

[113] M. Bosma, L.M. Sparks, G.J. Hooiveld, J.A. Jorgensen, S.M. Houten, P. Schrauwen, S. Kersten, M.K.C. Hesselink, Overexpression of PLIN5 in skeletal muscle promotes oxidative gene expression and intramyocellular lipid content without compromising insulin sensitivity, Biochim. Biophys. Acta - Mol. Cell Biol. Lipids. 1831 (2013) 844–852. doi:10.1016/j.bbalip.2013.01.007.

[114] L.-A. Harris, J.R. Skinner, T.M. Shew, T.A. Pietka, N.A. Abumrad, N.E. Wolins, Perilipin 5-Driven Lipid Droplet Accumulation in Skeletal Muscle Stimulates the Expression of Fibroblast Growth Factor 21., Diabetes. 64 (2015) 2757–68. doi:10.2337/db14-1035.

Chapter 4

HILPDA uncouples lipid droplet accumulation in adipose tissue macrophages from inflammation and metabolic dysregulation

Xanthe A.M.H. van Dierendonck†, Montserrat A. de la Rosa Rodriguez†, Anastasia Georgiadi, Frits Mattijssen, Wieneke Dijk, Michel van Weeghel, Rajat Singh, Jan Willem Borst, Rinke Stienstra*, Sander Kersten*

Cell Rep., vol. 30, no. 6, pp. 1811-1822.e6, 2020
† equal contribution
* shared senior authors

Summary

Obesity leads to a state of chronic low-grade inflammation that features the accumulation of lipid-laden macrophages in adipose tissue. Here, we determined the role of macrophage lipid droplet accumulation in the development of obesity-induced adipose tissue inflammation, using mice with myeloid-specific deficiency of the lipid-inducible HILPDA protein. HILPDA deficiency markedly reduced intracellular lipid levels and accumulation of fluorescently-labeled fatty acids. Decreased lipid storage in HILPDA-deficient macrophages could be rescued by inhibition of adipose triglyceride lipase (ATGL) and was associated with increased oxidative metabolism. In diet-induced obese mice, HILPDA deficiency did not alter inflammatory and metabolic parameters, despite markedly reducing lipid accumulation in macrophages. Overall, we find that HILPDA is a lipid-inducible physiological inhibitor of ATGL-mediated lipolysis in macrophages that uncouples lipid storage in adipose tissue macrophages from inflammation and metabolic dysregulation. Our data question the contribution of lipid droplet accumulation in adipose tissue macrophages in obesity-induced inflammation and metabolic dysregulation.

Keywords: Hilpda, ATGL, fatty acid metabolism, lipid droplets, macrophages, inflammation, obesity

Introduction

The prevalence of obesity across the world has risen steeply in the past decades and has become a huge public health concern. It is well established that obesity is associated with a state of chronic low-grade inflammation. This low-grade inflammation is characterized by increased production of several inflammatory cytokines and adipokines and has been suggested to be an important pathophysiological mechanism underlying many of the adverse health effects of obesity (Gregor and Hotamisligil, 2011). In particular, the increase in inflammatory cytokines and adipokines is believed to disrupt insulin signalling and contribute to obesity-induced insulin resistance (Hotamisligil, 2017).

Adipose tissue mainly consists of adipocytes but also harbours numerous immune cells, including macrophages. These macrophages are important for maintaining homeostasis in healthy adipose tissue, yet also contribute to the development of inflammation during obesity (Boutens and Stienstra, 2016). In lean states, adipose tissue macrophages mainly show anti-inflammatory phenotypes and are distributed evenly throughout the adipose tissue. In contrast, in obese adipose tissue, macrophages accumulate in so-called crown-like structures around dead adipocytes and display a metabolically activated phenotype (Cinti et al., 2005; Lumeng, Bodzin and Saltiel, 2007; Xu et al., 2013). Metabolically activated macrophages form multiple intracellular lipid droplets and display distinct transcriptional profiles (Lumeng et al., 2008; Shapiro et al., 2013; Xu et al., 2013). These features reflect an attempt by macrophages to buffer excess lipids, which is adaptive in the lean state but becomes maladaptive in obese adipose tissue (Boutens and Stienstra, 2016). The lipid-laden macrophages observed in obese adipose tissue are reminiscent of the foamy macrophages present in atherosclerotic plaques. Although foam cell formation and adipose tissue inflammation are known to co-exist in obesity, the exact role of lipid droplet accumulation in adipose tissue macrophages in the development of obesity-induced adipose tissue inflammation and associated metabolic disturbances remains unclear.

HILPDA (Hypoxia Inducible Lipid Droplet Associated) is a small lipid droplet-associated protein expressed in several tissues (Mattijssen et al., 2014). The expression of *Hilpda* is induced by different stimuli including hypoxia, beta-adrenergic activation, and PPAR transcription factors (Gimm et al., 2010; Mattijssen et al., 2014; Dijk et al., 2017). Gain and loss of function studies have shown that HILPDA promotes lipid deposition in hepatocytes, adipocytes, and macrophages (Gimm et al., 2010; Mattijssen et al., 2014; DiStefano et al., 2015, 2016; Dijk et al., 2017; Maier et al., 2017). The mechanism by which HILPDA promotes lipid storage in cells has not been completely elucidated but evidence has been presented that HILPDA directly binds and inhibits adipose triglyceride lipase (ATGL) (Zhang et al., 2017; Padmanabha Das et al., 2018), consistent with the ability of HILPDA to inhibit lipolysis (DiStefano et al., 2015; Dijk et al., 2017). Interestingly, endothelial cell marker Tie2-Cre

driven deletion of *Hilpda* was found to decrease fatty acid and oxLDL-driven lipid droplet formation in macrophages, and reduce lesion formation and progression of atherosclerosis in *Apoe-/-* mice (Maier et al., 2017).

Here, we aimed to determine the exact role of HILPDA in lipid storage in macrophages, and explore the potential causal relationship between lipid droplet accumulation in adipose tissue macrophages, and the development of adipose tissue inflammation and insulin resistance during obesity.

Results

Hilpda as gene of interest in obese adipose tissue

To identify genes that may be able to modify lipid storage in adipose tissue macrophages, we searched for genes that are induced by lipids and upregulated in adipose tissue macrophages by obesity. To that end, we co-analyzed the transcriptomics data from three experiments: 1) adipose tissue macrophages isolated from obese versus lean mice, 2) mouse peritoneal macrophages treated with the fatty acid oleate, 3) mouse peritoneal macrophages treated with intralipid, a triglyceride emulsion. Scatter plot analysis identified *Hilpda* as a gene of particular interest (Fig 1A), as it was the only gene that was strongly upregulated in all three experiments. Moreover, *Hilpda* was the most highly induced gene in peritoneal macrophages by oleate. Consistent with a potential role for *Hilpda* in obese-induced adipose tissue inflammation, transcriptome analysis indicated that *Hilpda* expression in adipose tissue is upregulated by high fat feeding in mice in parallel with macrophage and inflammatory markers, such as *Ccl2* (MCP1), *Cd68*, and *Itgax* (Cd11c) (Fig 1B), as confirmed by qPCR (Fig 1C). Immunohistochemistry of adipose tissue of obese mice indicated that HILPDA co-localized with adipose tissue macrophages in crown-like structures, thus supporting the expression of HILPDA in adipose tissue macrophages (Fig 1D). Together, these data suggest that HILPDA may be implicated in obesity-induced adipose tissue inflammation and foam cell formation.

Hilpda in macrophages is responsive to lipids

To further investigate the regulation of HILPDA by lipids, we treated RAW264.7 and primary peritoneal macrophages with fatty acids. Confirming the transcriptomics data, oleate markedly upregulated *Hilpda* mRNA in RAW264.7 and peritoneal macrophages (Fig 1E). Similarly, intralipid significantly induced *Hilpda* mRNA in both types of macrophages (Fig 1F). The induction of HILPDA by intralipid in RAW264.7 and peritoneal macrophages was particularly evident at the protein level (Fig 1G). *Hilpda* was originally identified as hypoxia-inducible gene 2 (Hig2) (Denko et al., 2000). Since hypoxic areas are characteristic of obese adipose tissue (Rausch et al., 2008), we tested the effect of a combination of intralipid and a chemical hypoxia mimic. Together, they synergistically increased *Hilpda* mRNA (Fig 1H).

Macrophage-specific *Hilpda* deficiency impairs lipid droplet accumulation

To study the effect of HILPDA on lipid storage in macrophages, we overexpressed HILPDA in RAW264.7 macrophages using an adenoviral vector (Fig 1I). Interestingly, the marked increase in HILPDA protein levels was not accompanied by any changes in lipid droplet accumulation, as visualized by Oil Red O staining (Fig 1J). These data indicate that overexpression of HILPDA in macrophages has no discernible effect on lipid storage.

We next switched to bone-marrow derived macrophages (BMDMs) as a robust primary in vitro model. Similar to RAW264.7 and peritoneal macrophages, intralipid and chemical hypoxia synergistically upregulated *Hilpda* mRNA in BMDMs (Fig 2A). To be able to study the effects of HILPDA deficiency in macrophages, we generated mice with a myeloid-specific *Hilpda* inactivation (*Hilpda*$^{\Delta M\Phi}$) by crossing *Hilpda*$^{flox/flox}$ with mice expressing Cre-recombinase driven by the LysM promoter. BMDMs obtained from *Hilpda*$^{\Delta M\Phi}$ mice and their *Hilpda*$^{flox/flox}$ littermates were lipid-loaded with a combination of oleate and palmitate for 12 hours to induce maximal lipid droplet formation. The Cre-mediated excision in BMDMs led to an approximate 80% reduction in *Hilpda* mRNA (Fig 2B) and a corresponding decrease in HILPDA protein (Fig 2C). Strikingly, staining of neutral lipids by BODIPY in BMDMs showed that lipid droplets were much less visible in fatty acid-loaded *Hilpda*$^{\Delta M\Phi}$ than *Hilpda*$^{flox/flox}$ macrophages (Fig 2D). Quantitative analysis indicated that the number of lipid droplets per cell and the size of the lipid droplets were significantly lower in *Hilpda*$^{\Delta M\Phi}$ than in *Hilpda*$^{flox/flox}$ macrophages (Fig 2E). This reduction of lipid droplets was confirmed by Oil Red O staining (Fig 2F). In addition, triglyceride levels were markedly decreased in fatty acid-loaded *Hilpda*$^{\Delta M\Phi}$ compared to *Hilpda*$^{flox/flox}$ macrophages (Fig 2G, Fig S1). Together, these data show that HILPDA deficiency in macrophages leads to a pronounced decrease in lipid storage.

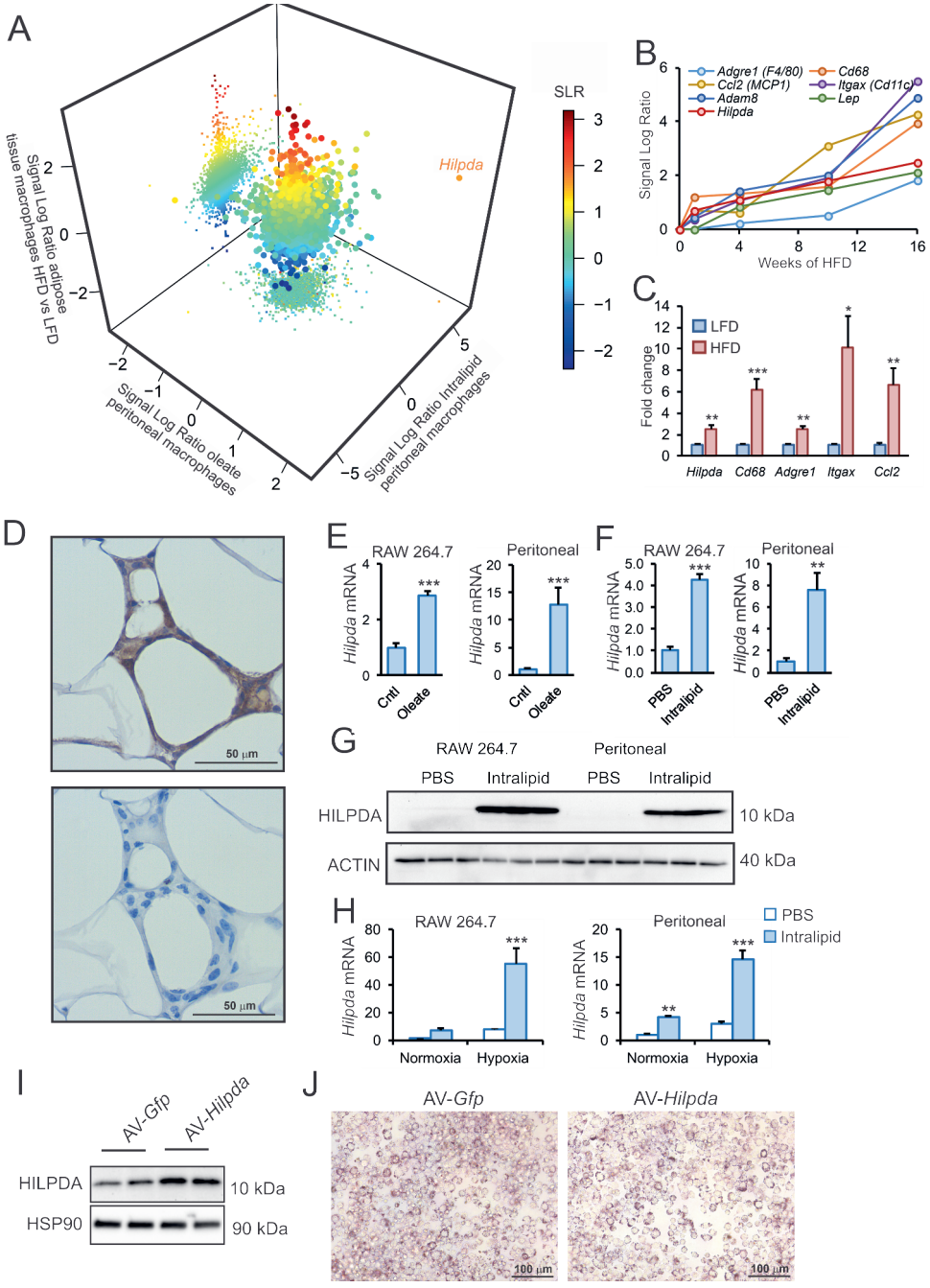
A
Hilpda
SLR
Signal Log Ratio adipose tissue macrophages HFD vs LFD
Signal Log Ratio oleate peritoneal macrophages
Signal Log Ratio Intralipid peritoneal macrophages
B
Adgre1 (F4/80)
Ccl2 (MCP1)
Adam8
Hilpda
Cd68
Itgax (Cd11c)
Lep
Signal Log Ratio
Weeks of HFD
C
LFD
HFD
Fold change
Hilpda
Cd68
Adgre1
Itgax
Ccl2
D
50 µm
50 µm
E
RAW 264.7
Peritoneal
Hilpda mRNA
Cntl
Oleate
F
RAW 264.7
Peritoneal
Hilpda mRNA
PBS
Intralipid
G
RAW 264.7
Peritoneal
PBS
Intralipid
PBS
Intralipid
HILPDA
10 kDa
ACTIN
40 kDa
H
RAW 264.7
Peritoneal
PBS
Intralipid
Hilpda mRNA
Normoxia
Hypoxia
I
AV-Gfp
AV-Hilpda
HILPDA
10 kDa
HSP90
90 kDa
J
AV-Gfp
AV-Hilpda
100 µm
100 µm

Figure 1 Lipid-responsive *Hilpda* as gene of interest in obese adipose tissue. A: Transcriptomics co-analysis of ATMs isolated from C57Bl/6 mice fed a HFD versus a LFD, C57Bl/6 mouse peritoneal macrophages treated with oleate and C57Bl/6 *Angptl4*$^{-/-}$ mouse peritoneal macrophages treated with intralipid. B: Signal log ratio patterns of *Hilpda*, inflammatory genes and macrophage markers in gonadal adipose tissue of C57Bl/6 mice fed a HFD for 1, 4, 8, 12 or 16 weeks. C: Gene expression of *Hilpda*, *Cd68*, *Adgre1*, *Itgax, Ccl2* in gonadal adipose tissue of C57Bl/6 mice fed a HFD for 20 weeks (LFD, n=8; HFD, n=10). D: Immunohistochemical staining of HILPDA in gonadal adipose tissue from C57Bl/6 mice fed a HFD for 20 weeks (representative data for n=10). Lower panel is without primary antibody. *Hilpda* mRNA expression in RAW264.7 and C57Bl/6 mouse peritoneal macrophages exposed to 250µM oleate (E) or 1mM intralipid (F) for 6h versus BSA (Cntl) or PBS. G: HILPDA protein levels in RAW 264.7 and peritoneal macrophages exposed to 1mM intralipid or PBS for 6h. ACTIN was used as loading control. H: *Hilpda* mRNA expression in RAW264.7 and C57Bl/6 mouse peritoneal macrophages exposed to 1mM intralipid or PBS in combination with normoxia or chemical hypoxia mimic induced by 100µM 2,2'-bipyridyl for 6h. I: HILPDA protein levels in RAW264.7 macrophages transduced with recombinant adenovirus expressing *Gfp* (AV-*Gfp*) or *Hilpda* (AV-*Hilpda*) at a multiplicity of infection of 500 for 48 hours. J: Oil Red O staining of RAW264.7 macrophages transduced with AV-*Gfp* or AV-*Hilpda*, followed by lipid loading with 667µM oleate and 333µM palmitate or BSA for 24h. Bar graphs are presented as mean ±SEM (*in vivo* studies) or mean ±SD (*in vitro* studies). Statistical testing was performed by Student's t-test or by two-way ANOVA followed by Bonferroni's post hoc multiple comparisons test. The effect of treatment was significant in H. *P<0.05, **P≤0.01, ***P≤0.001. LFD: low fat diet, HFD: high fat diet.

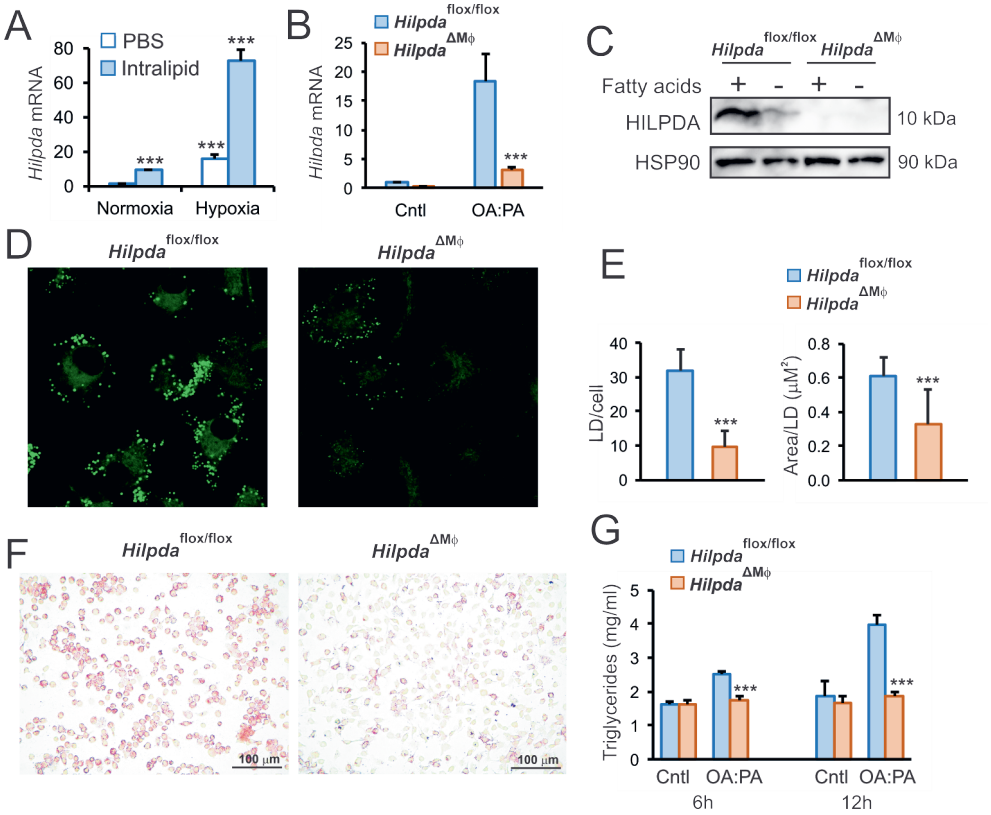

Figure 2 Myeloid-specific HILPDA deficiency impairs lipid droplet formation. A: *Hilpda* mRNA expression in C57Bl/6 BMDMs exposed to 1mM intralipid or PBS, combined with normoxia or chemical hypoxia induced by 100µM 2,2'-bipyridyl for 6h. Gene expression of *Hilpda* (B) and protein levels (C) of HILPDA in *Hilpda*$^{flox/flox}$ and *Hilpda*$^{\Delta M\Phi}$ BMDMs lipid loaded with 400µM oleate and 200µM palmitate (oleate:palmitate) or BSA (Cntl) for 12h (n = 3). HSP90 was used as loading control. BODIPY (D and E) and Oil Red O (F) staining in *Hilpda*$^{flox/flox}$ and *Hilpda*$^{\Delta M\Phi}$ BMDMs lipid loaded with oleate:palmitate or BSA (Cntl) for 24h. Data is shown from or is representative for at least three independent experiments. G: Triglyceride measurement in BMDMs from *Hilpda*$^{flox/flox}$ and *Hilpda*$^{\Delta M\Phi}$ lipid loaded with oleate:palmitate or BSA (Cntl) for 6 or 12h. See also Figure S1. Bar graphs are presented as mean ±SD. Statistical testing was performed by Student's t-test or by two-way ANOVA followed by Bonferroni's post hoc multiple comparisons test. The effect of treatment was significant in B and G. *P<0.05, ***P≤0.001. OA:PA: oleate:palmitate, LD: lipid droplet.

HILPDA does not regulate fatty acid uptake or triglyceride synthesis

We next explored potential mechanisms underlying the decreased lipid storage in HILPDA-deficient macrophages. To determine if the reduction in lipid storage in HILPDA-deficient macrophages is due to decreased lipid uptake, we measured fatty acid uptake 6 and 35 min after addition of a mixture of oleate and BODIPY-labeled C12 (BODIPY FL). Confocal microscopy showed no difference in fluorescence intensity between *Hilpda*$^{\Delta M\Phi}$ and *Hilpda*$^{flox/flox}$ macrophages at 6 and 35 min (Fig 3A), which was corroborated by quantitative image analysis (Fig 3B), indicating that HILPDA deficiency did not influence fatty acid uptake. Expression of the fatty acid transporter Cd36 was comparable in *Hilpda*$^{\Delta M\Phi}$ and *Hilpda*$^{flox/flox}$ macrophages (Fig 3C). In addition, the early induction of gene expression by fatty acids was not different between *Hilpda*$^{\Delta M\Phi}$ and *Hilpda*$^{flox/flox}$ macrophages, regardless of whether the fatty acids were provided as free fatty acids (Fig 3D), or intralipid (Fig S2), clearly indicating that HILPDA does not regulate fatty acid uptake. Accordingly, we hypothesized that HILPDA may have two—not necessarily mutually exclusive—functions: 1) Activator of fatty acid esterification, and/or 2) Inhibitor of triglyceride lipolysis. If HILPDA acts by activating fatty acid esterification in macrophages, suggested before by Maier et al. (Maier et al., 2017), it would be expected that HILPDA deficiency leads to accumulation of intermediates in the triglyceride synthesis pathway. To explore that possibility, we performed shotgun lipidomics on *Hilpda*$^{\Delta M\Phi}$ and *Hilpda*$^{flox/flox}$ BMDMs loaded with oleate:palmitate for 24h. Partial least squares discriminant analysis clearly separated the two genotypes (Fig 3E), indicating that the lipidomics profiles of *Hilpda*$^{\Delta M\Phi}$ and *Hilpda*$^{flox/flox}$ macrophages are very distinct. Volcano plot analysis indicated that while a number of lipids were increased in *Hilpda*$^{\Delta M\Phi}$ macrophages, the majority of lipids were reduced (Fig 3F). Indeed, levels of phosphatidic acids, diacylglycerols, and triglycerides were significantly decreased in *Hilpda*$^{\Delta M\Phi}$ versus *Hilpda*$^{flox/flox}$ macrophages (Fig 3G), as were cholesteryl-esters, while lysophosphatidic acids were hardly detectable. The decrease in triglycerides and diacylglycerols was accounted for by the major subspecies within each lipid class (Fig 3H). These data suggest that HILPDA probably does not regulate the fatty acid esterification pathway in macrophages.

HILPDA regulates lipid droplet mobilization through ATGL inhibition

To further investigate the molecular basis for the decreased lipid storage in HILPDA-deficient macrophages, we determined the trafficking of lipids after loading with a mixture of oleate and BODIPY FL for either 5 or 24 hours. Strikingly, after lipid loading *Hilpda*$^{flox/flox}$ macrophages for 5 hours, the BODIPY FL had largely accumulated in lipid droplets, whereas in *Hilpda*$^{\Delta M\Phi}$ macrophages, the BODIPY FL was mainly distributed throughout the ER and showed only minor presence in lipid droplet-like structures (Fig 4A). After lipid loading for

24 hours, the size and number of lipid droplets had further increased in *Hilpda*$^{flox/flox}$ macrophages, whereas in *Hilpda*$^{\Delta M\Phi}$ macrophages, the lipid droplet-like structures that had initially formed at 5h were no longer visible (Fig 4A). These data indicate that *Hilpda*$^{\Delta M\Phi}$ BMDMs, while being able to take up similar amounts of fatty acids as *Hilpda*$^{flox/flox}$ BMDMs, are unable to retain them in lipid droplets.

Using various biochemical and cellular assays, we and others previously found that HILPDA is able to inhibit ATGL, the rate-limiting enzyme for lipolysis (Zhang et al., 2017; Padmanabha Das et al., 2018). However, it is unclear whether HILPDA is a physiological regulator of ATGL in macrophages. To investigate if the decrease in lipid droplet and triglyceride accumulation in *Hilpda*$^{\Delta M\Phi}$ macrophages is due to enhanced ATGL-mediated lipolysis, we loaded *Hilpda*$^{\Delta M\Phi}$ and *Hilpda*$^{flox/flox}$ BMDMs with oleate:palmitate in the presence of Atglistatin, a small-molecule inhibitor of ATGL (Mayer et al., 2013). Strikingly, inhibiting ATGL markedly increased lipid droplets in *Hilpda*$^{\Delta M\Phi}$ BMDMs (Fig 4B), almost completely rescuing the *Hilpda*$^{\Delta M\Phi}$ phenotype. Quantitative analysis showed that the lipid droplet surface area was not significantly affected by Atglistatin in *Hilpda*$^{flox/flox}$ BMDMs and markedly induced by Atglistatin in *Hilpda*$^{\Delta M\Phi}$ BMDMs (Fig S3A). Similarly, the defective retention of BODIPY FL in lipid droplets in *Hilpda*$^{\Delta M\Phi}$ macrophages was almost completely abolished by Atglistatin (Fig 4C, Fig S3B). These studies indicate that the decrease in lipid droplet and triglyceride accumulation in *Hilpda*$^{\Delta M\Phi}$ macrophages is caused by accelerated lipid droplet breakdown via enhanced ATGL-mediated lipolysis. Our data thus suggest that HILPDA functions as a potent endogenous inhibitor of ATGL in macrophages.

To determine whether HILPDA may influence the abundance of ATGL and other lipid droplet-associated proteins in macrophages, we performed Western blot on *Hilpda*$^{\Delta M\Phi}$ and *Hilpda*$^{flox/flox}$ BMDMs loaded with oleate:palmitate for 24h. As expected, lipid loading increased HILPDA levels, as well as PLIN3 levels (Fig 4D). Remarkably, ATGL levels were markedly higher in *Hilpda*$^{\Delta M\Phi}$ than *Hilpda*$^{flox/flox}$ BMDMs, suggesting that HILPDA not only inhibits ATGL but also decreases ATGL protein levels. G0S2 protein levels, despite being difficult to detect, were also higher in *Hilpda*$^{\Delta M\Phi}$ than *Hilpda*$^{flox/flox}$ BMDMs.

Figure 3 HILPDA does not regulate fatty acid uptake or triglyceride synthesis. A: Confocal microscopy of *Hilpda*$^{flox/flox}$ and *Hilpda*$^{\Delta M\Phi}$ BMDMs incubated with BODIPY FL for 6 or 35 minutes. B: Fluorescence quantification reflecting fatty acid uptake. C: *Cd36* mRNA in *Hilpda*$^{flox/flox}$ and *Hilpda*$^{\Delta M\Phi}$ BMDMs. D: Gene expression of *Hilpda*, *Ddit3*, *Ptgs2* and *Plin2* in BMDMs from *Hilpda*$^{flox/flox}$ and *Hilpda*$^{\Delta M\Phi}$ lipid loaded with oleate:palmitate or BSA (Cntl) for 6h, (n=3). See also figure S2. Partial least square discriminant analysis (E), volcano plot analysis (F), differences in abundancy of CE, DAG, PA, TAG and total lipid species (G) and heatmap of most abundant DG and TG species (H) based on shotgun lipidomics on *Hilpda*$^{flox/flox}$ and *Hilpda*$^{\Delta M\Phi}$ BMDMs loaded with oleate:palmitate for 24h. Bar graphs are presented as mean ±SD. Statistical testing was performed by Student's t-test or by two-way ANOVA followed by Bonferroni's post hoc multiple comparisons test. The effect of treatment was significant in C. *P<0.05, ***P≤0.001. SLR, signal log ratio.

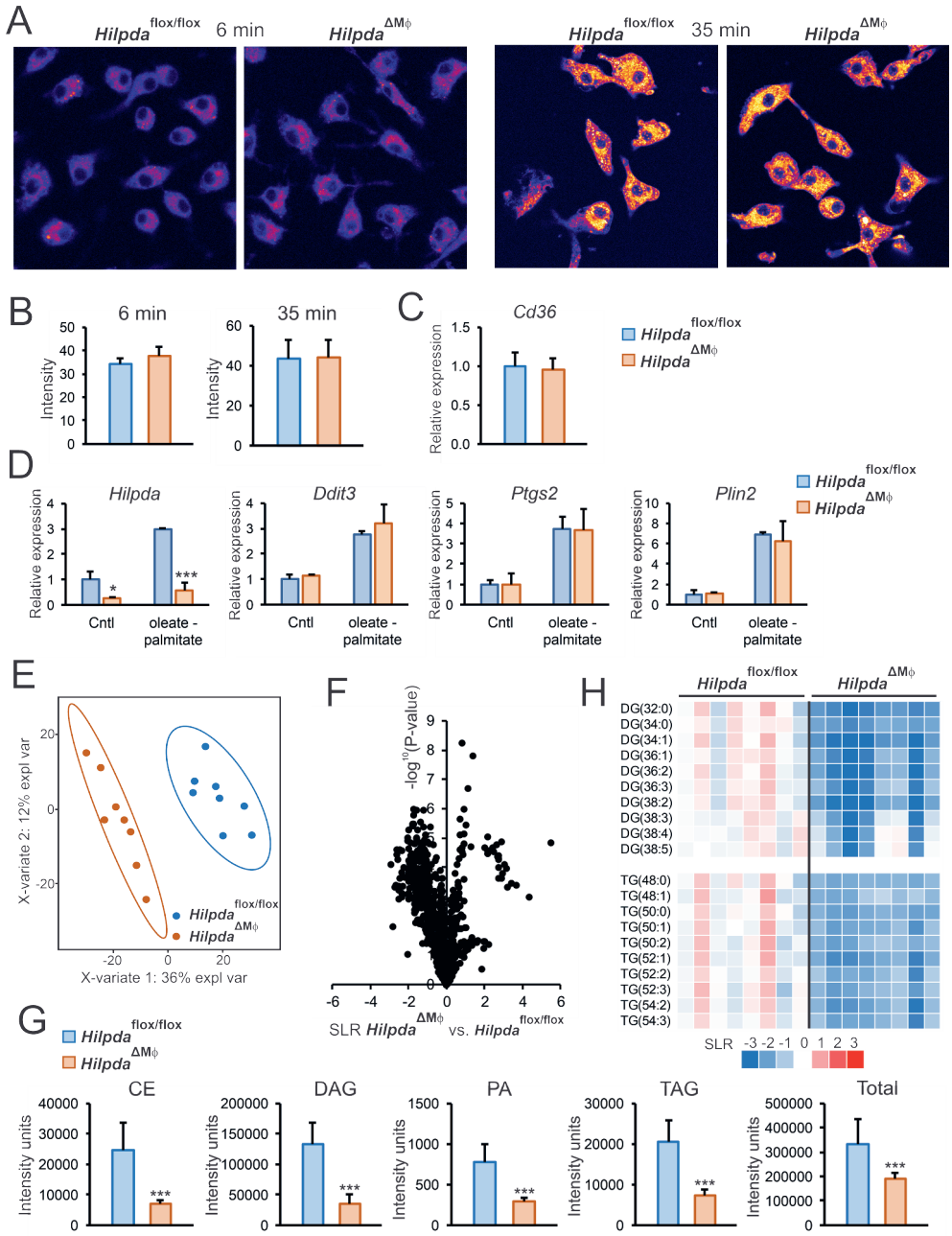
A
Hilpda flox/flox 6 min
Hilpda ΔMϕ
Hilpda flox/flox 35 min
Hilpda ΔMϕ
B
6 min
35 min
Intensity
C
Cd36
Relative expression
Hilpda flox/flox
Hilpda ΔMϕ
D
Hilpda
Ddit3
Ptgs2
Plin2
Relative expression
Cntl
oleate - palmitate
E
X-variate 2: 12% expl var
X-variate 1: 36% expl var
F
-log10(P-value)
SLR Hilpda ΔMϕ vs. Hilpda flox/flox
H
DG(32:0)
DG(34:0)
DG(34:1)
DG(36:1)
DG(36:2)
DG(36:3)
DG(38:2)
DG(38:3)
DG(38:4)
DG(38:5)
TG(48:0)
TG(48:1)
TG(50:0)
TG(50:1)
TG(50:2)
TG(52:1)
TG(52:2)
TG(52:3)
TG(54:2)
TG(54:3)
SLR -3 -2 -1 0 1 2 3
G
CE
DAG
PA
TAG
Total
Intensity units

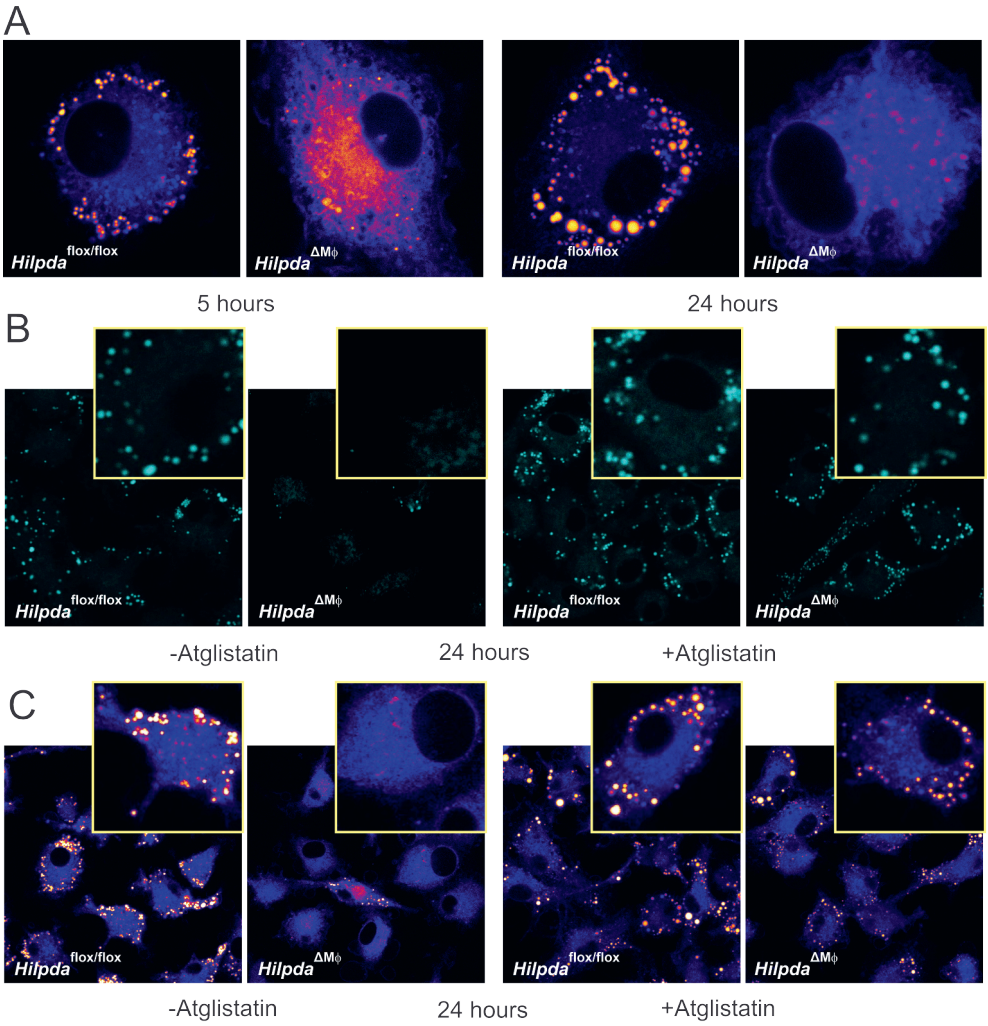
A
Hilpda flox/flox
Hilpda ΔMϕ
Hilpda flox/flox
Hilpda ΔMϕ
5 hours
24 hours
B
Hilpda flox/flox
Hilpda ΔMϕ
Hilpda flox/flox
Hilpda ΔMϕ
-Atglistatin
24 hours
+Atglistatin
C
Hilpda flox/flox
Hilpda ΔMϕ
Hilpda flox/flox
Hilpda ΔMϕ
-Atglistatin
24 hours
+Atglistatin
D
Hilpda flox/flox
Hilpda ΔMϕ
Hilpda flox/flox
Hilpda ΔMϕ
Fatty acids - - + +
HILPDA
PLIN3
ATGL
G0S2
HSP90
10 kDa
50 kDa
60 kDa
15 kDa
90 kDa

Figure 4 HILPDA regulates lipid droplet mobilization through ATGL inhibition. A: Fatty acid trafficking in *Hilpda*$^{flox/flox}$ and *Hilpda*$^{\Delta M\Phi}$ BMDMs lipid loaded with oleate and BODIPY FL for 5 or 24h. B: BODIPY staining in *Hilpda*$^{flox/flox}$ and *Hilpda*$^{\Delta M\Phi}$ BMDMs lipid loaded with oleate:palmitate for 24h, treated with 20μM Atglistatin or vehicle. C: Fatty acid trafficking in *Hilpda*$^{flox/flox}$ and *Hilpda*$^{\Delta M\Phi}$ BMDMs lipid loaded with oleate and BODIPY FL for 24h, treated with 20μM Atglistatin or vehicle. D. Protein expression of selected lipid droplet-associated proteins in *Hilpda*$^{flox/flox}$ and *Hilpda*$^{\Delta M\Phi}$ BMDMs lipid loaded with oleate:palmitate or BSA for 12h. See also figure S3. LD: lipid droplet.

HILPDA deficiency promotes respiration

It could be expected that if lipolysis is enhanced, the free fatty acid levels in the cell may rise, thereby stimulating fatty acid-dependent gene regulation. Consistent with this notion, the expression of fatty acid-inducible *Gdf15*, *Cpt1a* and *Il7r* was significantly higher in lipid-loaded *Hilpda*$^{\Delta M\Phi}$ than *Hilpda*$^{flox/flox}$ BMDMs (Fig 5A). To analyze this further, we performed transcriptomics on *Hilpda*$^{\Delta M\Phi}$ and *Hilpda*$^{flox/flox}$ BMDMs loaded with oleate:palmitate for 24h and co-analyzed the data together with a transcriptomics dataset of Robblee et al. on wild-type BMDMs loaded with stearate for 20h (Robblee et al., 2016), as well as with the transcriptomics dataset of adipose tissue macrophages from obese and lean mice. In line with enhanced fatty acid-dependent gene regulation in *Hilpda*-deficient macrophages, genes that were highly upregulated after stearate in wild-type BMDMs, such as *Gdf15, Il7r* and *Ddit3*, were also higher in fatty acid loaded *Hilpda*$^{\Delta M\Phi}$ than *Hilpda*$^{flox/flox}$ BMDMs (Fig 5B). In addition, pro-inflammatory genes such as *Ccl2* and *Il1b* were downregulated by stearate in wild-type BMDMs and were also lower in fatty acid-loaded *Hilpda*$^{\Delta M\Phi}$ compared to *Hilpda*$^{flox/flox}$ BMDMs. Interestingly, genes induced by obesity in adipose tissue macrophages, such as *Lpl*, *Lipa*, and *Itgax*, were only weakly regulated by stearate and by HILPDA deficiency, suggesting distinct regulatory mechanisms (Fig 5B).

Of the 6600 genes that passed the expression threshold, only 49 were induced more than 2-fold in fatty acid-loaded *Hilpda*$^{\Delta M\Phi}$ compared to *Hilpda*$^{flox/flox}$ BMDMs. The limited effect of impaired triglyceride retention in *Hilpda*$^{\Delta M\Phi}$ BMDMs suggests that the excess fatty acids may be disposed of, for instance by enhanced oxidation. To explore that option, cellular respiration was determined in fatty acid-loaded *Hilpda*$^{\Delta M\Phi}$ and *Hilpda*$^{flox/flox}$ BMDMs. As a marker for oxidative phosphorylation, oxygen consumption of fatty acid-loaded *Hilpda*$^{\Delta M\Phi}$ and *Hilpda*$^{flox/flox}$ BMDMs was measured by extracellular flux analysis during a mitochondrial stress test (Fig 5C). After 6 hours of oleate:palmitate loading, basal and maximal respiration were slightly lower in *Hilpda*$^{\Delta M\Phi}$ than *Hilpda*$^{flox/flox}$ BMDMs (Fig 5D). Remarkably, however, after 24h fatty acid loading, basal and maximal respiration were significantly higher in *Hilpda*$^{\Delta M\Phi}$ compared to *Hilpda*$^{flox/flox}$ BMDMs (Fig 5D), indicating an increased maximal

oxidative capacity. These data suggest that the enhanced lipolysis in *Hilpda*$^{\Delta M\Phi}$ BMDMs is accompanied by increased fatty acid oxidation through oxidative phosphorylation.

Next we tested whether HILPDA might influence lipid droplet accumulation in macrophages in adipose tissue. To mimic the adipose environment in vitro, BMDMs were treated with conditioned medium of adipose tissue explants. Adipose-conditioned medium markedly increased *Hilpda* expression, along with that of several other lipid sensitive genes, such as Plin2, Cd36 and Angptl4 (Fig 5E). Consistent with our previous studies with fatty acid-loaded macrophages, *Hilpda*$^{\Delta M\Phi}$ BMDMs incubated with adipose-conditioned medium showed substantially reduced BODIPY staining compared with *Hilpda*$^{flox/flox}$ BMDMs (Fig 5F). These data suggest that HILPDA may also influence lipid droplet accumulation in macrophages in adipose tissue.

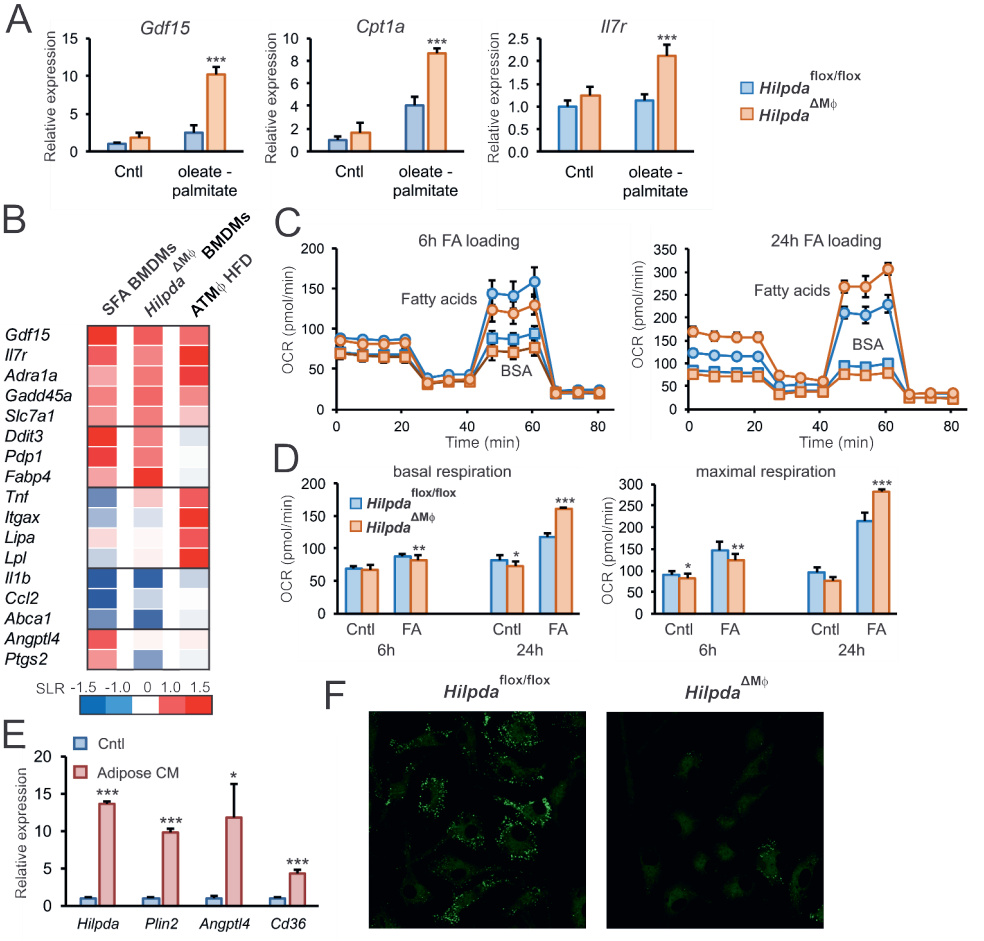

Figure 5 Lack of ATGL inhibition by HILPDA does not affect lipid-induced inflammation, but increases oxidative respiration. A: Gene expression of *Gdf15, Cpt1a*, *Il7r* and *Fabp4* in *Hilpda*$^{flox/flox}$ and *Hilpda*$^{\Delta M\Phi}$ BMDMs lipid loaded with oleate:palmitate or BSA (Cntl) for 12h (n=3). B: Microarray-based gene expression of relevant genes in WT C57Bl/6 mouse BMDMs loaded with stearate (250μM) for 20h, *Hilpda*$^{\Delta M\Phi}$ BMDMs loaded with oleate:palmitate for 24h and adipose tissue macrophages isolated from mice fed a HFD vs LFD. Oxygen consumption rate of *Hilpda*$^{flox/flox}$ and *Hilpda*$^{\Delta M\Phi}$ lipid loaded with oleate:palmitate or BSA (cntl) for 6 or 24h (C) and corresponding basal and maximal respiration levels (D). Data are representative of three independent experiments. Gene expression levels of *Hilpda*, *Plin2*, *Angptl4* and *Cd36* in C57Bl/6 mouse BMDMs loaded with adipose-conditioned medium (CM) or control medium (cntl) for 6h (E) and BODIPY staining after loading with CM for 24h (F) (n=3). Bar graphs are presented as mean ±SD. Statistical testing was performed by Student's t-test or by two-way ANOVA followed by Bonferroni's post hoc multiple comparisons test. The effect of treatment was significant in A and D. *P<0.05, **P≤0.01, ***P≤0.001. FA: fatty acid loading with oleate:palmitate. SLR, signal log ratio.

Myeloid-specific deficiency of *Hilpda* decreases lipid droplets in ATMs without altering adipose tissue inflammation

To enable studying the effect on HILPDA deficiency in macrophages in vivo, we used *Hilpda*$^{\Delta M\Phi}$ mice and their *Hilpda*$^{flox/flox}$ littermates. As expected, myeloid-specific inactivation of *Hilpda* significantly decreased *Hilpda* expression in the stromal vascular fraction of adipose tissue, but not in the adipocyte fraction (Fig 6A). To test the functional consequences of macrophage HILPDA deficiency in the context of obesity-induced adipose tissue inflammation and foam cell formation, *Hilpda*$^{\Delta M\Phi}$ mice and their *Hilpda*$^{flox/flox}$ littermates were rendered obese and insulin resistant by high fat feeding for 20 weeks, using a low fat diet as control. Bodyweight gain (Fig 6B), feed intake (Fig 6C), and liver and adipose tissue weights (Fig 6D) were not different between *Hilpda*$^{\Delta M\Phi}$ and *Hilpda*$^{flox/flox}$ littermates. Consistent with the data shown in Fig 1C, high fat feeding increased *Hilpda* mRNA in adipose tissue. Interestingly, the relative increase in *Hilpda* mRNA was considerably lower in *Hilpda*$^{\Delta M\Phi}$ than in *Hilpda*$^{flox/flox}$ adipose tissue (Fig 6E), suggesting that the increase in *Hilpda* expression by high fat feeding is mainly driven by its expression in macrophages. Immunoblot for HILPDA confirmed this notion by showing markedly reduced HILPDA protein levels in *Hilpda*$^{\Delta M\Phi}$ versus *Hilpda*$^{flox/flox}$ adipose tissue (Fig 6F).

Based on the studies in BMDMs, we hypothesized that lipid accumulation would be reduced in adipose tissue macrophages from *Hilpda*$^{\Delta M\Phi}$ mice compared to *Hilpda*$^{flox/flox}$ mice. Indeed, Oil Red O staining showed significantly lower lipid droplet content in adipose tissue macrophages isolated from HFD-fed *Hilpda*$^{\Delta M\Phi}$ mice compared with HFD-fed *Hilpda*$^{flox/flox}$ mice (Fig 7A, B). Interestingly, however, the decrease in lipid droplets was not associated with any change in the secretion of the classical inflammatory cytokines IL6 and TNFα (Fig 7C). These data indicate that HILPDA deficiency reduces lipid accumulation in adipose tissue macrophages but does not have any effect on their ex vivo inflammatory properties.

To investigate the potential impact of macrophage HILPDA on adipose tissue inflammation in vivo, we performed flow cytometry analysis of the stromal vascular fraction isolated from the adipose tissue of the various groups of mice. The results showed an increased percentage of populations of CD45+, CD11b+CD206+ and CD11b+CD11c+ cells by high fat feeding, but no clear differences in the percentages of these populations between *Hilpda*$^{\Delta M\Phi}$ and *Hilpda*$^{flox/flox}$ mice (Fig 7D). To further examine the influence of macrophage HILPDA deficiency on inflammation in adipose tissue, we determined the expression of selected genes. Interestingly, mRNA levels of both inflammatory macrophage marker Itgax (Cd11c) and general macrophage marker Cd68 were significantly lower in adipose tissue of *Hilpda*$^{\Delta M\Phi}$ mice versus *Hilpda*$^{flox/flox}$ mice fed a HFD (Fig 7E), while the general macrophage marker Adgre1 (F4/80) showed a trend towards a decreased expression (Fig S4). Despite being induced by high fat feeding, adipose expression of other pro- or anti-inflammatory genes, such as Gdf15, Il10, Arg1, Ccl2 and Il1ra, was not significantly different between *Hilpda*$^{\Delta M\Phi}$ and *Hilpda*$^{flox/flox}$ mice (Fig S4). Expression of Adipoq and Leptin also was not different between *Hilpda*$^{\Delta M\Phi}$ and *Hilpda*$^{flox/flox}$ mice (Fig S4).

To further investigate the inflammatory status of adipose tissue, the density of crown-like structures was determined in adipose tissue of *Hilpda*$^{\Delta M\Phi}$ and *Hilpda*$^{flox/flox}$ mice fed a HFD. A trend towards lower density was found in the *Hilpda*$^{\Delta M\Phi}$ mice (Fig 7F), which, however, did not reach statistical significance (Fig 7G). Additionally, we measured the ex vivo release of cytokines from adipose tissue explants. While high fat feeding stimulated the release of IL10 and IL6, no significant difference in IL10 and IL6 release was observed between adipose tissue explants from *Hilpda*$^{\Delta M\Phi}$ and *Hilpda*$^{flox/flox}$ mice (Fig 7H).

Finally, to determine whether macrophage HILPDA deficiency has any influence on obesity-induced metabolic derailments, we measured plasma metabolic parameters and assessed glucose tolerance in *Hilpda*$^{\Delta M\Phi}$ and *Hilpda*$^{flox/flox}$ mice fed the low and high fat diets. High fat feeding significantly increased plasma levels of cholesterol, triglycerides, glucose, non-esterified fatty acids, leptin, and insulin (Fig S5). However, no difference in these parameters were observed between *Hilpda*$^{\Delta M\Phi}$ and *Hilpda*$^{flox/flox}$ mice, either on a low or high fat diet (Fig S5). Similarly, although high fat feeding caused a marked decrease in glucose tolerance, no differences were observed between *Hilpda*$^{\Delta M\Phi}$ and *Hilpda*$^{flox/flox}$ mice (Fig 7I).

Collectively, our data indicate that myeloid-specific HILPDA deficiency reduces lipid droplet accumulation in adipose tissue macrophages, yet does not influence the inflammatory status of adipose tissue, nor does it have any effect on obesity-induced metabolic complications.

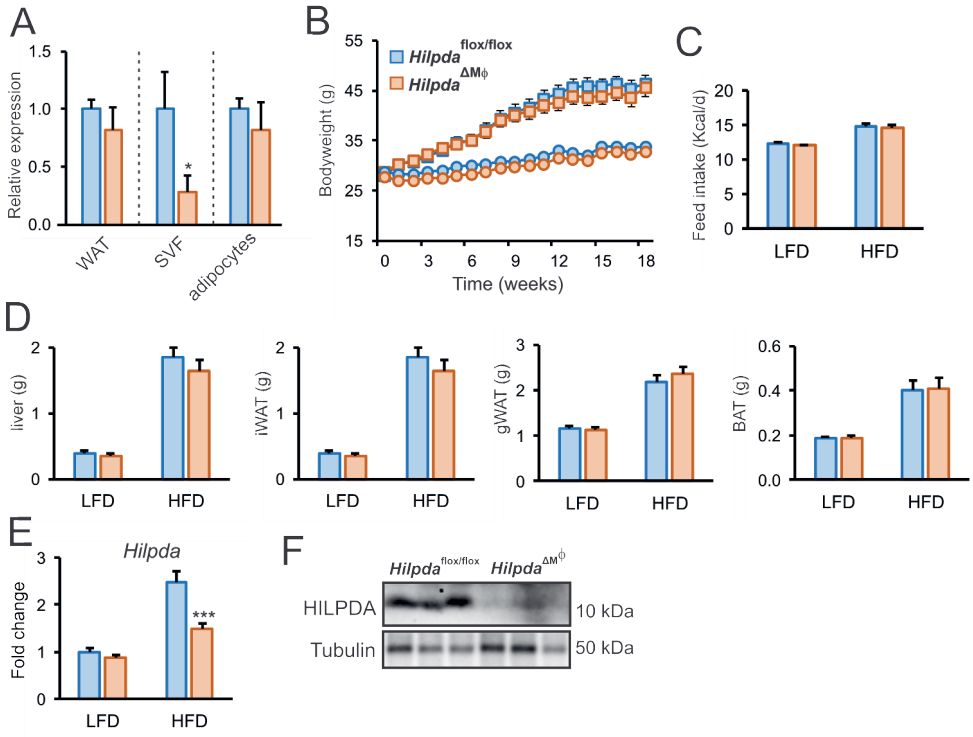

Figure 6 *Hilpda* deficiency in myeloid cells results in a decrease in HILPDA in gWAT after high fat feeding, without influencing body and organ weight. A: Relative gene expression of *Hilpda* in whole gWAT, stromal vascular fraction and adipocyte fraction of *Hilpda*$^{flox/flox}$ and *Hilpda*$^{\Delta M\Phi}$ (n=3-7). Body weight (B), feed intake (C) and weight of liver, iWAT, gWAT and BAT (D) in *Hilpda*$^{flox/flox}$ and *Hilpda*$^{\Delta M\Phi}$ mice fed a LFD or HFD for 20 weeks. *Hilpda* gene expression in gWAT (E) and HILPDA protein expression in gWAT (F). Bar graphs are presented as mean ±SEM, (n = 10-12 mice per group). Statistical testing was performed by Student's t-test or by two-way ANOVA followed by Bonferroni's post hoc multiple comparisons test. The effect of diet was significant in C, D and E. *P<0.05, ***P≤0.001. WAT: white adipose tissue, SVF: stromal vascular fraction, LFD: low fat diet, HFD: high fat diet, iWAT: inguinal adipose tissue, gWAT: gonadal adipose tissue, BAT: brown adipose tissue.

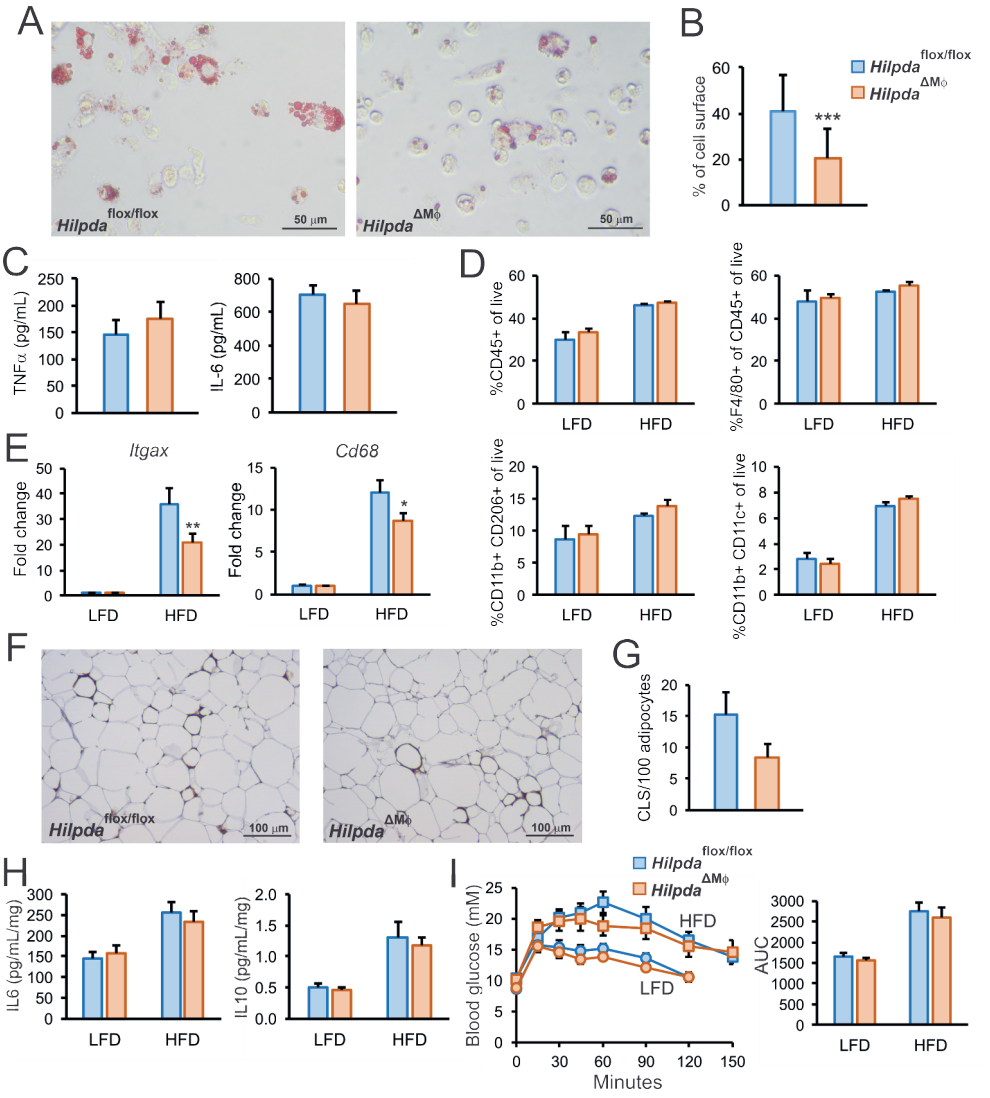

Figure 7 Myeloid-specific deficiency of *Hilpda* decreases lipid droplets in ATMs without altering adipose tissue inflammation or glucose tolerance. Oil red O staining of adipose tissue macrophages isolated from *Hilpda*$^{flox/flox}$ and *Hilpda*$^{\Delta M\Phi}$ mice fed a HFD for 20 weeks (A and B). Data are mean ±SD. C: Corrected TNFα and IL6 secretion of adipose tissue macrophages from *Hilpda*$^{flox/flox}$ and *Hilpda*$^{\Delta M\Phi}$ mice fed a HFD for 20 weeks (n=10-12 per group, pooled per 3-4). D: Flow cytometry based percentages of CD45+, CD45+F4/80+, CD11b+CD206+ and CD11b+CD11c+ populations in the SVF of gWAT from *Hilpda*$^{flox/flox}$ and *Hilpda*$^{\Delta M\Phi}$ mice (n=10-12, pooled per 3-4). Gene expression of *Itgax*, *Adgre1*, *Cd68*, *Ccl2*, *Il10*, *Il1ra* (E), see also figure S4. Density of CLSs in gWAT coupes stained for F4/80 (F and G, only for HFD) and secretion of IL6 and IL10 (H) in gWAT explants (n=10-12 per group). I: Glucose tolerance test after 18 weeks of LFD or HFD feeding, see also figure S5. Bar graphs are presented as mean ±SEM, (n=10-12 mice per group). Statistical testing was performed by Student's t-test or by two-way ANOVA followed by Bonferroni's post hoc multiple comparisons test. The effect of diet was significant in D, E, H and the AUCs of I. *P<0.05, **P≤0.01, ***P≤0.001. LFD: low fat diet, HFD: high fat diet, CLS: crown-like structure, AUC: Area under the curve.

Discussion

Here we show that HILPDA deficiency in macrophages disrupts stable lipid droplet formation after lipid loading. The reduction in lipid droplets is caused by impaired retention of lipids due to elevated ATGL-mediated lipolysis, which in turn is associated with increased oxidative metabolism (Fig S6). Overall, our data demonstrate that HILPDA is an endogenous and physiological inhibitor of ATGL in macrophages. Strikingly, despite reducing lipid storage in adipose tissue macrophages, HILPDA deficiency in macrophages does not alter the inflammatory status of adipose tissue in diet-induced obesity, arguing against the notion that lipid droplet accumulation in adipose tissue macrophages promotes adipose tissue inflammation and associated metabolic complications such as insulin resistance.

During obesity, macrophages infiltrate the adipose tissue and take up adipocyte-released lipids. The resulting lipid-laden macrophages are found in crown-like structures in murine and human obesity (Lumeng et al., 2008; Prieur et al., 2011; Shapiro et al., 2013). These macrophages form a distinct subpopulation with a characteristic activation that is likely triggered by the adipocyte-released lipids (Kratz et al., 2014; Coats et al., 2017; Hill et al., 2018). Inasmuch as lipid droplet formation often serves as a cytoprotective mechanism to prevent lipotoxicity by lipid intermediates or free fatty acids (Saraswathi and Hasty, 2009), it could be hypothesized that the enhanced lipid droplet breakdown in HILPDA-deficient macrophages may result in elevated inflammation. However, HILPDA deficiency not only reduced intracellular triglyceride levels but also the levels of potentially lipotoxic intermediates, such as diacylglycerols, likely via enhanced fatty acid oxidation, which may be predicted to lead to reduced inflammation (Namgaladze and Brüne, 2016). Intriguingly, however, no clear effect of HILPDA deficiency was observed on cytokine release by adipose tissue macrophages, on the percentage of different macrophage populations in adipose tissue, on inflammatory gene expression in adipose tissue, and on cytokine release by adipose tissue explants. Also, genes typically elevated in adipose tissue macrophages of obese mice, such as Lipa, Lpl, and Itgax, were not induced by fatty acid loading or altered by HILPDA deficiency. The data argue against the notion that excessive lipid droplet accumulation in adipose tissue macrophages is the major driver of adipose tissue inflammation and of the composition of macrophage populations in obese adipose tissue. Rather, the unique profile of adipose tissue macrophages may be determined by other factors active in the obese adipose tissue environment, the identity of which requires further study.

As indicated above, HILPDA-deficient macrophages exhibited a marked decrease in intracellular levels of all the major lipid species, including triglycerides, diacylglycerols, phosphatidic acids, and cholesteryl-esters, likely due to enhanced fatty acid oxidation. Previously, a strong link was made between ATGL activity and fatty acid oxidation in liver

and heart. It was found that ATGL-mediated lipolysis activates a transcriptional network involving PGC-1α/PPAR-α that controls fatty acid oxidation and mitochondrial biogenesis (Reid et al., 2008; Sapiro et al., 2009; Haemmerle et al., 2011; Ong et al., 2011). Accordingly, it is likely that the loss of ATGL inhibition is directly responsible for the enhanced oxidative capacity, reducing the total intracellular lipid levels. In general, increased lipolysis and increased oxidative respiration are two traits essential for macrophage polarization towards alternative, M2-like phenotypes, which may be protective in the context of adipose tissue inflammation (Huang et al., 2014; Van den Bossche et al., 2016; Jung et al., 2018). In our experiments, increased oxidative respiration seemed a mere consequence following overactive ATGL-mediated lipolysis, and did not contribute to any anti-inflammatory effects. Although increased oxidation of fatty acids is often proposed as an alternative cytoprotective pathway in lipid-laden macrophages, the interplay between fatty acid oxidation, concomitant ROS formation, and ER stress complicates this mechanism (Namgaladze and Brüne, 2016).

Apart from fatty acid oxidation, ATGL has also been linked to the autophagic degradation of lipid droplets, termed lipophagy (Sathyanarayan, Mashek and Mashek, 2017). It was suggested that ATGL acts as a signaling node to promote lipophagy, which then controls bulk lipid droplet breakdown. Whether HILPDA, via ATGL, connects to lipophagy requires further study.

In contrast to the cytoprotective effect of normal lipid droplet formation, the adverse effects of excessive triglyceride storage becomes apparent in ATGL-/- macrophages, underlining the importance of functional ATGL in macrophages (Chandak et al., 2010; Aflaki, Balenga, et al., 2011; Aflaki, Radović, et al., 2011; Aflaki et al., 2012). Indeed, the elevated triglyceride accumulation in ATGL-/- macrophages is accompanied by mitochondrial dysfunction and apoptosis, ER stress, reduced macrophage migration, and decreased phagocytosis ability (Chandak et al., 2010; Aflaki, Balenga, et al., 2011; Aflaki, Radović, et al., 2011; Aflaki et al., 2012), suggesting that proper macrophage function is dependent on the liberation of free fatty acids from intracellular triglyceride stores. The ATGL-mediated release of fatty acids is also necessary for the production of lipid mediators, at least in neutrophils (Schlager et al., 2015). Similar to ATGL-/- macrophages, macrophages deficient in the ATGL activator CGI-58 (a.k.a. ABHD5) also have elevated lipid storage and decreased phagocytic capacity, yet show no signs of mitochondrial apoptosis and ER stress, suggesting that triglyceride accumulation per se does not drive mitochondrial dysfunction (Goeritzer et al., 2014). Our data show that HILPDA deficiency, despite leading to markedly reduced lipid storage, raises markers of ER stress, suggesting that triglyceride storage protects against lipid-induced ER stress. Presumably, the mechanism leading to ER stress is different in HILPDA-deficient macrophages as compared with ATGL/CGI-58-deficient macrophages.

HILPDA was initially identified in a screen for hypoxia-inducible genes in human cervical cancer cells and was later found to be associated with lipid droplets (Denko et al., 2000; Gimm et al., 2010). We identified *Hilpda* as a novel PPARα target gene in liver (Mattijssen et al., 2014). In addition, *Hilpda* is well expressed in adipocytes (DiStefano et al., 2016; Dijk et al., 2017). Several studies have shown that overexpression of *Hilpda* increases intracellular lipid storage in cells (Gimm et al., 2010; Mattijssen et al., 2014; Dijk et al., 2017). In the present study, *Hilpda* emerged from a screen for genes elevated by obesity in adipose tissue macrophages and upregulated in macrophages by fatty acids. Induction of HILPDA by fatty acids and subsequent inhibition of triglyceride hydrolysis is likely part of a lipid buffering effort of the cell to effectively store excess energy and neutralize the potentially reactive free fatty acids (Fig S6).

The observation that the decrease in lipid storage in HILPDA-deficient macrophages can be almost completely abolished by inhibition of ATGL indicates that HILPDA is an endogenous inhibitor of ATGL in macrophages, which is in line with previous data showing direct inhibition of ATGL by HILPDA (Zhang et al., 2017; Padmanabha Das et al., 2018). Intriguingly, HILPDA reduced ATGL protein levels in BMDMs, which supports our previous finding that HILPDA reduces ATGL protein levels in 3T3-L1 adipocytes (Dijk et al., 2017). It can be hypothesized that binding of HILPDA to ATGL might destabilize it, leading to enhanced ATGL degradation. This option should be investigated in future experiments. Of note, our observation that forced upregulation of HILPDA levels in macrophages does not noticeably increase lipid droplet accumulation suggests that inhibition of ATGL is nearly maxed out in lipid-loaded macrophages.

The inhibition of ATGL by HILPDA is analogous to the inhibition by G0/G1 switch gene 2 (G0S2), with which HILPDA shares extensive sequence homology (Yang et al., 2010; Zhang et al., 2017; Padmanabha Das et al., 2018). However, the inhibitory potency of HILPDA was low compared to G0S2, which raised questions on the physiological relevance of HILPDA as ATGL inhibitor. Our studies demonstrate that HILPDA is a potent endogenous inhibitor of ATGL-mediated lipolysis in macrophages. A number of questions emerge from this work. First, why does HILPDA, despite allegedly being a much weaker ATGL inhibitor than G0S2, have such a marked influence on lipid storage in macrophages? We hypothesize that HILPDA may require an interaction with an auxiliary factor for full activity. Further research is necessary to identify the mechanism for the differential potency of HILPDA in cell-free systems compared to live cells. Second, what is the reason for having two related ATGL inhibitors? Although our preliminary data suggest that HILPDA is much more abundant in BMDMs than G0S2, it seems that at least in certain cells, such as cultured hepatocytes, HILPDA and G0S2 co-exist. Inasmuch as HILPDA and G0S2 are induced by different stimuli, they may be active under different circumstances. So far there is no evidence for any functional dependency between the two proteins. Further research is necessary to better

characterize the relationship and relative roles of these two homologous proteins in different cell types.

In conclusion, our data demonstrate that HILPDA is a lipid-inducible physiological inhibitor of ATGL-mediated lipolysis in macrophages. In obese mice, HILPDA uncouples lipid droplet accumulation in adipose tissue macrophages from inflammation and metabolic dysregulation. Overall, our data question the importance of lipid storage in adipose tissue macrophages in obesity-induced inflammation and metabolic dysregulation.

Acknowledgements

We would like to thank Shohreh Keshtkar, Karin Mudde, Jenny Jansen, Anneke Hijmans, Tessa de Bie and Jacqueline Ratter for their technical assistance. This work was financed by grants from the Netherlands Organisation of Scientific Research (2014/12393/ALW), the Dutch Diabetes Foundation (2015.82.1824), and the Netherlands Heart Foundation (ENERGISE grant CVON2014-02).

Author contributions

X.v.D., M.d.l.R, A.G., F.M., W.D., J.B. R.St. and S.K. conceived and planned the research and experiments. X.v.D. carried out the *Hilpda*$^{\Delta M\Phi}$ mouse studies. X.v.D., M.d.l.R., A.G., F.M. and W.D. carried out the experiments and analyzed the data. M.v.W. carried out the lipidomics analysis. R.Si. and J.B. contributed to the interpretation of the results. X.v.D. carried out the statistical analyses. X.v.D., R.St. and S.K. wrote the manuscript. All authors provided critical feedback and helped to shape the research, analysis and manuscript. Co-first author order was determined by contribution.

Declaration of interests

The authors declare no competing interests.

Star methods

Lead contact and materials availability

Further information and requests for resources should be directed to and will be fulfilled by the Lead Contact, Sander Kersten (sander.kersten@wur.nl). This study did not generate new unique reagents.

Experimental model and subject details

Animal studies

Studies were performed using purebred wildtype C57BL/6 mice, *Hilpda*$^{\Delta M\Phi}$ mice and their *Hilpda*$^{flox/flox}$ littermates. *Hilpda*$^{flox/flox}$ were acquired (Jackson Laboratories, Bar Harbor, ME; *Hilpda*tm1.1Nat/J, JAX: #017360, RRID: MGI:5285399) and backcrossed onto a C57Bl/6 background in our facility for at least 5 generations. LysM-Cre transgenic mice (B6.129P2-Lyz2tm1(cre)Ifo/J, JAX:#004781, RRID: IMSR_JAX:004781) were acquired from Jackson laboratories. Prior to arrival at Jackson laboratories, the lysM-Cre transgenic mice have been backcrossed onto a C57BL/6 background for at least six generations. In our facility, the *Hilpda*$^{flox/flox}$ were crossed with lysM-Cre transgenic mice to generate mice with a mature myeloid cell-specific Cre-mediated deletion of *Hilpda* on a C57BL/6 background. The identity of the C57BL/6 background strain was not confirmed by sequencing. Mice were individually housed under normal light-dark cycles in temperature- and humidity-controlled specific pathogen-free conditions. Mice had ad libitum access to food and water. The experimenter was blinded to group assignments during all analyses. For in vivo studies, male mice were used with an age of 9-12 weeks. For the isolation of primary cell cultures, both male and female mice were used with an age of 8-12 weeks. All animal experiments were approved by the local animal welfare committee of Wageningen University (AVD104002015236, 2016.W-0093.001).

Cell lines and primary cultures

RAW264.7 macrophage cells (Cat#91062702; RRID: CVCL_0493, Sigma-Aldrich, Darmstadt, Germany) and bone-marrow derived macrophages were cultured in Dulbecco's modified Eagle's medium (DMEM, Corning, NY, USA), supplemented with 1% penicillin/streptomycin (P/S, Corning). Adipose tissue macrophages and peritoneal macrophages were cultured in Roswell Park Memorial Institute (RPMI)-1630 medium (Lonza, Basel, Zwitserland) supplemented with 10% FCS and 1% P/S. All cells were kept in incubators at 37°C/5% CO2. Primary cell cultures were isolated from male and female wildtype C57Bl/6, *Hilpda*$^{\Delta M\Phi}$ and

Hilpda$^{flox/flox}$ mice aged 8-12 weeks. RAW264.7 macrophages were purchased as authenticated cell line from Sigma-Aldrich.

Method details

Mouse studies

Per genotype, 12 male *Hilpda*$^{\Delta M\Phi}$ mice aged 9-12 weeks or their male *Hilpda*$^{flox/flox}$ littermates were randomly allocated using an online randomisation tool to either a standardized high fat diet or a low fat diet (formula D12451 and formula D12450H respectively, Research Diets, New Brunswick, USA; γ-irradiated with 10-20 kGy) for 20 weeks. Body weight and feed intake were assessed weekly. At the end of the study, mice were anaesthetised with isoflurane and blood was collected via orbital puncture in tubes containing EDTA (Sarstedt, Nümbrecht, Germany). Subsequently, mice were immediately euthanized by cervical dislocation, after which tissues were excised, weighed and frozen in liquid nitrogen or prepared for histology. Frozen samples were stored at -80°C.

Intraperitoneal glucose tolerance test

In the HFD-LFD study, an intraperitoneal glucose tolerance test was performed after 18 weeks. Mice were fasted for 5 hours and blood was collected via tail bleeding at 0, 15, 30, 45, 60, 90 and 120 minutes after i.p. injection of 1g/kg bodyweight glucose (Baxter, Deerfield, IL, USA). Blood glucose was measured with a GLUCOFIX Tech glucometer and glucose sensor test strips (GLUCOFIX Tech, Menarini Diagnostics, Valkenswaard, The Netherlands). A time point of 150 minutes after injection of glucose was added for the high fat diet fed groups.

Plasma measurements

Blood collected in EDTA tubes was spun down for 15 minutes at 5000 RPM at 4°C. Plasma was aliquoted and stored at -80°C until measurement of cholesterol (Liquicolor, Human GmbH, Wiesbaden, Germany), triglycerides (Liquicolor), glucose (Liquicolor), NEFAs (NEFA-HR set R1, R2 and standard, WAKO Diagnostics, Instruchemie, Delfzijl, The Netherlands), adiponectin (ELISA duoset kit, R&D Systems, Bio-techne, MN, USA), leptin (ELISA duoset kit, R&D Systems) and insulin (ultra-sensitive mouse insulin ELISA kit, Crystal Chem Inc., IL, USA) following manufacturer's instructions.

gWAT explants and adipose macrophage isolation

For SVF, adipocytes and adipose tissue macrophages isolation, gonadal adipose tissue (gWAT) was collected and kept in with DMEM supplemented with 1% P/S and 1% FFA-free Bovine Serum Albumin (BSA fraction V, Roche via Merck, Darmstadt, Germany) on ice. gWAT explants were taken into culture for 24h in DMEM, supplemented with 10% fetal calf serum (FCS, BioWest, Nuaillé, France) and 1% P/S. Supernatant was stored for ELISA measurements or as conditioned medium. For high fat diet groups, the stromal vascular fractions were isolated by digesting gWAT for 45 minutes in Roswell Park Memorial Institute (RPMI)-1630 medium (Lonza, Basel, Zwitserland) supplemented with 10% FCS, 1% P/S, 0.5% FFA-free BSA, 1M CaCl2, 1M HEPES and 0.15% collagenase (from Clostridium histolyticum, Sigma-Aldrich, Cat#C6885; CAS: 9001-12-1). Per three mice of the same group, gWAT was pooled after digestion, filtered through a 100µm cell strainer and centrifuged at 200g for 10 min. Floating mature adipocytes were removed and stored separately and stromal vascular pellet was resuspended in erythrocyte lysis buffer and subsequently washed twice in phosphate buffered saline (PBS, Corning) supplemented with 0.5% FFA-free BSA and 2mM EDTA. Resulting stromal vascular fractions were used to isolate ATMs using mouse anti-F4/80-FITC antibodies (Cat#130-117-509; RRID: AB_2727970, Miltenyi Biotec, Bergisch Gladbach, Germany), anti-FITC MicroBeads (Cat#130-048-701; RRID: AB_244371, Miltenyi Biotec) and MS columns (Miltenyi Biotec) on an OctoMACS™ Cell Separator system (Miltenyi Biotec). ATMs were cultured for 24h in RPMI-1630 supplemented with 10% FCS and 1% P/S. ATMs were either cultured for 2h after which cells were washed with PBS, fixed in 3.7% paraformaldehyde and stained with Oil red O following standard protocols, or were cultured for 24h to obtain supernatants.

Flow cytometry of SVF

Before isolation of ATMs, SVF pools were resuspended in PBS containing 0.5% BSA and 2mM EDTA and 500 000 cells were sampled and stained with antibodies against CD45-ECD (Cat#A07784, Beckman Coulter, Brea, CA, USA), F4/80-FITC (Cat#123107; RRID: AB_893500), CD206-APC (Cat#141707; RRID: AB_10896057), CD11c-PE-Cy7 (Cat#117317; RRID: AB_493569) and CD11b-PE (Cat#101207; RRID: AB_312790, Biolegend, San Diego, CA, USA). Samples were measured on a flow cytometer (FC500, Beckman Coulter) and results were analyzed using Kaluza analysis software 2.1 (RRID: SCR_016182, Beckman Coulter).

Histological studies

Samples of gWAT for histological analysis were fixed in 3.7% paraformaldehyde immediately upon collection, embedded in paraffin, sectioned and stained with hematoxylin eosin according to standard protocols. After preincubation with 20% normal goat serum, paraffin-embedded sections were incubated at 4°C overnight with antibodies for F4/80 (Cat#MCA497G; RRID: AB_872005, Bio-Rad Laboratories, Hercules, CA, USA), HILPDA (sc-137518 HIG2 Antibody (C-14); RRID: AB_2011522, Santa-Cruz Biotechnology, Dallas, TX, USA Biotechnology) or CD68 (Cat#MCA1957; RRID: AB_322219, AbD Serotec, Bio-Rad Laboratories) dissolved in PBS supplemented with 1% BSA (Merck). Anti-rat or anti-rabbit IgG conjugated to HRP (Cell Signaling Technology, Danvers, MA, USA) were used as secondary antibody. Negative controls were prepared without using primary antibody.

Peritoneal macrophages and BMDMs

To harvest peritoneal macrophages, 8-12 week old WT C57Bl/6 mice were injected intraperitoneally with 1mL 4% thioglycolic acid. Three days post-injection, mice were anesthetised with isoflurane and euthanized by CO2. Peritoneal cells were harvested by washing the peritoneal cavity with ice-cold RPMI-1630 supplemented with 10% heat-inactivated FCS (BioWest) and 1% P/S. Cells were plated after lysis of erythrocytes and non-adherent cells were washed away three hours post plating. To isolate BMDMs, 8-12 week old *Hilpda*$^{\Delta M\Phi}$ mice and their *Hilpda*$^{flox/flox}$ littermates were euthanized by cervical dislocation. Both femurs and hind legs were isolated at the hip joint, keeping femur and tibia intact. Bone marrow was extracted from the femur and tibia and differentiated in DMEM, supplemented with 10% FCS, 1% P/S and 15% L929 conditioned medium. After seven days of differentiation, BMDMs were scraped and plated as appropriate.

Cell culture experiments

RAW 264.7 macrophage cells (Cat#91062702; RRID: CVCL_0493, Sigma-Aldrich) were cultured in DMEM supplemented with 10% FCS and 1% P/S. Overexpression of *Hilpda* was achieved by transfection with an adenoviral construct containing either *Hilpda* (Ad-m-2310016C08RIK, ADV-250639, Vector Biolabs, Malvern, USA) or GFP (Ad-GFP, Cat#1060, Vector Biolabs, Malvern, USA) in a dose of 500 MOI for 48 hours. Palmitate (Cat#P0500; CAS: 57-10-3, Sigma-Aldrich) and oleate (Cat#O1008; CAS: 112-80-1, Sigma-Aldrich) were solubilized using EtOH and KOH and conjugated to FFA-free BSA in sterile water (Versol, Aguettant, Lyon, France) at 37°C for 30 min. Palmitate was used in concentrations of 200, 250 or 500µM. Oleate was used in a concentration of 250µM or 400µM together with 20

µM BODIPY-FL C12 (Cat#D3822, ThermoFisher Scientific, MA, USA) for fatty acid trafficking experiments. A mixture of oleate and palmitate (oleate:palmitate) was made in a ratio of 1:2 and used in a final concentration of 600 µM. Intralipid (Fresenius Kabi AB, Uppsala, Sweden) was used in a concentration of 1 or 2mM. The addition of 100µM iron chelator 2,2'-bipyridyl (Cat#D216305; CAS: 366-18-7, Sigma-Aldrich) was used to chemically mimic hypoxia. Atglistatin (Cat#SML1075, Sigma-Aldrich) was used in a concentration of 20µM in 100% DMSO and cells were pre-treated for 2 hours before fatty acid loading. 24 hour treatments containing Atglistatin were refreshed every 12 hours. All cells were washed with PBS (Corning) after treatment. BMDMs were stained with Oil Red O following standard procedures.

Confocal Imaging

To visualise fatty acid uptake, accumulation and trafficking, BMDMs were plated on 8-well µ glass bottom slides (Ibidi, Martinsried, Germany). Confocal imaging was performed on a Leica confocal TCS SP8 X system equipped with a 63× 1.20 NA water-immersion objective lens. Images were acquired using 1,024 × 1,024 pixels with pinhole set at 1 Airy Unit (AU). Excitation of the fluorescent probes used in this study was performed using white light laser (WLL, 50% laser output) selecting the 488 nm laser line. Fluorescence emission was detected using internal Hybrid (HyD) detector selecting a spectral window from either 520 - 580 nm (fatty acid uptake) or from 510 – 565 nm (fatty acid trafficking).

Fatty acid trafficking was assessed after lipid loading for 5h and 24h with 400 µM oleate and 20 µM BODIPY® FL C12, treated either with vehicle or Atglistatin. The WLL laser line (488 nm) was set at a laser power of 1.6% for 5 h incubated cells and 0.3% for 24 h incubated cells. Cells were washed with PBS, fixed for 15 min with 3.7% formaldehyde and mounted with Vectashield-H (Vector Laboratories, Peterborough, UK). Fire LUT was applied using Fiji.

To assess fatty acid accumulation, BMDMs treated with oleate:palmitate were washed with PBS and fixed for 15 minutes with 3.7% paraformaldehyde. Fixed cells were stained with 2µg/mL BODIPY® 493/503 (Thermo Fisher Scientific) and mounted with Vectashield-H (Vector Laboratories). Images were processed and analyzed with Fiji. Briefly, images were converted to binary, watershed and LD size and number was measured with particle analysis set 0.07 µm2-infinity.

Extracellular flux assay

Extracellular flux of lipid-loaded BMDMs was measured using the Agilent Seahorse XF96 Analyzer (Agilent Technologies, Santa Clara, CA, USA). Cells were seeded in a density of 200

000 cells per well in XF-96 plates (Agilent Technologies), treated appropriately and kept in a 37°C/5% CO2 incubator. An hour before the measurement, cells were washed and cultured in Seahorse XF base medium (Agilent Technologies) without sodium bicarbonate, supplemented with 25mM glucose and 2mM L-glutamine for one hour at 37°C in a non-CO2 incubator. For the mitochondrial stress test, the following compounds were added during four injections: oligomycin (1.5µM), FCCP (1.5 µM), pyruvate (1mM), antimycin A (2.5 µM) and rotenone (1.25 µM). The oxygen consumption rate (OCR) was automatically measured by the sensor cartridge at baseline and following injections. Calculations were made using the Seahorse XF-96 software Wave Desktop 2.6 (RRID: SCR_014526, Agilent Technologies).

Real-time PCR

For cells, total RNA was isolated using TRIzol® Reagent (Invitrogen, ThermoFisher Scientific). For tissues, total RNA was isolated using the RNeasy Micro Kit (Qiagen, Venlo, The Netherlands). cDNA was synthesized from 500ng RNA using the iScript cDNA kit (Bio-Rad Laboratories, Hercules, CA, USA) according to manufacturer's instructions. Real time polymerase chain reaction (RT-PCR) was performed with the CFX96 or CFX384 Touch™ Real-Time detection system (Bio-Rad Laboratories), using a SensiMix™ (BioLine, London, UK) protocol for SYBR green reactions. Mouse 36b4 expression was used for normalization.

Immunoblotting

Cell or tissue protein lysates were separated by electrophoresis on pre-cast 4-15% polyacrylamide gels and transferred onto nitrocellulose membranes using a Trans-Blot® Semi-Dry transfer cell (all purchased from Bio-Rad Laboratories), blocked in non-fat milk and incubated overnight at 4°C with primary antibody for HILPDA (Cat#sc-137518; RRID: AB_2011522, Santa Cruz Biotechnology), ATGL (Cat#sc-365278, RRID:AB_10859044, Santa Cruz Biotechnology), PLIN3 (Cat#10694-1-AP, RRID:AB_2297252, Proteintech), G0S2 (Cat#sc-518067, Santa Cruz Biotechnology), ACTIN (Cat#5057; RRID: AB_10694076, Cell Signaling Technology), TUBULIN (Cat#2146; RRID: AB_2210545, Cell Signaling Technology) or HSP90 (Cat#4874S; RRID: AB_2121214, Cell Signaling Technology). Membranes were incubated with secondary antibody (Anti-rabbit IgG, HRP-linked Antibody, 7074, Cell Signaling Technology) and developed using Clarity ECL substrate (Bio-Rad Laboratories). Images were captured with the ChemiDoc MP system (Bio-Rad Laboratories).

Enzyme-linked immunosorbent assay (ELISA)

DuoSet sandwich ELISA kits for TNFα, IL10 and IL6 (Cat#DY410/Cat#DY417/Cat#DY406, R&D systems) were used to measure cytokine concentrations in cell or explant supernatant according to manufacturer's instructions. Data was normalized for the amount of adipose tissue macrophages by determining the concentration of DNA per well (Quant-iT dsDNA Assay Kit high sensitivity, Thermo Fisher Scientific) and normalized for gWAT explants to the weight per explant.

Lipidomics

Lipidomics analysis was performed as described (Herzog et al., 2016). The HPLC system consisted of an Ultimate 3000 binary HPLC pump, a vacuum degasser, a column temperature controller, and an auto sampler (Thermo Fisher Scientific). The column temperature was maintained at 25°C. The lipid extract was injected onto a "normal phase column" LiChrospher 2x250-mm silica-60 column, 5 µm particle diameter (Merck) and a "reverse phase column" Acquity UPLC HSS T3, 1.8 µm particle diameter (Waters, Milford, MA, USA). A Q Exactive Plus Orbitrap (Thermo Fisher Scientific) mass spectrometer was used in the negative and positive electrospray ionization mode. Nitrogen was used as the nebulizing gas. The spray voltage used was 2500 V, and the capillary temperature was 256°C. S-lens RF level: 50, auxiliary gas: 11, auxiliary temperature 300°C, sheath gas: 48, sweep cone gas: 2. In both the negative and positive ionization mode, mass spectra of the lipid species were obtained by continuous scanning from m/z 150 to m/z 2000 with a resolution of 280,000 full width at half maximum (FWHM). Data was analyzed and visualised using R programming language (CRAN, RRID: SCR_003005, https://www.r-project.org).

Microarray analyses

Microarray analysis was performed on a several experiments: 1) Peritoneal macrophages treated with various fatty acids (500 µM) for 6 hours. 2) Peritoneal macrophages treated with intralipid (2mM) for 6 hours. 3) BMDM samples from *Hilpda*$^{\Delta M\Phi}$ mice and *Hilpda*$^{flox/flox}$ mice lipid loaded with oleate:palmitate (600µM) for 12 and 24 hours. RNA was isolated as described above and purified with the RNeasy Micro kit from Qiagen. Integrity of the RNA was verified with RNA 6000 Nano chips using an Agilent 2100 bioanalyzer (Agilent Technologies). Purified RNA (100 ng per sample) was labeled with the Whole-Transcript Sense Target Assay kit (Affymetrix, Santa Clara, CA, USA; P/N 900652) and hybridized to an Affymetrix Mouse Gene 1.0 arrays or 2.1 ST array plate (Affymetrix). Hybridization, washing,

and scanning were carried out on an Affymetrix GeneTitan platform according to the manufacturer's instructions.

Visualisation

The 3D scatterplot of signal log ratio's (Fig 1A) was created using R programming language (https://www.r-project.org) and the R package "plot3D". Heat-maps for the lipidomics were created using the package "gplots" and. The graphical abstract was created with BioRender.

Quantification and statistical analysis

Power calculation

From earlier studies it is known that fasting glucose values of mice fed a high fat diet differs on average 3mM (+ 8 mM – 11mM) compared to mice fed a low fat diet. Differences in responses lead to a standard deviation around 2mM or higher. For the power calculation, we used a one-way ANOVA with a significance level of 0.05 and a power of 90%, leading to an estimation of around n = 11 mice needed per group. To allow compensation for unforeseen circumstances or potential loss of mice during the study, n = 12 mice were included per group.

Statistical analysis

Normalization of the arrays was performed with the Robust Multi-array Average method (Bolstad et al., 2003; Irizarry et al., 2003). Probe sets were redefined according to Dai et al. (Dai et al., 2005) based on annotations provided by the Entrez Gene database. Data for the 3D scatterplot of signal log ratio's (Fig 1A) was created using R programming language (https://www.r-project.org). Partial least squares regression analysis for the lipidomics data was performed using the R package "mixOMICS".

Details on statistical analyses are given in figure legends. In experiments where animals were included, n represents the number of animals used. For cell experiments, n represents the number of replications performed. Data are represented as means ±SD or SEM as indicated. Assumptions for statistical methods were tested and statistical analyses were carried out using an unpaired Student's t test or two-way ANOVA followed by Bonferroni's post hoc multiple comparisons test, if genotype and diet or genotype and treatment both were found significant (GraphPad Software, San Diego, CA, USA). A value of $p < 0.05$ was considered statistically significant.

Data and code availability

A publicly available dataset (GSE77104) was downloaded from Gene Expression Omnibus and further processed as described above to obtain individual gene expression data (Robblee et al., 2016). The microarray analysis of the adipose tissue macrophages (GSE84000) and peritoneal macrophages treated with intralipid (GSE136240) are already described elsewhere (Boutens and Stienstra, 2016; Oteng et al., 2019). The microarray datasets generated during this study have been submitted to the Gene Expression Omnibus (GSE142296).

References

Aflaki, E., Balenga, N. A. B., Luschnig-Schratl, P., Wolinski, H., Povoden, S., Chandak, P. G., Bogner-Strauss, J. G., Eder, S., Konya, V., Kohlwein, S.-D., et al. (2011). Impaired Rho GTPase activation abrogates cell polarization and migration in macrophages with defective lipolysis. Cell. Mol. Life Sci. 68, 3933–3947.

Aflaki, E., Radović, B., Chandak, P. G., Kolb, D., Eisenberg, T., Ring, J., Fertschai, I., Uellen, A., Wolinski, H., Kohlwein, S.-D., et al. (2011). Triacylglycerol Accumulation Activates the Mitochondrial Apoptosis Pathway in Macrophages. J. Biol. Chem. 286, 7418–7428.

Aflaki, E., Doddapattar, P., Radović, B., Povoden, S., Kolb, D., Vujić, N., Wegscheider, M., Koefeler, H., Hornemann, T., Graier, W. F., et al. (2012). C16 ceramide is crucial for triacylglycerol-induced apoptosis in macrophages. Cell Death Dis. 3, e280.

Bolstad, B. M., Irizarry, R. A., Astrand, M. and Speed, T. P. (2003). A comparison of normalization methods for high density oligonucleotide array data based on variance and bias. Bioinformatics 19, 185–193.

Boutens, L. and Stienstra, R. (2016). Adipose tissue macrophages: going off track during obesity. Diabetologia 59, 879–894.

Chandak, P. G., Radović, B., Aflaki, E., Kolb, D., Buchebner, M., Fröhlich, E., Magnes, C., Sinner, F., Haemmerle, G., Zechner, R., et al. (2010). Efficient Phagocytosis Requires Triacylglycerol Hydrolysis by Adipose Triglyceride Lipase. J. Biol. Chem. 285, 20192–20201.

Cinti, S., Mitchell, G., Barbatelli, G., Murano, I., Ceresi, E., Faloia, E., Wang, S., Fortier, M., Greenberg, A. S. and Obin, M. S. (2005). Adipocyte death defines macrophage localization and function in adipose tissue of obese mice and humans. J. Lipid Res. 46, 2347–55.

Coats, B. R., Schoenfelt, K. Q., Barbosa-Lorenzi, V. C., Peris, E., Cui, C., Hoffman, A., Zhou, G., Fernandez, S., Zhai, L., Hall, B. A., et al. (2017). Metabolically Activated Adipose Tissue Macrophages Perform Detrimental and Beneficial Functions during Diet-Induced Obesity. Cell Rep. 20, 3149–3161.

Dai, M., Wang, P., Boyd, A. D., Kostov, G., Athey, B., Jones, E. G., Bunney, W. E., Myers, R. M., Speed, T. P., Akil, H., et al. (2005). Evolving gene/transcript definitions significantly alter the interpretation of GeneChip data. Nucleic Acids Res. 33, e175.

Denko, N., Schindler, C., Koong, A., Laderoute, K., Green, C. and Giaccia, A. (2000). Epigenetic regulation of gene expression in cervical cancer cells by the tumor microenvironment. Clin. Cancer Res. 6, 480–487.

Dijk, W., Mattijssen, F., de la Rosa Rodriguez, M., Loza Valdes, A., Loft, A., Mandrup, S., Kalkhoven, E., Qi, L., Borst, J. W. and Kersten, S. (2017). Hypoxia-Inducible Lipid Droplet–Associated Is Not a Direct Physiological Regulator of Lipolysis in Adipose Tissue. Endocrinology 158, 1231–1251.

DiStefano, M. T., Danai, L. V., Roth Flach, R. J., Chawla, A., Pedersen, D. J., Guilherme, A. and Czech, M. P. (2015). The Lipid Droplet Protein Hypoxia-inducible Gene 2 Promotes Hepatic Triglyceride Deposition by Inhibiting Lipolysis. J. Biol. Chem. 290, 15175–15184.

DiStefano, M. T., Roth Flach, R. J., Senol-Cosar, O., Danai, L. V., Virbasius, J. V., Nicoloro, S. M., Straubhaar, J., Dagdeviren, S., Wabitsch, M., Gupta, O. T., et al. (2016). Adipocyte-specific Hypoxia-inducible gene 2 promotes fat deposition and diet-induced insulin resistance. Mol. Metab. 5, 1149–1161.

Gimm, T., Wiese, M., Teschemacher, B., Deggerich, A., Schödel, J., Knaup, K. X., Hackenbeck, T., Hellerbrand, C., Amann, K., Wiesener, M. S., et al. (2010). Hypoxia-inducible protein 2 is a novel lipid droplet protein and a specific target gene of hypoxia-inducible factor-1. FASEB J. 24, 4443–4458.

Goeritzer, M., Schlager, S., Radovic, B., Madreiter, C. T., Rainer, S., Thomas, G., Lord, C. C., Sacks, J., Brown, A. L., Vujic, N., et al. (2014). Deletion of CGI-58 or adipose triglyceride lipase differently affects macrophage function and atherosclerosis. J. Lipid Res. 55, 2562–2575.

Gregor, M. F. and Hotamisligil, G. S. (2011). Inflammatory Mechanisms in Obesity. Annu. Rev. Immunol. 29, 415–445.

Haemmerle, G., Moustafa, T., Woelkart, G., Büttner, S., Schmidt, A., van de Weijer, T., Hesselink, M., Jaeger, D., Kienesberger, P. C., Zierler, K., et al. (2011). ATGL-mediated fat catabolism regulates cardiac mitochondrial function via PPAR-α and PGC-1. Nat. Med. 17, 1076–1085.

Herzog, K., Pras-Raves, M. L., Vervaart, M. A. T., Luyf, A. C. M., van Kampen, A. H. C., Wanders, R. J. A., Waterham, H. R. and Vaz, F. M. (2016). Lipidomic analysis of fibroblasts from Zellweger spectrum disorder patients identifies disease-specific phospholipid ratios. J. Lipid Res. 57, 1447–1454.

Hill, D. A., Lim, H.-W., Kim, Y. H., Ho, W. Y., Foong, Y. H., Nelson, V. L., Nguyen, H. C. B., Chegireddy, K., Kim, J., Habertheuer, A., et al. (2018). Distinct macrophage populations direct inflammatory versus physiological changes in adipose tissue. Proc. Natl. Acad. Sci. U. S. A. 115, E5096–E5105.

Hotamisligil, G. S. (2017). Inflammation, metaflammation and immunometabolic disorders. Nature 542, 177–185.

Huang, S. C.-C., Everts, B., Ivanova, Y., O'Sullivan, D., Nascimento, M., Smith, A. M., Beatty, W., Love-Gregory, L., Lam, W. Y., O'Neill, C. M., et al. (2014). Cell-intrinsic lysosomal lipolysis is essential for alternative activation of macrophages. Nat. Immunol. 15, 846–855.

Irizarry, R. A., Bolstad, B. M., Collin, F., Cope, L. M., Hobbs, B. and Speed, T. P. (2003). Summaries of Affymetrix GeneChip probe level data. Nucleic Acids Res. 31, e15.

Jung, S.-B., Choi, M. J., Ryu, D., Yi, H.-S., Lee, S. E., Chang, J. Y., Chung, H. K., Kim, Y. K., Kang, S. G., Lee, J. H., et al. (2018). Reduced oxidative capacity in macrophages results in systemic insulin resistance. Nat. Commun. 9, 1551.

Kratz, M., Coats, B. R., Hisert, K. B., Hagman, D., Mutskov, V., Peris, E., Schoenfelt, K. Q., Kuzma, J. N., Larson, I., Billing, P. S., et al. (2014). Metabolic Dysfunction Drives a Mechanistically Distinct Proinflammatory Phenotype in Adipose Tissue Macrophages. Cell Metab. 20, 614–625.

Lumeng, C. N., DelProposto, J. B., Westcott, D. J. and Saltiel, A. R. (2008). Phenotypic Switching of Adipose Tissue Macrophages With Obesity Is Generated by Spatiotemporal Differences in Macrophage Subtypes. Diabetes 57, 3239–3246.

Lumeng, C. N., Bodzin, J. L. and Saltiel, A. R. (2007). Obesity induces a phenotypic switch in adipose tissue macrophage polarization. J. Clin. Invest. 117, 175–184.

Maier, A., Wu, H., Cordasic, N., Oefner, P., Dietel, B., Thiele, C., Weidemann, A., Eckardt, K.-U. and Warnecke, C. (2017). Hypoxia-inducible protein 2 Hig2/*Hilpda* mediates neutral lipid accumulation in macrophages and contributes to atherosclerosis in apolipoprotein E–deficient mice. FASEB J. 4971–4984.

Mattijssen, F., Georgiadi, A., Andasarie, T., Szalowska, E., Zota, A., Krones-Herzig, A., Heier, C., Ratman, D., De Bosscher, K., Qi, L., et al. (2014). Hypoxia-inducible Lipid Droplet-associated (HILPDA) Is a Novel Peroxisome Proliferator-activated Receptor (PPAR) Target Involved in Hepatic Triglyceride Secretion. J. Biol. Chem. 289, 19279–19293.

Mayer, N., Schweiger, M., Romauch, M., Grabner, G. F., Eichmann, T. O., Fuchs, E., Ivkovic, J., Heier, C., Mrak, I., Lass, A., et al. (2013). Development of small-molecule inhibitors targeting adipose triglyceride lipase. Nat. Chem. Biol. 9, 785–787.

Namgaladze, D. and Brüne, B. (2016). Macrophage fatty acid oxidation and its roles in macrophage polarization and fatty acid-induced inflammation. Biochim. Biophys. Acta - Mol. Cell Biol. Lipids 1861, 1796–1807.

Ong, K. T., Mashek, M. T., Bu, S. Y., Greenberg, A. S. and Mashek, D. G. (2011). Adipose triglyceride lipase is a major hepatic lipase that regulates triacylglycerol turnover and fatty acid signaling and partitioning. Hepatology 53, 116–126.

Oteng, A.-B., Ruppert, P. M. M., Boutens, L., Dijk, W., van Dierendonck, X. A. M. H., Olivecrona, G., Stienstra, R. and Kersten, S. (2019). Characterization of ANGPTL4 function in macrophages and adipocytes using Angptl4-knockout and Angptl4-hypomorphic mice. J. Lipid Res. 60, 1741–1754.

Padmanabha Das, K. M., Wechselberger, L., Liziczai, M., De la Rosa Rodriguez, M., Grabner, G. F., Heier, C., Viertlmayr, R., Radler, C., Lichtenegger, J., Zimmermann, R., et al. (2018). Hypoxia-inducible lipid droplet-associated protein inhibits adipose triglyceride lipase. J. Lipid Res. 59, 531–541.

Prieur, X., Mok, C. Y. L., Velagapudi, V. R., Núñez, V., Fuentes, L., Montaner, D., Ishikawa, K., Camacho, A., Barbarroja, N., O'Rahilly, S., et al. (2011). Differential Lipid Partitioning Between Adipocytes and Tissue Macrophages Modulates Macrophage Lipotoxicity and M2/M1 Polarization in Obese Mice. Diabetes 60, 797–809.

Rausch, M. E., Weisberg, S., Vardhana, P. and Tortoriello, D. V. (2008). Obesity in C57BL/6J mice is characterized by adipose tissue hypoxia and cytotoxic T-cell infiltration. Int. J. Obes. 32, 451–463.

Reid, B. N., Ables, G. P., Otlivanchik, O. A., Schoiswohl, G., Zechner, R., Blaner, W. S., Goldberg, I. J., Schwabe, R. F., Chua, S. C. and Huang, L.-S. (2008). Hepatic Overexpression of Hormone-sensitive Lipase and Adipose Triglyceride Lipase Promotes Fatty Acid Oxidation, Stimulates Direct Release of Free Fatty Acids, and Ameliorates Steatosis. J. Biol. Chem. 283, 13087–13099.

Robblee, M. M., Kim, C. C., Abate, J. P., Valdearcos, M., Sandlund, K. L. M., Shenoy, M. K., Volmer, R., Iwawaki, T. and Koliwad, S. K. (2016). Saturated Fatty Acids Engage an IRE1α-Dependent Pathway to Activate the NLRP3 Inflammasome in Myeloid Cells. Cell Rep. 14, 2611–2623.

Rueden, C. T., Schindelin, J., Hiner, M. C., DeZonia, B. E., Walter, A. E., Arena, E. T. and Eliceiri, K. W. (2017). ImageJ2: ImageJ for the next generation of scientific image data. BMC Bioinformatics 18, 529.

Sapiro, J. M., Mashek, M. T., Greenberg, A. S. and Mashek, D. G. (2009). Hepatic triacylglycerol hydrolysis regulates peroxisome proliferator-activated receptor α activity. J. Lipid Res. 50, 1621–1629.

Saraswathi, V. and Hasty, A. H. (2009). Inhibition of Long-Chain Acyl Coenzyme A Synthetases During Fatty Acid Loading Induces Lipotoxicity in Macrophages. Arterioscler. Thromb. Vasc. Biol. 29, 1937–1943.

Sathyanarayan, A., Mashek, M. T. and Mashek, D. G. (2017). ATGL Promotes Autophagy/Lipophagy via SIRT1 to Control Hepatic Lipid Droplet Catabolism. Cell Rep. 19, 1–9.

Schindelin, J., Arganda-Carreras, I., Frise, E., Kaynig, V., Longair, M., Pietzsch, T., Preibisch, S., Rueden, C., Saalfeld, S., Schmid, B., et al. (2012). Fiji: An open-source platform for biological-image analysis. Nat. Methods 676–682.

Schlager, S., Goeritzer, M., Jandl, K., Frei, R., Vujic, N., Kolb, D., Strohmaier, H., Dorow, J., Eichmann, T. O., Rosenberger, A., et al. (2015). Adipose triglyceride lipase acts on neutrophil lipid droplets to regulate substrate availability for lipid mediator synthesis. J. Leukoc. Biol. 98, 837–50.

Shapiro, H., Pecht, T., Shaco-Levy, R., Harman-Boehm, I., Kirshtein, B., Kuperman, Y., Chen, A., Blüher, M., Shai, I. and Rudich, A. (2013). Adipose Tissue Foam Cells Are Present in Human Obesity. J. Clin. Endocrinol. Metab. 98, 1173–1181.

Van den Bossche, J., Baardman, J., Otto, N. A., van der Velden, S., Neele, A. E., van den Berg, S. M., Luque-Martin, R., Chen, H.-J., Boshuizen, M. C. S., Ahmed, M., et al. (2016). Mitochondrial Dysfunction Prevents Repolarization of Inflammatory Macrophages. Cell Rep. 17, 684–696.

Xu, X., Grijalva, A., Skowronski, A., van Eijk, M., Serlie, M. J. and Ferrante, A. W. (2013). Obesity Activates a Program of Lysosomal-Dependent Lipid Metabolism in Adipose Tissue Macrophages Independently of Classic Activation. Cell Metab. 18, 816–830.

Yang, X., Lu, X., Lombès, M., Rha, G. B., Chi, Y.-I., Guerin, T. M., Smart, E. J. and Liu, J. (2010). The G0/G1 Switch Gene 2 Regulates Adipose Lipolysis through Association with Adipose Triglyceride Lipase. Cell Metab. 11, 194–205.

Zhang, X., Saarinen, A. M., Hitosugi, T., Wang, Z., Wang, L., Ho, T. H. and Liu, J. (2017). Inhibition of Intracellular Lipolysis Promotes Cancer Cell Adaptation to Hypoxia. Elife 6, e31132.

Supplemental information

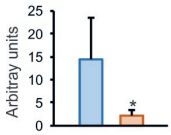

Figure S1, related to Figure 2G Quantification of triglycerides on Thin Layer Chromatography plates in *Hilpda*$^{flox/flox}$ and *Hilpda*$^{\Delta M\Phi}$ BMDMs lipid loaded with oleate:palmitate for 24h. B: BODIPY staining in *Hilpda*$^{flox/flox}$ and *Hilpda*$^{\Delta M\Phi}$ BMDMs treated with palmitate for 6h or 24h. Bar graphs are presented as mean ± SD. *P < 0.05.

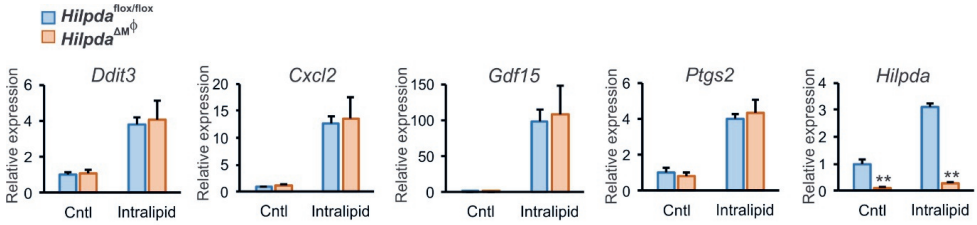

Figure S2, related to Figure 3D Gene expression of *Ddit3*, *Cxcl2*, *Gdf15*, *Ptgs2* and *Hilpda* in *Hilpda*$^{flox/flox}$ and *Hilpda*$^{\Delta M\Phi}$ BMDMs treated with 1mM intralipid or PBS control (Cntl) for 6h. Bar graphs are presented as mean ± SD. The effect of treatment was significant. **P ≤ 0.01. Cntl: Control.

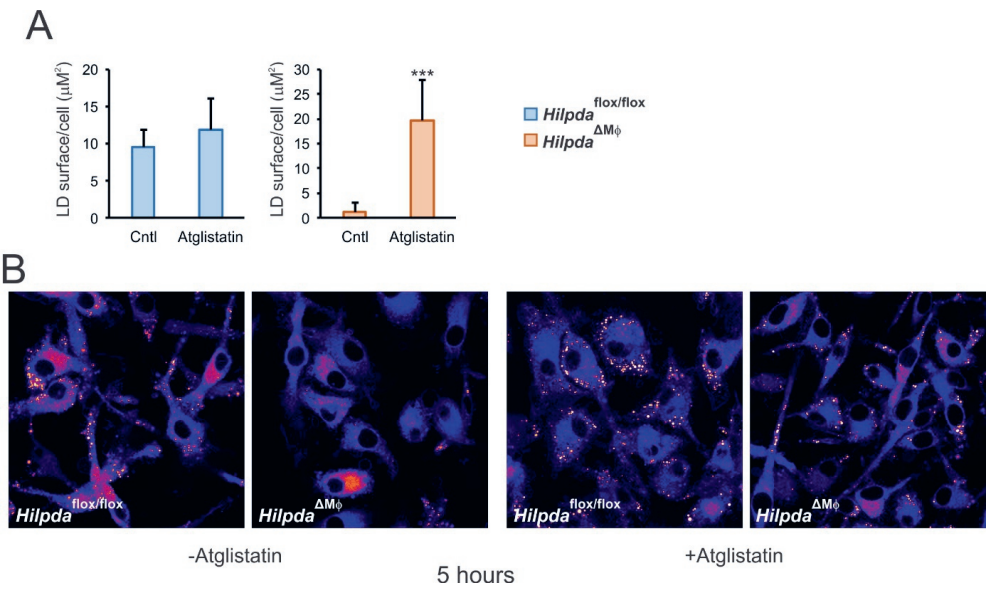

Figure S3, related to Figure 4 A: Quantification of the amount of lipid droplet surface area per cell in *Hilpda*$^{flox/flox}$ and *Hilpda*$^{\Delta M\Phi}$ BMDMs lipid loaded with oleate:palmitate for 24h and treated with 20μM atglistatin or vehicle (DMSO). B: BODIPY FL trafficking and incorporation in lipid droplets in *Hilpda*$^{flox/flox}$ and *Hilpda*$^{\Delta M\Phi}$ BMDMs lipid loaded with 400μM oleate and 20μM BODIPY FL, treated with 20μM atglistatin or vehicle (DMSO) for 5 hours. Bar graphs are presented as mean ± SD. ***P ≤ 0.001 LD: lipid droplet, Cntl: Control.

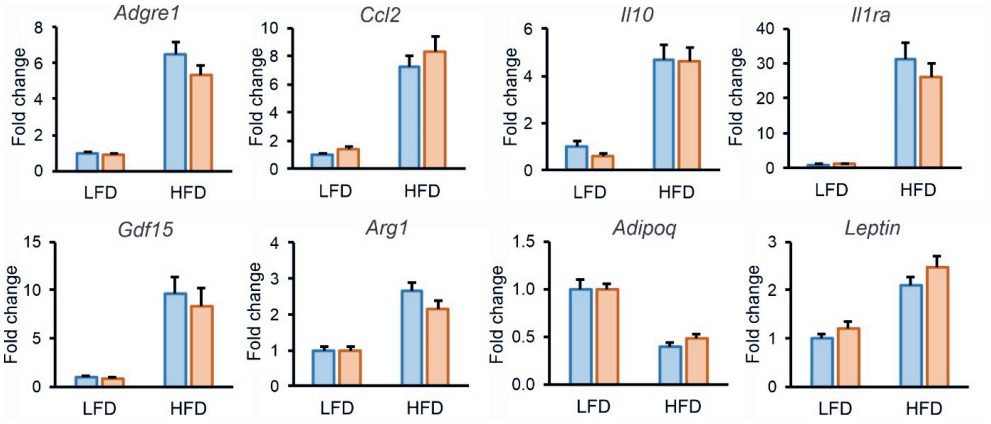

Figure S4, related to Figure 7E Gene expression of *Adgre1, Ccl2, Il10, Il1ra, Gdf15*, *Arg1*, *Adipoq* and *Leptin* in gWAT of *Hilpda*$^{flox/flox}$ and *Hilpda*$^{\Delta M\Phi}$ mice fed a LFD or HFD for 20 weeks. Gene expression levels in gWAT from *Hilpda*$^{flox/flox}$ fed a LFD diet are set to one. Bar graphs are presented as mean ± SEM. The effect of diet was significant. LFD: low fat diet, HFD: high fat diet.

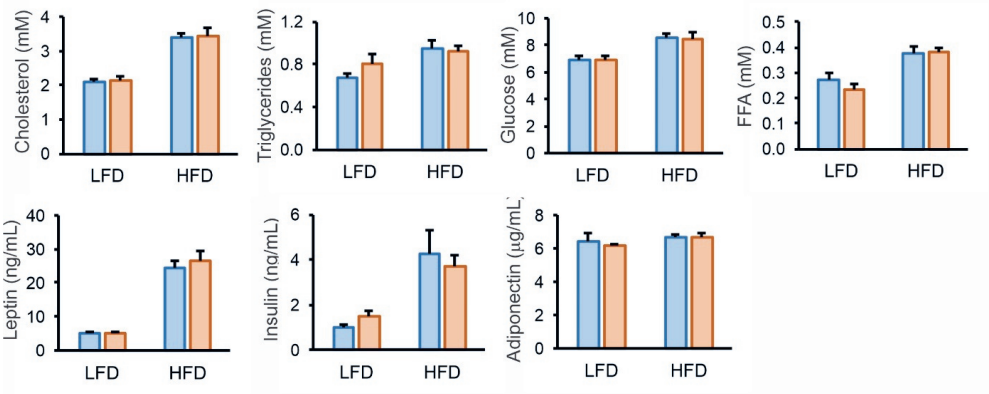

Figure S5, related to Figure 7I Plasma levels of cholesterol, triglycerides, glucose, free-fatty acids, leptin, insulin and adiponectin in *Hilpda*$^{flox/flox}$ and *Hilpda*$^{\Delta M\Phi}$ mice fed a LFD or HFD for 20 weeks. Bar graphs are presented as mean ± SEM, (n = 10 – 12 mice per group). Statistical testing was performed by two-way ANOVA followed by Bonferroni's post hoc multiple comparisons test. The effect of diet was significant in cholesterol, triglycerides, glucose, FFA, leptin and insulin. LFD: low fat diet, HFD: high fat diet.

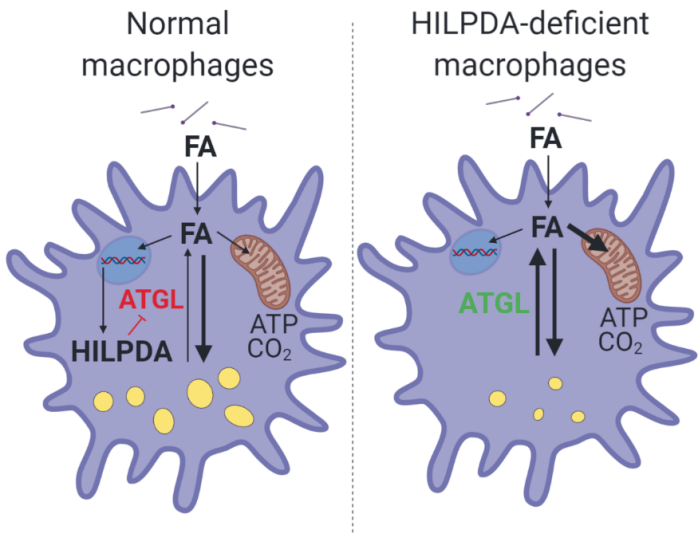

Figure S6 Effect of HILPDA deficiency on lipid metabolism in BMDMs. In normal BMDMs, HILPDA is produced in response to lipid load, resulting in enhanced lipid storage via inhibition of ATGL-mediated lipolysis. HILPDA deficiency in BMDMs relieves inhibition of adipose tissue lipolysis, leading to enhanced degradation of lipid droplets and promoting oxidation of fatty acids in mitochondria.

Table S1, related to STAR methods Primers used for qPCR

Primer name	Forward	Reverse
mHilpda	TCGTGCAGGATCTAGCAGCAG	GCCCAGCACATAGAGGTTCA
mAdgre1	CTTTGGCTATGGGCTTCCAGTC	GCAAGGAGGACAGAGTTTATCGTG
mCcl2	CCCAATGAGTAGGCTGGAGA	TCTGGACCCATTCCTTCTTG
mCd68	CCAATTCAGGGTGGAAGAAA	CTCGGGCTCTGATGTAGGTC
mItgax	CTGGATAGCCTTTCTTCTGCTG	GCACACTGTGTCCGAACTCA
mLep	AGAAGATCCCAGGGAGGAAA	TGATGAGGGTTTTGGTGTCA
mCd36	TCCAGCCAATGCCTTTGC	TGGAGATTACTTTTCAGTGCAGAA
mDdit3	TATCTCATCCCCAGGAAACG	GGGCACTGACCACTCTGTTT
mPtgs2	TGAGCAACTATTCCAAACCAGC	GCACGTAGTCTTCGATCACTATC
mPlin2	CTTGTGTCCTCCGCTTATGTC	GCAGAGGTCACGGTCTTCAC
mGdf15	GAACTGCGCTTACGGGTAG	CTGCACAGTCTCCAGGTGA
mCpt1a	CTCAGTGGGAGCGACTCTTCA	GGCCTCTGTGGTACACGACAA
mIl7r	GCGGACGATCACTCCTTCTG	AGCCCCACATATTTGAAATTCCA
mAngptl4	GTTTGCAGACTCAGCTCAAGG	CCAAGAGGTCTATCTGGCTCTG

Chapter 5

Hypoxia-inducible lipid droplet-associated induces DGAT1 and promotes lipid storage in hepatocytes

Montserrat A. de la Rosa Rodriguez, Lei Deng, Anne Gemmink, Michel van Weeghel, Marie Louise Aoun, Christina Warnecke, Rajat Singh, Jan Willem Borst*, Sander Kersten*

Mol Metab. 2021 Jan 16;47:101168.
* shared senior author

Abstract

The storage of lipids in cells is determined by the balance between triglyceride synthesis and degradation. The rate-limiting step in triglyceride synthesis is catalyzed by diacylglycerol acyltransferases (DGAT). Here we find that the lipid droplet-associated protein HILPDA physically interacts with DGAT1 and increases DGAT activity. Deficiency of HILPDA in liver cells significantly reduced lipid storage in vitro and in vivo. Fluorescence microscopy showed that HILPDA partly colocalizes with LD and with the endoplasmic reticulum, is especially abundant in perinuclear areas, and mainly associates with newly added fatty acids. Real-time fluorescence live-cell imaging further revealed that HILPDA preferentially localizes to LD that are being remodelled. Overexpression of HILPDA in liver cells increased DGAT activity and DGAT1 protein levels, concurrent with increased lipid storage. Confocal microscopy coupled to Förster resonance energy transfer-fluorescence lifetime imaging microscopy analysis demonstrated that HILPDA physically interacts with DGAT1 in living liver cells. The stimulatory effect of HILPDA on lipid storage via DGAT1 was corroborated in adipocytes. Our findings suggest a novel regulatory mechanism by which fatty acids promote triglyceride synthesis and storage.

Introduction

Fatty acids are an important fuel for many cell types. When the supply of fatty acids exceeds the demand for oxidation, excess fatty acids can be stockpiled by converting them to triglycerides. Triglycerides are synthesized in the endoplasmic reticulum and are stored in specialized organelles called lipid droplets (LD) [1]. With the exception of adipocytes, most cell types have tiny LD that collectively only take up a very small portion of the total cell volume. However, in certain pathological conditions, LD may become enlarged and occupy considerable cell volume, potentially interfering with important cellular functions [2].

The liver plays a central role in the regulation of lipid metabolism. Under conditions of obesity and insulin resistance, storage of lipids in the liver is often elevated [3]. A chronic increase in intra-hepatic fat is referred to as steatosis and is a key feature of non-alcoholic fatty liver disease (NAFLD) [4]. In many high-income countries, NAFLD has become the most common liver disorder and growing clinical concern [4].

Fatty acids in hepatocytes can originate from several sources: from circulating triglycerides in chylomicron and very low-density lipoprotein remnants taken up by the liver, from endogenous synthesis (de novo lipogenesis), and from circulating non-esterified fatty acids released by adipose tissue [5]. A portion of the incoming fatty acids are oxidized to provide energy to hepatocytes and, depending on nutritional status, converted into ketone bodies. The remainder is esterified into triglycerides, part of which is incorporated in and secreted as very low-density lipoproteins, and part of which is stored in LD in hepatocytes. Accordingly, excess storage of lipids in the liver can be due to changes in several metabolic pathways, including defective fatty acid oxidation, enhanced lipogenesis, impaired triglyceride secretion, and increased uptake of fatty acids from the circulation [6].

LD are dynamic organelles that can rapidly expand and shrink, driven by fluctuations in the rate of triglyceride synthesis and degradation [2]. The synthesis of triglycerides, their storage in LD, and the subsequent breakdown of triglycerides into fatty acids are governed by a complex set of enzymes and LD-associated proteins. LD-associated proteins encompass a large group of proteins that physically and functionally interact with LD. According to proteomic profiling, the number of LD-associated proteins easily runs into hundreds [7-10]. This group includes lipid synthesis and degradation enzymes, proteins involved in membrane trafficking, lipid signaling proteins, and proteins involved in protein degradation [10]. An important group of LD-associated proteins is the perilipin family, composed of PLIN1-PLIN5 [11]. Other known LD-associated proteins include CIDEA, CIDEB, CIDEC, FITM1, FITM2, G0S2, and ABHD5 [12-14].

A relatively poorly characterized LD-associated protein is HILPDA. The first identification of HILPDA as LD-associated protein was in HeLa cells, where its overexpression was found to

increase intracellular lipid accumulation [15]. HILPDA raised our attention when trying to identify novel target genes of the transcription factors PPARα and PPARγ in hepatocytes and adipocytes, respectively, and when screening for novel genes induced by fatty acids in peritoneal macrophages [16-18]. In mouse liver, HILPDA overexpression via adeno-associated viral delivery raised intrahepatic triglyceride levels by approximately 4-fold, likely by suppressing the secretion of triglycerides in very low-density lipoproteins [17]. Consistent with these data, deficiency of HILPDA in cultured hepatocytes lowered hepatic lipid accumulation, which was explained by a combination of decreased fatty acid uptake, increased fatty acid beta-oxidation, and increased triglyceride lipolysis [19]. Somewhat surprisingly, hepatocyte-specific HILPDA deficiency did not influence liver triglyceride content in mice chronically fed a high-fat diet [19].

Recently, we and others found that HILPDA is able to bind to the intracellular triglyceride hydrolase ATGL and inhibits ATGL-mediated triglyceride hydrolysis [18, 20-22]. Studies in HILPDA-deficient macrophages and cancer cells have firmly established the physiological relevance of ATGL inhibition by HILPDA [18, 20-22]. Currently, very little is known about the molecular mechanism of action of HILPDA in hepatocytes. Accordingly, the present study was aimed at better characterizing the molecular role of HILPDA in hepatocytes.

Materials and Methods

Mice experiments

Hilpda$^{flox/flox}$ mice (Jackson Laboratories, Bar Harbor, ME; Hilpdatm1.1Nat, #017360) were acquired and crossed with C57Bl/6J mice for at least 5 generations. Thereafter, the *Hilpda*$^{flox/flox}$ mice were crossed with Albumin-Cre transgenic mice (Jackson Laboratories, Bar Harbor, ME; B6.Cg-Speer6-ps1$^{Tg(Alb\text{-}cre)21Mgn}$/J, #003574) or Adiponectin-Cre transgenic mice (Jackson Laboratories, Bar Harbor, ME; B6.FVB-Tg (Adipoq-cre)1Evdr/J, # 028020) to generate mice with hepatocyte-specific Cre-mediated deletion of *Hilpda* (*Hilpda*$^{\Delta hep}$) or adipocyte-specific Cre-mediated deletion of *Hilpda* (*Hilpda*$^{\Delta ADIPO}$). Mice were group housed under normal light-dark cycles in temperature- and humidity-controlled specific pathogen-free conditions. Mice had ad libitum access to regular chow and water. A power calculation was performed based on fasting glucose level, assuming a standard deviation of 2.5 mM, using a power of 0.8, a significance level of 0.05, and an effect size of 3 mM. Using an online statistics tool from the University of British Columbia (https://www.stat.ubc.ca/~rollin/stats/ssize/n2.html), the sample size was calculated as

n = 11 mice per group. To allow compensation for potential loss of mice during the study, n = 12 mice were included per group.

Male *Hilpda*$^{\Delta hep}$ mice aged 3-4 months and their *Hilpda*$^{flox/flox}$ littermates were given a semi-purified low fat diet (10% kcal fat, A08051501) or high fat diet lacking choline and methionine (45% kcal fat, A06071309) (Research Diets, Inc. New Brunswick, NJ). During the dietary intervention, the mice were housed individually. After 11 weeks, mice were euthanized in the ad libitum fed state between 8:15h and 10.00h. The number of mice per group was 12.

Prior to euthanasia, mice were anaesthetised with isoflurane and blood was collected via orbital puncture in tubes containing EDTA (Sarstedt, Nümbrecht, Germany). Immediately thereafter, mice were euthanized by cervical dislocation, after which tissues were excised, weighed, and frozen in liquid nitrogen or prepared for histology. Frozen samples were stored at -80°C. Liver tissue was fixed in 4% formaldehyde solution in PBS. All animal experiments were approved by the local animal welfare committee of Wageningen University (AVD104002015236, 2016.W-0093.007 and 2016.W-0093.017). The experimenter was blinded to group assignments during all analyses.

Plasma measurements

Blood collected in EDTA tubes (Sarstedt, Numbrecht, Germany) was spun down for 10 minutes at 2000 g at 4°C. Plasma was aliquoted and stored at -80°C until further measurements. The plasma concentration of various metabolites was determined used specialized kits: cholesterol (Liquicolor, Human GmbH, Wiesbaden, Germany), triglycerides (Liquicolor), glucose (Liquicolor), NEFA (NEFA-HR set R1, R2 and standard, WAKO Diagnostics, Instruchemie, Delfzijl, The Netherlands), Alanine Transaminase Activity Assay Kit (ab105134, Abcam, Cambridge, UK), following the manufacturer's instructions.

Liver triglycerides

2% liver homogenates were prepared in a buffer (10 mM Tris, 2 mM EDTA and 0.25 M sucrose, pH 7.5) using a Tissue Lyser II (Qiagen, Hilden, Germany). Liver triglyceride content was then quantified using Triglyceride liquicolor mono kit from HUMAN Diagnostics (Wiesbaden, Germany) according to the manufacturer's instructions.

Cell treatments and gene expression

Human HepG2, mouse Hepa 1-6 and rat Fao hepatoma cells at 75% confluency were incubated with a mixture of oleate and palmitate (ratio 2:1, total concentration 1.2 mM) coupled to FA-free Bovine Serum Albumin (BSA) (Roche Applied Sciences). All fatty acid stocks were initially reconstituted in absolute ethanol. Sub-stocks of fatty acids at 25 mM were prepared in filter-sterilised KOH at 70 mM. Fatty acids were diluted in DMEM containing 3% FA-free BSA to obtain the desired final concentrations. After treatment, cells were washed with ice-cold phosphate-buffered saline (PBS) (Lonza) and stored at -20°C for further analysis.

Total RNA was isolated using TRIzol® Reagent (Invitrogen, ThermoFisher Scientific). cDNA was synthesized from 500 ng RNA using the iScript cDNA kit (Bio-Rad Laboratories, Hercules, CA, USA) according to manufacturer's instructions. Real time polymerase chain reaction (RT-PCR) was performed with the CFX96 or CFX384 Touch™ Real-Time detection system (Bio-Rad Laboratories), using a SensiMix™ (BioLine, London, UK) protocol for SYBR green reactions. Mouse 36b4 expression was used for normalization.

Liver slices

Precision cut liver slices were prepared from *Hilpda*$^{\Delta hep}$ and *Hilpda*$^{flox/flox}$ mice as described previously [23]. Briefly, 5 mm cylindrical liver cores were obtained with a surgical biopsy punch and sectioned to 200 µm slices using a Krumdieck tissue slicer (Alabama Research and Development, Munford, AL, USA) filled with carbonated Krebs-Henseleit buffer (pH 7.4, supplemented with 25 mM glucose). At this time point, some liver slices were snap-frozen in liquid nitrogen for RNA isolation. The rest was incubated in William's E Medium (Gibco, Paisley, Scotland) supplemented with penicillin/streptomycin in 6-well plates at 37°C/5% CO_2/80% O_2 under continuous shaking (70 rpm). 3 liver slices were incubated per well. After 1 h, medium was replaced with either fresh William's E Medium 1% BSA in the presence or absence of a mix of 0.8 mM oleic acid and 0.02 mM BODIPY FL C12 (ThermoFisher Scientific, Breda, Netherlands) for imaging, or William's E Medium 1% BSA in the presence or absence of a mixture of oleate and palmitate (ratio 2:1, total concentration 0.8 mM) for RNA and protein isolation. After overnight incubation, liver slices were snap-frozen in liquid nitrogen and stored in −80°C for RNA and protein isolation. Alternatively, liver slices were fixed for 1h in 3.7% formaldehyde, transferred into an 8-well removable chamber (ibidi, GmbH, Martinsried, Germany) and coated with vectashield. Slices were imaged on a Leica TCS SP8 X confocal. BODIPY FL C12 was excited at 488 nm and detected using HyD in a spectral window of 505-550 nm.

Primary Hepatocytes

Buffers: Hanks:112 mM NaCl, 5.4 mM KCl, 0.9 mM KH_2PO_4, 0.7 mM $Na_2HPO_4.12H_2O$. Hanks I: Hanks supplemented with 25 mM $NaHCO_3$, 10 mM D-glucose, 0.5 mM EGTA at pH 7.42. Hanks II: same as Hanks I with the addition of 5 mM $CaCl_2$. Krebs: 25 mM $NaHCO_3$, 10 mM D-glucose, 10 mM Hepes. Hepatocyte culture medium: Williams E without phenol red (Fisher) supplemented with Primary hepatocyte maintenance supplement (Fisher). All buffers were saturated with carbogen before use.

Primary hepatocytes were prepared from *Hilpda*$^{\Delta hep}$ and *Hilpda*$^{flox/flox}$ mice. Briefly, mice were anesthetized with isoflurane. Livers were infused through the portal vein with Hanks buffer I for 10 min and with 100 mL of Hanks buffer II. Next, livers were infused with 200 mL Liver Digest Medium (Fisher). Livers were excised and washed in Krebs Buffer. Primary hepatocytes were passed through a 100 µm mesh and centrifuged at 450 rpm for 4 min at 4ºC. Supernatant was discarded and cells were washed again in cold Krebs medium. Supernatant was discarded and cells were resuspended in hepatocyte culture medium with 5% FCS and seeded on collagen-coated 8-well µ-slide glass bottoms (Ibidi, Martinsried, Germany). After 2h medium was refreshed with hepatocyte culture medium with 10% FCS and left overnight. Next day, cells were treated with 20 µM Atglistatin (Sigma-Aldrich) or DMSO control and left overnight. Next morning, treatments were refreshed for 2h before adding a mixture of oleate and palmitate (ratio 2:1, total concentration 0.8 mM). Cells were lipid loaded for 6h and then fixed for 20 min in 3.7% paraformaldehyde. Lipid droplets were stained with 3 µg/mL BODIPY® 493/503 and mounted with vectashield for imaging. Cells were imaged on a Leica TCS SP8 X confocal. BODIPY was excited at 488 nm and detected using HyD in a spectral window of 505-550 nm. Images were acquired 1024 × 1024 pixels with pinhole set at 1 airy unit (AU), pixel saturation was avoided. Images were processed and analyse with Fiji. Briefly, images were converted to binary images, watershed, and LD size and number was measured with particle analysis set 0.07 μm^2-infinity.

Primary Adipocytes

Primary adipocytes were differentiated from the stromal vascular fraction, which was obtained from inguinal white adipose tissue of *Hilpda*$^{\Delta ADIPO}$ and *Hilpda*$^{flox/flox}$ mice. Briefly, dissected adipose tissue depots were kept and cleaned in ice-cooled transport medium (DMEM plus 1% fatty acid–free BSA (Sigma-Aldrich)). Cleaned adipose tissue samples were minced into small pieces and incubated with collagenase solution (DMEM, 3.2 mM $CaCl_2$, 15 mM HEPES, 0.5% BSA, 10% fetal calf serum (FCS), and 1.5 mg/mL collagenase type II (Sigma-Aldrich; C6885) at 37°C for 30 minutes. Afterwards, the digested tissue suspensions were filtered using a 100-mm cell strainer and centrifuged at 300g for 10 minutes at room

temperature. The pellet SVF were resuspended and grown in cell culture flasks until around 90% confluency. Cells were seeded in the culture plate with a density of 15000 cells/ cm^2 in DMEM, 10% FCS and 1% penicillin/streptomycin. 2-3 days post seeding (at full confluency), differentiation was started by supplementing with 0.5 mM 3-Isobutyl-1-methylxanthine (Sigma-Aldrich; I5879), 1 µM Dexamethasone (Sigma-Aldrich; D4902), 7 µg/ml human Insulin (Sigma-Aldrich; I2643) and 1 µM Rosiglitazone (Sigma-Aldrich; R2408). After 3 days stimulation, cells were further cultured in insulin medium (DMEM containing 7 µg/ml human Insulin) for another 3 days followed by normal growth medium (DMEM, 10% FCS and 1% penicillin/streptomycin). Gene expression of *Fabp4*, *Slc2a4*, *Adipoq*, *Pnpla2* and *G0S2* was used as an indicator of cell differentiation.

For confocal imaging the SVF was seeded and differentiated in 8-well µ-slide glass bottoms coated with collagen. Differentiated adipocytes were stained with 2 µg/mL BODIPY® 493/503 and mounted with vectashield after fixation with 3.7% paraformaldehyde. Imaging settings were as described previously. The size and fluorescent intensity of BODIPY stained LD were analysed using Image J (LOCI, University of Wisconsin). The size was measured from 0 μm^2-infinity. To measure the release of non-esterified free fatty acids into the cell culture medium, adipocytes were starved with DMEM supplied with 0.5% BSA for 2 hours and medium was then collected and analyzed using a kit (Instruchemie, Delfzijl, the Netherlands) following the manufacturer's instruction. Adipocytes were treated with the ATGL inhibitor Atglistatin (50 µM) or the DGAT1 inhibitor T863 (20 µM) (Sigma-Aldrich) during starvation.

TG quantification in HepG2 cells

HepG2 cells were seeded in 24-well plates. Next day, cells were transduced with Adenovirus-GFP (AV-*Gfp*) or Adenovirus-mHilpda (AV-*Hilpda*) at $5x10^6$ IFU/mL media in DMEM (Lonza, Verviers, Belgium) supplemented with 10% fetal calf serum (Lonza) and 1% penicillin/streptomycin (Lonza), from now on referred as complete DMEM, and left overnight. Recombinant adenoviruses were generated by cloning *GFP* or mouse *Hilpda* cDNA in human adenovirus type5 (dE1/E3). Expression regulated by CMV promoter. Viruses were produced and titrated by Vector Biolabs (Philadelphia, PA, USA). Cells were then incubated with DMEM 3% BSA and a mixture of oleate and palmitate (ratio 2:1, total concentration 1 mM) for 3 hours. Cells were washed twice with PBS and frozen in 25 mM Tris/HCl, 1mM EDTA, pH 7.5. TG quantification plates were thawed and a mixture of 4:1 tertiary butanol:methanol was added to cells, followed by an incubation of 10 minutes on a shaking platform. Plates were left to evaporate on a hot plate at 50°C. Next, 300 µL of triglyceride Liquicolor reagent (Human Diagnostics, Wiesbaden, Germany) was added to the cells and incubated for 10 minutes while shaking. 100 µL was transferred to a 96 well plate

and absorption measured at 492 nm. A calibration curve of a standard solution was used to determine the TG content of the cells. The triglyceride content relative to protein content was then calculated. For protein quantification Pierce BCA kit (ThermoFisher Scientific) was used according to manufacturer's protocol.

LD count

HepG2 and Hepa1-6 cells were plated on collagen-coated 8-well µ-slide glass bottoms (ibidi, Martinsried, Germany). The next day, cells were transduced with AV-*Hilpda* in complete DMEM at $5x10^6$ IFU/mL media and left overnight. HepG2 cells were incubated with a mixture of oleate and palmitate (ratio 2:1, total concentration 0.8 mM) for 8h to promote LD formation. Hepa 1-6 cells were incubated with 1 mM oleate:palmitate for 24h. Cells were washed with PBS, fixed for 15 min with 3.7% formaldehyde, stained with 3 µg/mL BODIPY® 493/503 and Hoechst for 45 min, and mounted with Vectashield-H (Vector Laboratories). Cells were imaged on a Leica confocal TCS SP8 X system equipped with a 63× 1.20 NA water-immersion objective lens. BODIPY® 493/503 was excited at 488 nm and fluorescence emission was detected using internal Hybrid (HyD) in a spectral window of 505nm - 578nm. Images were acquired 1024 × 1024 pixels with pinhole set at 1 AU, pixel saturation was avoided. Images were processed and analyse with Fiji. Briefly, images were converted to binary, watershed and LD size and number was measured with particle analysis set 0.07 μm^2-infinity.

Western blot

Cell or tissue protein lysates were separated by SDS-PAGE on pre-cast 8-16% polyacrylamide gels and transferred onto nitrocellulose membranes using a Trans-Blot® Semi-Dry transfer cell (all purchased from Bio-Rad Laboratories), blocked in non-fat milk and incubated overnight at 4°C with primary antibody for HILPDA (1:750, Santa Cruz Biotechnology, sc-137518 or rabbit antisera against the C-terminal half (aa 37–64) of murine HILPDA generated by Pineda (Berlin, Germany) [24]), ACTIN (Cell Signaling Technology), ATGL (Santa Cruz Biotechnology), DGAT1 (Santa Cruz Biotechnology, sc-271934) or HSP90 (1:5000, Cell Signaling Technology, #4874). Membranes were incubated with a secondary antibody (Anti-rabbit IgG, HRP-linked Antibody, 7074, Cell Signaling Technology) and developed using Clarity ECL substrate (Bio-Rad Laboratories). Images were captured with the ChemiDoc MP system (Bio-Rad Laboratories).

Plasmid constructs

Plasmids for *Plin2*, *Plin3*, *Gpat1*, *Gpat4*, *Dgat1*, *Dgat2* and *Hilpda* were constructed by fusing the full-length mouse cDNA into pEGFP-N2 (Clonetech, Mountain View, California, USA) and substituting the EGFP sequence by the sequence of the fluorescent proteins (FP) mCherry, sYFP2 or mEGFP. Briefly, RNA from mouse WAT or liver was reverse transcribed with First Strand cDNA synthesis kit (Thermo Scientific) and amplified with Phusion High fidelity DNA Polymerase (Thermo Scientific) using gene-specific primers. The PCR products were cloned into pEGFP-N2 vector using the XhoI and KpnI-HF or NheI and BamHI (New England Biolabs Inc.) restriction enzyme sites. Afterwards, MAX Efficiency ® DH5α™ Competent Cells (Invitrogen) were transformed by heat-shock and grown in Luria-Bertani (LB) agar plates with kanamycin (Sigma-Aldrich). The vector was isolated using Qiagen plasmid maxi kit (Qiagen) according to manufacturer instructions. The EGFP sequence was then excised from the pEGFP-N2 parent vector by enzyme digestion with KpnI-HF and NotI-HF. The vector was gel-purified with QIAquick Gel Extraction Kit (Qiagen) and the fragments of mCherry, sYFP2 or mEGFP were ligated into KpnI and NotI restriction enzyme site using T4 DNA ligase (Thermo Scientific). For plasmids of mGPAT1 and mGPAT4 the original pEGFP-N2 plasmid was used.

Stimulated Emission Depletion (STED) microscopy

HepG2 cells were plated on collagen coated 8 well µ-slide glass bottom (ibidi, Martinsried, Germany). Next day cells were transfected with 750 ng of *Hilpda*_sYFP2 complexed to polyethylenimine (PEI) (Polyscience Inc., PA, USA) in serum free medium. After 6h, the transfection medium was changed to DMEM 1% FA-free BSA with 0.8 mM OA and 15 µM BODIPY C12 558/568. Cells were fixed after 18h lipid loading for 20 min in 3.7% PFA. Images were acquired on a Leica TCS SP8 STED microscope. A 100x 1.4 N.A. oil immersion objective was used in combination with a 5x optical zoom resulting in a pixel size of 23x23 nm. The pinhole was set at 0.9 AU and imaging speed at 700 Hz. For excitation of the fluorescent probes a white light laser line was used. HILPDA-sYFP2 and BODIPY-558 were excited at 470 nm and 558 nm respectively, and fluorescence emission was detected using HyD in a spectral window of 480-540 nm and 570-650 nm, respectively. The HILPDA-sYFP2 emission was partly depleted with the 592 depletion laser set at a 40% laser intensity with a power output of 1.3530 W. For both fluorophores the gating was set at 0.3-6.5 ns. Images were corrected for chromatic aberration and deconvolved using the Deconvolution Express modus in Huygens Professional Software (Scientific Volume Imaging B.V., Hilversum, the Netherlands).

HILPDA and fluorescently labeled fatty acid colocalization

HepG2 cells were plated on collagen coated 8 well µ-slide glass bottom (Ibidi, Martinsried, Germany). Next day cells were transfected with Hilpda_mTurquoise2 plasmid complexed to PEI in serum-free DMEM. After 6 h, the medium was replaced by complete DMEM and left overnight. Cells were then incubated 16h with 0.6 mM oleate and 15 µM BODIPY C12 558/568 and next day for 20 min with QBT fatty acid uptake solution, which uses a BODIPY FL ®-dodecanoic acid fluorescent fatty acid analogue (BODIPY FL C12), prepared according to manufacturer's protocol (Molecular Devices, California, USA). Cells were washed with PBS and fixed with 3.7% formaldehyde for 30 min, and mounted with vectashield (Molecular Devices, California, USA). Imaging was performed on a Leica TCS SP8 X system equipped with a 63x 1.20 NA water-immersion objective lens. Images were acquired sequentially 1024x1024 pixel scans with pinhole set at 1 AU. mTurquoise2 was excited at 440 nm and fluorescence emission was detected using internal HyD in a spectral window of 450-480 nm. BODIPY C12 558/568 was excited at 561 nm and fluorescence emission was detected using internal Hybrid (HyD) in a spectral window of 570-620 nm. BODIPY FL C12 was excited at 488 nm and fluorescence emission was detected using internal HyD in a spectral window of 505-558 nm. During image acquisition, fluorescence bleed-through and pixel saturation were avoided. All images were deconvolved using Deconvolution Express modus with Huygens Essential version 18.10 (http://svi.nl, The Netherlands). Further images were process with ImageJ. Briefly, channels were split, the entire cell was selected as a ROI, colocalization threshold was used to obtain colocalized pixels image and Mander`s colocalization (overlap) coefficient and Pearson correlation coefficient were measured using Coloc2 plugin.

2D Time Lapse

HepG2 cells were seeded on 15 µ-8 well glass bottom slide (Ibidi, Martinsried, Germany) and let grown overnight before transfection. Cells were transfected with 800 ng of mHilpda_mCherry plasmid complexed to polyethylenimine (PEI) (Polyscience Inc., PA, USA) in serum-free DMEM. After 6 h, the medium was replaced by complete medium. Next day cells were starved for 1h with HBSS 0.2% FA-free BSA. Medium was then replaced with QBT fatty acid uptake assay kit and after 4h incubation cells were imaged on a Leica TCS SP8 X system equipped with a 63x 1.20 NA water-immersion objective lens. Images were acquired sequentially using 512 x 512 pixels, and a total of 491 frames were acquired with a frame interval of ± 5 seconds. All images were deconvolved using Deconvolution Express modus with Huygens Essential version 18.10 (Scientific Volume Imaging, The Netherlands, http://svi.nl). Further images were processed with Fiji to assign different coloring LUTs for visualization.

Lipophagy assay

HepG2 cells were transduced with AV-*GFP* or AV-*Hilpda* in complete DMEM at $5x10^6$ IFU/mL media and left overnight. Next day, HepG2 cells were incubated with a mixture of 8 mM oleate:palmitate (ratio 2:1) for 8h to promote LD formation. 2h before collection, cells were treated with lysosomal inhibitor cocktail 20 mM ammonium chloride and 100 uM leupeptin. Cells were then lysed in RIPA buffer with protease and phosphatase inhibitors, and centrifuged at 10,000 rpm for 10 min.

FRET-FLIM analysis

FRET is a process in which the excitation energy is transferred from a donor fluorophore to an acceptor chromophore in very close proximity (<10 nm). FRET determined using FLIM is independent of the protein concentration, but very sensitive to the local microenvironment of the fluorophores. In FRET-FLIM, the fluorescence lifetime of the donor molecule is reduced in the presence of a nearby acceptor molecule, because energy transfer to the acceptor will introduce an additional relaxation path from the excited to the ground state of the donor (34).

HepG2 cells were cultivated in complete DMEM (at standard conditions (37 °C, 5% CO2, 95% humidified atmosphere). Cells were seeded on a rat tail collagen coated (Ibidi, Martinsried, Germany) 15 µ-8 well glass bottom slide (Ibidi, Martinsried, Germany) and let to grow for 24h before transfection. Transfections were performed with 800 ng of single or 1600 ng of mixed plasmid DNA complexed to polyethylenimine (PEI) (Polyscience Inc., PA, USA) in serum-free DMEM. After 5 h, the medium was replaced by serum free DMEM supplemented with 1% fatty acid free BSA (Roche Applied Sciences) and a mixture of oleate and palmitate (ratio 2:1, total concentration 0.8 mM) and left overnight. For imaging, medium was replaced with FluoroBrite DMEM supplemented with 1% BSA and 0.8 mM fatty acid mix.

Colocalization imaging was performed on a Leica TCS SP8 X system equipped with a 63x 1.20 NA water-immersion objective lens. Images were acquired sequentially 512x512 pixels with pinhole set at 1 AU. mEGFP was excited at 488 nm and fluorescence emission was detected using internal HyD in a spectral window of 505-550 nm. mCherry was excited at 561 nm and detected using HyD in a spectral window of 580-650 nm. All images were deconvolved using Deconvolution Express modus with Huygens Essential version 18.10 (Scientific Volume Imaging, The Netherlands, http://svi.nl). Further images were process with Fiji. Briefly, brightness and contrast levels were adjusted and images were merged.

Förster resonance energy transfer-Fluorescence lifetime imaging microscopy (FRET-FLIM) was performed on a Leica TCS SP8 X confocal microscope. Donor and acceptor (mEGFP and mCherry, respectively) molecules were excited using a 40 MHz tunable supercontinuum laser at 488 nm and 561 nm, respectively. Fluorescence emission was detected using HyD detectors with 100 ps time resolution and collected in a spectral window of 505-550 nm for the donor (mEGFP) and 580-650 nm for the acceptor (mCherry). The signal output from the HyD detector was coupled to an external time-correlated single photon counting module (Becker&Hickl) for acquiring FLIM data. Typical images had 256 x 256 pixels (pixel size ± 300 nm), and the analogue to digital converter (ADC) was set to 256 time channels and FLIM images were acquired by imaging for 120 seconds per image. From the time resolved fluorescence intensity images, the fluorescence decay curves were calculated for each pixel and fitted with a double-exponential decay model using the SPCImage v7.1 software (Becker & Hickl). Fitting was performed without fixing any parameters. FRET-FLIM analysis provided fluorescence intensity as well as false-colored fluorescence lifetime images. The raw data was subjected to the following criteria to analyze and omit false positive negatives in the fluorescence lifetime scoring: minimum photon count per pixel of 1000 photons, 2 component analysis, goodness of fit ($\chi 2<2$) and fluorescence lifetime range of 500–3500 ps. For data analysis, we set pixel binning at 1 to have sufficient number of photons per pixel required for accurate fluorescence lifetime analysis.

DGAT assay

Our protocol is a modification of the method described by McFie and Stone [25]. HepG2 cells were seeded in 6-well plates at a density of 4 x 105 cells/ well or in 60x15mm round cell culture dishes at a cell density of 3.5 x 106 cells/dish in DMEM supplemented with 10% Fetal Calf Serum (FCS) and 1% penicillin/streptomycin. Next day, cells were transduced with AV-Gfp or AV-Hilpda at 5x106 PFU/mL medium. After 6h, the medium was changed to complete DMEM with 40 µM Atglistatin (3-(4'-(Dimethylamino)-[1,1'-biphenyl]-3-yl)-1,1-dimethylurea, Sigma-Aldrich) or control, and incubated overnight. Atglistatin is a specific high-affinity inhibitor of ATGL [26]. For the samples treated with Atglistatin, Atglistatin was added again the next morning 2 h prior to cell lysate isolation. In addition, Atglistatin was added to the resuspension buffer during the fluorescence assay. Cells were detached with trypsin, washed, and resuspended in 100 µL of 50 mM Tris-HCl (pH 7.6)/250 mM sucrose buffer supplemented with protease inhibitors (Roche Diagnostics GmbH). Cells were disrupted by 20 passages through a 27-gauge needle. Prepared cell lysate samples were placed on a spinning wheel for 20 min at 4°C. Cell debris was pelleted by centrifugation at 2500 rpm for 5 min. The supernatant was transferred to a new tube and used for the assay. Protein concentration was determined using a Pierce BCA kit (Thermo Fisher Scientific). A

master mix containing 20 µL of 1 M Tris-HCl (pH 7.6), 4 µL of 1 M MgCl2, 10 µL of 4 mM DOG (Sigma-Aldrich), 10 µL of 12.5 mg/mL BSA, 10 µL of 500 µM NBD-palmitoyl CoA (Avanti Polar Lipids), and 96 µL of water per reaction, was prepared. Volumes were scaled up proportionally to accommodate the desired number of reactions. The master mix was protected from direct light during the entire experiment by wrapping the glass test tubes in aluminium foil. Assays were performed in 13 × 100 mm glass KIMAX Test Tubes with Teflon Liner Caps (DWK Life Sciences, Kimble) in a final reaction volume of 250 µL. A master mix volume of 150 µL was aliquot per test tube, and tubes pre-incubated in a 37°C water bath for 2 min. The reaction was started by adding 300 ug in 100 µL of protein sample and incubated at 37°C Shaking Water Bath (GFL Gesellschaft für Labortechnik mbH, Product No. 1086) for 30, 90 and/or 180 min with steady shaking at 60 rpm. For the co-treatment with Atglistatin (40 µM), DGAT1 inhibitor (A922500, 1 µM) and DGAT2 inhibitor (PF-06424439, 40 µM), the incubation was carried on for 180 min. The reaction was terminated by adding 4 mL CHCl3/methanol (2:1, v/v) and 800 µL of water mixed by vortex. After 1 h, the test tubes containing samples were re-vortexed and centrifuged at 3,000 rpm for 5 min to separate aqueous and organic phases. The upper aqueous phase was aspirated, and the organic phase dried under stream of nitrogen. To help the solvents evaporate faster, the test tubes were placed in a thermal block pre-warmed to 54°C. Lipids were finally resuspended in 50 µL CHCl3/methanol (2:1) and stored at -20°C overnight. Samples were vortexed and re-centrifuged at 3,000 rpm for 2 min, before being spot on channelled 20 × 20 cm TLC plates with pre-adsorbent silica gel HLF zone (Analtech). The TLC plates were developed in the solvent system containing hexane/ethyl ether/acetic acid (80:20:1, v/v/v). The plates were air dried for 1 h before quantification of reaction products.

The newly synthesized NBD-TG was analysed with a ChemiDocTM MP molecular imaging system (Bio-Rad Laboratories, Inc.), and fluorescence was quantified with Quantity One software 4.1 (Bio-Rad Laboratories, Inc.). The excitation and emission wavelengths of NBD are 465 nm and 535 nm, respectively. Extinction source UV Trans illumination and Standard Emission Filter, together with Application SYBER Green and Applied (UV Trans Orange) Flat Field, were used. Data is presented as arbitrary fluorescence intensity units.

Microarray analysis

Microarray analysis was performed on Hepa1-6 hepatoma cells incubated with different fatty acids. RNA was purified with RNeasy Minikit columns (Qiagen) and analysed for quality with RNA 6000 Nano chips on the Agilent 2100 bioanalyzer (Agilent Technologies, Amsterdam, The Netherlands). One microgram of RNA was used for cDNA synthesis using the First Strand cDNA synthesis kit (Thermo Scientific). Purified RNA (100 ng) was labeled with the Ambion WT expression kit (Invitrogen) and hybridized to an Affymetrix Mouse

Gene 1.1 ST array plate (Affymetrix, Santa Clara, CA). Hybridization, washing, and scanning were carried out on an Affymetrix GeneTitan platform. Scans of the Affymetrix arrays were processed using packages from the Bioconductor project. Arrays were normalized using the robust multi-array average method [27, 28]. Probe sets were defined by assigning probes to unique gene identifiers, e.g., Entrez ID [29]. The total gene set (24,973 probe sets) was filtered to only include genes with mean signal > 20, yielding 10,379 genes. Microarray data were submitted to the Gene Expression Omnibus (accession number pending).

Statistical analysis

Details of statistical analyses are given in the figure legends. Statistical analyses were carried out using an unpaired Student's t test or two-way ANOVA. A value of $p<0.05$ was considered statistically significant.

Results

Hilpda expression is induced by fatty acids in hepatoma cells

To examine the regulation of *Hilpda* expression by fatty acids in liver cells, we treated mouse Hepa1-6 cells for 6h with different types of fatty acids: cis-unsaturated (oleate), trans-unsaturated (elaidate), or saturated (palmitate). Besides *Plin2*, *Hilpda* was one of the 65 genes that was induced at least 1.5 fold by palmitate (3.3 fold), oleate (1.5 fold) and elaidate (3.9 fold) (Figure 1a). The regulation of *Hilpda* strongly resembled the pattern observed for *Plin2* (Figure 1b). To further investigate the induction of *Hilpda* by fatty acids, different hepatoma cell types were treated with a mixture of oleate and palmitate. In mouse Hepa1-6, rat Fao, and human HepG2 cells, a mixture of oleate and palmitate significantly induced *Hilpda* mRNA, along with *Plin2* (Figure 1c). The upregulation of HILPDA by oleate and palmitate was confirmed at the protein level in Hepa1-6 cells and Fao cells (Figure 1d). These data indicate that *Hilpda* expression is induced by fatty acids in liver cells.

HILPDA deficiency modestly decreases liver triglyceride storage in mice with NASH

Previously, it was found that hepatocyte-specific deficiency of HILPDA reduced hepatic triglyceride levels under chow-fed conditions, although not after chronic high fat feeding [19]. A possible reason for the inconsistent effect of HILPDA deficiency on liver triglycerides is the relatively low *Hilpda* expression in liver. To identify conditions where deficiency of HILPDA may be expected to have a larger effect, we screened mouse liver transcriptome data for upregulation of *Hilpda*. Interestingly, hepatic *Hilpda* mRNA levels were increased during non-alcoholic steatohepatitis (NASH) caused by feeding mice a methionine and choline deficient diet (Figure 2a, based on GSE35961). Accordingly, we hypothesized that the effect of HILPDA deficiency may be more pronounced during NASH. Hepatocyte-specific HILPDA-deficient mice were generated by crossing *Hilpda*$^{flox/flox}$ mice with mice expressing Cre-recombinase driven by the albumin promoter. To induce NASH, *Hilpda*$^{\Delta hep}$ and *Hilpda*$^{flox/flox}$ mice were fed a high-fat diet deficient in methionine and choline for 11 weeks (HFmcd), using a low-fat (LF) diet as control. This diet does not lead to weight loss and has been reported to be a better model for human NASH than the traditional methionine and choline-deficient diet [30, 31]. After 11 weeks, hepatic expression of *Hilpda* was significantly higher in mice fed the HFmcd than the LF diet, and was significantly lower in *Hilpda*$^{\Delta hep}$ than in *Hilpda*$^{flox/flox}$ mice, which was accompanied by a modest compensatory increase in *G0s2* mRNA (Figure 2b). HILPDA protein levels were also markedly reduced in livers of *Hilpda*$^{\Delta hep}$ compared to *Hilpda*$^{flox/flox}$ mice (Figure 2c). Mice fed HFmcd were significantly lighter than the mice fed LFD, but no differences were observed between the genotypes (Figure 2d). Similarly, weight of the epididymal fat pad was significantly lower in the mice fed HFmcd,

but no differences were observed between *Hilpda*$^{\Delta hep}$ and *Hilpda*$^{flox/flox}$ mice (Figure 2e). Intriguingly, in mice fed HFmcd but not the LF diet, the weight of the liver was modestly but significantly lower in *Hilpda*$^{\Delta hep}$ than in *Hilpda*$^{flox/flox}$ mice (Figure 2f). Consistent with a stimulatory effect of HILPDA on liver fat, hepatic triglyceride levels were modestly but significantly lower in *Hilpda*$^{\Delta hep}$ compared to *Hilpda*$^{flox/flox}$ mice, both on the HFmcd and LF diet (Figure 2g).

HILPDA deficiency did not have any significant effect on mRNA levels of *Pnpla2*, *Dgat1*, *Dgat2*, and *Plin3* (Figure 2h). Also, despite a marked induction by HFmcd of the expression of macrophage/inflammatory markers *Cd68* and *Ccl2*, and fibrosis markers *Timp1* and *Col1a1*, no significant differences were observed between *Hilpda*$^{\Delta hep}$ and *Hilpda*$^{flox/flox}$ mice (Figure 2h). Histological analysis by hematoxylin and eosin (Figure 2i) and Syrius Red (Figure 2j) staining indicated that mice fed HFmcd exhibited classical features of NASH, including ballooning, inflammation, steatosis, and fibrosis. However, no clear and consistent differences were noticeable between *Hilpda*$^{\Delta hep}$ and *Hilpda*$^{flox/flox}$ mice. By contrast, and in agreement with the liver triglyceride levels, plasma ALT levels were modestly but significantly lower in *Hilpda*$^{\Delta hep}$ compared to *Hilpda*$^{flox/flox}$ mice, both on the HFmcd and LF diet (Figure 2k). Finally, plasma levels of cholesterol, triglycerides, and glucose were not significantly different between *Hilpda*$^{\Delta hep}$ and *Hilpda*$^{flox/flox}$ mice on either diet (Figure 2l). Overall, these data indicate that hepatocyte-specific HILPDA deficiency causes a modest but significant decrease in hepatic triglyceride storage, liver weight, and plasma ALT levels, without having a clear impact on features of NASH and various metabolic parameters.

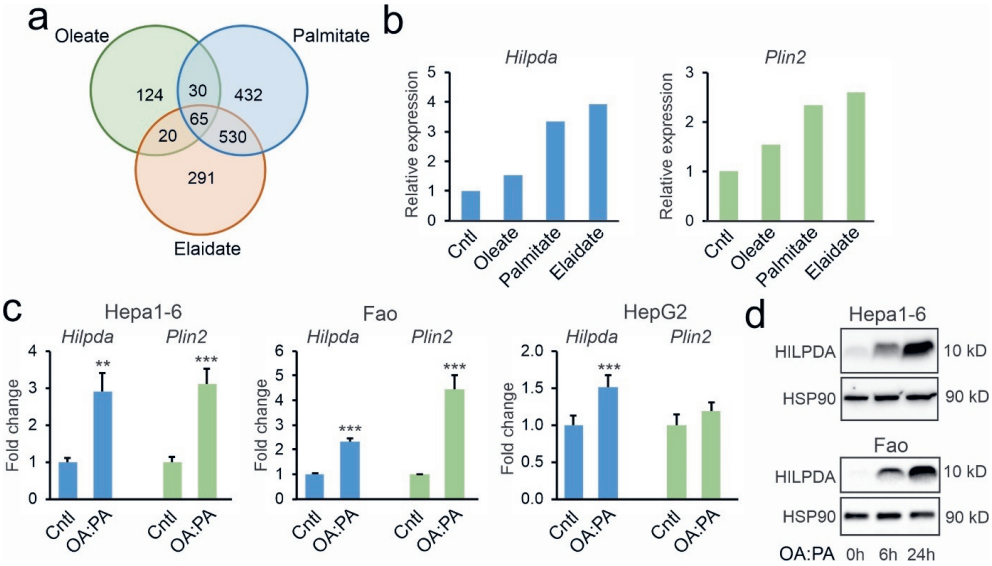

Figure 1: *Hilpda* expression is induced by fatty acids in various hepatoma cell lines. a) Venn diagram of upregulated genes (fold change>1.5) in murine Hepa1-6 hepatoma cells treated with different fatty acids (500 µM) for 6h. b) Relative changes in *Hilpda* and *Plin2* mRNA in Hepa1-6 cells treated with different fatty acids (500 µM) for 6h based on microarray analysis. c) Relative changes in *Hilpda* and *Plin2* mRNA in Hepa1-6, Fao and HepG2 hepatoma cells treated for 24h with a 2:1 mixture of oleate and palmitate (OA:PA, total concentration 1.2 mM, n=4-5 per condition). d) HILPDA protein levels in Hepa1-6 and Fao cells treated with a 2:1 mixture of oleate and palmitate (total concentration 1.2 mM) for different duration. Bar graphs are presented as mean ±SD. Asterisk indicates significantly different from control-treated cells according to Student's t test; **P < 0.01; ***P < 0.001.

Figure 2: Effect of hepatocyte-specific HILPDA deficiency in mice with NAFLD. a) Upregulation of hepatic *Hilpda* mRNA by a methionine and choline-deficient diet (GSE35961). N=4 mice/group. b) *Hilpda* and *G0s2* mRNA levels in livers of *Hilpda*$^{\Delta hep}$ and *Hilpda*$^{flox/flox}$ mice fed a low fat diet (LF) or high fat diet deficient in methionine and choline (HFmcd). c) HILPDA protein levels in livers of *Hilpda*$^{\Delta hep}$ and *Hilpda*$^{flox/flox}$ mice fed a low fat diet. d) Body weight. e) Gonadal adipose tissue weight. f) Liver weight. g) Liver triglyceride levels. h) mRNA levels of various LD-associated proteins, inflammatory markers. and fibrosis markers. i) H&E staining. j) Syrius Red staining. k) Plasma ALT levels. l) Plasma levels of various metabolites. Data are mean ± SEM; N=12 mice/group. Asterisk indicates significantly different from *Hilpda*$^{flox/flox}$ mice according to Student's t test; *P < 0.05; **P<0.01; ***P < 0.001.

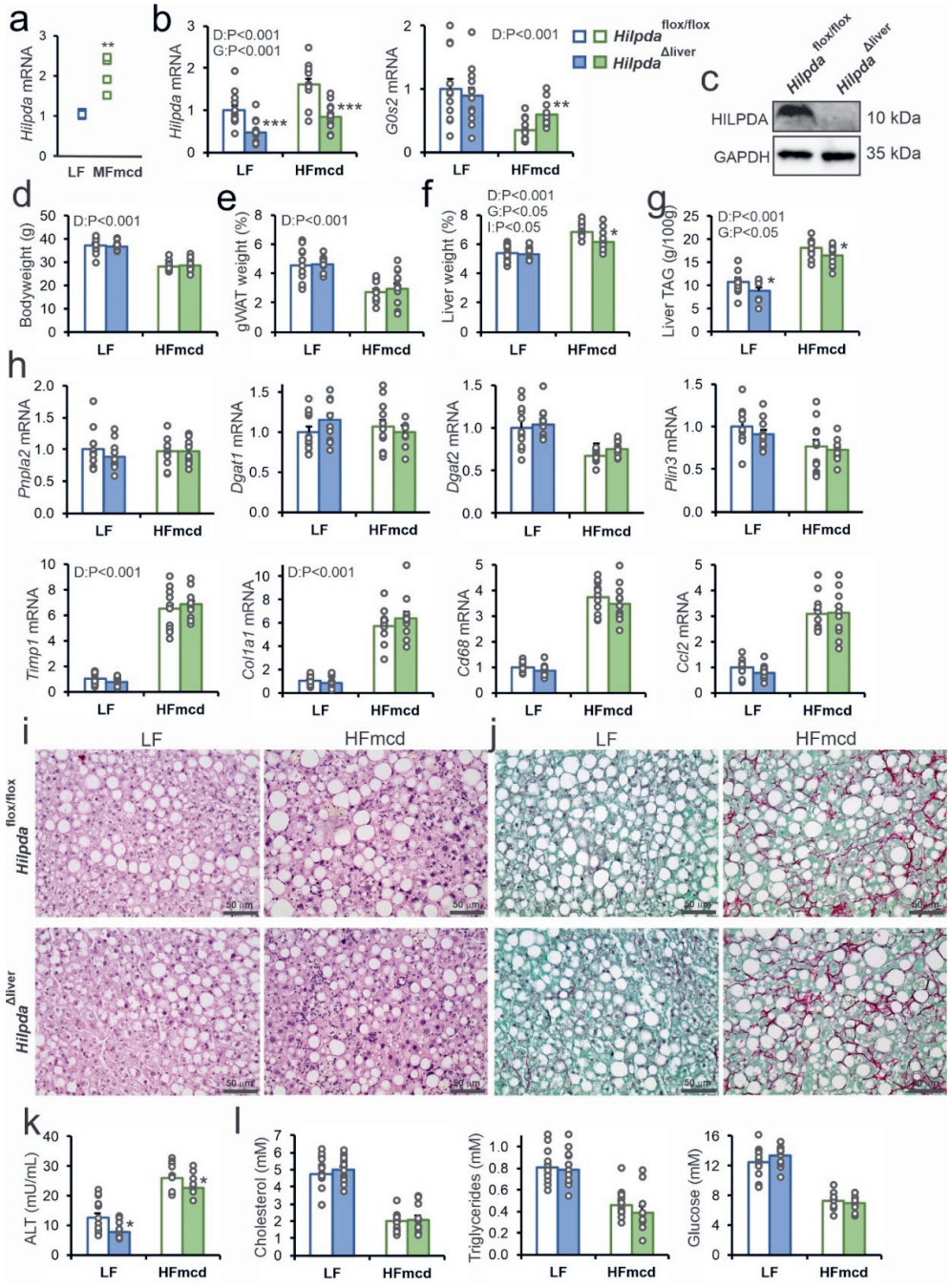
a
Hilpda mRNA
LF MFmcd
b
Hilpda mRNA
D:P<0.001
G:P<0.001
G0s2 mRNA
D:P<0.001
Hilpda flox/flox
Hilpda ΔliverΔliver
LF HFmcd
c
Hilpda flox/flox
Hilpda ΔliverΔliver
HILPDA
GAPDH
10 kDa
35 kDa
d
Bodyweight (g)
D:P<0.001
e
gWAT weight (%)
D:P<0.001
f
Liver weight (%)
D:P<0.001
G:P<0.05
I:P<0.05
g
Liver TAG (g/100g)
D:P<0.001
G:P<0.05
h
Pnpla2 mRNA
Dgat1 mRNA
Dgat2 mRNA
Plin3 mRNA
Timp1 mRNA
D:P<0.001
Col1a1 mRNA
D:P<0.001
Cd68 mRNA
Ccl2 mRNA
i
LF
HFmcd
Hilpda flox/flox
Hilpda ΔliverΔliver
50 µm
j
LF
HFmcd
k
ALT (mU/mL)
l
Cholesterol (mM)
Triglycerides (mM)
Glucose (mM)

HILPDA promotes lipid storage at least in part independently of ATGL

To further study the functional role of HILPDA in liver cells, we used precision cut liver slices and primary hepatocytes. These model systems were chosen because they both express very high levels of *Hilpda* compared to mouse liver (Figure 3a). Liver slices were prepared from *Hilpda*$^{\Delta hep}$ and *Hilpda*$^{flox/flox}$ mice and incubated overnight with a mixture of oleate and palmitate, as well as with BODIPY FL C12, followed by visualization of the stored fatty acids using fluorescence confocal microscopy. Levels of *Hilpda* mRNA were about 60% lower in *Hilpda*$^{\Delta hep}$ than *Hilpda*$^{flox/flox}$ liver slices, and HILPDA protein levels were also markedly reduced (Figure 3b). Consistent with a stimulatory effect of HILPDA on lipid storage, hepatocyte-specific deficiency of HILPDA led to a marked reduction in BODIPY FL accumulation in LD (Figure 3c).

We next moved to primary hepatocytes. In these cells, *Hilpda* mRNA was significantly induced by fatty acids (Figure 3d). To examine the effect of HILPDA deficiency on lipid storage, primary hepatocytes of *Hilpda*$^{\Delta hep}$ and *Hilpda*$^{flox/flox}$ mice were incubated overnight with a mixture of oleate and palmitate, followed by visualization of lipid storage by BODIPY 493/503 staining and fluorescence confocal microscopy. Again, consistent with a stimulatory effect of HILPDA on lipid storage, LD were considerably smaller in *Hilpda*$^{\Delta hep}$ than *Hilpda*$^{flox/flox}$ primary hepatocytes (Figure 3e). Quantification of the images revealed a significantly lower LD area in the *Hilpda*$^{\Delta hep}$ than *Hilpda*$^{flox/flox}$ hepatocytes (Figure 3f). Previously, we and others found that HILPDA inhibits ATGL [20, 22]. To investigate if the effect of loss of HILPDA on lipid storage in hepatocytes is mediated by hyperactivation of ATGL, we cotreated *Hilpda*$^{\Delta hep}$ and *Hilpda*$^{flox/flox}$ hepatocytes with the ATGL inhibitor Atglistatin. While Atglistatin and *Hilpda* genotype significantly increased the LD area, no statistical interaction was observed between Atglistatin treatment and *Hilpda* genotype (Figure 3e,f), suggesting no functional interaction between ATGL and HILPDA. In contrast to HILPDA deficiency in macrophages [18, 24], we also did not observe an increase in ATGL protein in HILPDA-deficient liver slices (Figure 3g). These data suggest that HILPDA promotes lipid storage at least partly via an ATGL-independent mechanism.

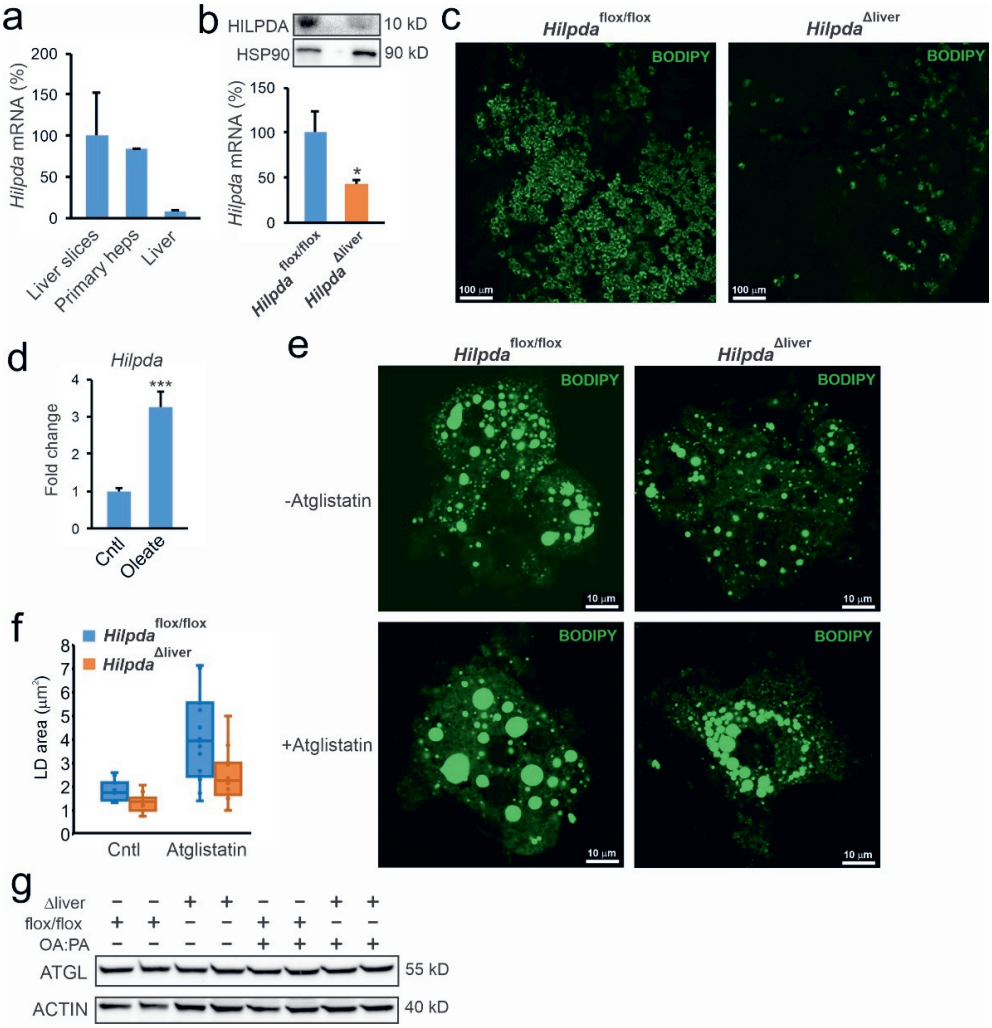

Figure 3: HILPDA stimulates lipid droplet formation partly independently of ATGL. a) Relative *Hilpda* mRNA levels in mouse precision cut liver slices, mouse primary hepactocytes, and mouse liver. b) HILPDA protein levels (top panel) and relative *Hilpda* mRNA levels (lower panel) in liver slices prepared from *Hilpda*$^{\Delta hep}$ and Hilpda$^{flox/flox}$ mice. Bar graphs are presented as mean ±SD. * indicates $P < 0.05$ according to Student's t test. c) Confocal microscopy of liver slices prepared from *Hilpda*$^{\Delta hep}$ and Hilpda$^{flox/flox}$ mice and incubated overnight with 800 µM oleate and 20 µM BODIPY FL C12. λex: 488nm, λem: 550-595 nm. d) Hilpda mRNA expression in wildtype mouse primary hepatocytes treated with oleate (500 µM) for 24h. * indicates $P < 0.001$ according to Student's t test. e) BODIPY 493/503 staining of primary hepatocytes prepared from *Hilpda*$^{\Delta hep}$ and Hilpda$^{flox/flox}$ mice and incubated overnight with 0.8 mM oleate:palmitate mix (2:1) in the presence or absence of Atglistatin (20 µM). λex: 488nm, λem: 550-595 nm. f) Quantification of the lipid droplet area. The total number of lipid droplets analyzed per condition varied between 1017 and 1958. Two-way ANOVA revealed significant effects for Atglistatin ($P<0.001$) and genotype ($P<0.001$), but not for an interaction effect. g) ATGL protein levels in liver slices from *Hilpda*$^{\Delta hep}$ and Hilpda$^{flox/flox}$ mice and incubated overnight with 0.8 mM oleate:palmitate mix (2:1). Bar graphs and images are representative of at least two independent experiments.

HILPDA preferentially associates with newly synthesised lipid droplets and active lipid droplets

To better understand the mechanism by which HILPDA promotes lipid storage in liver cells, we first investigated HILPDA localization. Previously, HILPDA protein was shown to partly localize to LD and to the LD-ER interface [15, 16, 19, 24]. Cellular fractionation confirmed the association of HILPDA with LD in mouse liver, which intriguingly was reduced by fasting (Supplemental figure 1a). The fractionation of the liver was confirmed by immunoblot of marker genes, showing the pronounced activation of autophagy by fasting in the LD fraction (Supplemental figure 1b).

To better zoom in on the intracellular localization of HILPDA, we used stimulated emission depletion (STED) microscopy, which generates images of very high spatial resolution (± 70 nm). HepG2 cells were transfected with HILPDA fused to sYFP2 and the LD were visualized by lipid loading the cells with a mix of oleate and BODIPY C12 558/568. Interestingly, while some HILPDA was observed around LD, most of the HILPDA was localized in the perinuclear area, presumably representing the ER, where triglyceride synthesis occurs (Figure 4a). Interestingly, many LD were not surrounded by HILPDA. Visualization of the ER via co-transfection with pDsRed2-ER verified the partial localization of HILPDA in the ER (Figure 4b).

To examine the dynamics of the association of HILPDA with LD, we performed time-lapse fluorescence imaging in HepG2 cells transfected with HILPDA-sYFP2 and incubated with BODIPY FL C12 (Supplemental Video 1). Intriguingly, HILPDA was mainly present around LD that are being lipolyzed (disappear) and remodelled (form new LD). Little to no HILPDA was observed around stable LD. These data suggest a role of HILPDA in LD remodelling in liver cells.

To better characterize the functional role of HILPDA in LD homeostasis in hepatocytes, we transfected HepG2 cells with HILPDA fused to mTurquoise2 and treated the cells with two labelled fatty acids that could be visualized separately using different channels. One labelled fatty acid (BODIPY C12 558/568) was added for 16 hours, while the other labelled fatty acid (BODIPY FL C12) was added for 20 min, after which cells were fixed (Figure 4c). Colocalization was evaluated by Manders' Colocalization Coefficients and Pearson Correlation Coefficient (Figure 4d). Manders' Colocalization Coefficients are measurements of co-occurrence, which is the spatial overlap of two probes. The Pearson Correlation Coefficient is a measurement of correlation, which evaluates the spatial overlap and signal proportionality. Analysis of the confocal images showed that HILPDA colocalizes almost entirely with the old and newly added fatty acids (M2: 96-97% respectively), and that the proportion of fatty acids that colocalized with HILPDA is greater for the newly added fatty acids than for the fatty acids added the day before (new M1:91% vs. old M1:80%). In line

with this, the Pearson Correlation Coefficient was significantly higher for the newly added fatty acids than for the fatty acids added the day before (Figure 4d). These data indicate that HILPDA more strongly correlates with newly added fatty acids, which —assuming that most of the added fatty acids are converted into triglycerides—suggests that HILPDA preferentially colocalizes with newly synthesized triglycerides. A schematic depiction of the set-up and outcomes of the above experiments is presented in Figure 4e.

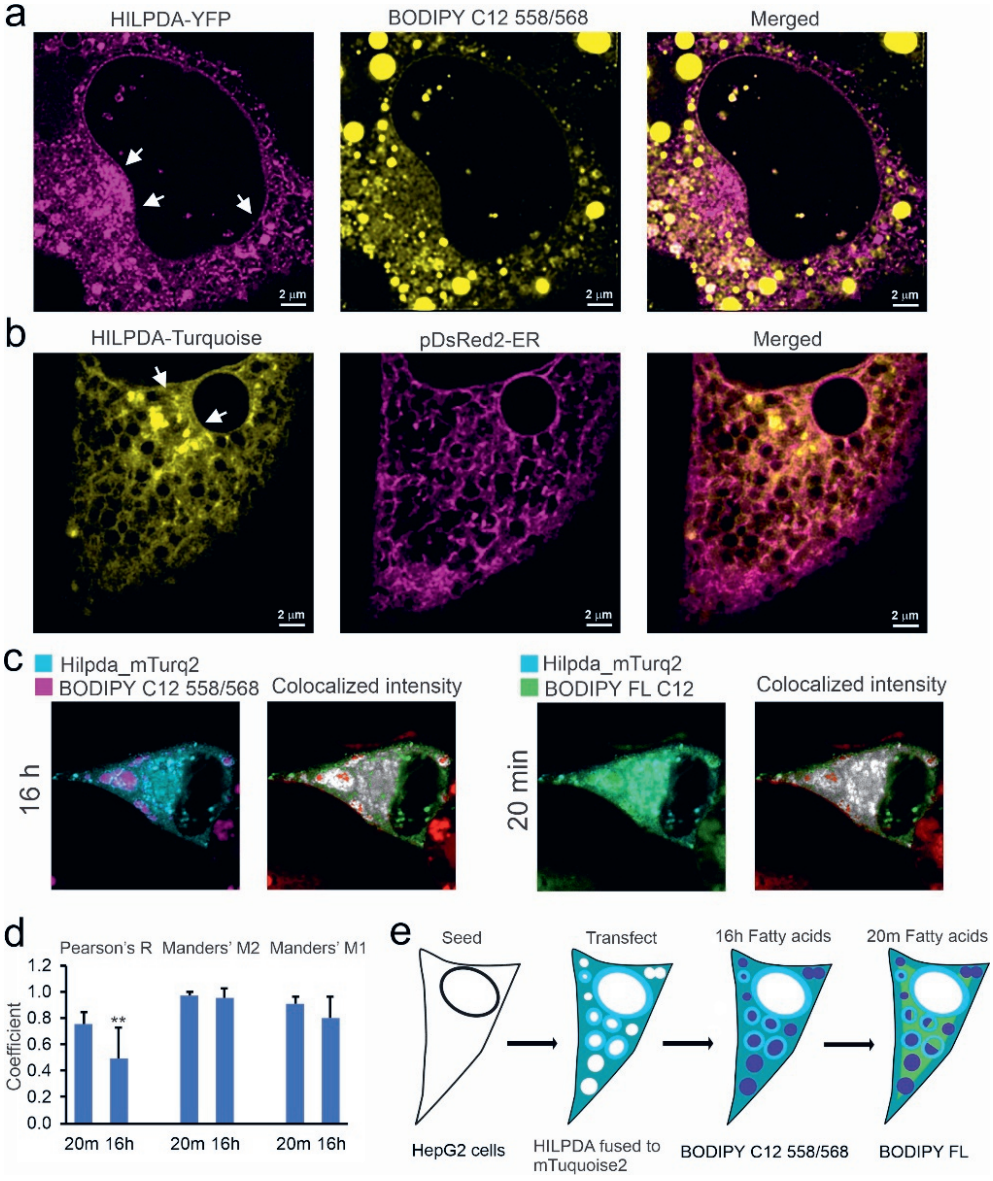

Figure 4: HILPDA is primarily localized to the perinuclear area and preferentially associated with new fat. a) STED microscopy of HepG2 cells transfected with HILPDA fused to sYFP2 and lipid loaded with 0.8 mM oleate and 15 µM BODIPY C12 558/568 for 18h. λex: 470 nm (YFP) and 558 nm (BODIPY-558/568). λem: 480-540 nm (sYFP2) and 570-650 nm (BODIPY 558/568). Left panel: HILPDA-sYFP2; middle panel: BODIPY-558, right panel: overlay. Arrows indicate perinuclear area. b) HepG2 cells cotransfected with HILPDA fused to Turquoise2 and with ER marker pDsRed2-ER (ClonTech) followed by incubation with 0.8mM oleate overnight. Left panel: HILPDA-Turquoise2; middle panel: ER marker pDsRed2-ER, right panel: overlay. Arrows indicate perinuclear area. c) Confocal microscopy of HepG2 cells transfected with HILPDA fused to Turquoise2 and lipid loaded with 0.6 mM oleate and 15 µM BODIPY C12 558/568 for 16h, followed by incubation for 20 min with BODIPY FL C12 and fixed with 3.7% PFA. λex: 440 nm (mTurquoise2), 561 nm (BODIPY 558/568), and 488 nm (BODIPY FL). λem: 450-480 nm (mTurquoise2), 570-620 nm (BODIPY 558/568), and 505-558 nm (BODIPY FL). Colocalized pixels of HILPDA and Fluorescent fatty acids are represented on gray scale, higher colocalization is depicted with lighter pixels; non-colocalized HILPDA pixels are coloured green; whereas non-colocalized fluorescent fatty acid pixels are coloured red. d) Mean Pearson correlation coefficient R, and mean Manders' colocalization coefficients M2 and M1 (pixel by pixel analysis, n=10 cells per group). Asterisk indicates significantly different according to Student's t test; $P<0.01$. e) Schematic depiction of the set-up and outcomes of the above experiments. Bar graphs and images are representative of multiple independent experiments.

HILPDA increases DGAT activity and DGAT1 levels

To further study how HILPDA promotes lipid storage, we overexpressed HILPDA in HepG2 cells via transduction with an adenoviral vector expressing *Hilpda.* HILPDA overexpression effectively raised HILPDA protein levels (Figure 5a) and was associated with a significant increase in triglyceride levels (Figure 5b) as well as LD size and abundance, as visualized by BODIPY staining (Figure 5c). Quantitative analysis showed that AV-*Hilpda* significantly increased the volume of the LD in both HepG2 and Hepa1-6 cells (Figure 5d). These data indicate that HILPDA overexpression promotes lipid storage in HepG2 cells.

Based on the finding that HILPDA increases lipid accumulation partly independently of ATGL, we considered the possibility that HILPDA may target the lipophagy pathway [32]. However, accumulation of the autophagosome marker LC3-II in the presence of lysosomal inhibitors was comparable between control and AV-*Hilpda* cells, indicating that increased LD content in AV-*Hilpda* cells is not due to stimulation of lipophagy (Figure 5e). Alternatively, we considered that HILPDA may promote the synthesis and/or storage of triglycerides. Interestingly, lipidomics indicated that AV-*Hilpda* significantly decreased levels of diacylglycerols (Figure 5f), but did not significantly affect levels of other major lipid species (data not shown). Accordingly, we hypothesized that HILPDA might stimulate the activity of diacylglycerol acyltransferase (DGAT), which catalyzes the last and purportedly the rate-limiting step in the formation of triglycerides, using diacylglycerol and acyl-CoA as substrates. To determine a possible stimulatory effect of HILPDA on DGAT activity, we measured the synthesis of fluorescently-labelled triglycerides from fluorescent NBD-

palmitoyl-CoA and 1,2 dioleoyl-sn-glycerol in lysates of HepG2 cells transduced with AV-*Hilpda* or AV-*Gfp*. Strikingly, the DGAT-mediated incorporation of fluorescent NBD-palmitoyl-CoA into triglycerides, as determined by quantification of TLC plates, was markedly increased by HILPDA overexpression (Figure 5g). This increase in triglyceride synthesis in HepG2 cells was unaltered in the presence of Atglistatin, suggesting it is independent of ATGL (Figure 5h). DGAT activity is catalyzed by two different isozymes: DGAT1 and DGAT2 [33]. Whereas DGAT2 has a preference for endogenously synthesized fatty acids, DGAT1 mainly esterifies exogenous fatty acids to diacylglycerol [34-36]. Strikingly, the increase in triglyceride synthesis by HILPDA overexpression was unaltered by the DGAT2 inhibitor PF-06424439 but completely suppressed by the DGAT1 inhibitor A922500. Interestingly, the induction of DGAT activity in HepG2 cells by HILPDA overexpression was accompanied by a significant increase in DGAT1 protein levels (Figure 5i). The increase in DGAT1 protein was not associated with any change in mRNA levels of DGAT1, DGAT2 or other relevant proteins (Figure 5j), and was independent of ATGL activity (Figure 5k). The specificity of the DGAT1 antibody is shown in supplemental figure 2a. Neither the DGAT1 inhibitor nor the DGAT2 inhibitor affected endogenous HILPDA levels, as tested in Hepa1-6 cells (Supplemental figure 2b and 2c).

To assess the effect of HILPDA overexpression on hepatic lipid levels and DGAT1 protein levels in vivo, we used samples from a previous study in which mice were infected with AAV expressing HILPDA [17]. AAV-mediated HILPDA overexpression markedly changed the lipidomic profile in liver (Figure 6a) and markedly increased hepatic triglyceride levels (Figure 6b). In fact, out of 1479 lipids measured, the 30 most significantly altered lipids by HILPDA overexpression were nearly all triglycerides, the remainder being cholesteryl-esters (Figure 6c). Consistent with the data in HepG2 cells, HILPDA overexpression increased DGAT1 protein levels in mouse liver (Figure 6d). These data suggest that HILPDA promotes triglyceride storage in liver concurrent with an increase in DGAT1 protein.

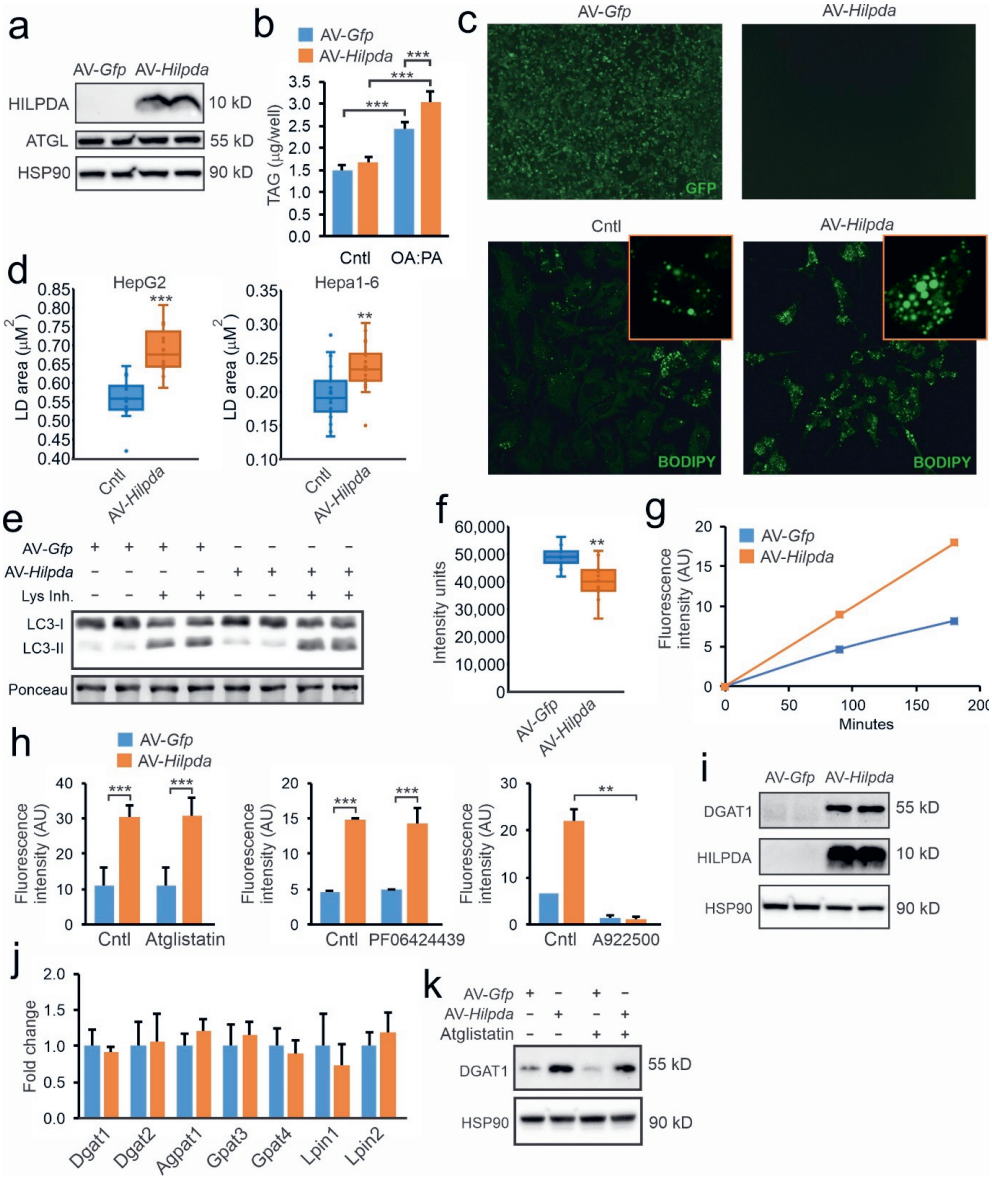
a
AV-Gfp AV-Hilpda
HILPDA
ATGL
HSP90
10 kD
55 kD
90 kD
b
AV-Gfp
AV-Hilpda
TAG (µg/well)
Cntl
OA:PA
c
AV-Gfp
AV-Hilpda
GFP
Cntl
AV-Hilpda
BODIPY
d
HepG2
Hepa1-6
LD area (µM²)
Cntl
AV-Hilpda
e
AV-Gfp
AV-Hilpda
Lys Inh.
LC3-I
LC3-II
Ponceau
f
Intensity units
AV-Gfp
AV-Hilpda
g
AV-Gfp
AV-Hilpda
Fluorescence intensity (AU)
Minutes
h
AV-Gfp
AV-Hilpda
Fluorescence intensity (AU)
Cntl
Atglistatin
PF06424439
A922500
i
AV-Gfp AV-Hilpda
DGAT1
HILPDA
HSP90
55 kD
10 kD
90 kD
j
Fold change
Dgat1
Dgat2
Agpat1
Gpat3
Gpat4
Lpin1
Lpin2
k
AV-Gfp
AV-Hilpda
Atglistatin
DGAT1
HSP90
55 kD
90 kD

Figure 5: HILPDA overexpression promotes LD storage and increases DGAT1 levels in HepG2 cells. HepG2 cells were transduced with AV-Hilpda, AV-GFP, or non-transduced and treated with oleate:palmitate (2:1 ratio). a) HILPDA protein levels. b) Triglyceride content in HepG2 cells incubated with serum free DMEM or 3h in 1 mM oleate:palmitate. c) GFP fluorescence and BODIPY 493/503 staining. d) Quantification of LD size in HepG2 treated with 0.8mM oleate:palmitate for 8h and Hepa 1-6 cells treated with 1mM for 24h. The graphs are representative of two independent experiments. e) LC3-I and LC3-II protein levels in HepG2 cells lipid loaded with 0.8mM oleate:palmitate for 8h, in the presence and absence of lysosomal inhibitors cocktail. f) Total DAG levels as determined by lipidomics in HepG2 cells incubated with 0.8mM oleate:palmitate for 5h. g) Time course of DGAT activity in HepG2 cells. The graph is representative of three independent experiments. h) DGAT activity in HepG2 cells in the presence and absence of ATGL, DGAT2 and DGAT1 inhibitor. The graphs are representative of two independent experiments. i) DGAT1 and HILPDA protein levels in HepG2 cells. j) mRNA levels of selected genes. k) DGAT1 protein levels in HepG2 cells in presence and absence of Atglistatin. Asterisk indicates significantly different according to Student's t test; **P<0.01; ***P < 0.001.

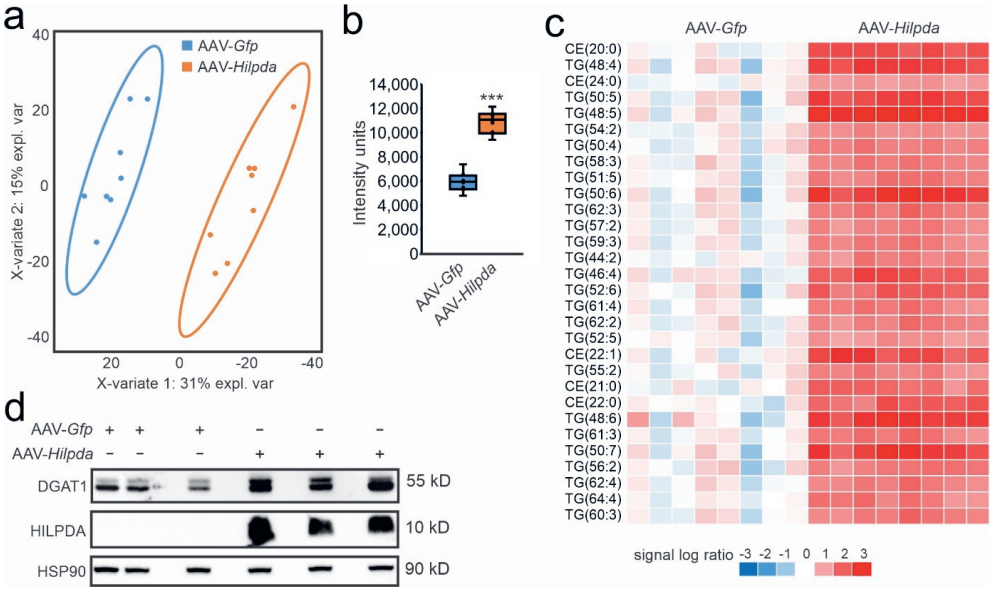

Figure 6: HILPDA overexpression promotes triglycerides storage and increases DGAT1 levels in mouse liver. Livers were collected from mice 4 weeks after injection with AAV-Gfp or AAV-Hilpda [17]. a) PLS-DA analysis of the liver lipidomics profiles. b) Cumulative hepatic concentration of all triglyceride species. c) Heatmap of the 30 most significantly altered lipid species. d) DGAT1 and HILPDA protein levels in livers of mice infected with AAV-Gfp or AAV-Hilpda. N=8 mice/group. Asterisk indicates significantly different according to Student's t test; ***P < 0.001.

HILPDA physically interacts with DGAT1

To investigate if HILPDA may physically interact with DGAT1 in cells, we performed FRET quantified by FLIM. In live HepG2 cells transfected with HILPDA-mEGFP and DGAT1-mCherry, HILPDA colocalized with DGAT1 (Figure 7a). Because confocal microscopy is diffraction limited to ~250 nm, our colocalization results do not directly demonstrate that HILPDA and DGAT1 are physically interacting. To determine protein interactions, we performed FRET quantified by FLIM. The mean fluorescence lifetime of the donor fluorophore HILPDA-EGFP was significantly decreased by the presence of the acceptor fluorophore DGAT1-mCherry (Figure 7b-c). This result demonstrates that HILPDA and DGAT1 are in very close proximity, indicating a direct physical interaction between these two proteins. Transfection of HepG2 cells with HILPDA-mEGFP and DGAT2-mCherry showed that HILPDA also partially colocalizes with DGAT2 (Figure 7d). As for DGAT1, the mean fluorescence lifetime of the donor HILPDA-EGFP was significantly decreased upon co-transfection of the acceptor DGAT2-mCherry (Figure 7e-f). These data indicate that HILPDA is able to physically interact with both DGAT1 and DGAT2. By contrast, although GPAT4-EFGP and HILPDA-mCherry showed substantial colocalization, FRET-FLIM analysis did not reveal a significant change in donor lifetime, indicating that these proteins do not interact (Supplemental figure 3a-c). Also, no significant change in donor lifetime was observed for HILPDA-mEGFP in combination with PLIN3-mCherry or GPAT1-EGFP in combination with HILPDA-mCherry (Supplemental figure 3d). Furthermore, HILPDA-mEGFP showed little to no colocalization with PLIN2-mCherry (Figure 7g-h). The latter observation was confirmed in Hepa1-6 and 3T3-L1 cells (Supplemental figure 3e).

We repeated the FRET-FLIM experiments in fixed HepG2 cells and obtained similar outcomes. Specifically, co-expression of HILPDA-mEGFP with DGAT1-mCherry (Supplemental figure 4a-c) and DGAT2-mCherry (Supplemental figure 4d-f) led to a significant reduction in donor fluorescence lifetime. Collectively, these data indicate that HILPDA physically interacts with DGAT1 and DGAT2, but not with any of the other proteins studied.

Finally, to investigate if HILPDA may promote lipid storage via DGAT in other cell types, we turned our attention to adipocytes. Adipocyte-specific HILPDA-deficient mice (*Hilpda*$^{\Delta ADIPO}$) were generated by crossing *Hilpda*$^{flox/flox}$ mice with mice expressing Cre-recombinase under control of the adiponectin promoter and used for the production of HILPDA-deficient primary adipocytes. HILPDA protein levels were markedly reduced in *Hilpda*$^{\Delta ADIPO}$ adipocytes (Figure 8a). Deficiency of HILPDA in primary mouse adipocytes did not influence adipogenesis per se, as indicated by unaltered expression of adipogenic markers genes, nor did it influence the expression of *G0s2*, *Dgat1*, or *Dgat2* (Figure 8b). However, lipid accumulation was markedly reduced by HILPDA deficiency (Figure 8c), as revealed by a

significant decrease in the size of the lipid droplets (Figure 8d) and the Bodipy fluorescence (Figure 8e). To determine the underlying mechanism, we measured the release of non-esterified fatty acids into the medium. Interestingly, HILPDA deficiency significantly increased fatty acid secretion (Figure 8f). Secretion of fatty acids was completely blunted by the ATGL inhibitor Atglistatin, indicating that fatty acid secretion is entirely driven by ATGL-mediated lipolysis. Theoretically, the increased fatty acid secretion in HILPDA-deficient adipocytes may be caused by enhanced lipolysis or reduced fatty acid re-esterification. As expected, blocking fatty acid (re)esterification by inhibiting DGAT1 increased fatty acid release. Intriguingly, however, the relative increase in fatty acid secretion by HILPDA deficiency was markedly reduced upon DGAT1 inhibition (Figure 8f), suggesting that the elevated fatty acid secretion in HILPDA-deficient adipocytes cannot solely be explained by enhanced ATGL-mediated lipolysis but also involves impaired DGAT1-mediated fatty acid re-esterification. Finally, in agreement with a stimulatory effect of HILPDA on lipid storage, the weights of the epididymal and inguinal fat depots were significantly lower in *Hilpda*$^{\Delta ADIPO}$ mice than *Hilpda*$^{flox/flox}$ mice (Figure 8g).

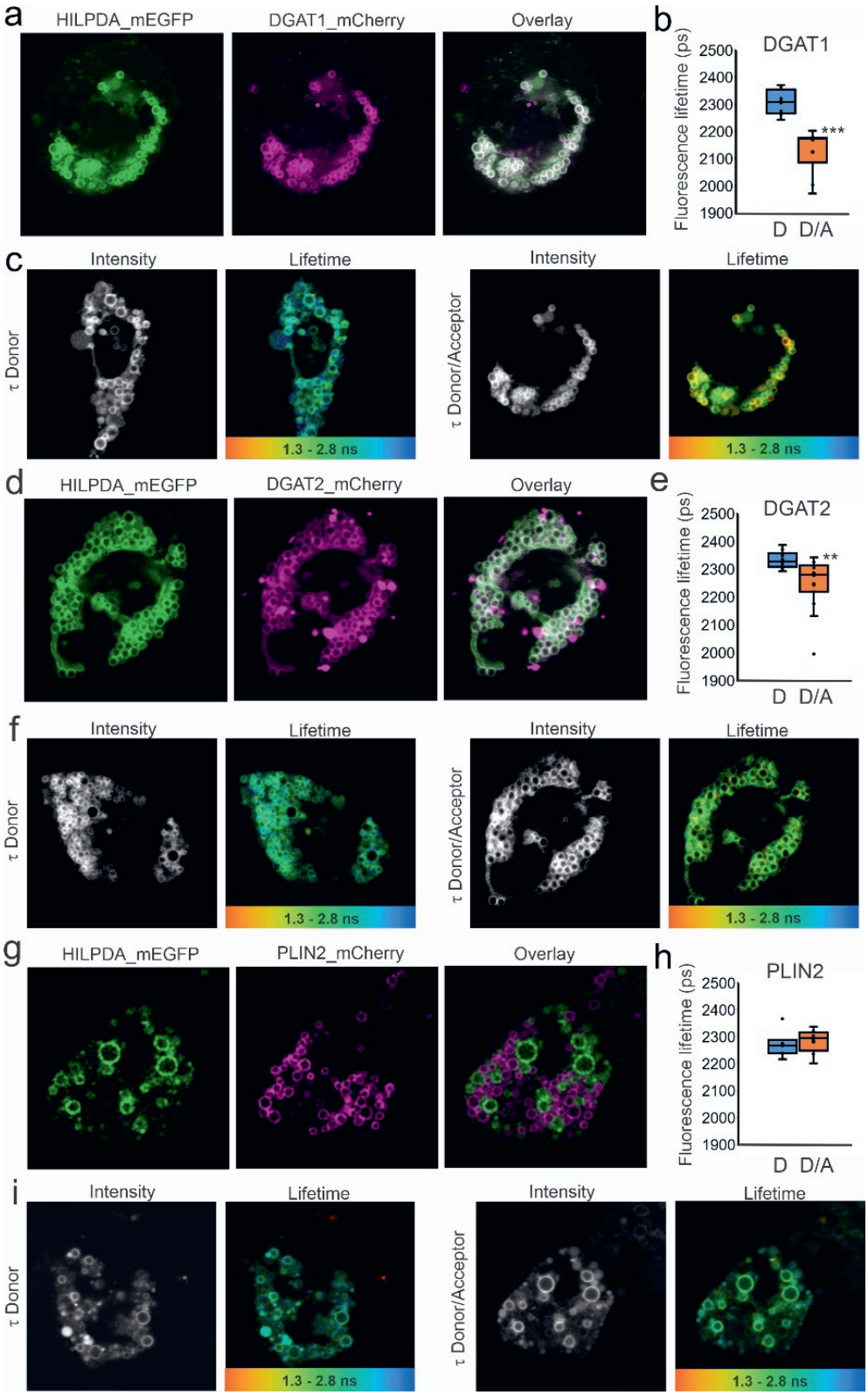
a
HILPDA_mEGFP
DGAT1_mCherry
Overlay
b
DGAT1
Fluorescence lifetime (ps)
2500
2400
2300
2200
2100
2000
1900
***
D
D/A
c
Intensity
Lifetime
τ Donor
1.3 - 2.8 ns
Intensity
Lifetime
τ Donor/Acceptor
1.3 - 2.8 ns
d
HILPDA_mEGFP
DGAT2_mCherry
Overlay
e
DGAT2
Fluorescence lifetime (ps)
2500
2400
2300
2200
2100
2000
1900
**
D
D/A
f
Intensity
Lifetime
τ Donor
1.3 - 2.8 ns
Intensity
Lifetime
τ Donor/Acceptor
1.3 - 2.8 ns
g
HILPDA_mEGFP
PLIN2_mCherry
Overlay
h
PLIN2
Fluorescence lifetime (ps)
2500
2400
2300
2200
2100
2000
1900
D
D/A
i
Intensity
Lifetime
τ Donor
1.3 - 2.8 ns
Intensity
Lifetime
τ Donor/Acceptor
1.3 - 2.8 ns

Figure 7: HILPDA and DGAT1/DGAT2 colocalize and physically interact intracellularly. HepG2 cells were transfected with HILPDA_mEGFP and DGAT1_mCherry or DGAT2_mCherry under lipid loaded conditions. Microscopy was carried out on live cells. a) HILPDA_EGFP and mDGAT1_mCherry partially colocalize in HepG2 cells. b) Fluorescence lifetime (τ) of HILPDA_EGFP in absence and presence of acceptor DGAT1_mCherry (n=8 per condition). c) Intensity image and LUT coloured lifetime image from red (1300 ps) to blue (2800 ps) from HILPDA_EGFP lifetime (τ) in the absence (left) or presence (right) of DGAT1_mCherry indicating where interaction occurs d) HILPDA_EGFP and DGAT2_mCherry partially colocalize in HepG2 cells. e) Fluorescence lifetime (τ) of HILPDA_EGFP in absence and presence of acceptor DGAT2_mCherry (n= 12-14). f) Intensity image and LUT coloured lifetime image from red (1300 ps) to blue (2800 ps) from HILPDA_EGFP lifetime (τ) in the absence (left) or presence (right) of DGAT2_mCherry indicating where interaction occurs g) HILPDA_EGFP and PLIN2_mCherry do not colocalize in HepG2 cells. h) Fluorescence lifetime (τ) of HILPDA_EGFP in absence and presence of acceptor PLIN2_mCherry (n=5-6). Asterisk indicates significantly different from donor-only according to Student's t test; **P < 0.01; ***P < 0.001. D=donor, D/A=donor/acceptor. Graphs and images are representative of at least two independent experiments in live and fixed cells.

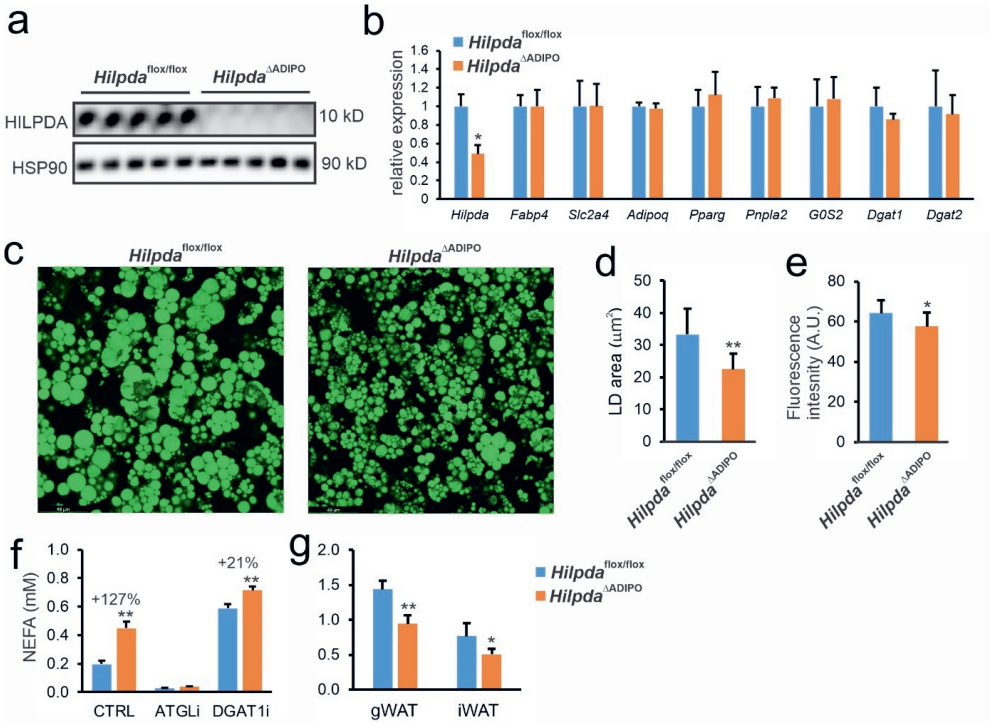

Figure 8. HILPDA promotes lipid storage and reduces fatty acid secretion in adipocytes via DGAT1. Primary adipocytes were differentiated using the adipose tissue of Hilpda$^{\Delta ADIPO}$ and Hilpda$^{flox/flox}$ mice. a) HILPDA protein levels as determined by Western blot. b) mRNA levels of selected genes determined by qPCR. c) Confocal fluorescence microscopy of Bodipy-stained Hilpda$^{\Delta ADIPO}$ and Hilpda$^{flox/flox}$ adipocytes. d) Quantification of the lipid droplet area. e) Quantification of the Bodipy fluorescence. f) Concentration of fatty acids in the medium of Hilpda$^{\Delta ADIPO}$ and Hilpda$^{flox/flox}$ adipocytes treated with Atglistatin (ATGLi) or T863 (DGAT1i). Graphs and images are representative of at least two independent experiments. g) Weight of the gonadal and inguinal fat depots in Hilpda$^{\Delta ADIPO}$ and Hilpda$^{flox/flox}$ mice. N=11-13 mice/group. Asterisk indicates significantly different from Hilpda$^{flox/flox}$ mice/cells according to Student's t test; *P < 0.05; **P<0.01.

Discussion

The purpose of this study was to better define the role and mechanism of action of HILPDA in liver cells. We find that HILPDA is induced by fatty acids in liver cells and stimulates lipid storage, which is at least partly independently of ATGL. Fluorescence microscopy showed that HILPDA partly colocalizes with LD and with the endoplasmic reticulum, is especially abundant in perinuclear areas, mainly associates with newly added fatty acids, and preferentially localizes to LD that are being remodelled. Mechanistically, HILPDA physically interacts with DGAT1, stimulates DGAT activity, and increases DGAT1 protein levels. Studies in adipocytes further support the stimulatory effect of HILPDA on lipid storage via DGAT1. Our data suggest that in addition to inhibiting ATGL-mediated lipolysis, HILPDA stimulates DGAT1-mediated triglyceride synthesis. Based on our and other data, it can be hypothesized that HILPDA is part of a larger triglyceride turnover complex ("lipolysome") that includes enzymes involved in triglycerides synthesis and triglyceride breakdown, including ATGL and DGAT1, as well as regulatory proteins such as ABHD5 and G0S2 [33, 37, 38].

HILPDA and G0S2 share extensive sequence homology, and both proteins are able to inhibit ATGL. Recently, evidence was provided that G0S2 not only suppresses lipolysis but also promotes triglyceride synthesis by carrying glycerol-3-phosphate acyltransferase (GPAT/LPAAT/AGPAT) enzymatic activity [39]. Given the very small size of HILPDA (63 amino acids), it is unlikely that HILPDA can itself function as a fatty acid esterification enzyme. Rather, our data suggest that HILPDA increases the level and activity of the DGAT1 enzyme via a direct physical interaction between the two proteins. DGAT1 catalyzes the esterification of exogenous fatty acids and fatty acids released from LD [35, 40]. How HILPDA increases DGAT1 levels is unclear but it can be hypothesized that the binding of HILPDA may stabilize DGAT1. Currently, nothing is known about how DGAT1 is degraded, complicating the study of the possible role of HILPDA in DGAT1 degradation.

PLIN2 is considered to represent a general lipid droplet-coating protein that occurs in essentially all cells, including hepatocytes. Evidence abounds indicating that PLIN2 promotes LD formation and thereby protects stored triglycerides from lipolysis [41]. Although PLIN2 is believed to resides on most LD in hepatocytes, we found that HILPDA-mEGFP did not colocalize with PLIN2-mCherry and that HILPDA and PLIN2 coat distinct sets of LD. Based on this observation, it can be hypothesized that the presence of HILDPA on LD may lead to the exclusion of PLIN2 or vice-versa. Whereas coating with PLIN2 may define more stable LD, coating with HILPDA may be a feature of LD that are being remodelled via active triglyceride synthesis and lipolysis. This intriguing possibility merits further experimental investigation.

In this paper, deficiency of HILPDA in mouse liver led to a modest reduction in triglyceride storage after inducing NASH. Previous studies found that HILPDA deficiency does not significantly influence hepatic triglyceride levels in mice fed chow or a high fat diet [19]. The reason for the divergent results is unclear but could be related to the different types of diets used. Although statistically significant, the magnitude of the effect of HILPDA deficiency on hepatic triglyceride levels in mice was modest, which may be explained by the relatively low expression of *Hilpda* in mouse liver. By contrast, raising liver HILPDA levels by adeno-associated virus markedly elevates triglyceride storage.

Whereas HILPDA deficiency only had a modest effect on triglyceride storage in mouse liver, deficiency of HILPDA markedly reduced lipid storage in primary hepatocytes, which is consistent with the much higher *Hilpda* expression in primary mouse hepatocytes compared to mouse liver. Specific physiological, pathological, and pharmacological stimuli may elevate HILPDA levels, thereby rendering HILPDA more important. A pathological condition associated with upregulation of *Hilpda* is infection with hepatitis C virus [42], which, interestingly, uses lipid droplets for replication [43, 44]. Also, as HILPDA is highly induced by hypoxia and HIF1α, HILPDA is an excellent candidate to mediate the stimulatory effect of hypoxia/HIF1α on hepatic triglyceride levels [22, 45]. We speculate that an elevated expression of HIF1α may also explain the higher expression of HILDPA in primary hepatocytes compared to mouse liver.

The observed reduction in lipid storage in HILPDA-deficient hepatocytes is consistent with the data by DiStefano and colleagues [19]. According to their fatty acid flux data, the decrease in lipid storage is explained by a combination of decreased fatty acid uptake, increased fatty acid beta-oxidation, and increased triglyceride lipolysis. While triglyceride lipolysis is known to be directly targeted by HILPDA, it is unclear if fatty acid uptake and β-oxidation are as well, or if they are affected indirectly.

Currently, hardly anything is known about HILPDA in human liver. If the expression level of *HILPDA* in human liver is sufficiently high, inactivation of HILPDA could in theory be a promising strategy to treat non-alcoholic fatty liver disease. Whether NAFLD is associated with a change in the expression of *HILPDA* in human liver is unknown. Because loss-of-function variants in *HILPDA* would be expected to lead to reduced hepatic lipid storage, *HILPDA* is unlikely to emerge from any genome-wide association screens on NAFLD. Using multiple tools, we searched for SNP missense variants in the protein-coding region of the *HILPDA* gene. We identified several missense variants, a number of which was predicted to have a negative impact on protein structure. However, all identified missense variants are rare or very rare with a minor allele frequency <0.1%. Accordingly, human genetic studies are unlikely to clarify the role of HILPDA in human liver.

As our gene targeting strategy was directed towards HILPDA in hepatocytes, our conclusions are also limited to the role of HILPDA in these cells. The fact that albumin Cre-mediated *Hilpda* deletion only reduced hepatic *Hilpda* mRNA by about 50-60% suggests that *Hilpda* is expressed in other liver cell types as well, including possibly Kupffer cells, stellate cells, and endothelial cells. Given the important role of HILPDA in lipid storage in macrophages, it would be of interest to study the effect of LysM-Cre mediated HILPDA deficiency on NASH and on lipid storage in Kupffer cells.

In our study, expression of HILPDA in liver cells was induced by fatty acids, which is consistent with the very sensitive upregulation of HILPDA by fatty acids in macrophages [18, 24]. Besides activating *Hilpda* transcription via PPARs [17, 24], it is possible that fatty acids also specifically upregulate HILPDA at the protein level. The marked upregulation of *Hilpda* by fatty acids is likely part of a feed-forward mechanism to properly dispose of the fatty acids by promoting their storage as triglycerides, either by activating the last step in triglyceride synthesis and/or inhibiting the first step in triglyceride breakdown, thereby avoiding potentially lipotoxic levels of fatty acids.

Our study has several limitations. First, studies in cell culture were performed with overexpressed and tagged proteins, which may have influenced the results. It should be noted, though, that the colocalization of HILPDA to the ER and lipid droplets is fully in agreement with previous immunofluorescence studies on endogenous HILPDA [24, 46]. Moreover, to be able to study protein-protein interactions in live cells via FRET-FLIM, it is necessary to overexpress and tag proteins. Second, the expression of *Hilpda* in mouse liver is low, certainly compared to macrophages, limiting the impact of HILPDA deficiency. Nevertheless, we could clearly detect HILPDA protein by Western blot in mouse liver, and observed a marked decrease in HILPDA abundance in hepatocyte-specific HILPDA-deficient mice. Third, direct evidence showing that physiological levels of HILPDA regulate triglyceride storage in mouse liver via DGAT1 is lacking. Addressing this question is technically extremely challenging. Instead, we showed that the stimulatory effect of HILPDA overexpression on triglyceride synthesis in liver cells is mediated by DGAT1. Furthermore, we show in adipocytes that the inhibitory effect of HILPDA on fatty acid release is dependent on DGAT1. Fourth, the only direct evidence for a physical interaction between HILPDA and DGAT1 is via FRET-FLIM. Unfortunately, numerous efforts to try to immunoprecipitate HILPDA in cells failed, which is common for LD-associated proteins.

In conclusion, HILPDA serves as an intracellular sensor for fatty acids that couples changes in intracellular fatty acid levels to lipid storage. Specifically, our data suggest that besides inhibiting ATGL-mediated lipolysis, HILPDA increases lipid storage in cells by stimulating DGAT1-catalyzed triglyceride synthesis.

Acknowledgements/Grant support

Funding from the Netherlands Organisation for Scientific Research (2014/12392/ALW), Consejo Nacional de Ciencia y Tecnologia de México (CONACYT-455071) and from the Netherlands Cardiovascular Research Initiative (CVON2014-02 ENERGISE), an initiative with support of the Dutch Heart Foundation, is gratefully acknowledged. The authors would like to thank Matthijs Hesselink for valuable comments on the manuscript and Venetia Bazioti, Marialena Chrysanthou, Kaja Hribar, Anneke Hempel, Fabian Rood, and Shohreh Keshtkar for their help in carrying out the experiments.

References

[1] Gross, D.A., Silver, D.L., 2014. Cytosolic lipid droplets: from mechanisms of fat storage to disease. Critical reviews in biochemistry and molecular biology 49:304-326.

[2] Greenberg, A.S., Coleman, R.A., Kraemer, F.B., McManaman, J.L., Obin, M.S., Puri, V., et al., 2011. The role of lipid droplets in metabolic disease in rodents and humans. J Clin Invest 121:2102-2110.

[3] Yki-Jarvinen, H., 2014. Non-alcoholic fatty liver disease as a cause and a consequence of metabolic syndrome. Lancet Diabetes Endocrinol 2:901-910.

[4] Perlemuter, G., Bigorgne, A., Cassard-Doulcier, A.M., Naveau, S., 2007. Nonalcoholic fatty liver disease: from pathogenesis to patient care. Nat Clin Pract Endocrinol Metab 3:458-469.

[5] Hodson, L., 2019. Hepatic fatty acid synthesis and partitioning: the effect of metabolic and nutritional state. The Proceedings of the Nutrition Society 78:126-134.

[6] Ipsen, D.H., Lykkesfeldt, J., Tveden-Nyborg, P., 2018. Molecular mechanisms of hepatic lipid accumulation in non-alcoholic fatty liver disease. Cell Mol Life Sci 75:3313-3327.

[7] Beller, M., Riedel, D., Jansch, L., Dieterich, G., Wehland, J., Jackle, H., et al., 2006. Characterization of the Drosophila lipid droplet subproteome. Mol Cell Proteomics 5:1082-1094.

[8] Brasaemle, D.L., Dolios, G., Shapiro, L., Wang, R., 2004. Proteomic analysis of proteins associated with lipid droplets of basal and lipolytically stimulated 3T3-L1 adipocytes. J Biol Chem 279:46835-46842.

[9] Turro, S., Ingelmo-Torres, M., Estanyol, J.M., Tebar, F., Fernandez, M.A., Albor, C.V., et al., 2006. Identification and characterization of associated with lipid droplet protein 1: A novel membrane-associated protein that resides on hepatic lipid droplets. Traffic 7:1254-1269.

[10] Yang, L., Ding, Y., Chen, Y., Zhang, S., Huo, C., Wang, Y., et al., 2012. The proteomics of lipid droplets: structure, dynamics, and functions of the organelle conserved from bacteria to humans. J Lipid Res 53:1245-1253.

[11] Sztalryd, C., Brasaemle, D.L., 2017. The perilipin family of lipid droplet proteins: Gatekeepers of intracellular lipolysis. Biochimica et biophysica acta. Molecular and cell biology of lipids 1862:1221-1232.

[12] Brown, A.L., Mark Brown, J., 2017. Critical roles for alpha/beta hydrolase domain 5 (ABHD5)/comparative gene identification-58 (CGI-58) at the lipid droplet interface and beyond. Biochimica et biophysica acta. Molecular and cell biology of lipids 1862:1233-1241.

[13] Gao, G., Chen, F.J., Zhou, L., Su, L., Xu, D., Xu, L., et al., 2017. Control of lipid droplet fusion and growth by CIDE family proteins. Biochimica et biophysica acta. Molecular and cell biology of lipids 1862:1197-1204.

[14] Zhang, X., Heckmann, B.L., Campbell, L.E., Liu, J., 2017. G0S2: A small giant controller of lipolysis and adipose-liver fatty acid flux. Biochimica et biophysica acta. Molecular and cell biology of lipids 1862:1146-1154.

[15] Gimm, T., Wiese, M., Teschemacher, B., Deggerich, A., Schodel, J., Knaup, K.X., et al., 2010. Hypoxia-inducible protein 2 is a novel lipid droplet protein and a specific target gene of hypoxia-inducible factor-1. FASEB J 24:4443-4458.

[16] Dijk, W., Mattijssen, F., de la Rosa Rodriguez, M., Loza Valdes, A., Loft, A., Mandrup, S., et al., 2017. Hypoxia-inducible lipid droplet-associated (HILPDA) is not a direct physiological regulator of lipolysis in adipose tissue. Endocrinology 158:1231-1251.

[17] Mattijssen, F., Georgiadi, A., Andasarie, T., Szalowska, E., Zota, A., Krones-Herzig, A., et al., 2014. Hypoxia-inducible lipid droplet-associated (HILPDA) is a novel peroxisome proliferator-activated receptor (PPAR) target involved in hepatic triglyceride secretion. J Biol Chem 289:19279-19293.

[18] van Dierendonck, X., de la Rosa Rodriguez, M.A., Georgiadi, A., Mattijssen, F., Dijk, W., van Weeghel, M., et al., 2020. HILPDA Uncouples Lipid Droplet Accumulation in Adipose Tissue Macrophages from Inflammation and Metabolic Dysregulation. Cell reports 30:1811-1822 e1816.

[19] DiStefano, M.T., Danai, L.V., Roth Flach, R.J., Chawla, A., Pedersen, D.J., Guilherme, A., et al., 2015. The Lipid Droplet Protein Hypoxia-inducible Gene 2 Promotes Hepatic Triglyceride Deposition by Inhibiting Lipolysis. J Biol Chem 290:15175-15184.

[20] Padmanabha Das, K.M., Wechselberger, L., Liziczai, M., De la Rosa Rodriguez, M., Grabner, G.F., Heier, C., et al., 2018. Hypoxia-inducible lipid droplet-associated protein inhibits adipose triglyceride lipase. J Lipid Res 59:531-541.

[21] VandeKopple, M.J., Wu, J., Auer, E.N., Giaccia, A.J., Denko, N.C., Papandreou, I., 2019. HILPDA Regulates Lipid Metabolism, Lipid Droplet Abundance, and Response to Microenvironmental Stress in Solid Tumors. Mol Cancer Res 17:2089-2101.

[22] Zhang, X., Saarinen, A.M., Hitosugi, T., Wang, Z., Wang, L., Ho, T.H., et al., 2017. Inhibition of intracellular lipolysis promotes human cancer cell adaptation to hypoxia. eLife 6.

[23] Szalowska, E., Tesfay, H.A., van Hijum, S.A., Kersten, S., 2014. Transcriptomic signatures of peroxisome proliferator-activated receptor alpha (PPARalpha) in different mouse liver models identify novel aspects of its biology. BMC genomics 15:1106.

[24] Maier, A., Wu, H., Cordasic, N., Oefner, P., Dietel, B., Thiele, C., et al., 2017. Hypoxia-inducible protein 2 Hig2/Hilpda mediates neutral lipid accumulation in macrophages and contributes to atherosclerosis in apolipoprotein E-deficient mice. FASEB J 31:4971-4984.

[25] McFie, P.J., Stone, S.J., 2011. A fluorescent assay to quantitatively measure in vitro acyl CoA:diacylglycerol acyltransferase activity. J Lipid Res 52:1760-1764.

[26] Mayer, N., Schweiger, M., Romauch, M., Grabner, G.F., Eichmann, T.O., Fuchs, E., et al., 2013. Development of small-molecule inhibitors targeting adipose triglyceride lipase. Nat Chem Biol 9:785-787.

[27] Bolstad, B.M., Irizarry, R.A., Astrand, M., Speed, T.P., 2003. A comparison of normalization methods for high density oligonucleotide array data based on variance and bias. Bioinformatics 19: 185-193.

[28] Irizarry, R.A., Bolstad, B.M., Collin, F., Cope, L.M., Hobbs, B., Speed, T.P., 2003. Summaries of Affymetrix GeneChip probe level data. Nucleic Acids Res 31:e15.

[29] Dai, M., Wang, P., Boyd, A.D., Kostov, G., Athey, B., Jones, E.G., et al., 2005. Evolving gene/transcript definitions significantly alter the interpretation of GeneChip data. Nucleic Acids Res 33 e175.

[30] Chiba, T., Suzuki, S., Sato, Y., Itoh, T., Umegaki, K., 2016. Evaluation of Methionine Content in a High-Fat and Choline-Deficient Diet on Body Weight Gain and the Development of Non-Alcoholic Steatohepatitis in Mice. PLoS One 11:e0164191.

[31] Matsumoto, M., Hada, N., Sakamaki, Y., Uno, A., Shiga, T., Tanaka, C., et al., 2013. An improved mouse model that rapidly develops fibrosis in non-alcoholic steatohepatitis. Int J Exp Pathol 94:93-103.

[32] Singh, R., Kaushik, S., Wang, Y., Xiang, Y., Novak, I., Komatsu, M., et al., 2009. Autophagy regulates lipid metabolism. Nature 458:1131-1135.

[33] Bhatt-Wessel, B., Jordan, T.W., Miller, J.H., Peng, L., 2018. Role of DGAT enzymes in triacylglycerol metabolism. Arch Biochem Biophys 655:1-11.

[34] Qi, J., Lang, W., Geisler, J.G., Wang, P., Petrounia, I., Mai, S., et al., 2012. The use of stable isotope-labeled glycerol and oleic acid to differentiate the hepatic functions of DGAT1 and -2. J Lipid Res 53:1106-1116.

[35] Villanueva, C.J., Monetti, M., Shih, M., Zhou, P., Watkins, S.M., Bhanot, S., et al., 2009. Specific role for acyl CoA:Diacylglycerol acyltransferase 1 (Dgat1) in hepatic steatosis due to exogenous fatty acids. Hepatology 50:434-442.

[36] Wurie, H.R., Buckett, L., Zammit, V.A., 2012. Diacylglycerol acyltransferase 2 acts upstream of diacylglycerol acyltransferase 1 and utilizes nascent diglycerides and de novo synthesized fatty acids in HepG2 cells. The FEBS journal 279:3033-3047.

[37] Coleman, R.A., 2019. It takes a village: channeling fatty acid metabolism and triacylglycerol formation via protein interactomes. J Lipid Res 60:490-497.

[38] Zechner, R., Kienesberger, P.C., Haemmerle, G., Zimmermann, R., Lass, A., 2009. Adipose triglyceride lipase and the lipolytic catabolism of cellular fat stores. J Lipid Res 50:3-21.

[39] Zhang, X., Xie, X., Heckmann, B.L., Saarinen, A.M., Gu, H., Zechner, R., et al., 2019. Identification of an intrinsic lysophosphatidic acid acyltransferase activity in the lipolytic inhibitor G0/G1 switch gene 2 (G0S2). FASEB J 33 6655-6666.

[40] Chitraju, C., Mejhert, N., Haas, J.T., Diaz-Ramirez, L.G., Grueter, C.A., Imbriglio, J.E., et al., 2017. Triglyceride Synthesis by DGAT1 Protects Adipocytes from Lipid-Induced ER Stress during Lipolysis. Cell Metab 26:407-418 e403.

[41] Itabe, H., Yamaguchi, T., Nimura, S., Sasabe, N., 2017. Perilipins: a diversity of intracellular lipid droplet proteins. Lipids Health Dis 16:83.

[42] Hagist, S., Sultmann, H., Millonig, G., Hebling, U., Kieslich, D., Kuner, R., et al., 2009. In vitro-targeted gene identification in patients with hepatitis C using a genome-wide microarray technology. Hepatology 49:378-386.

[43] Barba, G., Harper, F., Harada, T., Kohara, M., Goulinet, S., Matsuura, Y., et al., 1997. Hepatitis C virus core protein shows a cytoplasmic localization and associates to cellular lipid storage droplets. Proc Natl Acad Sci U S A 94:1200-1205.

[44] Miyanari, Y., Atsuzawa, K., Usuda, N., Watashi, K., Hishiki, T., Zayas, M., et al., 2007. The lipid droplet is an important organelle for hepatitis C virus production. Nat Cell Biol 9:1089-1097.

[45] Gonzalez, F.J., Xie, C., Jiang, C., 2018. The role of hypoxia-inducible factors in metabolic diseases. Nat Rev Endocrinol 15: 21-32.

[46] DiStefano, M.T., Roth Flach, R.J., Senol-Cosar, O., Danai, L.V., Virbasius, J.V., Nicoloro, S.M., et al., 2016. Adipocyte-specific Hypoxia-inducible gene 2 promotes fat deposition and diet-induced insulin resistance. Molecular metabolism 5:1149-1161.

Supplemental figures

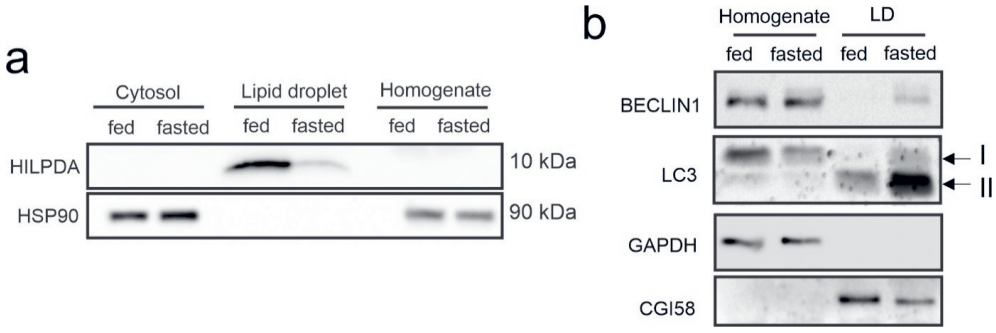

Supplemental figure 1. a) Enrichment of HILPDA in the lipid droplet fraction of fasted and fed wildtype livers as shown by immunoblot. b) Immunoblots showing the presence of autophagy-related proteins Beclin 1 and LC in homogenate and lipid droplets fractions of livers of fed and 24h fasted mice. Five livers of wildtype C57Bl/6 mice were pooled into each sample. Absence of GAPDH validates absence of cytosolic contamination of lipid droplet fractions. Presence of CGI58 (ABHD5) demonstrates enrichment of the LD fraction.

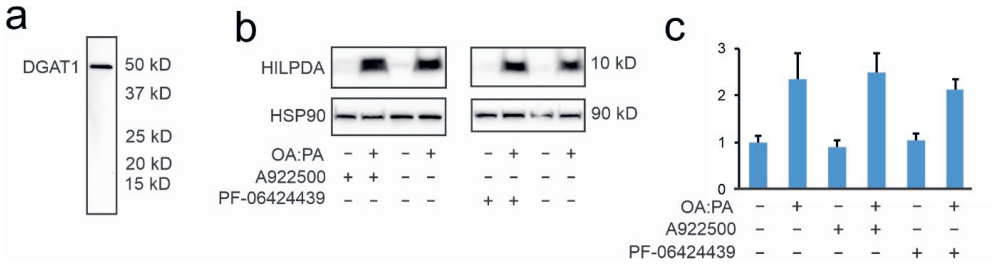

Supplemental figure 2. a) The DGAT1 antibody effectively detects DGAT1 in HepG2 cells transfected with DGAT1 expression vector. No effect of DGAT1 or DGAT2 inhibition on HILPDA protein levels (b) or mRNA levels (c) in Hepa1-6 cells. Hepa1-6 cells were pre-treated with DGAT1 inhibitor (A922500, 1 µM) or DGAT2 inhibitor (PF-06424439, 20 µM) for 30 minutes followed by co-treated for 24 hours with a 2:1 mixture of oleate and palmitate (total concentration (0.6 mM). Error bars represent SD.

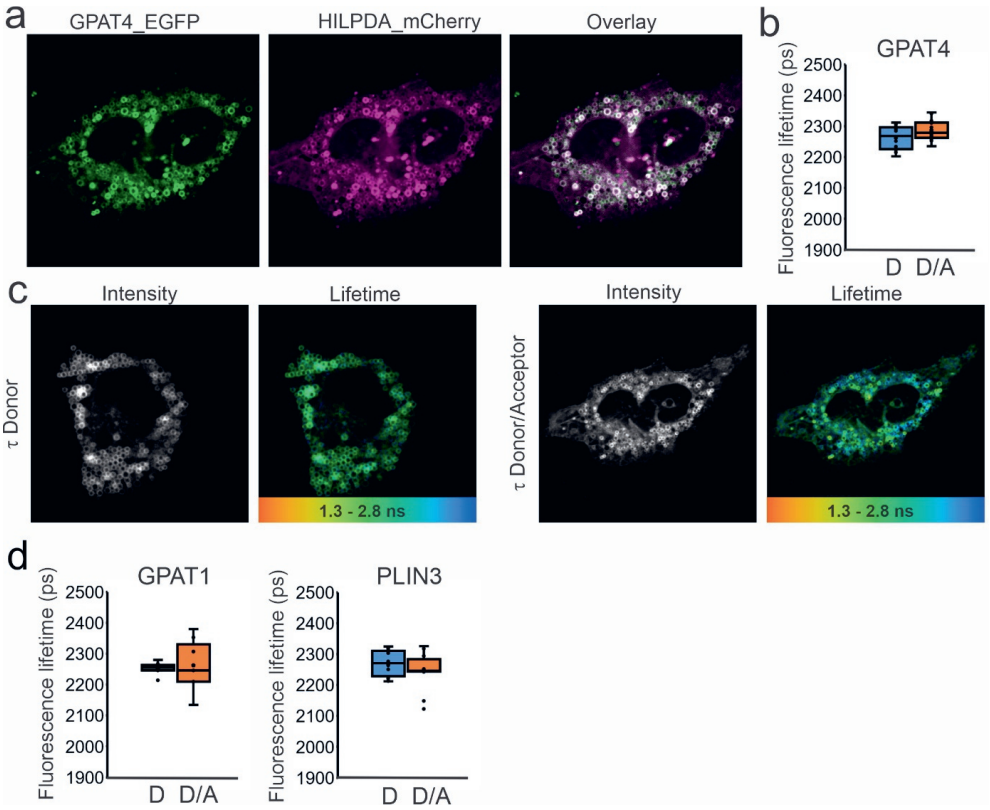

Supplemental figure 3. HepG2 cells were transfected with HILPDA_mCherry and GPAT4_EGFP, GPAT1_EGFP or HILPDA_EGFP and PLIN3_mCherry under lipid loaded conditions. Microscopy was carried out on live cells. a) HILPDA_mCherry and GPAT4_EGFP colocalize in HepG2 cells. b) Fluorescence lifetime (τ) of GPAT4_EGFP in absence and presence of acceptor HILPDA_mCherry. c) Intensity image and LUT coloured lifetime image from GPAT4_EGFP lifetime (τ) in the absence (left) or presence (right) of HILPDA_mCherry. d) Fluorescence lifetime (τ) of GPAT1_EGFP in absence and presence of acceptor HILPDA_EGFP and fluorescence lifetime (τ) of donor HILPDA_EGFP in the absence and presence of acceptor PLIN3_mCherry.

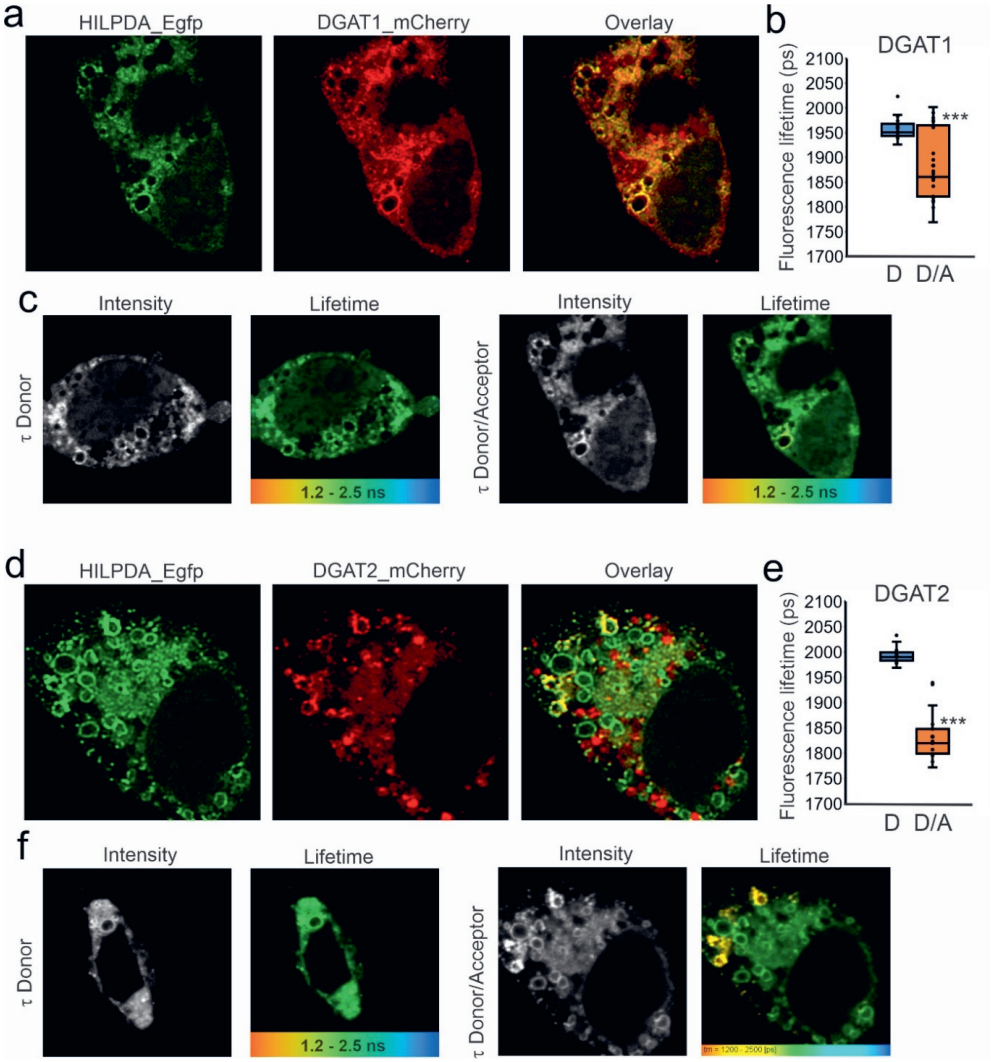

Supplemental figure 4: HILPDA and DGAT1/DGAT2 colocalize and physically interact intracellularly. HepG2 cells were transfected with HILPDA_EGFP and DGAT1_mCherry or DGAT2_mCherry under lipid loaded conditions. Microscopy was carried out on fixed cells. a) HILPDA_EGFP and mDGAT1_mCherry partially colocalize in HepG2 cells. b) Fluorescence lifetime (τ) of HILPDA_EGFP in absence and presence of acceptor DGAT1_mCherry. c) Intensity image and LUT coloured lifetime image from red (1200 ps) to blue (2500 ps) from HILPDA_EGFP lifetime (τ) in the absence (left) or presence (right) of DGAT1_mCherry indicating where interaction occurs) HILPDA_EGFP and DGAT2_mCherry partially colocalize in HepG2 cells. e) Fluorescence lifetime (τ) of HILPDA_EGFP in absence and presence of acceptor DGAT2_mCherry. f) Intensity image and LUT coloured lifetime image from red (1200 ps) to blue (2500 ps) from HILPDA_EGFP lifetime (τ) in the absence (left) or presence (right) of DGAT2_mCherry indicating where interaction occurs. Asterisk indicates significantly different from donor only according to Student's t test; ***P < 0.001.

Supplemental Video 1. HILPDA concentrates in active (lipolyzed/re-emerged) lipid droplets. HepG2 cells were transfected with HILPDA fused to mCherry, the day after transfection cells were starved for 1h with HBSS 0.2% FA-free BSA. Medium was then replaced with QBT fatty acid uptake assay kit, which contains a BODIPY dodecanoic acid fluorescent fatty acid and after 4h incubation cells were imaged on a Leica TCS SP8 X system. λ^{ex}: 561 nm (mCherry) and 488 nm (BODIPY). λ^{em}: 570-620 nm (mCherry) and 505-550 nm (BODIPY). Images were acquired sequentially using 512 x 512. Left, Hilpda in magenta LUTs and fatty acid BODIPY in green LUTs. White tone depicts higher signal intensity from HILPDA_mCherry. Right, Hilpda_mCherry distribution is delineated in white and the underneath fatty acid BODIPY can be visualized in green LUTs. Access code: Delarosa

Chapter 6

Regulation of Lipid Droplet Homeostasis by Hypoxia Inducible Lipid Droplet Associated HILPDA

Montserrat A. de la Rosa Rodriguez, Sander Kersten

Biochim. Biophys. Acta - Mol. Cell Biol. Lipids, vol. 1865, no. 9, p. 158738, 2020

Summary

Nearly all cell types have the ability to store excess energy as triglycerides in specialized organelles called lipid droplets. The formation and degradation of lipid droplets is governed by a diverse set of enzymes and lipid droplet-associated proteins. One of the lipid droplet-associated proteins is Hypoxia Inducible Lipid Droplet Associated (HILPDA). HILPDA was originally discovered in a screen to identify novel hypoxia-inducible proteins. Apart from hypoxia, levels of HILPDA are induced by fatty acids and adrenergic agonists. HILPDA is a small protein of 63 amino acids in humans and 64 amino acids in mice. Inside cells, HILPDA is located in the endoplasmic reticulum and around lipid droplets. Gain- and loss-of-function experiment have demonstrated that HILPDA promotes lipid storage in hepatocytes, macrophages and cancer cells. HILPDA increases lipid droplet accumulation at least partly by inhibiting triglyceride hydrolysis via ATGL and stimulating triglyceride synthesis via DGAT1. Overall, HILPDA is a novel regulatory signal that adjusts triglyceride storage and the intracellular availability of fatty acids to the external fatty acid supply and the capacity for oxidation.

Introduction

Fatty acids are a major fuel for many different types of cells. Indeed, nearly all cells have the ability to oxidize fatty acids in mitochondria, leading to the production of ATP. Fatty acids enter cells via fatty acid transporters. After uptake, they are bound by fatty acid-binding proteins, which direct the fatty acids to their different metabolic fates. When uptake of fatty acids exceeds the requirements and capacity for oxidation, the excess fatty acids are esterified into triglycerides and stored in specialized organelles called lipid droplets [1]. The ability to store energy as triglycerides in lipid droplets endows cells with the ability to overcome periods of limited nutrient supply. In addition, storing fatty acids as triglycerides permits cells to cope with fluctuations in fatty acid supply and avoid lipotoxicity. Nearly all types of cells contain lipid droplets. Whereas an adipocyte contains one large lipid droplet, most cell types have multiple small lipid droplets. Under normal circumstances, these lipid droplets only take up limited space in the cell. However, in certain physiological and pathological conditions, lipid droplets may expand and occupy substantial cell volume [2]. For example, alcoholic and non-alcoholic steatohepatitis are characterized by proliferation and expansion of lipid droplets in hepatocytes [3, 4]. A similar phenomenon is observed in hepatocytes during fasting.

A unique feature of lipid droplets is that they are very dynamic and can quickly expand or shrink depending on cellular demands. The synthesis of triglycerides, their storage in lipid droplets, and the subsequent breakdown of triglycerides into fatty acids is regulated by a complex set of enzymes and lipid droplet-associated proteins. These lipid droplet-associated proteins serve structural roles in lipid droplets and regulate the activity of key lipogenic and lipolytic enzymes [5]. An important group of lipid droplet-associated proteins are the five members of the perilipin family, PLIN1-PLIN5, and the three members of the Cell Death Inducing DFFA Like Effectors (CIDE) family. Detailed information on these groups of lipid droplet-associated proteins can be found elsewhere [6-8]. Recently, the Hypoxia Inducible Lipid Droplet Associated (HILPDA) protein emerged as a novel modulator of intracellular lipid droplet homeostasis in liver, macrophages, and other cell types. This review provides a detailed overview of the role of HILPDA in lipid homeostasis in various cell types.

Cell-specific expression and regulation of HILPDA

HILPDA gene

HILPDA was originally discovered in a subtractive hybridization screen to identify novel genes upregulated by hypoxia in cultured human cervical epithelial cells [9]. The human HILPDA gene is located on chromosome 7 and consists of two exons and one intron, covering a genomic region of 2.6 kb. The human cDNA is almost 1.4 kb and gives rises to a protein of 63 amino acids. The mouse HILPDA protein is slightly larger at 64 amino acids. The primary structure of HILPDA in several mammals is shown in Figure 1A.

According to Genevestigator, HILPDA mRNA is expressed at high levels in numerous tissues and cell types [10]. In humans, high HILPDA mRNA expression is reported in peripheral blood CD8 activated T cells, adipocytes, esophagus, blood vessels, dendritic cells, and various epithelial cells, while in mice, the highest Hilpda mRNA expression is observed in various types of immune cells, including dendritic cells, neutrophils, eosinophils, macrophages, B cells, and T cells, as well as cultured hepatocytes. At the protein level, high HILPDA levels are found in murine white and brown adipose tissue, heart, and lung [11-13].

Regulation of HILPDA expression

The expression of HILPDA in different cell types is controlled by several stimuli. As reflected by its full name, HILPDA is induced by hypoxia. Induction of HILPDA mRNA and protein by hypoxia was first observed in human cervical epithelial cells [9], and was subsequently confirmed in numerous cancer cells and cell lines [9, 14-16], and macrophages [12, 17]. Induction of HILPDA by hypoxia is mediated by HIF-1α via a number of hypoxia-response elements located 300 nucleotides upstream of the transcriptional start site of the *Hilpda* gene [14].

Another potent stimulus of *Hilpda* mRNA expression are fatty acids, which has been observed in various types of macrophages [12, 17], hepatocytes [18], mouse embryonic fibroblasts [15], and in the HCT116 human colon cancer cell line [15]. The relative increase in HILPDA protein by fatty acids is more pronounced than the increase in *Hilpda* mRNA, which is consistent with the observation that fatty acids protect HILPDA from degradation [14]. Induction of *Hilpda* mRNA is likely mediated in part by the fatty acid-inducible PPAR transcription factors. In human and mouse hepatocytes, *Hilpda* mRNA is upregulated by PPARα via a conserved PPAR response element located 1200 base pairs upstream of the transcription start site [19]. Regulation by PPARα is not responsible for the induction of hepatic *Hilpda* mRNA and protein during fasting [19, 20]. In human and mouse adipocytes, *HILPDA* mRNA is upregulated by PPARγ via a prominent PPARγ superenhancer covering

about 8 kb upstream of the *HILPDA* gene and containing several conserved PPARγ binding sites.

Other stimuli that increase HILPDA mRNA and protein levels are numerous β-adrenergic agonists and forskolin. These effects were observed in adipocytes and suggest a stimulatory effect of cAMP [11, 13]. Fasting induces *Hilpda* mRNA and protein levels in mouse adipose tissue, which may be mediated by cAMP [11]. In bone marrow-derived macrophages, HILPDA protein is highly induced by lipopolysaccharide [17].

Lastly, *HILPDA* mRNA and protein levels were found to be upregulated in different types of tumor cells, including renal cell carcinoma, ovarian clear cell adenocarcinoma, colorectal adenoma and carcinoma, and in different solid tumors [16, 21, 22]. In renal cell carcinoma cell lines, *HILPDA* expression is under positive transcriptional control of the β-catenin/Wnt pathway. Induction of *HILPDA* expression by the β-catenin/Wnt pathway was shown to be mediated by a TCF/LEF binding site about 2.1 kb upstream of the transcriptional start site [23].

Intracellular localization of HILPDA

HILPDA has been shown to localize to lipid droplets in several different cell types [11, 14, 20]. Nevertheless, not all lipid droplets are surrounded by HILPDA. In contrast to PLIN2, a ubiquitously expressed and constitutive lipid droplet-associated protein, HILPDA only colocalizes with a subpopulation of the lipid droplets [14, 18]. Apart from lipid droplets, HILPDA has also been shown to localize to and migrate through the endoplasmic reticulum, the site of lipid droplet synthesis [17, 18]. In addition, it was found that HILPDA preferably accumulates in lipid droplets undergoing remodelling (shrinking and expansion), and that HILPDA is present in the perinuclear area, where it correlates significantly with newly synthesized triglycerides [18]. Consistent with this observation, HILPDA was shown to colocalize with the lipolytic and lipogenic enzymes ATGL and DGAT1/2 respectively [16, 18, 24, 25]. Together, these observations suggest that HILPDA is coupled to a functionally distinct subpopulation of lipid droplets that is undergoing active remodelling, which fits with its alleged role as small molecule inhibitor and activator of lipolysis and triglyceride synthesis, respectively (see below).

Molecular mechanism of action of HILPDA

HILPDA is a small protein that bears no homology with any other protein, except for a conserved region that is predicted to be a transmembrane domain. This stretch of 24 amino acids, which is close to the N-terminus and targets HILPDA to lipid droplets, is highly

homologous to a region in the protein G0S2 (Figure 1B, 1C). G0S2 functions as an inhibitor of ATGL in several tissues, including adipose tissue, liver, and skeletal muscle [26]. Recent research suggests that HILPDA also inhibits ATGL. In HILPDA-deficient HTC116 cells, mouse embryonic fibroblasts, and bone marrow-derived macrophages, ATGL inactivation restored the decrease in lipid droplets and triglyceride storage, whereas it had minimal effect on lipid storage in wildtype cells [12, 15, 16]. Moreover, the increase in lipolysis in HILPDA-deficient cells was restored by ATGL inactivation [15, 16]. These data indicate that HILPDA is an endogenous and physiological inhibitor of ATGL. Biochemical studies indicate that HILPDA directly inhibits ATGL triglyceride hydrolase activity via a direct physical interaction between the two proteins [16, 24]. This interaction was also observed intracellularly in live cells using FRET-FLIM [24]. The ATGL interaction and inhibition by HILPDA are mediated by the conserved N-terminus of HILPDA and crucially depend on residues 7-11 [15, 16, 24]. The HILPDA interacting region in ATGL covers the N-terminal patatin domain-containing region, which also mediates triglyceride hydrolysis and the interaction with CGI-58/ABHD5, Atglistatin, acyl-CoA, and G0S2.

Interestingly, in a cell-free system, the interaction between ATGL and HILPDA was found to be substantially weaker than the interaction between ATGL and G0S2 [24], which may also explain why initial studies failed to provide support for ATGL inhibition by HILPDA [19]. Nevertheless, studies in HILPDA-deficient cells indicate that HILPDA effectively inhibits ATGL-mediated lipolysis. Additional research is needed to determine why HILPDA is less potent in cell-free systems compared to live cells, but it can be hypothesized that HILPDA requires interaction with an auxiliary factor to gain full activity. It should be noted that apart from binding and inhibiting ATGL, HILPDA also seems to reduce ATGL protein levels, possibly by destabilizing ATGL protein [11, 12].

Besides inhibiting lipolysis, in a recent preprint, HILPDA was shown to promote intracellular lipid accumulation by enhancing triglyceride synthesis [18]. The final rate-limiting step in the formation of triglycerides is catalyzed by diacylglycerol acyltransferases (DGAT), consisting of two evolutionarily unrelated enzymes DGAT1 and DGAT2. It has been shown that DGAT2 preferentially catalyzes triglyceride synthesis from *de novo* synthesized fatty acids, whereas DGAT1 catalyzes triglyceride synthesis from exogenous fatty acids or fatty acids released by lipolysis [27] . In the preprint, HILPDA was shown to colocalize and physically interact with DGAT1 and DGAT2 in HepG2 cells and promotes DGAT activity. Although HILPDA colocalized with DGAT2 it needs exogenous fatty acids to increase triglyceride accumulation. This indicates that DGAT1 is the preferred target of HILPDA. In addition, HILPDA increases protein levels of DGAT1, possibly by serving as a protein stabilizer. Collectively, HILPDA may thus promote intracellular lipid storage by suppressing

lipolysis via inhibition of ATGL and inducing triglyceride synthesis via activation of DGAT1[18].

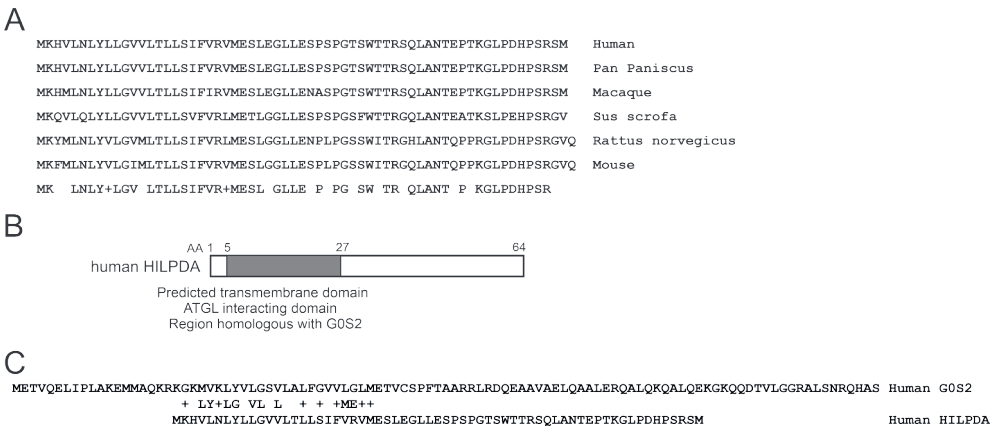

Figure 1. Primary sequence of HILPDA. A) Comparative analysis of the amino acid sequence of HILPDA in different species. B) Graphical presentation of the primary sequence of HILPDA, highlighting the N-terminal domain involved in interactions with lipid droplets and ATGL. C) Comparative analysis of the amino acid sequence of human HILPDA and G0S2, showing significant homology in the N-terminal region of HILPDA.

Role of HILPDA in lipid metabolism in various cells and tissues

Numerous studies have demonstrated that HILPDA promotes lipid storage in various cells and tissues. Below, an overview is given of the functional data on HILPDA in different cell types.

Hepatocytes

Overexpression of HILPDA in primary hepatocytes or hepatoma cells significantly increases intracellular lipid accumulation [18, 20]. Similarly, in vivo AAV-mediated HILPDA over-expression markedly increases liver triglyceride content, which is at least in part due to a decrease in VLDL-TG secretion [19]. Conversely, hepatic HILPDA deficiency was found to lower liver triglycerides, yet only in mice fed chow, a semi-purified low fat diet, and a choline and methionine deficient high fat diet [18, 20]. The overall magnitude of the decrease in hepatic triglycerides by HILPDA deficiency is modest. No significant decrease in liver triglycerides was found in HILPDA deficient mice fed a regular semi-purified high fat

diet or mice in the fasted or refed state [18, 20]. In vitro, HILPDA deficiency caused a very pronounced decrease in cellular lipid accumulation in primary hepatocytes and liver slices. The modest effect of HILPDA deficiency on triglyceride levels in mouse liver compared to primary mouse hepatocytes or mouse liver slices may be explained by the relatively low expression of *Hilpda* in mouse liver as compared to ex vivo [18].

Mechanistically, it was shown that HILPDA deficiency in hepatocytes increases triglyceride turnover and lipolysis, as well as fatty acid β-oxidation [20]. The elevated triglyceride turnover in HILPDA-deficient hepatocytes is likely mediated by an inhibitory and stimulatory effect of HILPDA on ATGL and DGAT1 activity, respectively. [18]

Neither HILPDA overexpression nor deficiency in liver has any influence on plasma cholesterol, triglyceride, ketone body, or non-esterified fatty acid (NEFA) levels [18-20]. Interestingly, hepatic HILPDA deficiency significantly improved glucose tolerance in mice fed chow or a high fat diet, while no significant effect of HILPDA deficiency was observed on insulin tolerance [20]. Currently, the mechanism underlying the changes in glucose tolerance remains unclear.

Adipocytes

HILPDA is expressed at high levels in brown and white adipocytes and increases during mouse 3T3-L1, mouse primary brown fat, and human SGBS adipogenesis [11, 13, 28]. Nevertheless, HILPDA does not seem to be directly implicated in adipogenesis [11]. The effect of HILPDA deficiency in adipocytes has been studied in vivo and in vitro. In vivo, adipocyte-specific HILPDA deficiency significantly decreased weight of the epididymal fat depot in mice fed a high fat diet [28]. In contrast, no effect of HILPDA deficiency on weight of adipose tissue depots was observed under conditions of 24-hour fasting, 10-day cold exposure, acute injection of a β3-adrenergic agonist, and when mice were fed a high fat diet at thermoneutrality [11, 28]. In all of the above conditions, HILPDA deficiency in adipocytes did not alter plasma NEFAs and glycerol, two systemic measures of lipolysis, nor did it influence plasma triglycerides [11, 28]. The effects of HILPDA deficiency on ex vivo and in vitro lipolysis are mixed. HILPDA deficiency did not influence basal or isoproterenol-induced ex vivo NEFAs and glycerol release from adipose tissue explants and primary adipocytes [11, 13, 28]. Also, *Hilpda* silencing did not influence fatty acid and glycerol release in 3T3-L1 adipocytes, despite lower triglyceride storage. By contrast, AV-mediated HILPDA overexpression significantly decreased fatty acid release by 3T3-L1 adipocytes, concurrent with a marked reduction in ATGL protein levels. Interestingly, HILPDA deficiency in adipocytes raised liver triglycerides in mice after fasting, which may reflect increased delivery of NEFAs from adipose tissue [11]. Collectively, these data lead to the tentative

conclusion that HILPDA is not a major physiological regulator of adipocyte lipolysis, although additional studies are warranted.

Interestingly, in vivo adipocyte-specific HILPDA deficiency was associated with worsened glucose tolerance in mice fed a high fat diet at thermoneutrality, but improved glucose tolerance at 23°C [28]. The latter result appears to be due to deficiency of HILPDA in brown adipocytes. How deficiency of HILPDA in brown adipocytes may improve glucose tolerance is unknown. By contrast, whole body *Hilpda*-/- mice fed chow and kept at 22°C exhibited no change in glucose tolerance [13].

Macrophages

The functional role of HILPDA in macrophages has been studied by crossing *Hilpda*$^{flox/flox}$ mice with mice expressing Cre under the Tie2 promoter (endothelial and hematopoietic cells) or LysM promoter (myeloid cells). These models, which both lead to a very pronounced reduction in HILPDA levels in bone marrow-derived macrophages, consistently show a marked reduction in intracellular lipid droplets and total lipid levels, which are not caused by decreased fatty acid uptake but rather by decreased triglyceride retention [12, 17]. The decrease in triglyceride retention was shown to be mediated by elevated ATGL-mediated lipolysis. Enhanced lipolysis without efficient disposal of the released fatty acids may be expected to lead to lipotoxicity. Indeed, fatty acid-loaded HILPDA-deficient macrophages exhibited increased formation of reactive oxygen species, decreased cell viability, and elevated fatty acid-dependent gene regulation [12, 17]. However, lipotoxicity may be limited in HILPDA-deficient macrophages by increased oxidative disposal of fatty acids [12].

Lipid-laden macrophages (also known as foam cells) are abundant in atherosclerotic plaques and are a key feature of atherosclerosis. Immunohistochemical studies located HILPDA to foam cells in human atherosclerotic plaques, suggesting a potential role for HILPDA in atherogenesis [14]. In agreement with this notion, in atherosclerosis-prone *Apoe*-/- mice, Tie2-driven HILPDA-deficiency was associated with a marked reduction in atherosclerotic lesions and plaque lipid content [17]. These data suggest that HILPDA may be a potential therapeutic target for atherosclerosis. Another tissue enriched in lipid-laden macrophages is adipose tissue, where foam cells are believed to contribute to the inflammatory phenotype during obesity. Despite reducing lipid storage in adipose tissue macrophages, LysM-driven HILPDA-deficiency did not alter the inflammatory status of adipose tissue in diet-induced obesity, nor did it influence any metabolic perturbations associated with obesity [12]. This study suggests that the contribution of foam cells in

obesity-induced inflammation and metabolic dysregulation may be less important than previously envisioned.

Tumor cells

Expression of *HILPDA* has been found to be upregulated in several cancers, including renal [23], ovarian [22], uterine [29], and colon cancers [21]. The functional role of HILPDA has been studied in HTC116 cells, a human colon cancer cell line. In these cells, hypoxia was found to increase intracellular triglycerides by inhibiting lipolysis in a HILPDA-dependent manner [15, 16]. Similarly, fatty acids increased lipid droplet abundance and intracellular triglycerides in HTC116 cells via HILPDA [15]. HILPDA deficiency in hypoxic HTC116 cells led to enhanced apoptosis, elevated ROS production, and increased fatty acid oxidation, concomitant with upregulation of PPAR target genes [15, 16]. Co-ablation of ATGL was able to rescue these effects of HILPDA deficiency, indicating that the pro-survival effect of HILPDA against apoptosis during hypoxia is mediated by inhibition of lipolysis [16]. Interestingly, the growth of HCT116 tumors in nude mice was slower for the HILPDA deficient cells than for wildtype cells [15, 16]. Consistent with HILPDA acting via ATGL, deficiency of ATGL along with HILPDA restored tumor growth and rescued the effects elicited by HILPDA deficiency alone [16]. Overall, these data suggest that HILPDA promotes cancer cell survival via inhibition of lipolysis by decreasing lipotoxicity, ROS production, and oxidative damage.

Whole body

Experiments using whole body *Hilpda*-/- mice have shown that HILPDA is not required for viability, growth and reproduction [13]. However, at 22℃, *Hilpda*-/- mice were less active, had lower energy expenditure, and lower food intake. In addition, *Hilpda*-/- mice had lower body temperature after fasting, suggesting that HILPDA is required for maintaining body temperature during fasting. *Hilpda*-/- mice did not exhibit any significant change in plasma cholesterol, triglycerides, creatine kinase, lactate dehydrogenase, and in the triglyceride content of adipose tissue, liver and muscle [13].

HILPDA and G0S2

G0S2 was recognized by Zhang et al. as an interacting partner and selective inhibitor of ATGL(10.1016/j.cmet.2010.02.003). The human cDNA is almost 0.9 kb and gives rises to a protein of 103 amino acids. Compared to G0s2 the Hilpda gene is evolutionary younger (24).

G0S2 and HILPDA interact with ATGL through the LY(V/L)LG motif conserved between their hydrophobic domain (DOI: 10.7554/eLife.31132). However, on a cell-free system HILPDA showed a lower inhibitory capacity than G0S2 (IC50 value 2 μM vs. 22 nM for HILPDA and G0S2, respectively) (PMID: 29326160). Nonetheless, as previously mentioned, in-vivo HILPDA can effectively inhibit ATGL-mediated lipolysis. Whereas both proteins are ubiquitously present their expression level varies among tissues and cells. G0S2 is highly expressed in murine white and brown adipose tissue, heart, and liver ((10.1016/j.cmet.2010.02.003). HILPDA is highly express in immune cells, white and brown adipose tissue, heart, and lung. Interestingly, in several types of human cancers G0s2 is methylated and silenced (PMID: 19706769, PMID: 20399149, PMID: 26837760,). Similarly to Hilpda, G0s2 is induced by fatty acids via PPARs but also via LXRα in liver (10.1172/jci.insight.88735, doi: 10.1042/BJ20050636). Although HILPDA and ATGL share a common function and activation by PPARs they have slight differences in their expression pattern, environmental drivers, and inhibitory efficiency. Nonetheless, under conditions were both are upregulated, like fatty acid induction it can be hypothesize G0s2 and HILPDA act on different subpopulations of lipid droplets (Fig·#). On the one hand G02s may completely inhibit lipolysis from a specific subpopulation of lipid droplets and HILPDA partially inhibiting lipolysis while activating TG synthesis via DGAT1. Through this mechanism mammalian cells can finely select the LD undergoing lipolysis, control the availability and possibly the type of fatty acids for cellular function. Further research on protein-protein interactions to identifying the protein network of G0S2 and HILPDA will aid to further understand the co-existence of these proteins.

Concluding remarks and Future perspectives

Studies over the past decade have shown that HILPDA has a profound impact on intracellular fatty acid metabolism. Tissue-specific *Hilpda*-deficient mouse models suggest that the importance of HILPDA in regulating cellular triglyceride storage is cell-type specific and is likely dictated by the level of HILPDA expression, as well as by the expression of related proteins such as G0S2. Mechanistically, HILPDA promotes triglyceride storage by inhibiting ATGL-mediated lipolysis and stimulating DGAT1-mediated triglyceride synthesis (Figure 2). It can be hypothesized that HILPDA may be part of a larger triglyceride turnover complex ("lipolysome") that includes enzymes involved in triglyceride synthesis and triglyceride breakdown, including ATGL and DGAT1, as well as regulatory proteins such as ABHD5 and G0S2 [30-32]. Exactly how HILPDA regulates the activity of these enzymes is still unknown. It is conceivable that HILPDA functions as small protein binding partner of ATGL and DGAT1, causing their destabilization (ATGL) or stabilization (DGAT1).

One of the unique features of HILPDA is its marked upregulation by several external stimuli, including hypoxia, fatty acids, and β-adrenergic agonists. It thus seems that HILPDA functions as an adaptive signal that is called into action under specific circumstances. The induction by fatty acids acids is likely part of a feed forward mechanism to properly dispose of intracellular fatty acids by promoting their storage as triglycerides, either by activating the last step in triglyceride synthesis and/or inhibiting the first step in triglyceride breakdown (Figure 2). The induction of HILPDA by hypoxia likely serves to shift fuel utilization towards glucose by lowering the intracellular concentration of fatty acids, which cannot be used as fuel under low oxygen conditions.

A major effect of HILPDA deficiency on lipid metabolism has been observed in macrophages, showing markedly reduced lipid storage as a result of enhanced lipolysis. So far, the functional impact of HILPDA deficiency in macrophages has only been studied in relation to atherosclerosis and adipose tissue inflammation. In the future, it would be of interest to investigate the role of macrophage HILPDA in non-alcoholic steatohepatitis. In addition, HILPDA may be involved in other diseases characterized by foamy macrophages, including tuberculosis, multiple sclerosis, and kidney disease. Finally, it would be interesting to explore whether HILPDA plays an important role in lipid storage in microglial cells, especially since it was recently proposed that lipid accumulation in microglial cells is connected with aging in mouse and human brains [33].

As mentioned previously, HILPDA is not only highly expressed in macrophages but also in numerous other immune cells, including dendritic cells, neutrophils, eosinophils, B cells, and T cells. Currently, the role of HILPDA in these immune cells is unknown. Inactivation of

HILPDA may be an effective tool to study the functional roles of lipid droplets in immune cells, which are still poorly characterized.

Overall, it can be concluded that HILPDA is a novel regulator of intracellular lipid metabolism. Specific stimuli such as hypoxia and fatty acids promote intracellular lipid storage at least partly via upregulation of HILPDA. HILPDA thus adjusts triglyceride storage and the intracellular availability of fatty acids to the external fatty acid supply and the capacity for oxidation.

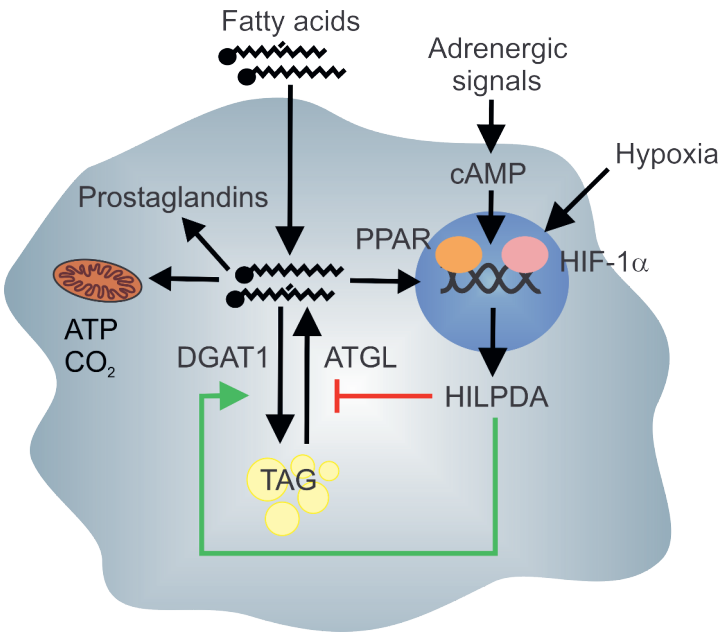

Figure 2. Role of HILPDA in cellular lipid metabolism. Fatty acids increase HILPDA levels in cells via a transcriptional mechanism. Hypoxia increases HILPDA levels via HIF-1α-mediated transcriptional regulation. HILPDA suppresses lipolysis via inhibition of ATGL and induces triglyceride synthesis via activation of DGAT1. Induction of HILPDA by fatty acids and hypoxia can be considered an adaptive mechanism to lower the intracellular concentration of fatty acids.

References

[1] D.A. Gross, D.L. Silver, Cytosolic lipid droplets: from mechanisms of fat storage to disease, Critical reviews in biochemistry and molecular biology, 49 (2014) 304-326.

[2] A.S. Greenberg, R.A. Coleman, F.B. Kraemer, J.L. McManaman, M.S. Obin, V. Puri, Q.W. Yan, H. Miyoshi, D.G. Mashek, The role of lipid droplets in metabolic disease in rodents and humans, J Clin Invest, 121 (2011) 2102-2110.

[3] N.L. Gluchowski, M. Becuwe, T.C. Walther, R.V. Farese, Jr., Lipid droplets and liver disease: from basic biology to clinical implications, Nat Rev Gastroenterol Hepatol, 14 (2017) 343-355.

[4] D.G. Mashek, S.A. Khan, A. Sathyanarayan, J.M. Ploeger, M.P. Franklin, Hepatic lipid droplet biology: Getting to the root of fatty liver, Hepatology, 62 (2015) 964-967.

[5] S. Xu, X. Zhang, P. Liu, Lipid droplet proteins and metabolic diseases, Biochim Biophys Acta Mol Basis Dis, 1864 (2018) 1968-1983.

[6] H. Itabe, T. Yamaguchi, S. Nimura, N. Sasabe, Perilipins: a diversity of intracellular lipid droplet proteins, Lipids Health Dis, 16 (2017) 83.

[7] G. Gao, F.J. Chen, L. Zhou, L. Su, D. Xu, L. Xu, P. Li, Control of lipid droplet fusion and growth by CIDE family proteins, Biochimica et biophysica acta. Molecular and cell biology of lipids, 1862 (2017) 1197-1204.

[8] C. Sztalryd, D.L. Brasaemle, The perilipin family of lipid droplet proteins: Gatekeepers of intracellular lipolysis, Biochimica et biophysica acta. Molecular and cell biology of lipids, 1862 (2017) 1221-1232.

[9] N. Denko, C. Schindler, A. Koong, K. Laderoute, C. Green, A. Giaccia, Epigenetic regulation of gene expression in cervical cancer cells by the tumor microenvironment, Clin Cancer Res, 6 (2000) 480-487.

[10] T. Hruz, O. Laule, G. Szabo, F. Wessendorp, S. Bleuler, L. Oertle, P. Widmayer, W. Gruissem, P. Zimmermann, Genevestigator v3: a reference expression database for the meta-analysis of transcriptomes, Adv Bioinformatics, 2008 (2008) 420747.

[11] W. Dijk, F. Mattijssen, M. de la Rosa Rodriguez, A. Loza Valdes, A. Loft, S. Mandrup, E. Kalkhoven, L. Qi, J.W. Borst, S. Kersten, Hypoxia-inducible lipid droplet-associated (HILPDA) is not a direct physiological regulator of lipolysis in adipose tissue, Endocrinology, 158 (2017) 1231-1251.

[12] X. van Dierendonck, M.A. de la Rosa Rodriguez, A. Georgiadi, F. Mattijssen, W. Dijk, M. van Weeghel, R. Singh, J.W. Borst, R. Stienstra, S. Kersten, HILPDA Uncouples Lipid Droplet Accumulation in Adipose Tissue Macrophages from Inflammation and Metabolic Dysregulation, Cell reports, 30 (2020) 1811-1822.e6.

[13] M.J. VandeKopple, J. Wu, L.A. Baer, N.C. Bal, S.K. Maurya, A. Kalyanasundaram, M. Periasamy, K.I. Stanford, A.J. Giaccia, N.C. Denko, I. Papandreou, Stress-responsive HILPDA is necessary for thermoregulation during fasting, J Endocrinol, 235 (2017) 27-38.

[14] T. Gimm, M. Wiese, B. Teschemacher, A. Deggerich, J. Schodel, K.X. Knaup, T. Hackenbeck, C. Hellerbrand, K. Amann, M.S. Wiesener, S. Honing, K.U. Eckardt, C. Warnecke, Hypoxia-inducible protein 2 is a novel lipid droplet protein and a specific target gene of hypoxia-inducible factor-1, FASEB J, 24 (2010) 4443-4458.

[15] M.J. VandeKopple, J. Wu, E.N. Auer, A.J. Giaccia, N.C. Denko, I. Papandreou, HILPDA Regulates Lipid Metabolism, Lipid Droplet Abundance, and Response to Microenvironmental Stress in Solid Tumors, Mol Cancer Res, 17 (2019) 2089-2101.

[16] X. Zhang, A.M. Saarinen, T. Hitosugi, Z. Wang, L. Wang, T.H. Ho, J. Liu, Inhibition of intracellular lipolysis promotes human cancer cell adaptation to hypoxia, eLife, 6 (2017) e31132.

[17] A. Maier, H. Wu, N. Cordasic, P. Oefner, B. Dietel, C. Thiele, A. Weidemann, K.U. Eckardt, C. Warnecke, Hypoxia-inducible protein 2 Hig2/Hilpda mediates neutral lipid accumulation in macrophages and contributes to atherosclerosis in apolipoprotein E-deficient mice, FASEB J, 31 (2017) 4971-4984.

[18] M.A. de la Rosa Rodriguez, A. Gemmink, M. van Weeghel, M.L. Aoun, R. Singh, J.W. Borst, S. Kersten, Hypoxia-inducible lipid droplet-associated interacts with DGAT1 to promote lipid storage in hepatocytes. bioRxiv 2020.02.26.966374.

[19] F. Mattijssen, A. Georgiadi, T. Andasarie, E. Szalowska, A. Zota, A. Krones-Herzig, C. Heier, D. Ratman, K. De Bosscher, L. Qi, R. Zechner, S. Herzig, S. Kersten, Hypoxia-inducible lipid droplet-associated (HILPDA) is a novel peroxisome proliferator-activated receptor (PPAR) target involved in hepatic triglyceride secretion, J Biol Chem, 289 (2014) 19279-19293.

[20] M.T. DiStefano, L.V. Danai, R.J. Roth Flach, A. Chawla, D.J. Pedersen, A. Guilherme, M.P. Czech, The Lipid Droplet Protein Hypoxia-inducible Gene 2 Promotes Hepatic Triglyceride Deposition by Inhibiting Lipolysis, J Biol Chem, 290 (2015) 15175-15184.

[21] S.H. Kim, D. Wang, Y.Y. Park, H. Katoh, O. Margalit, M. Sheffer, H. Wu, V.R. Holla, J.S. Lee, R.N. DuBois, HIG2 promotes colorectal cancer progression via hypoxia-dependent and independent pathways, Cancer Lett, 341 (2013) 159-165.

[22] S. Nishimura, H. Tsuda, K. Ito, M. Takano, Y. Terai, T. Jobo, J. Kigawa, T. Sugiyama, N. Yaegashi, D. Aoki, Differential expression of hypoxia-inducible protein 2 among different histological types of epithelial ovarian cancer and in clear cell adenocarcinomas, Int J Gynecol Cancer, 20 (2010) 220-226.

[23] A. Togashi, T. Katagiri, S. Ashida, T. Fujioka, O. Maruyama, Y. Wakumoto, Y. Sakamoto, M. Fujime, Y. Kawachi, T. Shuin, Y. Nakamura, Hypoxia-inducible protein 2 (HIG2), a novel diagnostic marker for renal cell carcinoma and potential target for molecular therapy, Cancer Res, 65 (2005) 4817-4826.

[24] K.M. Padmanabha Das, L. Wechselberger, M. Liziczai, M. De la Rosa Rodriguez, G.F. Grabner, C. Heier, R. Viertlmayr, C. Radler, J. Lichtenegger, R. Zimmermann, J.W. Borst, R. Zechner, S. Kersten, M. Oberer, Hypoxia-inducible lipid droplet-associated protein inhibits adipose triglyceride lipase, J Lipid Res, 59 (2018) 531-541.

[25] R. Schreiber, H. Xie, M. Schweiger, Of mice and men: The physiological role of adipose triglyceride lipase (ATGL), Biochimica et biophysica acta. Molecular and cell biology of lipids, 1864 (2019) 880-899.

[26] X. Zhang, B.L. Heckmann, L.E. Campbell, J. Liu, G0S2: A small giant controller of lipolysis and adipose-liver fatty acid flux, Biochimica et biophysica acta. Molecular and cell biology of lipids, 1862 (2017) 1146-1154.

[27] C.L. Yen, S.J. Stone, S. Koliwad, C. Harris, R.V. Farese, Jr., Thematic review series: glycerolipids. DGAT enzymes and triacylglycerol biosynthesis, J Lipid Res, 49 (2008) 2283-2301.

[28] M.T. DiStefano, R.J. Roth Flach, O. Senol-Cosar, L.V. Danai, J.V. Virbasius, S.M. Nicoloro, J. Straubhaar, S. Dagdeviren, M. Wabitsch, O.T. Gupta, J.K. Kim, M.P. Czech, Adipocyte-specific Hypoxia-inducible gene 2 promotes fat deposition and diet-induced insulin resistance, Molecular metabolism, 5 (2016) 1149-1161.

[29] S. Nishimura, H. Tsuda, H. Nomura, F. Kataoka, T. Chiyoda, H. Tanaka, K. Tanaka, N. Susumu, D. Aoki, Expression of hypoxia-inducible 2 (HIG2) protein in uterine cancer, Eur J Gynaecol Oncol, 32 (2011) 146-149.

[30] B. Bhatt-Wessel, T.W. Jordan, J.H. Miller, L. Peng, Role of DGAT enzymes in triacylglycerol metabolism, Arch Biochem Biophys, 655 (2018) 1-11.

[31] R.A. Coleman, It takes a village: channeling fatty acid metabolism and triacylglycerol formation via protein interactomes, J Lipid Res, 60 (2019) 490-497.

[32] R. Zechner, P.C. Kienesberger, G. Haemmerle, R. Zimmermann, A. Lass, Adipose triglyceride lipase and the lipolytic catabolism of cellular fat stores, J Lipid Res, 50 (2009) 3-21.

[33] J. Marschallinger, T. Iram, M. Zardeneta, S.E. Lee, B. Lehallier, M.S. Haney, J.V. Pluvinage, V. Mathur, O. Hahn, D.W. Morgens, J. Kim, J. Tevini, T.K. Felder, H. Wolinski, C.R. Bertozzi, M.C. Bassik, L. Aigner, T. Wyss-Coray, Lipid-droplet-accumulating microglia represent a dysfunctional and proinflammatory state in the aging brain, Nat Neurosci, 23 (2020) 194-208.

Chapter 7

Regulation and functional characterization of the mitochondrial transporter SLC25A47

Montserrat A. de la Rosa Rodriguez, Brecht Attema, Evert M. van Schothorst, Sander Grefte, Sander Kersten

Manuscript in preparation

Introduction

The liver plays a central role in governing lipid metabolism in various nutritional conditions. In the fed state, the liver actively synthesizes cholesterol, bile acids, and fatty acids. In the fasted state, the liver takes up large quantities of fatty acids coming from the adipose tissue. These fatty acids are oxidized, converted into ketone bodies, or esterified into triglycerides (1). The latter are stored in lipid droplets or are secreted as a component of very low-density lipoproteins (2).

The changes in lipid metabolism during feeding and fasting are partly driven by changes in circulating levels of key metabolic hormones and are largely effectuated through enzyme regulation at the transcriptional, translational, and post-translational levels. Whereas post-translational mechanisms are crucial for the acute regulation of enzymatic activity, transcriptional mechanisms are particularly important for the more chronic regulation of metabolic pathways. In the last few decades, numerous transcription factors have been identified that are involved in the transcriptional regulation of hepatic lipid metabolism. Many of these transcription factors belong to the superfamily of nuclear hormone receptors (3). A specific group of nuclear receptors that play a central role in the regulation of lipid metabolism are the peroxisome proliferator-activated receptors (PPARs) (4). PPARs are activated by a variety of fatty acids and fatty acid-derived compounds, as well as by certain drugs and other synthetic compounds. Three different PPARs can be distinguished: PPARα (Nr1c1), PPARβ/δ (Nr1c2), and PPARγ (Nr1c3) (4). Although all PPARs are expressed to some extent in the liver, the role of the PPARα isotype in the liver has been characterized in the greatest detail. Transcriptome analyses of the liver of whole body and liver-specific PPARα−/− mice have demonstrated that PPARα induces the expression of hundreds of genes involved in fatty acid metabolism, including fatty acid uptake, transport, activation, elongation, esterification, storage, and oxidation (5-7). Consistent with the classification of PPARα as a master regulator of hepatic lipid metabolism during fasting (8, 9), the transcriptional regulation of hepatic lipid metabolism by PPARα mainly becomes manifest in the fasted state (5-7).

Studies in human hepatocytes, human liver slices, humanized PPARα mice, and hepatocyte humanized mice support the major role of PPARα in regulating hepatic lipid metabolism in human hepatocytes but also underscore the more modest effect of PPARα activation on gene regulation in the human liver compared to mouse liver (10-14). In agreement with this notion, it was observed in hepatocyte humanized mice that the upregulation of genes involved in various PPARα-dependent pathways of fatty acid catabolism and storage by fasting was generally more modest in the human liver cells than mouse livers cells (15). Nevertheless, many genes can be identified that are consistently induced by fasting and PPARα in mouse and human hepatocytes, including *ACOX1*, *HMGCS2*, *CPT1A*, *APOA5*, and

ANGPTL4. Considering that most of the genes that are induced by PPARα are involved in lipid homeostasis, regulation by PPARα could be used as a screening tool to identify novel genes involved in hepatic lipid metabolism.

Uncoupled respiration has been described in many types of cells but its existence in the liver remains controversial. Uncoupled respiration describes the flow of electrons through the electron transport chain, the resultant generation of a proton motive force, and the return of the protons to the mitochondrial matrix without it being coupled to the synthesis of ATP (16). It has been estimated that from 15 to 40% of oxygen consumption by mitochondria in liver cells of vertebrate animals is not associated with ATP synthesis and is due to a passive leak of protons across the inner mitochondrial membrane (17). In most cells, the physiological function of uncoupled respiration is to lower the formation of reactive oxygen species by complexes I and III (16). In brown adipocytes, uncoupled respiration is used to generate heat during cold exposure as part of adaptive thermogenesis. In these cells, uncoupled respiration is critically dependent on uncoupling protein 1, a membrane transport protein that is part of the SLC25 family of nuclear-encoded transporters embedded in the inner mitochondrial membrane (17). UCP1 catalyzes the flow of protons from the intermembrane space to the mitochondrial matrix without it being coupled to ATP synthesis. The expression of UCP1 is specific to brown adipocytes and brite adipocytes (18). Brite adipocytes are cold-activated white adipocytes that have adopted features of white adipocytes. Besides UCP1, the UCP subfamily also includes UCP2 and UCP3. Although these proteins are able to transport protons, it is plausible that their protonophoric function may be complementary to an as yet unknown transport function (19).

Whether the liver engages in uncoupled respiration has remained unclear. Tan and colleagues suggested that uncoupled respiration occurs in the liver and is mediated by Hepatocellular Downregulated Mitochondrial Carrier Protein (HDMCP, now renamed SLC25A47) (20). It was shown that transient overexpression of SLC25A47 in cancer cells results in the dissipation of mitochondrial membrane potential, concomitant with a significant reduction of cellular ATP. Studies in yeast cells confirmed the ability of SLC25A47 to uncouple mitochondrial respiration (21). These two studies were the first to hint at the existence of a physiological "proton leak" in the liver, which is purportedly catalyzed by SLC25A47. So far, any follow-up studies on the concept of liver-specific uncoupling and specifically on the role of SLC25A47 in energy metabolism and liver-specific uncoupling have been lacking.

Here, we identify SLC25A47 as a gene that is potently induced by fasting and PPARα activation in human hepatocytes. Furthermore, we performed extensive in vitro and in vivo studies to characterize the functional role of SLC25A47.

Methods

Animals

All mice included in the studies described below were male mice on a C57BL/6 background. During the intervention, the mice were housed at 21-22ºC under specific pathogen–free conditions and followed a 6:00-18:00 day-night cycle. Mice were fed a standard chow diet after weaning. At the end of the studies, mice were euthanized between 8.30 – 10.00 in the morning. The mice were first anesthesized with a mixture of isoflurane (1.5%), nitrous oxide (70%), and oxygen (30%), followed by collection of blood by eye extraction into EDTA tubes. Mice were euthanized by cervical dislocation, after which tissues were excised and snap frozen in liquid nitrogen.

SLC25A47-mutant mice (Slc25a47tm1a(EUCOMM)Hmgu) were acquired from the EUCOMM/KOMP repository. Mice heterozygous for the initial allele (Tm1a) were cross-bred with transgenic mice in which Cre recombinase is expressed in hepatocytes under the control of the Albumin gene promoter (Albumin-Cre, B6.Cg-Speer6-ps1$^{Tg(Alb\text{-}cre)21Mgn}$/J, #003574; Jackson Laboratories, Bar Harbor, ME), leading over several generations to the generation of homozygous Tm1b mice.

The animal studies were all carried out at the Centre for Small Animals, which is part of the Centralized Facilities for Animal Research at Wageningen University and Research (CARUS), and were approved by the Local Animal Ethics Committee of Wageningen University (2014091.b, 2016015.e, 2016.W-0093.012, 2016.W-0093.016).

Determination optimal dose AAV-Slc25a47

Twelve male wildtype C57BL/6 mice were randomly divided over 4 groups with 3 mice each. At x weeks of age, mice were injected via the tail vein with AAV-*Slc25a47* dissolved in 100 uL PBS at the following titers: 0, $0.25*10^{11}$, $1.0*10^{11}$, $2.5*10^{11}$ and $6*10^{11}$. Eight weeks after injection, mice were euthanized via cervical dislocation.

High fat diet AAV-Slc25a47

Twenty-four male wildtype C57BL/6 mice were randomly divided over 2 groups with 12 mice each. At 9-12 weeks of age, 12 mice were injected via the tail vein with AAV-*Slc25a47* dissolved in 100 uL PBS at a titer of $2.5*10^{11}$. Another group of 12 mice were injected with an equivalent amount of AAV-*Gfp*. Two weeks after injection, the mice were placed on a high fat diet containing 60 energy percent fat (D12492, Research Diets, Inc, New Brunswick)

for 11 weeks. During the entire study, the mice were individually housed. Ten weeks after injection, blood was collected and mice were euthanized as described above.

Fasting-refeeding AAV-Slc25a47

Forty-eight male wildtype C57BL/6 mice were randomly divided over 2 groups with 24 mice each. At 9-12 weeks of age, 24 mice were injected via the tail vein with AAV-*Slc25a47* dissolved in 100 uL PBS at a titer of $2.5*10^{11}$. Another group of 24 mice were injected with an equivalent amount of AAV-*Gfp*. Three weeks after injection, half of the mice in each group (n=12) was fasted for 24 hours before blood was collected and the mice were euthanized. The other half of the mice (n=12) was fasted for 18 hours, after which the food was returned for 6 hours followed by blood collection and euthanasia.

High fat diet Slc25a47-/- mice

Male wildtype C57BL/6 mice and *Slc25a47-/-* littermates at 15-18 weeks of age were placed on a LFD containing 10 energy percent fat (D12450, Research Diets, Inc.) or a high fat diet containing 45 energy percent fat (D12451, Research Diets, Inc.) for 20 weeks. Mice were group housed under regular light–dark cycles (6.00 a.m. – 6 p.m.) in temperature- and humidity-controlled specific pathogen-free conditions. One mouse was removed from analysis for the WT HFD group due to ambiguous genotype. One mouse in the WT HFD group became ill and had to be removed from the study. Two mice were removed from the *Slc25a47-/-* HFD group because they were heterozygous according to re-genotyping and assessment of *Slc25a47* gene expression. One mouse in the *Slc25a47-/-* HFD group became ill and had to be removed from the study.

Power calculation

A power calculation was performed based on fasting glucose level, assuming a standard deviation of 2.5 mM, using a power of 0.8, a significance level of 0.05, and an effect size of 3 mM. Using an online statistics tool from the University of British Columbia (https://www.stat.ubc.ca/~rollin/stats/ssize/n2.html), the sample size was calculated as n = 11 mice per group. To allow compensation for potential loss of mice during the dietary interventions, n = 12 mice were included per group. Accordingly, all mouse studies mentioned above started with 12 mice per group.

Intraperitoneal glucose tolerance test

Three weeks before euthanasia, wildtype and *Slc25a47*-/- mice fed the high fat diet were subjected to an intraperitoneal glucose tolerance test. After a 5-hour fast, the mice were injected intraperitoneally with glucose (1 g/kg body weight) (Baxter, Deerfield, IL). Blood samples from tail vein bleeding were tested for glucose levels at different time points after glucose injection using a GLUCOFIX Tech glucometer and glucose sensor test strips (Menarini Diagnostics, Valkenswaard, The Netherlands). Blood glucose values for 2 mice per group could not be used because they exceeding the maximal detection level.

Quantification of plasma parameters

Blood samples were collected into EDTA-coated tubes and centrifuged at 4°C for 15 min at 12,000 g. Plasma was collected and stored at −80°C. Plasma concentrations of glucose (Sopachem, Ochten, the Netherlands), triglycerides (TG), cholesterol (Instruchemie, Delfzijl, the Netherlands), glycerol (Sigma-Aldrich, Houten, the Netherlands) and free fatty acids (Wako Chemicals, Neuss, Germany; HR(2) Kit) were determined according to manufacturers' instructions.

Liver triglycerides

Liver pieces of ~50 mg were homogenized to a 5% lysate (m/v) using 10 mM Tris, 2 mM EDTA, 0.25 M sucrose, pH 7.5. Homogenates were assayed for triglycerides using a kit for triglycerides (Instruchemie, Delfzijl, the Netherlands).

Plasmid constructs

Plasmid for *pSlc25*a47*_Egfp N2* was constructed by cloning the full-length mouse *Slc25a47* cDNA into *pEgfp-N2* (Clonetech, Mountain View, California, USA). Briefly, RNA from mouse liver was reverse transcribed with First Strand cDNA synthesis kit (Thermo Scientific) and amplified with Phusion High fidelity DNA Polymerase (Thermo Scientific) Fwd_NheI_slc25A47: *GCATGAGCTAGCACCATGGATTTTGTTGCTGGGGCC* and Rev_BamHI_slc25A47: *GCATGAGGATCCTTGTGAGCAGGCTCTGCGTGAG*. The PCR products were cloned into pEGFP-N2 vector using the NheI-HF and BamHI-HF (New England Biolabs Inc.) restriction enzyme sites. Afterwards, MAX Efficiency ® DH5α™ Competent Cells (Invitrogen) were transformed by heat-shock and grown in Luria-Bertani (LB) agar plates with kanamycin (Sigma-Aldrich). The vector was isolated using Qiagen plasmid maxi kit (Qiagen) according to manufacturer instructions.

Transient transfection and stable cell line

For transient transfections the plasmids p*Slc25a47_Egfp N2* and empty p*Egfp-N2* for control were complexed to polyethylenimine (PEI) (Polyscience Inc., PA, USA) 1:3 plasmid:PEI ratio in serum free DMEM (Lonza, Belgium). After 6h, the transfection medium was changed to DMEM with 10% FCS. For selection of stably-transfected cells, 24h after transfection medium was changed to selection medium DMEM with 600 ug/mL G418 (Sigma-Aldrich, The Netherlands). After 48h incubation, cells were diluted and seeded on 96 well plates with selection medium. At 70% confluency, fluorescent positive wells were re-selected, diluted and replated in 96 well plates. Selected colonies were incubated in maintenance medium (DMEM with 10%FCS and 250ug/ml G418) and gradually grown into larger volumes.

Colocalization and intensity analysis using Mitotrack FM

Hepa1-6 cell transiently transfected with *Slc25a47_Egfp-N2* or non-transfected Hepa 1-6 cells were cultured in complete DMEM at standard conditions (37 °C, 5% CO2, 95% humidified atmosphere). Cells were seeded on rat tail collagen-coated 15 µ-8 well glass bottom slide (Ibidi, Martinsried, Germany). After 24h, cells were washed and stained for 30min with 50 nM MitoTrack Red FM (ThermoFisher, Netherlands). For imaging, medium was replaced with FluoroBrite DMEM (ThermoFisher, Netherlands). Cells were imaged *in vivo* on a Leica TCS SP5 X. Images were acquired sequentially. SLC25A47_EGFP-N2 was excited at 488 nm and fluorescence emission was detected in a spectral window of 495-540 nm. MitoTrack Red FM was excited at 581 nm ab and detected in a spectral window of 602-650 nm. Every cell was only imaged once. Laser power, zoom factor, and acquisition speed was unchanged through the experiment. For image analysis, zero-zero pixels were removed and mean of values above the median were calculated.

Mitochondria isolation and Western Blot

Different centrifugation steps were conducted in order to isolate mitochondria of cells and liver tissues. Hepa1-6 cells stably transfected with *Slc25a47_Egfp-N2* or *Egfp-N2* were cultured in antibiotic-free medium in order to ensure an optimal mitochondrial function. The cells were harvested by using trypsin 1% and washed and centrifuged down two times in ice cold Isolation mitochondrial buffer (IMB) (210 mM mannitol, 70 mM sucrose, 1 mM EDTA, 10 mM HEPES. Complete EDTA -Free Protein inhibitor cocktail tablet (Roche, USA) and 2mg/ml Free-fatty acid-BSA was added prior to usage, pH 7.5). This was followed by resuspension of the pellet in IMB including 2 mg/mL albumin to bind fatty acids. The cells

were homogenized using a glass Dounce homogenizer performing 60 strokes on ice. The homogenate was centrifuged for 5 minutes at 2350 rpm to get rid of the whole cell lysate (pellet 1). In the next step, the supernatant was centrifuged for 45 minutes at 10.900 rpm in order to obtain the cytosolic fraction (supernatant 1) and the isolated mitochondrial fraction (pellet 2). For Western blot the mitochondrial pellet was resuspended in 1% CHAPS or gently resuspended in storage buffer for ATP analysis. For Western Blot analysis anti-GFP antibody was used to detect SLC25A_47- EGFP fused protein.

ATP content assay

The Molecular ProbesTM ATP Determination Kit (A22066) of Invitrogen with some modifications was used in order to detect the ATP content in isolated mitochondria of Hepa1-6 cells stably transfected with *Slc25a47_Egfp-N2* or *Egfp-N2*. Prior to assay, cells were cultured on antibiotic free medium for 2 passages. The substrates L-(-)-Malic acid (1M) and Sodium Pyruvate (1M) were added in a concentration of 1 µL substrate / 1 mL reaction solution. The reaction solution was gently mixed, protected from light and preheated for at least 15 minutes at the optimal reaction temperature of 28 °C. Luminometric absorption of the mitochondrial samples was measured in a dark 96-well Costar well plate (3915, Corning Incorporated) using a Fluoroskan plate reader, integration time 20 ms (Fluoroskan Ascent FLTM, ThermoFischer Scientific, USA). During the centrifugation step in order to spin down the mitochondrial pellet (i.e. 45 min. at 10.900 rpm), the ATP standard curve (0 nM – 1000 nM) was measured using 10 µL of ATP stock (5mM) dilutions in storage buffer. The measured values were subtracted from the background luminometric absorption values of the 90 µL reaction solution. As soon as the isolated mitochondrial pellet was retrieved, it was resuspended in storage buffer by gently pipetting up and down to keep the mitochondria intact. Mitochondrial function was measured within 20 minutes after the last centrifugation step, due to time-dependent degradation of mitochondria. Firstly, the background luminometric absorption of the 90 µl reaction solution was measured. This was followed by ATP content measurements by addition of 10 µL of the isolated mitochondria dissolved in storage buffer in technical triplicates. The measurement (90 µL reaction solution + 10 µL mitochondrial sample) minus the background value (90 µL reaction solution) minus the mean of the duplicate negative control samples (90 µL reaction solution + 10 µl of the storage buffer) represents the ATP content. Results were normalized to protein content as measured by Micro BCA Protein Assay Kit (Thermofisher Scientific, Rockford, USA).

High-resolution respirometry

Respirometry analysis were performed using high-resolution respirometry (Oroboros Oxygraph-2k; Oroboros Instruments, Innsbruck, Austria). Before experiments calibrations was performed according to manufacturer's recommendations.

Intact Hepa1-6 cells overexpressing Slc25a47 or Efgp

Hepa1-6 were transiently transfected with p*Slc25a47_Egfp-N2* and empty *pEgfp-N2* at least 90% transfection efficiency in T75 flasks. Each experiment was performed 48h after transfection with 10^6 cells per condition and afterwards results were normalized for protein content. Cells were cultured and measured in DMEM +10% FCS. For experiments with fatty acid loaded cells, 24h after transfection, Hepa1-6 cells were fatty acid loaded with 1.2 mM oleate:palmitate (2:1 ratio) coupled to 3% BSA-DMEM and incubated overnight. Respiratory states were assessed using a Coupling Control Protocol (CCP) (DOI 10.26124/bec:2020-0002). Briefly, Hepa1-6 cells were added to the OROBOROS chambers. Within the next 5-10 min, O_2 flux stabilized reflecting the cellular ROUTINE respiration. Cellular ROUTINE respiration is the aerobic metabolic activity under standard culture medium conditions in the physiological coupling state. Next, LEAK respiration was assessed by adding 2.5 uM oligomycin (an ATP-synthase inhibitor). LEAK respiration represents the O_2 flux that is maintained to compensate for the proton leak caused after ATP-synthase inhibition by oligomycin and thus represents the respiration independent of ADP phosphorylation. Afterwards, ETC (electron transport capacity) was assessed by the stepwise titration of 1 uM CCCP (a proton translocator that facilitates proton transfer across the membrane) until no further increase of O_2 flux was observed. ETC represents the uncoupler stimulated respiration, thus the electron-transport-system capacity at noncoupled respiration. Finally, ROX (residual oxygen consumption) was determined by adding 0.5 uM rotenone to inhibit Complex-I and 2.5 uM antimycin A to inhibit Complex-III. ROX is the oxygen consumption that remains after inhibition of the electron transfer pathway, thus the O_2 consumption that is not related to electron transfer. Finally, ATP-linked respiration was calculated as the difference between ROUTINE respiration and LEAK respiration.

Freshly isolated permeabilized liver overexpressing Slc25a47 or Egfp

Livers of mice infected with AAV-*Slc25a47* or AAV-*Gfp* were dissected and immediately transported in MiR05 medium (0.5 mM EGTA, 3 mM $MgCl_2$ $6H_2O$, 60 mM lactobionic acid, 20 mM taurine, 10 mM KH_2PO_4 , 20 mM HEPES, 110 mM D-Sucrose, 1g/l fatty acid-free BSA, pH 7.0) (DOI 10.1007/978-3-662-04162-8_45). The protocol for liver permeabilization was

adapted from Kuznetsov et al. (22). Briefly, 2 mg of freshly dissected livers were mechanically permeabilized in ice-cold MiR05 medium using two pairs of forceps. The tips of the forceps were inserted in the middle of the sample, and the tissue was repeatedly torn apart in different directions, until pieces of loosely connected liver were obtained. Permeabilized liver pieces were briefly rinsed in MiR05 medium chambers. Respiratory states were assessed using a Substrate-uncoupler-inhibitor titration protocol (SUIT) (DOI 10.26124/bec:2020-0002). Shortly after adding the samples to the chambers, 10 mM glutamate and 2 mM malate were injected to assess Complex I-linked LEAK respiration in the absence of ADP. Glutamate and malate activate dehydrogenases which generate, through coupled reaction, nicotinamide adenine dinucleotide (NADH). The generated NADH can subsequently deliver its electrons into Complex I (CI) and go down the electron transport chain for ATP production by ATP-synthase and O_2 consumption. However, in the absence of ADP, no oxidative phosphorylation can occur, thus the O_2 flux reflects the CI-linked LEAK respiration. Next, CI-linked OXIDATIVE respiration was assessed by the stepwise titration of 1mM ADP. Next, 10 uM of cytochrome C was added to evaluate the integrity of the mitochondrial outer membrane. An increase of respiration at this point would signify the outer mitochondrial membrane is damaged. Next, 10 mM succinate was added to assess CI&CII-linked OXIDATIVE respiration, immediately followed by 1mM ADP to ensure saturated ADP concentration. Next, CI&CII-linked LEAK respiration was assessed by titration of 2.5 uM oligomycin. Afterward, CI&CII-UNCOUPLED respiration was evaluated by the stepwise titration of 0.5 uM CCCP, until no further increase of O_2 flux was observed. Finally, CI&CII-ROX was determined by adding 0.5 uM rotenone and 2.5 uM antimycinA.

Results

To identify potential novel PPARα-induced genes in human hepatocytes, we analyzed transcriptome data of three independent studies in which human primary hepatocytes were treated with the PPARα agonist Wy14643 or GW7647 for 24 hours. Genes were considered to be significantly regulated if $P < 0.005$ and Signal Log Ratio >0.25 (fold change 1.1892). A total of 46 genes was significantly induced by PPARα activation in all three studies (Figure 1A). The changes in gene expression of these 46 genes in the hepatocytes from all donors is shown in figure 1B. Many well-known PPARα target genes are represented in this list, including *CPT1A*, *HMGCS2*, *PDK4*, *ANGPTL4*, *PLIN2* and *FABP1*. One relatively unknown gene that was consistently induced by PPARα activation in the three datasets was *SLC25A47*. Quantitative PCR confirmed the induction of *SLC25A47* mRNA by PPARα activation in human hepatocytes, human liver slices, and human hepatoma HepG2 cells (Figure 1C). In addition, *Slc25a47* expression was significantly induced by PPARα activation in mouse hepatocytes, rat FAO hepatoma cells, and in mouse liver (Figure 1D). Analysis of ChIP-SEQ data revealed several PPARα binding sites immediately upstream of the transcriptional start site, suggesting that *SLC25A47* is a direct PPARα target gene (Figure 1E) (23). Currently, only two papers exist about the SLC25A47 gene, both of which present evidence that SLC25A47 is a liver-specific mitochondrial uncoupler protein (20, 21). Tissue expression profiling by qPCR confirmed the liver specific expression of SLC25A47 in humans and mice (Figure 1F).

PPARα in liver is known to be activated by fasting (8, 9). Accordingly, we studied the expression of *Slc25a47* in liver in response to fasting. Expression of *Slc25a47* was induced by fasting, with highest induction observed after 12 hours (Figure 2A). In addition, fasting induced *Slc25a47* mRNA levels in hepatocyte humanized mice in both the mouse and human hepatocytes (Figure 2B). To study the functional role of SLC25A47 in mouse liver, we overexpressed *Slc25a47* in liver using adeno-associated virus. Injection of adeno-associated virus expressing *Slc25a47* increased hepatic *Slc25a47* expression to a maximum of 7-fold at the highest dose (Figure 2C). Further studies were done using an AAV titer of 2.5×10^{11} genomic copies. Inasmuch as hepatic *Slc25a47* expression is induced by fasting, we first studied the effect of *Slc25a47* overexpression in fed and fasted mice. AAV-mediated *Slc25a47* overexpression significantly increased *Slc25a47* mRNA levels in liver in the fed and fasted state (Figure 2D). No significant effect was observed of AAV-mediated *Slc25a47* overexpression on liver triglyceride levels (Figure 2E). Consistent with this finding, neutral lipid staining of the liver by Oil Red O did not reveal any differences between the AAV-*Slc25a47* and AAV-*Gfp* mice (Figure 2F). Plasma non-esterified fatty acids and β-hydroxybutyrate levels were not significantly different between AAV- *Slc25a47* and AAV-*Gfp* mice (Figure 2G), nor were plasma glucose, triglyceride, cholesterol, and glycerol levels

were not significantly affected by *Slc25a47* overexpression (Figure 2H). Finally, the expression of genes involved in various lipid metabolic pathways was not significantly changed by *Slc25a47* overexpression (Figure 2I).

Figure 1. *SLC24A47* is induced by PPARα in human and mouse hepatocytes. A) Venn diagram showing overlap in gene regulation in human primary hepatocytes treated with PPARα agonist for 24h. The following three datasets were included: GSE53399 (GW7647, 1 µM, n = 4)(31), GSE76148 (Wy14643, 50 µM, n = 6)(32), GSE17251 (Wy14643, 50 µM, n = 6)(14). Genes were considered to be significantly regulated if P < 0.005 and Signal Log Ratio >0.25 (fold change 1.1892). B) Heatmap showing the expression changes of the 46 genes significantly induced by PPARα activation in all three studies. Each vertical column represents one human donor. C) Effect of Wy14643 on *SLC25A47* mRNA in human hepatocytes (24h, 50 µM), precision cut liver slices (24h, 50 µM), and HepG2 cells (6h, 50 µM). D) Effect of Wy14643 on *Slc25a47* mRNA in mouse precision cut liver slices (24h, 20 µM), rat liver FAO hepatoma cells (24h, 5 µM), and mouse liver (5d, 0.1% in food). E) Screenshot of the mouse *Slc25a47* locus showing ChIP-seq profiles of PPARα in mouse liver. F) Expression profile of SLC25A47 in various human tissues (left panel) and mouse tissues (right panel). Error bars represent SD for in vitro experiments and SEM for in vivo studies. Asterisk indicates significantly different according to Student's t-test. *P<0.05, **P<0.01, ***P<0.001.

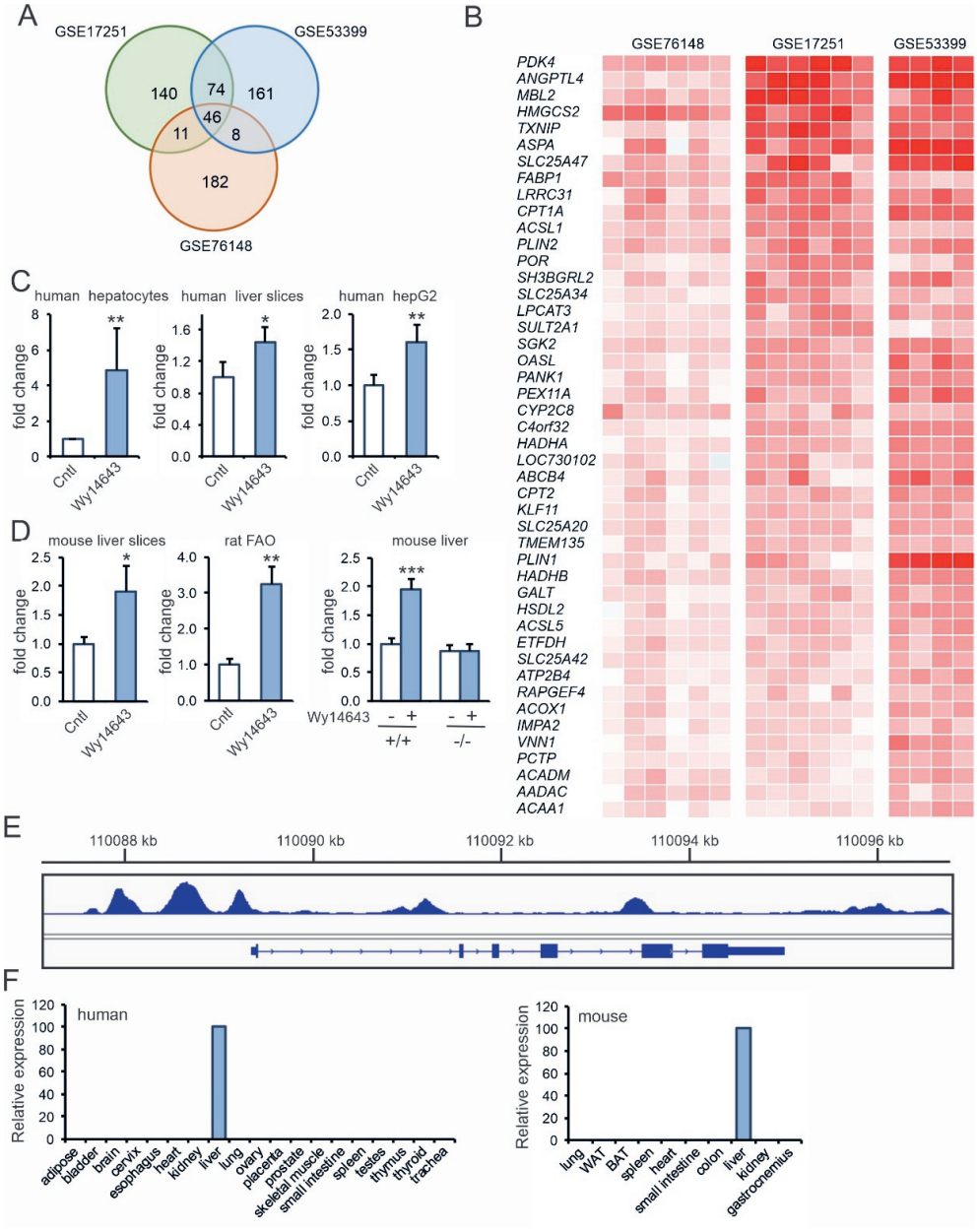
A
GSE17251
GSE53399
GSE76148
140
74
161
46
11
8
182
B
GSE76148
GSE17251
GSE53399
PDK4
ANGPTL4
MBL2
HMGCS2
TXNIP
ASPA
SLC25A47
FABP1
LRRC31
CPT1A
ACSL1
PLIN2
POR
SH3BGRL2
SLC25A34
LPCAT3
SULT2A1
SGK2
OASL
PANK1
PEX11A
CYP2C8
C4orf32
HADHA
LOC730102
ABCB4
CPT2
KLF11
SLC25A20
TMEM135
PLIN1
HADHB
GALT
HSDL2
ACSL5
ETFDH
SLC25A42
ATP2B4
RAPGEF4
ACOX1
IMPA2
VNN1
PCTP
ACADM
AADAC
ACAA1
C
human hepatocytes
human liver slices
human hepG2
fold change
Cntl
Wy14643
D
mouse liver slices
rat FAO
mouse liver
Wy14643
+/+
-/-
E
110088 kb
110090 kb
110092 kb
110094 kb
110096 kb
F
human
mouse
Relative expression
adipose
bladder
brain
cervix
esophagus
heart
kidney
liver
lung
ovary
placenta
prostate
skeletal muscle
small intestine
spleen
testes
thymus
thyroid
trachea
WAT
BAT
colon
gastrocnemius

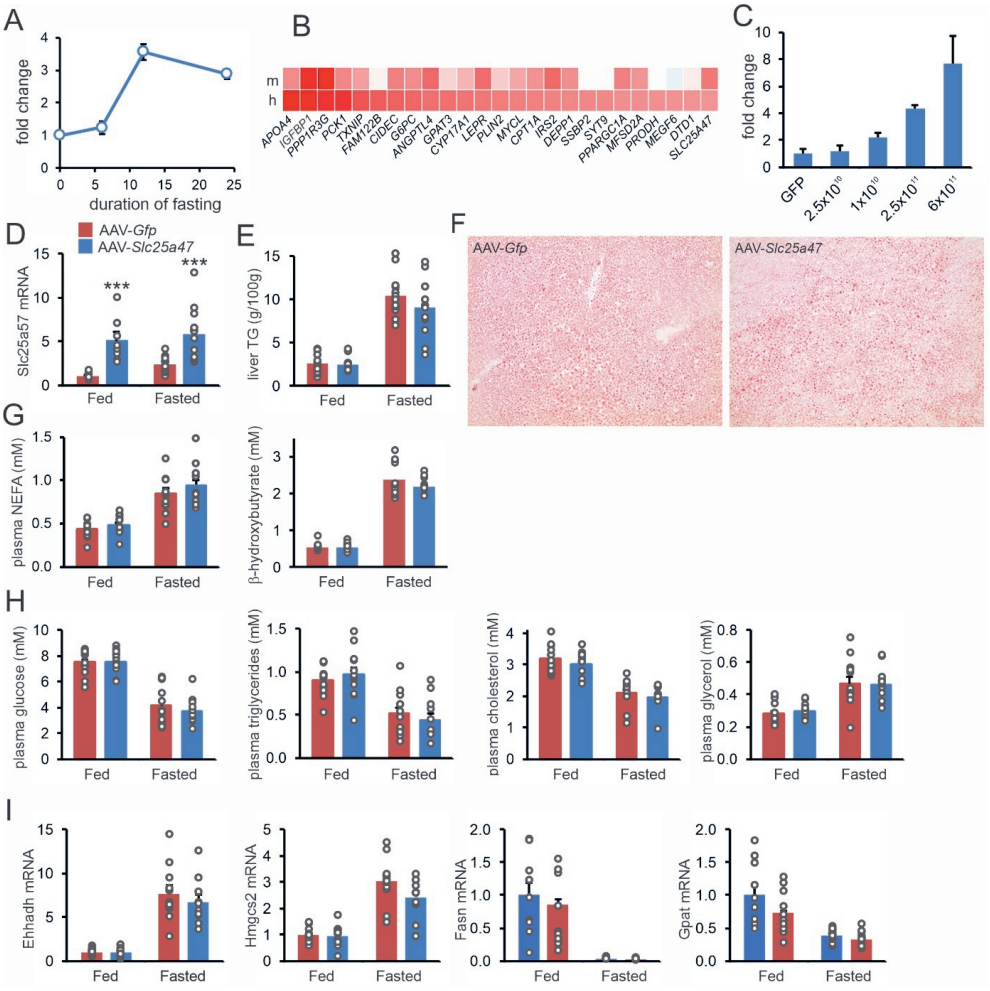

Figure 2. Effect of hepatic *Slc25a47* overexpression in refed and fasted mice. A) Effect of fasting on *Slc25a47* mRNA in mouse liver. B) Heatmap showing the top 25 genes induced by fasting in human and mouse hepatocytes of hepatocyte humanized mice. Data were extracted from GSE126587 (33). C) *Slc25a47* mRNA levels in livers of mice infected with different doses of AAV-*Slc25a47* (n=2 per group). D) *Slc25a47* mRNA levels in livers of refed and 24h fasted mice infected with 2.5×10^{11} genomic copies of AAV-*Slc25a47* or AAV-*Gfp*. E) Liver triglyceride content. F) Oil red O staining. G) Plasma levels of non-esterified fatty acids and β-hydroxybutyrate. H) Plasma levels of glucose, triglycerides, cholesterol, and glycerol. I) Hepatic mRNA levels of selected genes. N=12 per group. Asterisk indicates significantly different from AAV-*Gfp* according to the Student's T test (P<0.001).

We reasoned that the effects of *Slc25a47* overexpression may become more evident under conditions of obesity and fatty liver. Accordingly, mice were infected with AAV-*Slc25a47* and were placed on a high fat diet two weeks later. After 8 weeks of high fat diet and 10 weeks post-injection, *Slc25a47* mRNA levels were more than 4-fold higher in mice injected with AAV expressing *Slc25a47* as compared to *Gfp* (Figure 3A). Weight gain (Figure 3B) and food intake (Figure 3C) were not significantly affected by *Slc25a47* overexpression, as were liver and adipose tissue weights (Figure 3D). Plasma triglycerides, NEFA, glucose and cholesterol were not significantly different between AAV-*Slc25a47* and AAV-*Gfp* mice (Figure 3E), as were liver triglyceride levels (Figure 3F). To gain further insight into the effect of *Slc25a47* overexpression, we performed lipidomics analysis. No distinct clustering of the two sets of mice was observed (Figure 3G). Also, the levels of the major lipid classes was not significantly different between the two group (Figure 3H). Not a single lipid met the statistical significance threshold of FDR <0.05. To further examine the potential impact of *Slc25a47* overexpression on the liver we performed transcriptome analysis. As for the lipidomics data, no distinct clustering of the AAV-*Slc25a47* and AAV-*Gfp* mice was observed (not shown). The only gene that met the statistical significance threshold of FDR q-value <0.05 was *Slc25a47* (Figure 3I), indicating the overall minor effect of *Slc25a47* overexpression in hepatic genes expression. However, analysis at the pathway level showed that a number of gene sets related to cholesterol synthesis were significantly enriched among the upregulated genes, suggesting that SLC25A47 might stimulate cholesterol synthesis (Figure 3J). Overall, these data show that *Slc25a47* overexpression has minimal impact on the liver phenotype, except for a modest induction of the cholesterol synthesis pathway.

Figure 3. Effect of hepatic *Slc25a47* overexpression in diet-induced obese mice. Mice were injected with $2.5x10^{11}$ genomic copies of AAV-*Slc25a47* or AAV-*Gfp* and 2 weeks later were placed on a high fat diet for 8 weeks. A) Hepatic *Slc25a47* mRNA. B) Bodyweight. C) Average food intake during the 8 weeks of high fat diet. D) Tissue weights. E) Plasma metabolites. F) Liver triglyceride content. G) Principle component analysis on liver lipidomics. H) Hepatic levels of the main lipid species. I) Volcano plot of the liver transcriptome. J) Enrichment plot for the gene set Cholesterol Biosynthesis based on the liver transcriptome. N=12 per group. Asterisk indicates significantly different from AAV-*Gfp* according to the Student's T test (P<0.001).

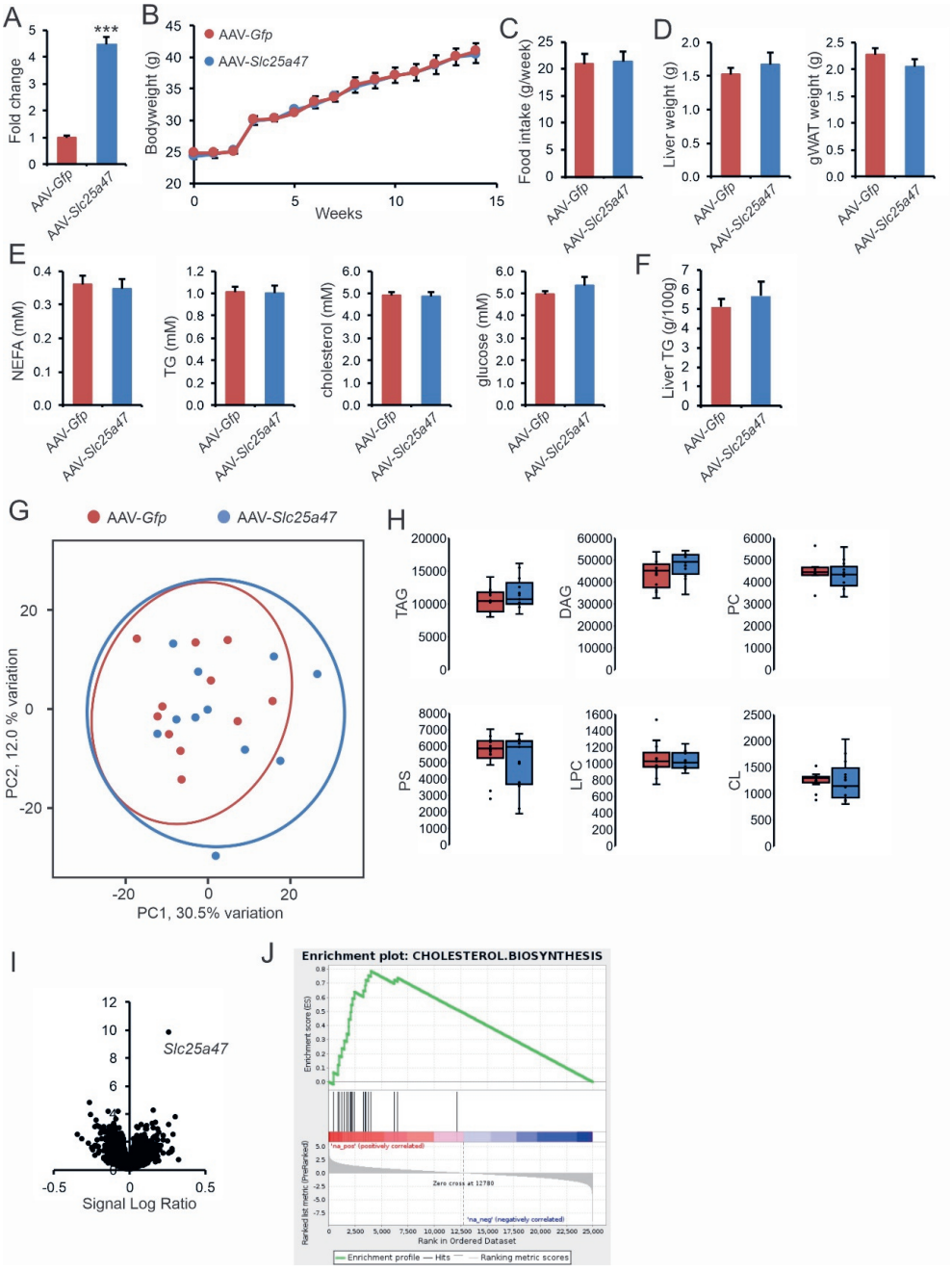
A
Fold change
***
AAV-Gfp
AAV-Slc25a47
B
Bodyweight (g)
AAV-Gfp
AAV-Slc25a47
Weeks
C
Food intake (g/week)
D
Liver weight (g)
gWAT weight (g)
E
NEFA (mM)
TG (mM)
cholesterol (mM)
glucose (mM)
F
Liver TG (g/100g)
G
AAV-Gfp
AAV-Slc25a47
PC2, 12.0 % variation
PC1, 30.5% variation
H
TAG
DAG
PC
PS
LPC
CL
I
Slc25a47
Signal Log Ratio
J
Enrichment plot: CHOLESTEROL.BIOSYNTHESIS
Enrichment score (ES)
Ranked list metric (PreRanked)
Zero cross at 12780
Rank in Ordered Dataset
Enrichment profile
Hits
Ranking metric scores

The reason why overexpression of *Slc25a47* does not lead to a pronounced metabolic phenotype may be that *Slc25a47* is already expressed at a high level in the liver. From that perspective, it could be reasoned that inactivation of *Slc25a47* is more likely to lead to a clear phenotype. To that end, we acquired *Slc25a47*-mutant mice from the EUCOMM/KOMP repository, which was generated by the knockout-first strategy (32). Mice heterozygous for the initial allele (Tm1a) were cross-bred with transgenic mice in which Cre recombinase was expressed in hepatocytes under the control of the Albumin gene promoter (Albumin-Cre), leading to the generation of homozygous Tm1b mice (Figure 4A). The Tm1b mice lack exon 5 and 6, as verified by qPCR (Figure 4B), giving rise to a truncated SLC25A47 protein.

Previously, evidence was presented that SLC25A47 functions as a liver-specific mitochondrial uncoupler. To verify these claims, we subjected the WT and *Slc25a47*-/- mice to indirect calorimetry and performed measurements in the fed and fasted state. Body mass, fat mass, and lean mass decreased upon fasting but were not significantly different between WT and *Slc25a47*-/- mice (Figure 4C). We next measured energy expenditure (Figure 4D,E), respiratory exchange ratio (Figure 4E), and activity (Figure 4F) in the fed and fasted state, and in the light and dark period. Energy expenditure and activity were higher in the dark period than in the light period. Interestingly, in the fed state the respiratory exchange ratio was higher in the dark period than in the light period, whereas the opposite pattern was observed in the fasted state. However, none of these parameters were significantly different between WT and *Slc25a47*-/- mice (Figure 4D-F). Our data thus indicate that SLC25A47 deficiency does not influence whole body energy expenditure.

To further study the possible metabolic role of SLC25A47, we placed the WT and *Slc25a47*-/- mice on a high fat diet for 20 weeks to induce obesity and insulin resistance. Another cohort of WT and *Slc25a47*-/- mice were fed a low fat diet for the same duration. No significant difference in body weight gain (Figure 5A) and food intake (Figure 5B) was observed between WT and *Slc25a47*-/- mice, either on the low fat diet or the high fat diet. Also, no significant differences in liver and white adipose tissue weight were observed between the two sets of mice (Figure 5C). By contrast, glucose tolerance was significantly improved in the *Slc25a47*-/- mice compared to the WT mice (Figure 5D), as shown by a significantly lower area under the curve. As expected, hepatic expression of *Slc25a47* was dramatically reduced in the *Slc25a47*-/- mice compared to the WT mice (Figure 5E). No significant differences between WT and *Slc25a47-/-* mice were observed for hepatic triglyceride (Figure 5F) and glycogen (Figure 5G) levels. Also, no significant differences were observed in plasma glucose, cholesterol, triglycerides, glycerol and non-esterified fatty acids between the two sets of mice (Figure 5G).

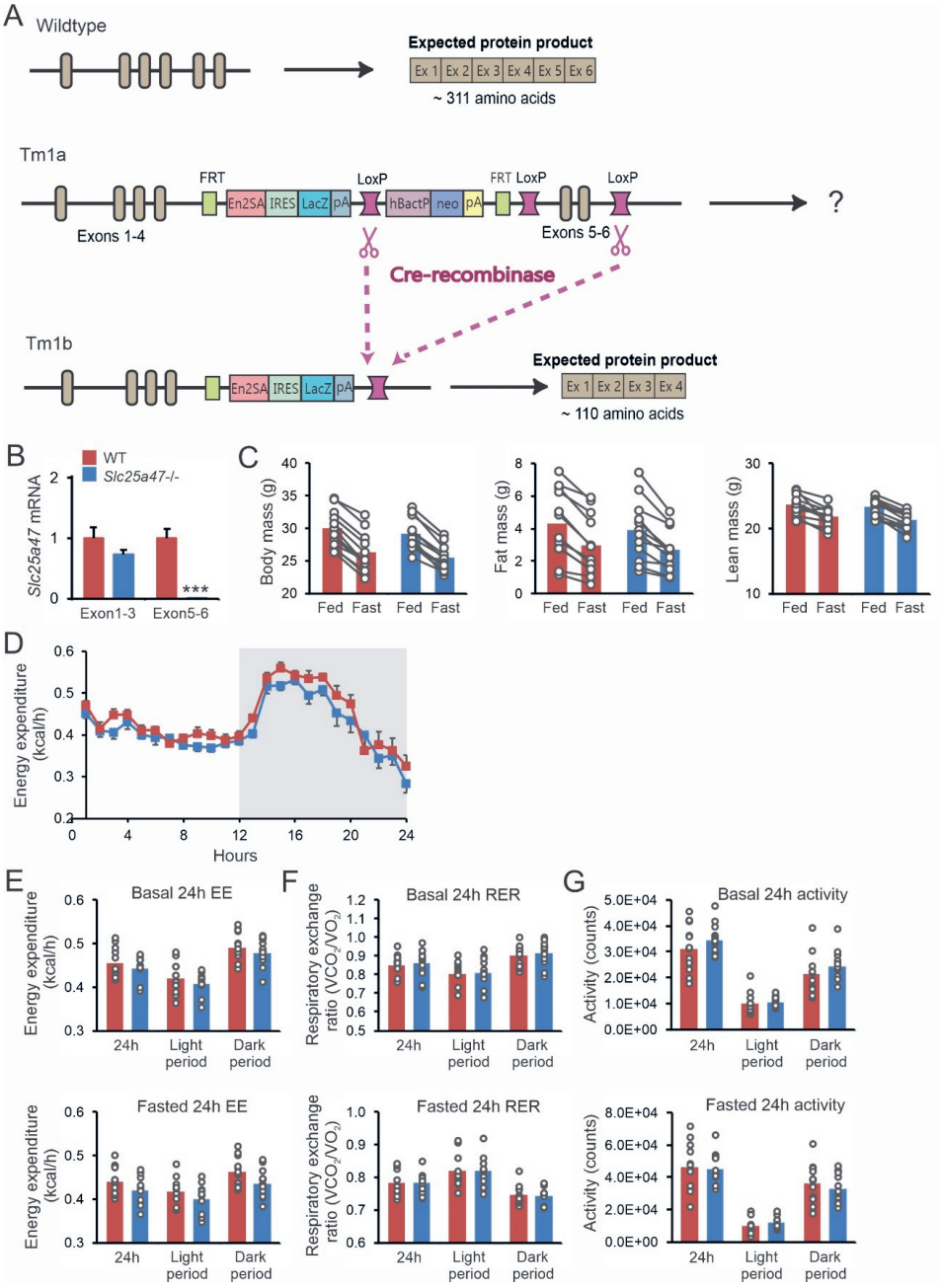

Figure 4. Effect of hepatic *Slc25A47* ablation on energy metabolism. A) Schematic map of the strategy for inactivation of *Slc25A47*. B) QPCR on livers of WT and *Slc25A47*-/- (Tm1b) mice using primers targeting exon 1-3 or exon 5-6. C) Body mass, lean mass, and fat mass in WT and *Slc25A47*-/- mice prior to and after a 24h fast. D) Energy expenditure across the 24h fasting period. E) Mean energy expenditure in the basal state (upper graph) or during the 24h fast (lower graph). F) Respiratory Exchange Ratio. G) Activity level. N= 12 per group. Asterisk indicates significantly different from WT according to the Student's T test (P<0.001).

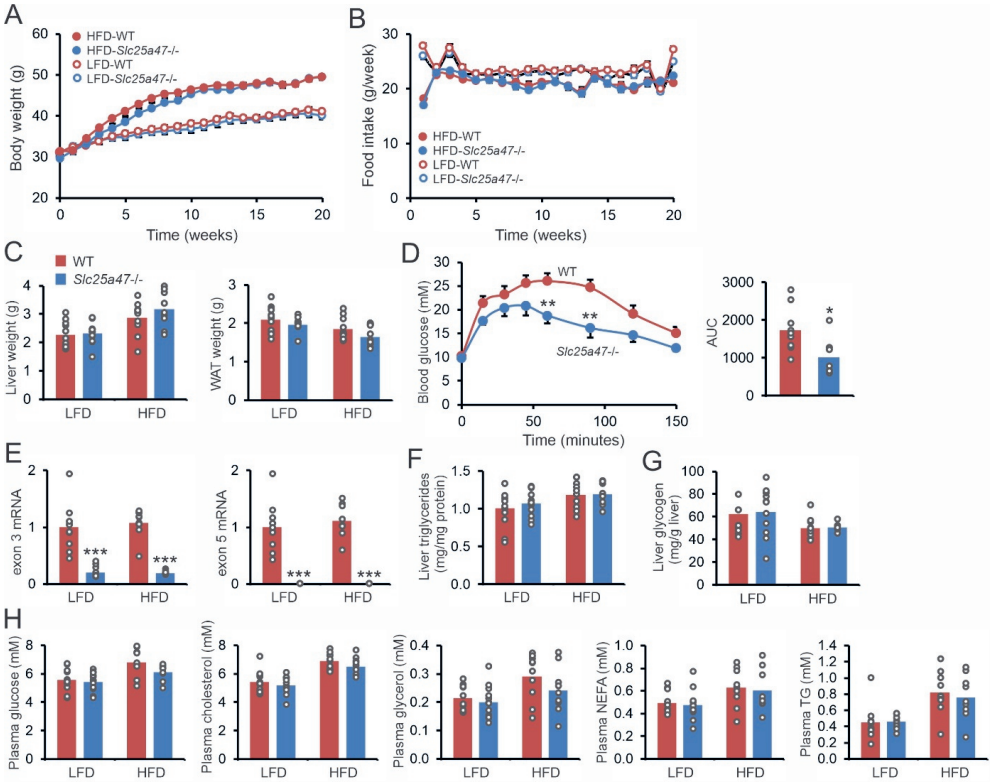

Figure 5. Effect of hepatic *Slc25A47* ablation on diet-induced obesity. A) Bodyweights of WT and *Slc25A47*-/- mice fed a low fat diet (LFD, n=12/group) or high fat diet (HFD, n=10/group) for 20 weeks. B) Mean energy intake per mouse per week. C) Liver and epipidymal adipose tissue weights. D) Results of intraperitoneal glucose tolerance test (1 g/kg bodyweight) and the area under the curve (AUC). E) qPCR for Slc25a47 mRNA in liver using primers directed against exon 3 and exon 5. F) Liver triglyceride levels. G) Liver glycogen levels. H) Plasma levels of glucose, non-esterified fatty acids, triglycerides, cholesterol, and glycerol. N=7-12 per group. Asterisk indicates significantly different from WT according to the Student's T test (*P<0.05, **P<0.01, ***P<0.001).

To further investigate the potential role of SLC25A47 as mitochondrial uncoupler, we performed studies in Hepa1-6 cells, which do not express *Slc25a47*, nor do any other cancer cell lines (24). Consistent with previous literature and with Protein Atlas (20, 21), we found SLC25A47 to be localized to mitochondria, as indicated by the overlap with the mitochondrial marker Mitotracker FM (Figure 6A). Western blotting on mitochondria isolated from Hepa1-6 cells stably transfected with *Slc25a47* fused to *Gfp*, followed by Western blotting for GFP, confirmed the mitochondrial localization of SLC25A47 (Figure 6B). Mitotracker FM is a cationic fluorescent dye whose accumulation inside the mitochondria is dependent on the mitochondrial membrane potential and can thus serve as a marker for

the mitochondrial membrane potential. Interestingly, after transient transfection of *Slc25a47*, the fluorescence intensity was significantly lower in cells expressing *Slc25a47* compared to the cells that do not express *Slc25a47* (Figure 6C,D). These data suggest that SLC25A47 reduces the mitochondrial membrane potential. Nevertheless, ATP content was not different between Hepa1-6 cells stably expressing *Slc25a47* or *Gfp* (Figure 6E).

To investigate if SLC25A47 may promote uncoupling, we performed high-resolution respirometry on an Oroboros Oxygraph 2k in Hepa1-6 cell transiently transfected with *Slc25a47* or *Gfp*. Transfection led to a huge increase in *Slc25a47* expression (Figure 6F). Respiratory states were assessed using a Coupling Control Protocol (CCP). First, cellular ROUTINE respiration was assessed within 5-10 min after adding the cells to the chambers. Next, LEAK respiration was determined by adding oligomycin. Afterward, ETC (electron transport capacity) was assessed by the stepwise titration of 1 uM CCCP until no further increase of O_2 flux was observed. Finally, ROX (residual oxygen consumption) was determined by adding 0.5 uM and 2.5 uM antimycin A. ATP-linked respiration was calculated as the difference between ROUTINE respiration and LEAK respiration. Neither under normal conditions (Figure 6G) nor after lipid-loading (Figure 6H) was there a significant difference between control and *Slc25a47*-expressing cells for any of the specific measurements performed. To further evaluate if SLC25A47 could affect mitochondrial respiration in a different system, we performed respirometry analysis on permeabilized livers of AAV-*Slc25a47* and AAV-*Gfp* infected mice. No significant differences were observed between AAV-*Slc25a47* and AAV-*Gfp* mice for any of the specific measurements performed (Figure 6I). These data do not support an uncoupling role of SLC25A47.

To investigate if SLC25A47 may impact cell viability, we tested the effect of *Slc25a47* overexpression on apoptosis markers. In lipid-loaded Hepa1-6 cells, *Slc25a47* overexpression was associated with a significant increase in apoptosis markers, including Caspase 3, Caspase 8a, and Caspase 8b (Figure 6J).

Figure 6. Effect of SLC25A47 on mitochondrial membrane potential and respiration. A) Hepa1-6 cells transiently transfected with p*Slc25a47_Egfp-N2* were incubated with MitoTracker™ Red FM and imaged lived on a on a Leica TCS SP5 X. B) Western blot on mitochondria isolated from Hepa1-6 cells stably transfected with p*Slc25a47_Egfp-N2* or p*Egfp-N2.* Over time, GFP expression was lost from the p*Egfp-N2* line. C) Hepa1-6 cells transiently transfected with p*Slc25a47_Egfp-N2* were stained with the membrane potential sensitive dye MitoTracker™ Red FM. D) Image intensity analysis of MitoTracker™ Red FM on Hepa1-6 cells transiently transfected with p*Slc25a47_Egfp-N2* or non-transfected Hepa1-6 cells. λ_{ex}: 488nm (EGFP), 581 nm (MitoTracker™), λ_{em}: 495-540 nm (EGFP), 602-650 nm (MitoTracker™). For image analysis, zero-zero pixels were removed and mean of values above the median were calculated (n=14 images per condition). E) ATP content in mitochondria isolated from Hepa1-6 cells stably transfected with p*Slc25a47_Egfp-N2* or p*Egfp-N2.* F) *Slc25a47* mRNA expression in Hepa1-6 cells transiently transfected with p*Slc25a47_Egfp-N2* or p*Egfp-N2.* SLR, signal log ratio. G) O_2 flux analysis in Hepa1-6

cells transiently transfected with p*Slc25a47_Egfp-N2* or p*Egfp-N2* (n=3 measurements per condition). H) O_2 flux analysis in Hepa1-6 cells transiently transfected with p*Slc25a47_Egfp-N2* or p*Egfp-N2* loaded with fatty acids overnight (1.2 mM oleate:palmitate 2:1) (n=3 measurements per condition). I) O_2 flux analysis on permeabilized mouse livers obtained mice infected with AAV-*Slc25a47* or AAV-*Gfp*. J) Western blot of apoptosis markers on lipid loaded and nonlipid loaded Hepa1-6 cells transiently transfected with p*Slc25a47_Egfp-N2*, p*Egfp-N2,* or vehicle.

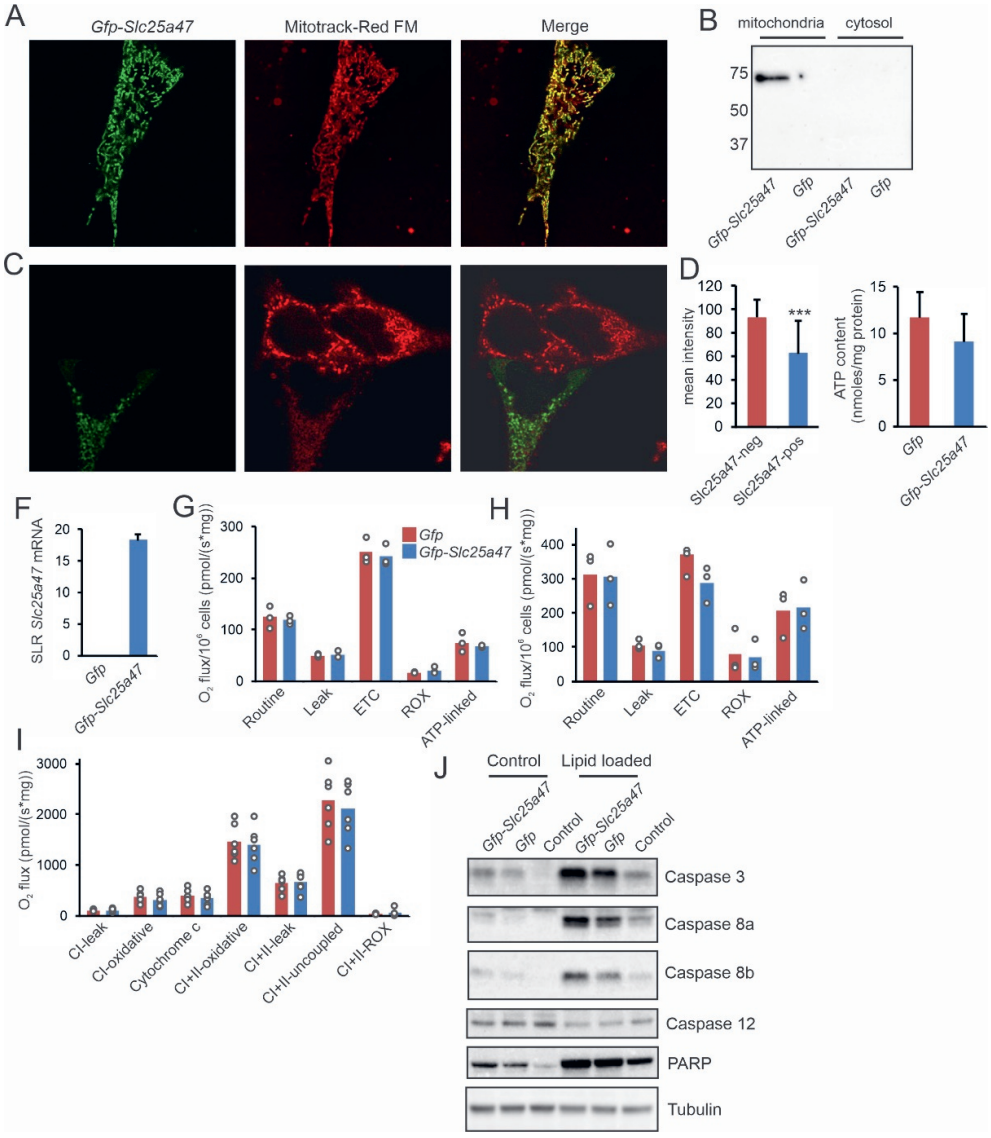

Discussion

Here we identify *SLC25A47* as a novel PPARα-induced gene in mouse and human hepatocytes. Previously, it was reported that SLC25A47 functions as an uncoupling protein. Studies in Hepa1-6 cells transiently and stably transfected with *Slc25a47* partly support that notion. By contrast, studies in *Slc25a47*-/- mice did not show any effect of SLC25A47 deficiency on whole body energy expenditure. Additional detailed studies in *Slc25a47*-overexpressing and deficient mice fed a high fat diet or subjected to fasting did not show a significant effect of SLC25A47 on lipid and glucose metabolism. Only the improvement in glucose tolerance in *Slc25a47*-/- compared to WT mice reached statistical significance. It is anticipated that additional measurements will reveal the role of SLC25A47 in lipid and/or glucose metabolism.

SLC25A47 is a member of the family of six-transmembrane-helix mitochondrial SLC25 (solute carrier family 25) transporters (25-27). These carriers facilitate the transport across the inner mitochondrial membrane of a chemically diverse set of solutes, including amino acids, acyl-carnitine, nucleotides, and protons. Based on a similar sequence and structural properties, 53 members of the SLC25 family have been identified in the human genome, including several orphan transporters (25-27). One of the unique features of SLC25A47 is that it is exclusively found in liver mitochondria. Accordingly, it can be predicted that SLC25A47 imports or exports a molecule that is specifically processed or synthesized in liver mitochondria. Inasmuch as the expression of *SLC25A47* is induced by fasting, fatty acids, and PPARα, it can be hypothesized that SLC25A47 transports a certain lipid metabolite, rather than just protons. We were able to dismiss ketone bodies as candidate molecule based on the lack of effect of SLC25A47 deficiency on fasting plasma levels of β-hydroxybutyrate. An attractive possibility that would merge the reported uncoupling property of SLC25A47 with the predicted lipid character of the transported molecule is that SLC25A47 is a carrier for fatty acids. In this scenario, the higher acidity outside the mitochondria will lead to the protonation of fatty acids, which are subsequently transported across the inner mitochondrial membrane and along a gradient by SLC25A47. In the mitochondrial matrix, the higher pH causes the deprotonation of the fatty acids to the anionic form, thus creating a gradient for the continuous influx of protonated fatty acids (17). The net effect of such a mechanism is that SLC25A47 not only catalyzes the import of fatty acids but also dissipates the protein-motive force. Why such a mechanism for fatty acid uptake would be confined to liver mitochondria is unclear.

Intriguingly, a set of fatty acids exclusively processed in the liver are the medium chain fatty acids. Unlike dietary long chain fatty acids, medium chain fatty acids are taken up by the portal circulation and are taken directly to the liver for metabolic processing (28). In the liver, medium chain fatty acids are further elongated and exported as part of VLDL-TG or

are oxidized in the mitochondria (28). The property to be able to oxidize octanoate seems to be specific for liver mitochondria (29). Due to their preferential oxidation in liver mitochondria, medium chain fatty acids are highly ketogenic (30). It has been reported that mitochondrial import of medium chain fatty acids is carnitine independent (28). However, exactly how medium chain fatty acids are imported into mitochondria is unclear. Future studies with isolated liver mitochondria from *Slc25a47*-/- and WT mice should explore the option that SLC25A47 catalyzes the mitochondrial import of medium chain fatty acids.

In addition to investigating the potential role of SLC25A47 as transporter of medium chain fatty acids, OMICS approaches could be employed as part of a more global strategy to characterize the metabolic role of SLC25A47. Specifically, metabolomics could be performed on isolated liver mitochondria, whole liver homogenates, and portal plasma of *Slc25a47*-/- and WT mice. The maximize the potential impact of *Slc25a47* deletion, these studies should be done on material collected from fasted mice. Based on the identity of the substrates for the other SLC25 transporters, the metabolomics analysis should concentrate on amino acids, carboxylic acids, fatty acids, cofactors, and nucleotides. Transcriptomics analysis might be useful as an indirect measurement responding to metabolic perturbation triggered by *Slc25a47* deficiency.

In our study, *Slc25a47* overexpression did not significantly influence any of the metabolic parameters tested. In addition, *Slc25a47* overexpression did not significantly change the expression of any gene above the threshold value. A possible reason why we didn't see any effect of *Slc25a47* overexpression is that hepatic expression of *Slc25a47* is already very high at baseline. In the fasted state, *Slc25a47* is among the most highly expressed genes in mouse liver. Accordingly, studying the effect of *Slc25a47* deficiency has a much better chance of generating important insights into the role of SLC25A47 in liver metabolism.

Slc25a47 mRNA levels were found to be induced by PPARα activation in various hepatocyte model systems, including primary human hepatocytes. In addition, ChIP-SEQ indicated that in mouse liver, PPARα is bound to the Slc25a47 gene at multiple sites immediately unstream of the transcriptional start site. These data suggest that *Slc25a47* is a direct PPARα target gene. Consistent with transcriptional regulation by PPARα, the expression of *Slc25a47* is induced by fasting in mouse liver and in the mouse and human hepatocytes of hepatocyte-humanized mice. This pattern of regulation is consistent with a role of *Slc25a47* in lipid metabolism during fasting.

In conclusion, we describe SLC25A47 as a novel PPARa-regulated gene in human and mouse hepatocytes. Metabolic studies in Slc25a47-overexpressing and Slc25a47-/- mice have so far not revealed any distinct phenotype. Further studies should be conducted to elucidate the functional role of SLC25A47 in liver mitochondrial metabolism.

References

1. Defour, M., G. Hooiveld, M. van Weeghel, and S. Kersten. 2020. Probing metabolic memory in the hepatic response to fasting. *Physiol Genomics* **52**: 602-617.

2. Mashek, D. G. 2020. Hepatic lipid droplets: A balancing act between energy storage and metabolic dysfunction in NAFLD. *Molecular metabolism*: 101115.

3. Xiao, Y., M. Kim, and M. A. Lazar. 2020. Nuclear receptors and transcriptional regulation in non-alcoholic fatty liver disease. *Molecular metabolism*: 101119.

4. Gross, B., M. Pawlak, P. Lefebvre, and B. Staels. 2017. PPARs in obesity-induced T2DM, dyslipidaemia and NAFLD. *Nat Rev Endocrinol* **13**: 36-49.

5. Rakhshandehroo, M., L. M. Sanderson, M. Matilainen, R. Stienstra, C. Carlberg, P. J. de Groot, M. Muller, and S. Kersten. 2007. Comprehensive analysis of PPARalpha-dependent regulation of hepatic lipid metabolism by expression profiling. *PPAR Res* **2007**: 26839.

6. Regnier, M., A. Polizzi, Y. Lippi, E. Fouche, G. Michel, C. Lukowicz, S. Smati, A. Marrot, F. Lasserre, C. Naylies, A. Batut, F. Viars, J. Bertrand-Michel, C. Postic, N. Loiseau, W. Wahli, H. Guillou, and A. Montagner. 2018. Insights into the role of hepatocyte PPARalpha activity in response to fasting. *Mol Cell Endocrinol* **471**: 75-88.

7. Regnier, M., A. Polizzi, S. Smati, C. Lukowicz, A. Fougerat, Y. Lippi, E. Fouche, F. Lasserre, C. Naylies, C. Betoulieres, V. Barquissau, E. Mouisel, J. Bertrand-Michel, A. Batut, T. A. Saati, C. Canlet, M. Tremblay-Franco, S. Ellero-Simatos, D. Langin, C. Postic, W. Wahli, N. Loiseau, H. Guillou, and A. Montagner. 2020. Hepatocyte-specific deletion of Pparalpha promotes NAFLD in the context of obesity. *Scientific reports* **10**: 6489.

8. Kersten, S., J. Seydoux, J. M. Peters, F. J. Gonzalez, B. Desvergne, and W. Wahli. 1999. Peroxisome proliferator-activated receptor alpha mediates the adaptive response to fasting. *J Clin Invest* **103**: 1489-1498.

9. Leone, T. C., C. J. Weinheimer, and D. P. Kelly. 1999. A critical role for the peroxisome proliferator-activated receptor alpha (PPARalpha) in the cellular fasting response: the PPARalpha-null mouse as a model of fatty acid oxidation disorders. *Proc Natl Acad Sci U S A* **96**: 7473-7478.

10. Cheung, C., T. E. Akiyama, J. M. Ward, C. J. Nicol, L. Feigenbaum, C. Vinson, and F. J. Gonzalez. 2004. Diminished hepatocellular proliferation in mice humanized for the nuclear receptor peroxisome proliferator-activated receptor alpha. *Cancer Res* **64**: 3849-3854.

11. de la Rosa Rodriguez, M. A., G. Sugahara, G. Hooiveld, Y. Ishida, C. Tateno, and S. Kersten. 2018. The whole transcriptome effects of the PPARalpha agonist fenofibrate on livers of hepatocyte humanized mice. *BMC genomics* **19**: 443.

12. Janssen, A. W., B. Betzel, G. Stoopen, F. J. Berends, I. M. Janssen, A. A. Peijnenburg, and S. Kersten. 2015. The impact of PPARalpha activation on whole genome gene expression in human precision cut liver slices. *BMC genomics* **16**: 760.

13. Kersten, S., and R. Stienstra. 2017. The role and regulation of the peroxisome proliferator activated receptor alpha in human liver. *Biochimie* **136**: 75-84.

14. Rakhshandehroo, M., G. Hooiveld, M. Muller, and S. Kersten. 2009. Comparative analysis of gene regulation by the transcription factor PPARalpha between mouse and human. *PLoS One* **4**: e6796.

15. Defour, M., C. Michielsen, S. D. O'Donovan, L. A. Afman, and S. Kersten. 2020. Transcriptomic signature of fasting in human adipose tissue. *Physiol Genomics* **52**: 451-467.

16. Mailloux, R. J. 2015. Teaching the fundamentals of electron transfer reactions in mitochondria and the production and detection of reactive oxygen species. *Redox Biol* **4**: 381-398.

17. Bertholet, A. M., and Y. Kirichok. 2017. UCP1: A transporter for H(+) and fatty acid anions. *Biochimie* **134**: 28-34.

18. Rui, L. 2017. Brown and Beige Adipose Tissues in Health and Disease. *Compr Physiol* **7**: 1281-1306.

19. Pohl, E. E., A. Rupprecht, G. Macher, and K. E. Hilse. 2019. Important Trends in UCP3 Investigation. *Front Physiol* **10**: 470.

20. Tan, M. G., L. L. Ooi, S. E. Aw, and K. M. Hui. 2004. Cloning and identification of hepatocellular carcinoma down-regulated mitochondrial carrier protein, a novel liver-specific uncoupling protein. *J Biol Chem* **279**: 45235-45244.

21. Jin, X., Y. D. Yang, K. Chen, Z. Y. Lv, L. Zheng, Y. P. Liu, S. H. Chen, C. H. Yu, X. Y. Jiang, C. Y. Zhang, and Y. M. Li. 2009. HDMCP uncouples yeast mitochondrial respiration and alleviates steatosis in L02 and hepG2 cells by decreasing ATP and H2O2 levels: a novel mechanism for NAFLD. *J Hepatol* **50**: 1019-1028.

22. Kuznetsov, A. V., D. Strobl, E. Ruttmann, A. Konigsrainer, R. Margreiter, and E. Gnaiger. 2002. Evaluation of mitochondrial respiratory function in small biopsies of liver. *Anal Biochem* **305**: 186-194.

23. Liang, N., A. Damdimopoulos, S. Goni, Z. Huang, L. L. Vedin, T. Jakobsson, M. Giudici, O. Ahmed, M. Pedrelli, S. Barilla, F. Alzaid, A. Mendoza, T. Schroder, R. Kuiper, P. Parini, A. Hollenberg, P. Lefebvre, S. Francque, L. Van Gaal, B. Staels, N. Venteclef, E. Treuter, and R. Fan. 2019. Hepatocyte-specific loss of GPS2 in mice reduces non-alcoholic steatohepatitis via activation of PPARalpha. *Nature communications* **10**: 1684.

24. Barretina, J., G. Caponigro, N. Stransky, K. Venkatesan, and A. A. Margolin. 2012. The cancer cell line encyclopedia enables predictive modelling of anticancer drug sensitivity. *Nature* **483**.

25. Kunji, E. R. S., M. S. King, J. J. Ruprecht, and C. Thangaratnarajah. 2020. The SLC25 Carrier Family: Important Transport Proteins in Mitochondrial Physiology and Pathology. *Physiology (Bethesda)* **35**: 302-327.

26. Palmieri, F. 2013. The mitochondrial transporter family SLC25: identification, properties and physiopathology. *Mol Aspects Med* **34**: 465-484.

27. Ruprecht, J. J., and E. R. S. Kunji. 2020. The SLC25 Mitochondrial Carrier Family: Structure and Mechanism. *Trends Biochem Sci* **45**: 244-258.

28. Schonfeld, P., and L. Wojtczak. 2016. Short- and medium-chain fatty acids in energy metabolism: the cellular perspective. *J Lipid Res* **57**: 943-954.

29. Pereyra, A. S., K. L. Harris, A. H. Soepriatna, Q. A. Waterbury, S. S. Bharathi, Y. Zhang, K. H. Fisher-Wellman, C. J. Goergen, E. S. Goetzman, and J. M. Ellis. 2021. Octanoate is differentially metabolized in liver and muscle and fails to rescue cardiomyopathy in CPT2 deficiency. *J Lipid Res* **62**: 100069.

30. St-Pierre, V., C. Vandenberghe, C. M. Lowry, M. Fortier, C. A. Castellano, R. Wagner, and S. C. Cunnane. 2019. Plasma Ketone and Medium Chain Fatty Acid Response in Humans Consuming Different Medium Chain Triglycerides During a Metabolic Study Day. *Front Nutr* **6**: 46.

31. McMullen, P. D., S. Bhattacharya, C. G. Woods, B. Sun, K. Yarborough, S. M. Ross, M. E. Miller, M. T. McBride, E. L. Lecluyse, R. A. Clewell, and M. E. Andersen. 2013. A map of the PPARalpha transcription regulatory network for primary human hepatocytes. *Chemico-biological interactions* **209C**: 14-24.

32. Kandel, B. A., M. Thomas, S. Winter, G. Damm, D. Seehofer, O. Burk, M. Schwab, and U. M. Zanger. 2016. Genomewide comparison of the inducible transcriptomes of nuclear receptors CAR, PXR and PPARalpha in primary human hepatocytes. *Biochim Biophys Acta* **1859**: 1218-1227.

33. Jiang, C., P. Li, X. Ruan, Y. Ma, K. Kawai, H. Suemizu, and H. Cao. 2020. Comparative Transcriptomics Analyses in Livers of Mice, Humans, and Humanized Mice Define Human-Specific Gene Networks. *Cells* **9**.

Chapter 8

General Discussion

PPARα is a ligand-activated transcription factor that belongs to the nuclear hormone receptor superfamily. Ligands for PPARα can be of natural origin, such as fatty acids and its derivatives, or synthetic like fibrate drugs, plasticizers, and insecticides (1,2). Following ligand- activation, PPARα forms a heterodimer with the nuclear receptor RXR and together bind to specific DNA-sequences, known as PPAR response elements (PPRE) around its target genes. Through gene expression PPARα regulates diverse biological pathways such as glucose metabolism, biotransformation, amino acid metabolism, inflammation, but most importantly lipid metabolism (3,4). Specifically, PPARα regulates fatty acid uptake, binding, activation, oxidation, elongation, and desaturation. Furthermore, it regulates formation and breakdown of triglycerides, lipid droplet-associated proteins (reviewed in Chapter 3), and plasma lipoprotein metabolism (5). Gene expression studies performed on mouse livers of PPARα null mice or in diverse in vitro hepatocyte models treated with PPARα agonists have shed light on the variety of genes regulated by PPARα (5–7). Nevertheless, there is limited data on the effects of PPARα in human liver in vivo. Most classical PPARα target genes involved in lipid metabolism (e.g. Angptl4, Pdk4, Cpt1a, Fabp4, G0s2) have been extensively characterized. However, the function of several top PPARα regulated genes is still unknown or has been poorly characterized. Amongst the poorly characterized target genes we have identified Hypoxia-induced lipid droplet associated (HILPDA) and Slc25a47.

The objectives of this research were to improve our knowledge on the transcriptional regulation by peroxisome proliferator-activated receptors (PPAR)-α activation on human liver in vivo. Furthermore, we aimed to characterize the physiological and molecular function of the PPAR target HILDPA in adipose tissue macrophages (ATM) in the context of obesity induced inflammation and in hepatocytes during non-alcoholic steatohepatitis (NASH). Likewise, we sought to identify the physiological function of the PPAR target Slc25a47 in liver lipid metabolism and energy expenditure. In this chapter, we will discuss the results of these studies and propose recommendations for future research.

Whole transcriptome effects of PPARα activation in chimeric mice with hepatocyte-humanized liver

Humanized liver has milder induction of PPARα target genes than mouse liver

Most of our current knowledge on PPARα regulation and function in liver has been acquired using PPARα null mice or by treating mice with synthetic agonists (8,9). Nonetheless, the translation to humans of the effects of PPARα activation in mice are somewhat questionable due to the discrepancy on inducing peroxisome proliferation and hepatocellular carcinoma as observed in mice livers (10,11). Hence, different models have emerged for studying the effects of PPARα activation on human liver including human primary hepatocytes, human cell lines, human liver slices, iPSC-derived human hepatocytes, and PPARα humanized mice. In our research, we used chimeric mice with hepatocyte-humanized liver generated by transplanting human hepatocytes into albumin enhancer–driven urokinase-type plasminogen activator transgenic/severe combined immunodeficiency (cDNA-uPA/SCID) mice to further characterize the whole transcriptome effect of PPARα activation by fenofibrate.

We first compared the whole genome expression profile of human liver tissue with the whole genome expression profile of hepatocyte humanized mouse livers, human primary hepatocytes, and human precision-cut liver slices. Interestingly, scatter plot analysis of transcriptomic data reveled that human liver tissue resembles more closely to hepatocyte humanized livers as compared to primary hepatocytes and human precision-cut liver slices. Nevertheless, there was a set of genes related to immunological pathways, focal adhesion, coagulation and complement that were remarkably higher in human liver tissue, which is reasonable in light of the fact that human hepatocytes were transplanted into the immunodeficient mice. However, we considered the hepatocyte humanized livers as a good model to study the whole transcriptome effect of PPARα agonist fenofibrate given the close similarity in whole transcriptomic gene expression and similar expression level of PPARα mRNA to the actual human liver. Therefore, we gave chimeric mice with hepatocyte humanized livers a daily oral dose of 300 mg/kg of fenofibrate or vehicle for 4 days and analyzed gene expression by qPCR. Fenofibrate treatment significantly increased the expression of known PPARα target genes in human and mouse hepatocytes as measured by qPCR using species-specific primers. However, the overall inductions in gene expression were higher in the mouse hepatocytes than the human hepatocytes. Following, we compared the transcriptomic data of hepatocyte-humanized liver treated with fenofibrate for 4 days to mouse livers harvested 6 h after a single oral dose of fenofibrate and mice treated daily with fenofibrate for 14 days. Interestingly, we also observed a milder effect of PPARα agonist on the gene expression profile in the hepatocyte humanized livers. This

difference cannot be attributed to a lower expression of PPARα in the humanized liver nor to different binding affinity of fenofibrate to human or mouse PPARα (12–14). A possible explanation of this quantitative difference in gene expression may arise on epigenetic regulation (15).

Species-specific and model-specific effects of PPARα activation

In mice, synthetic PPARα agonists are known to cause hepatocarcinogenesis by induction of genes involved in DNA synthesis and cell proliferation. Numerous studies performed in diverse human liver models have dismissed PPARα agonists are hepatocarcinogenic in humans. Nonetheless, it is still a matter of debate (16,17). We performed transcriptomics analysis on the fenofibrate vs. control treated humanized liver mouse. Pathway analysis revealed the most highly induced genes by fenofibrate were associated to fatty acid metabolism and immunity/interferon signaling. By contrast, the pathways repressed by fenofibrate were mainly related to cell cycle, mitosis, and DNA synthesis. Our results reinforce the notion of the species-specific effect of PPARα synthetic agonists on DNA synthesis and cell proliferation. We further compared the transcriptome effect of fenofibrate between normal mouse liver and hepatocyte humanized liver. As expected, among the most highly regulated pathways were PPARα signaling and fatty acid oxidation. Surprisingly, certain immune-related pathways such as interferon signaling were strongly upregulated in hepatocyte-humanized liver but were markedly downregulated in normal mouse liver. Additionally, we compared the 40 most up regulated genes on hepatocyte-humanized livers treated with fenofibrate to human primary hepatocytes and human precision cut liver slices treated with the PPARα agonist Wy14,643. As expected, in the three human liver models almost all significant genes involved in lipid metabolism were consistently induced by PPARα activation. However, we again observed a similar discrepancy in the regulation of several interferon-sensitive genes, which were upregulated by fenofibrate in the hepatocyte humanized mouse livers but downregulated by Wy-14,643 in human primary hepatocytes and human precision cut liver slices. Interferons (IFNs) are cytokines with antiviral, antiproliferative, and immune-modulatory effects (18). They are divided into three families: type I, type II and type III IFNs. In humans, type I IFNs can be secreted by many cell types in response to infection. The expression of the type II IFN is less ubiquitous and restricted to T cells and NK and NKT cells (19,20). Whether the upregulation of interferon signaling by PPARα activation in hepatocyte humanized liver is related to the lack of functional adaptive immune system of the SCID host mice, or to the interaction between human hepatocytes and mouse Kupffer cells, or it reflects PPARα signaling in human liver remains to be established. Overall, our data supports the notion that the effects

of PPARα activation on DNA synthesis, cell proliferation and hepatocarcinogenesis are distinct between mouse liver and human liver.

Humanized mouse as a model to study PPARα effects beyond transcription

Recently, the liver has been recognized as an endocrine organ due to its ability to secrete proteins, known as hepatokines, to communicate with other organs(21). Some of this hepatokines, like Angptl4 or FGF21, are also PPARα target proteins. In our research we were able to detect human Angptl4 in the plasma of humanized-liver mice. The humanized-hepatocyte mice may be a potential model to study the endocrine functions of the liver and its hepatokines. Nonetheless, this should be taken cautiously since there is a possibility of incompatibility between the mouse-human endocrine cell-signaling (22).

One of the most common liver lipid-dysregulation associated diseases is nonalcoholic fatty liver disease (NAFLD). NAFLD is accompanied by diverse liver lesions including steatosis, steatohepatitis and fibrosis. Progression of NAFLD is largely influenced by the degree of steatohepatitis. Although current research supports a mayor role of the innate immune system on hepatic inflammation, increasing evidence has point out to the role of the adaptive immunity on liver inflammation (23). The absence of functional adaptive immune system of our current model could potentially provide clues on the role of the adaptive immune system in NAFLD disease progression.

Overall, our study indicates the hepatocyte-humanized liver is a good model to study the transcriptional effects of PPARα agonist on human liver. By sheltering clusters of mouse and human hepatocytes, the hepatocyte-humanized mouse is an ideal tool to study the parallel effects of a particular treatment on both mouse and human hepatocytes. For example, in this model it has been possible to study the parallel effect of fasting on whole genome gene expression in mouse and human hepatocytes by RNAseq (24). Accordingly, we would like to encourage the broader implementation of the hepatocyte-humanized mouse model in research on lipid and glucose metabolism. By presenting an in vivo environment, it provides clear advantages over other models such as human liver organoids. A very promising feature of hepatocyte humanized mouse liver is that it could be used to model human (genetic) diseases, such as familial hypercholesterolemia (25), and can even be used as a model for correction of human genetic diseases (26). A major disadvantage for the broad implementation of the hepatocyte humanized mouse model is that it is very expensive.

Regulation of LD-associated proteins by PPARs

In cells, excess fatty acids are mainly stored as triglycerides inside specialized organelles known as lipid droplets (LD). Lipid droplets are composed of a hydrophobic core of neutral lipids and sterol esters surrounded by a monolayer of hydrophilic phospholipids. All cells have the ability to synthesize lipid droplets. However, most cells only contain minuscule lipid droplets, except for adipocytes which contains a single lipid droplet that takes-up most of the cell volume. LD are very dynamic; they can expand and shrink depending on the availability and requirement of fatty acids. LD homeostasis is regulated by different LD-associated proteins compromising a complex set of membrane proteins and enzymes. An important group of the membrane LD-associated proteins is the perilipin family which consists of PLIN1 to PLIN5. Other LD-associated proteins include the Cell death-inducing DNA fragmentation factor 45-like Effector family (CIDE-) comprised by CIDEA, CIDEB, and CIDEC. And more recently discovered, G0s2, HILPDA, FITM1, FITM2, among others. Several of these enzymes and LD-associated proteins are regulated by Peroxisome Proliferator-Associated Receptors (PPARs). PPARs are ligand-activated transcription factors that activate gene transcription by binding to a relatively conserved DNA sequence near to its target gene. PPARs have three different subtypes: PPARα, PPARδ, and PPARγ. PPARs mainly differ in their ligand specificity and expression profile among tissues. Through the regulation of LD-associated proteins, PPARs orchestrate the uptake, storage, and utilization of fatty acids.

Our current knowledge on lipid-droplet associated protein regulation by PPARs is mainly limited to cytoplasmic lipid droplets. However, lipid droplets haven been observed on the nucleus of mammalian cells (nLD), in particular in hepatocytes (27,28). In hepatocytes, nuclear lipid droplets represent 2-10% of total cellular lipid droplet population. Similar to cytosolic lipid-droplets, nLD are dynamic and respond to lipid availability (29). Little is known about the physiological relevance of nLD. However, it has been proposed they are involved in nuclear membrane growth (30), sequestration of transcription factors (31), and regulation of phosphatidylcholine synthesis via CCTα (32). Interestingly, we observed the presence of HILPDA, a PPAR target protein, around nLD (Chapter 4, Fig.4). Whether PPARs may regulate nLD or vice versa, whether nLD regulate PPARs requires further research.

Hypoxia inducible lipid droplet associated HILPDA

Our group first ran into HILPDA when screening for genes that are strongly upregulated in adipose tissue macrophages. HILPDA has now been widely recognized as a LD-associated protein by several research groups (33,34). Recent research has demonstrated that HILPDA promotes lipid storage in different types of cells and tissues in the form of lipid droplets

(Chapter 6). Lipid droplet accumulation has been recognized as a signature of metabolically activated macrophages in adipose tissue and of hepatocytes during NASH development (35–38). However, the exact role of lipid droplet accumulation in the development of both pathological conditions remains unclear (39). In this thesis, we studied the functional role of HILPDA in adipose tissue macrophages (ATM) in the context of obesity-induced inflammation (Chapter 4) and in hepatocytes in the context of non-alcoholic steatohepatitis (NASH) (Chapter 5).

Physiological effect of HILPDA in adipose tissue macrophages

Adipose tissue macrophages (ATM) are important for the maintenance of healthy adipose tissue by promoting clearance of adipocyte debris (40,41). During obesity, ATM increase in population accumulating around dead adipocytes in so-called "crown-like structures" and display a proinflammatory phenotype (42). Progressive lipid accumulation as lipid droplets within ATM and foam cell formation has been associated with severe obesity and insulin resistance (43,44). In Chapter 4, we aimed to characterize the role of HILPDA in ATM by exploring the causal association between lipid-droplet accumulation in ATM and the development of adipose tissue inflammation and glucose intolerance during obesity. For this aim, we generated mice with a myeloid-specific Hilpda inactivation (Hilpda$^{\Delta M\Phi}$) by crossing Hilpda$^{flox/flox}$ with mice expressing Cre-recombinase driven by the LysM promoter. Hilpda mRNA and protein level were decreased by approximately 80% in isolated BMDMs from Hilpda$^{\Delta M\Phi}$ mice compared to their Hilpda$^{flox/flox}$ littermates. Interestingly, after lipid loading, BMDMs from Hilpda$^{\Delta M\Phi}$ mice showed a marked decrease in lipid droplet accumulation accompanied by a decrease in di- and triacylglycerol content when compared to Hilpda$^{flox/flox}$ mice. Subsequently, cellular respiration was measured to explore if the excess fatty acids were disposed of by increased oxidation in Hilpda$^{\Delta M\Phi}$ and Hilpda$^{flox/flox}$ BMDMs. Oxygen consumption of fatty-acid-loaded Hilpda$^{\Delta M\Phi}$ and Hilpda$^{flox/flox}$ BMDMs was measured during a mitochondrial stress test with Seahorse. Remarkably, after 24 h of fatty acid loading, basal and maximal respiration were significantly higher in Hilpda$^{\Delta M\Phi}$ compared with Hilpda$^{flox/flox}$ BMDMs, indicating an increase in maximal oxidative capacity. Together, these data show that HILPDA deficiency leads to a pronounced decrease in lipid storage in macrophages accompanied by an increase in fatty acid oxidation. Next, to study the functional consequences of macrophage HILPDA deficiency in the context of obesity-induced adipose tissue inflammation, Hilpda$^{\Delta M\Phi}$ mice and their Hilpda$^{flox/flox}$ littermates were fed a high fat diet for 20 weeks, using a low-fat diet as control. As expected, Hilpda$^{\Delta M\Phi}$ showed pronounced decreased of Hilpda expression in the stromal vascular fraction of the adipose tissue but not in the adipocyte fraction. Similar to our previous finding in BMDMs, lipid droplet content was significantly lower in ATM isolated from high fat diet-fed Hilpda$^{\Delta M\Phi}$

mice than Hilpda$^{flox/flox}$ mice. Strikingly, the decrease in lipid-droplets was not associated with any change in the secretion of the classical inflammatory cytokines interleukin-6 (IL-6) and tumor necrosis factor alpha (TNF-α). Furthermore, flow cytometry analysis of the stromal vascular fraction isolated from the adipose tissue showed an increased percentage of populations of CD45+, CD11b+CD206+, and CD11b+CD11c+ cells by high-fat feeding, but no clear differences between genotypes. Also, gene expression analysis in adipose tissue of pro- or anti- inflammatory related genes showed no significant difference between Hilpda$^{\Delta M\Phi}$ and Hilpda$^{flox/flox}$ mice despite a marked induction by high fat diet. Last, to examine whether macrophage HILPDA deficiency had any influence on obesity-induced metabolic dysfunction, we measured plasma metabolic parameters and assessed glucose tolerance in Hilpda$^{\Delta M\Phi}$ and Hilpda$^{flox/flox}$ on both high- and low-fat diet. Although high-fat feeding significantly increased plasma levels of cholesterol, triglycerides, glucose, non-esterified fatty acids, leptin, and insulin, no differences were observed between Hilpda$^{\Delta M\phi}$ and Hilpda$^{flox/flox}$ mice, either on a low- or high-fat diet. Likewise, high-fat feeding caused a marked decrease in glucose tolerance, nonetheless no differences were observed between Hilpda$^{\Delta M\Phi}$ and Hilpda$^{flox/flox}$ mice. Altogether, our data indicate that myeloid-specific HILPDA deficiency reduces lipid droplet accumulation in adipose tissue macrophages but does not influence the inflammatory status of adipose tissue and does not have any effect on obesity- induced metabolic complications.

Our results do not invalidate the notion that ATMs contribute to obesity-induced adipose tissue inflammation, nor do they refute the model that lipid-activation of macrophages importantly underlies obesity-induced adipose tissue inflammation. Rather, they suggest that triglyceride storage as such does not drive the inflammatory phenotype. In contrast to our findings, a recent study on BMDMs stimulated with LPS indicated that DGAT1-mediated lipid droplet ablation resulted in a pronounced reduction of inflammatory mediators, thereby suggesting that lipid droplets play an essential role in the activation of macrophages (39). Possible explanations for this discrepancy may arise from the stimuli used to activate the macrophages (45) and from the lipid droplet-associated protein targeted to ablate the lipid droplet. Interestingly, a recently identified subset of ATM that expands during obese conditions suggests that the lipid storage capacity in this specific subset of ATMs, now named lipid-associated macrophages (LAMs), is crucial for adipose tissue remodeling and metabolic homeostasis. LAMs are characterized by a transcriptional signature of *Trem2*, *Lipa*, *Lpl*, *Ctsb*, *Ctsl*, *Fabp4*, *Fabp5*, *Lgals1*, *Lgals3*, *Cd9*, and *Cd36. In vivo* deletion of the lipid receptor Trem2 markedly reduced the expression level of signature genes in LAMs and consequently blunted the ability of LAMs to take up and storage lipid, accompanied by massive adipocyte hypertrophy, weight gain, increased in body fat content, plasma cholesterol, fasting insulin levels and glucose intolerance (46). The current

findings raise awareness of the complexity of lipid accumulation in ATMs and its relation to inflammation and metabolic homeostasis.

It could be argued that the enhanced lipolysis in Hilpda$^{\Delta M\Phi}$ macrophages may lead to intracellular accumulation of fatty acids, which in turn may exert a potential lipotoxic effect. Although we did observe increased fatty acid-induced gene regulation, the overall lipoxic effect of HILPDA deficiency seemed quite limited. Our Seahorse studies indicated that the enhanced lipolysis in HILPDA-deficient macrophages is accompanied by enhanced fatty acid oxidation, thereby limiting the intracellular accumulation of fatty acids and mitigating lipotoxicity.

Our research leaves open the possibility that inflammatory properties of macrophages might be influenced by lipid droplet-associated proteins. Current developments of novel therapies targeting ATM (47,48) highlights the importance of a clear understanding on the functionality of adipose tissue macrophages and its mechanisms to maintain healthy adipose tissue homeostasis.

Physiological effect of HILPDA in liver in the context of NASH

The liver has a vital role in regulating lipid metabolism. Liver lipids can become abnormally increased under conditions of obesity and insulin resistance. A chronic increase in intra-hepatic lipids is known as hepatic steatosis and is a characteristic sign of non-alcoholic fatty liver disease (NAFLD). NAFLD can progress to non-alcoholic steatohepatitis (NASH), which encompasses liver steatosis, inflammation and fibrosis (23). In this thesis, we further study the function of HILPDA in relation to hepatic lipid metabolism in the context of NASH. Liver-specific Hilpda knockout mice were fed with a high fat diet deficient in methionine and choline (HFmcd), using a low-fat (LF) diet as a control. This diet differs from the classical choline and methionine-deficient diet that is low in fat. When mice are fed the classical MCD, they quickly lose weight. The lack of obesity phenotype in MCD-fed mice is one of the major criticisms raised against this model, as most people with NASH are obese. In our study, we used a modified MCD diet that is high in fat (HFmcd) (49). When mice are fed HFmcd, it has been reported that they develop NASH without suffering from weight loss (49), which is exactly what we observed. Also, H&E staining of the livers of the mice fed HFmcd revealed all the pathological features of NASH. Accordingly, the HFmcd is a better model than the traditional MCD model for the study of NASH in mice.

Interestingly, after 11 weeks of feeding the diets, hepatic expression of Hilpda was significantly higher in mice fed the HFmcd than in mice fed the LF diet and was significantly lower in Hilpda$^{\Delta liver}$ than in Hilpda$^{flox/flox}$ mice. At the protein level, HILPDA was also considerably reduced in livers of Hilpda$^{\Delta liver}$ compared to Hilpda$^{flox/flox}$ mice. At the organ

level, liver weights of mice fed HFmcd but not the LF diet, were modestly but significantly lighter in Hilpda$^{\Delta liver}$ than in Hilpda$^{flox/flox}$ mice. In accordance with the previously observed effect of HILPDA on increasing liver triglyceride content (50), hepatic triglyceride levels were modestly but statistically significantly reduced in Hilpda$^{\Delta liver}$ compared to Hilpda$^{flox/flox}$ mice on both diets. In accordance with liver triglyceride levels, plasma alanine aminotransferase (ALT) levels were also significantly lower in Hilpda$^{\Delta liver}$ than in Hilpda$^{flox/flox}$ mice on both diets. However, no significant differences were observed between genotypes on the expression of inflammatory markers Cd68 and Ccl2, and the fibrosis markers Timp1 and Col1a1, despite a marked induction by HFmcd.

Overall, we found that Hilpda deletion in hepatocytes has a significant but modest effect on liver triglycerides storage after NASH induction. This result contrasts with the pronounced effect observed in macrophages, where the accumulation of triglycerides as lipid droplets was dramatically abolished by Hilpda deletion (51). Inversely, liver-specific overexpression of HILDPA led to a huge increase in liver triglycerides (52). The mild effect of HILPDA deficiency on liver triglyceride levels is likely related to the relatively low expression of Hilpda in mouse liver and to the molecular function of HILPDA as ATGL inhibitor and DGAT activator (see below). Consistent with this notion, HILPDA deficiency in mouse liver slices and primary mouse hepatocytes, which express much higher levels of HILPDA, markedly decreased triglyceride accumulation. It is not fully clear why HILPDA levels are much higher in cultured hepatocytes compared to hepatocytes in vivo. A possible explanation is that HIF1a, which stimulates HILPDA transcription, is activated when hepatocytes are put into culture. The high expression of HILPDA may explain why viral overexpression of HILPDA in primary hepatocytes did not influence triglyceride accumulation (data not shown), whereas HILPDA deficiency did. Conversely, in vivo we observed a much more pronounced effect of HILPDA overexpression as compared to HILPDA deficiency.

Hepatocyte specific HILPDA deletion using the albumin Cre-system led to a 50-60% decrease in liver Hilpda mRNA, suggesting it is still expressed in other liver cell-types like endothelial cells, stellate cells, or immune cells. Liver Kupffer cells are part of the liver innate immune system. They represent around 35% of liver non-parenchymal cells (53). Accumulating evidence has recognized the presence of activated foamy Kupffer cells at the early stage of NAFLD and not as a consequence of late steatosis (23,54,55). Given that Hilpda is abundantly expressed in macrophages and has an essential role in lipid storage in these cells (Chapter 4), it would be very interesting to further study the effect of Hilpda deficiency on lipid accumulation in liver Kupffer cells (KC) in relation to NASH.

Molecular aspects of HILPDA

In different cell types, HILPDA has been localized surrounding lipid droplets (56–58). In line with the notion that a cell contains distinct lipid droplet subpopulations (59), we observed that HILPDA is not present in all lipid droplets. In fact, co-transfected hepatocytes with HILPDA- mEGFP and PLIN2-mCherry showed that HILPDA and PLIN2 coat distinct sets of lipid droplets (Chapter 5). Besides its localization to lipid droplets, HILPDA was shown to colocalize and migrate through the endoplasmic reticulum, the site of lipid droplet synthesis, where it correlated significantly with newly synthesized triglycerides. Furthermore, HILPDA preferably accumulated in lipid droplets undergoing remodeling (shrinking and expansion) (Chapter 5). In macrophages, HILPDA deficiency substantially decreased lipid droplet accumulation. To investigate if the decrease in LD was due to reduced fatty acid uptake, BMDMs were loaded with a fluorescently labeled fatty acid. Confocal microscopy showed no difference in fluorescence intensity between Hilpda$^{\Delta M\phi}$ and Hilpda$^{flox/flox}$ macrophages at 6 and 35 min indicating that HILPDA deficiency did not influence fatty acid uptake. Similarly, expression of the fatty acid transporter Cd36 was not different between Hilpda$^{\Delta M\phi}$ and Hilpda$^{flox/flox}$ macrophages. Next, to determine the intracellular trafficking of lipids, BMDMs were loaded with a mixture of oleate and the fluorescent fatty acid BODIPY FL. Surprisingly, after lipid loading for 5h the Hilpda$^{flox/flox}$ had already accumulated BODIPY FL in lipid droplets, whereas in Hilpda$^{\Delta M\phi}$ macrophages, the BODIPY FL was distributed throughout the endoplasmic reticulum (ER) and with minor presence in lipid droplet-like structures. After lipid loading for 24 h, Hilpda$^{flox/flox}$ macrophages had an increased number and size of lipid droplets, whereas in Hilpda$^{\Delta M\phi}$ macrophages, the initially formed lipid-droplet-like structures faded. Previous research showed HILPDA can interact and inhibit ATGL (60,61). To evaluate if the inability to retain the fatty acids as lipid droplets is due to increased ATGL-mediated lipolysis, Hilpda$^{\Delta M\phi}$ and Hilpda$^{flox/flox}$ BMDMs were lipid loaded and incubated with Atglistatin, a small-molecule inhibitor of ATGL (62). Remarkably, inhibiting ATGL greatly increased lipid droplets in Hilpda$^{\Delta M\phi}$ BMDMs almost completely rescuing the Hilpda$^{\Delta M\phi}$ phenotype. (Chapter 4) These data suggest that the decrease in lipid content and lipid droplet growth in Hilpda$^{\Delta M\phi}$ macrophages is due to increased ATGL mediated triglyceride hydrolysis. Thus, in macrophages HILPDA acts as a potent endogenous inhibitor of ATGL. Contrastingly, in HILPDA-deficient primary mouse hepatocytes, no statistical interaction was observed between Atglistatin treatment and Hilpda genotype in relation to lipid droplet size, suggesting that in hepatocytes HILPDA promotes lipid storage at least partly via an ATGL-independent mechanism. A distinct mechanism from lipolysis to affect lipid accumulation is through lipid synthesis. Diacylglycerol acyl- transferase (DGAT) catalyzes the last and rate- limiting step in the synthesis of triglycerides by using diacylglycerol and acyl-CoA as substrates. To determine if HILPDA might stimulate DGAT activity, we transduced HepG2

cells with AV- Hilpda or AV-Gfp and incubated the lysate with fluorescent NBD-palmitoyl-CoA and 1,2 dioleoyl-sn-glycerol. Remarkably, the DGAT-mediated triglyceride synthesis was markedly increased by HILPDA overexpression, as determined by quantification of thin-layer chromatography (TLC). Triglyceride synthesis from diacylglycerol and acyl-CoA can be catalyzed by two different isozymes: DGAT1 and DGAT2 (63). Whereas DGAT2 catalyzes triacylglycerol synthesis from endogenous synthetized fatty acids, DGAT1 mainly esterifies exogenous fatty acids to diacylglycerol (64–66). Interestingly, the increase in triglyceride synthesis by HILPDA overexpression was unaltered by the DGAT2 inhibitor PF-06424439 but completely suppressed by the DGAT1 inhibitor A922500. Additionally, we corroborated the stimulatory effect of HILPDA on lipid storage via DGAT1 in adipocytes. Next, to investigate whether HILPDA may physically interact with DGAT1 in cells, we performed FRET quantified by FLIM in live and fixed HepG2 transfected with HILPDA-mEGFP and DGAT1-mCherry. The mean fluorescence lifetime of the donor fluorophore HILPDA-EGFP was significantly decreased by the presence of the acceptor fluorophore DGAT1-mCherry. This result demonstrates that HILPDA and DGAT1 are in very close proximity, indicating that they physically interact intracellularly.

Our cellular localization studies indicated that HILPDA coats a subpopulation of lipid droplets which presumably exclude PLIN2. PLIN2 is considered a general lipid droplet-associated protein present in essentially all cells. Evidence abounds indicating that PLIN2 promotes LD accumulation (67). We could hypothesize that PLIN2-coated LDs may define more stable LD population, whereas HILPDA-coated LDs may indicate that they are actively being remodeled via triglyceride lipolysis and synthesis as shown by our time-lapse live imaging. In line with this observation, we showed that the lipid droplet ablation in HILPDA-deficient macrophages is explained by increased ATGL-mediated lipolysis. Thus, in macrophages HILPDA acts as an important ATGL inhibitor. Previous research from our group and another group showed that HILPDA directly interacts and inhibits ATGL triglyceride hydrolase activity. This inhibitory interaction depends on the residues 7–11 of the conserved N-terminus of HILPDA and the N- terminal patatin domain-containing region of ATGL (60,68). This ATGL region also mediates triglyceride hydrolysis and the interaction with CGI-58/ABHD5, Atglistatin, acyl-CoA, and G0S2. Interestingly, despite the marked decrease in lipid storage of HILPDA-deficient mice and cells, in a cell-free system the inhibitory capacity of HILPDA was found to be substantially weaker than G0S2, another well-recognized ATGL inhibitor protein [26]. This could indicate that HILPDA might require an auxiliary factor to efficiently inhibit ATGL. However, further studies are needed to determine why HILPDA is less potent in cell-free systems compared to live cells.

Additionally, we found that HILPDA can interact and enhance DGAT1 activity in hepatocytes and adipocytes. Recent research showed that the N-terminal of DGAT1 is important for allosteric regulation and dimerization (69,70). DGAT1 forms homodimers through

hydrophilic and hydrophobic interactions. Deletion of the first 85 or 90 residues, which corresponds to important segments for dimerization, resulted in decreased activity and protein expression levels (70). Exactly how HILPDA increases DGAT1 activity and protein levels is unclear, but based on our and other data, it can be hypothesized that the interaction between HILPDA with DGAT1 might facilitate DGAT1 stability or dimerization, thus enhance DGAT1 activity. Further biochemical and microscopic studies should address how exactly HILPDA and DGAT1 interact.

Finally, it can be hypothesized that HILPDA may be part of a larger triglyceride turnover complex, “the lipolysome”. Lipolysome, is a term coined by Zechner et al. to designate the complex protein network regulating cytoplasmic lipolysis (71), including direct and indirect inhibitors or activators of lipolysis (72). Here we would like to propose to broaden this designation to the protein network regulating triglyceride turnover. Triglyceride turnover describes the concurrent synthesis and hydrolysis of stored triglycerides. It is a highly coordinated process that is partly aimed at minimizing fluctuations in intracellular fatty acid level. Mechanistically, HILPDA regulates triglyceride storage by inhibiting ATGL-mediated lipolysis (the first step in triglyceride breakdown) and/or activating DGAT1-mediated triglyceride synthesis (the last step in triglyceride synthesis) (Fig. 1). Several external stimuli, including hypoxia, fatty acids, and β-adrenergic agonists can upregulate Hilpda expression. Hence, HILPDA seems to function as an adaptive signal that is activated under specific circumstances. The induction of HILPDA by fatty acids is plausibly part of a feed-forward mechanism to regulate intracellular fatty acids availability by promoting their storage as triglycerides and attenuate lipolysis.

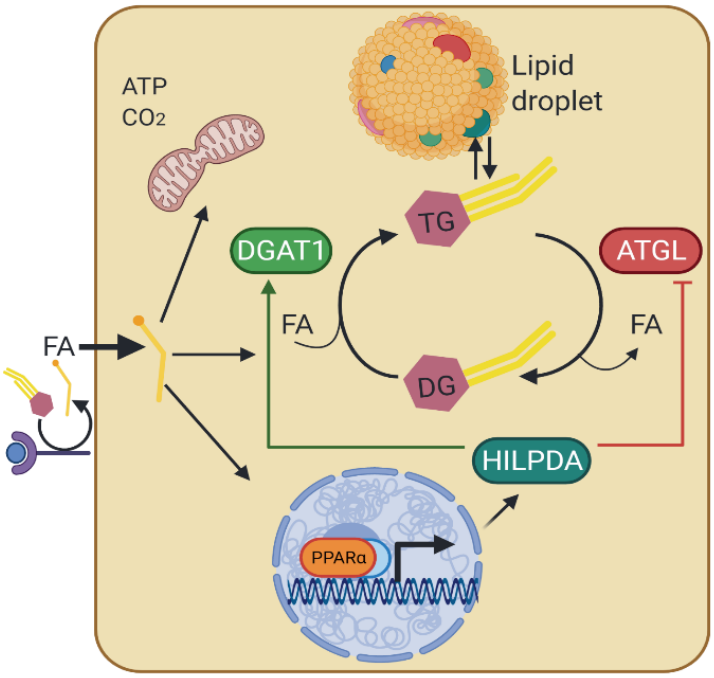

Figure 1. Schematic depiction of fatty acid disposition by HILPDA. HILPDA facilitates triglyceride storage by inhibiting ATGL-mediated lipolysis and/or activating DGAT1-mediated triglyceride synthesis.

Taken together, the results obtained with hepatocyte, adipocyte, and myeloid-specific Hilpda-deficient mouse models suggest that the main mechanism of HILPDA in regulating cellular triglyceride storage is cell-type specific and is likely dictated by the level of HILPDA expression, as well as by the expression of related proteins such as G0S2.

So far, our research has focused on the regulation of triglyceride synthesis or degradation by HILPDA. However, our lipidomic data reveled HILPDA overexpression or deletion results on increased or decreased cholesteryl esters (CE) levels, respectively. Cholesteryl ester synthesis is catalyzed by Sterol-o-acyltransferase (SOAT) from cholesterol and long-chain fatty acyl-CoA. CE can then be stored in lipid droplets or secreted in lipoproteins. Like DGAT1, SOAT belongs to the superfamily of membrane-bound O-acyl transferases (MBOAT). SOAT has been consider a potential therapeutical target for atherosclerosis, several types of cancer, and Alzheimer's disease (73). In the future, it would be of interest to investigate the function of HILPDA on cholesteryl ester regulation.

In this thesis we characterized the whole transcriptome effects of in vivo PPARα activation in a chimeric mouse model with hepatocyte humanized liver. Then we described the physiological function of the PPARα target HILPDA in adipose tissue macrophages in the context of obesity-induced inflammation and in liver in the context of non-alcoholic steatohepatitis. We further identified the molecular mechanism of HILPDA in relation to lipid metabolism in both hepatocytes and macrophages. We found that HILPDA promotes triglyceride accumulation mainly via enhancing DGAT1 activity in hepatocytes and via ATGL inhibition in macrophages. Lastly, we characterized the role of the PPARα target SLC25a47 in whole body and liver energy homeostasis and mitochondrial function. Overall, this thesis has generated more insight into the physiological role of PPARα and of genes regulated by PPARα.

References

1. Georgiadi A, Kersten S. Mechanisms of gene regulation by fatty acids. Adv Nutr. 2012 Mar 1;3(2):127–34.
2. Takeuchi S, Matsuda T, Kobayashi S, Takahashi T, Kojima H. In vitro screening of 200 pesticides for agonistic activity via mouse peroxisome proliferator-activated receptor (PPAR)α and PPARγ and quantitative analysis of in vivo induction pathway. Toxicol Appl Pharmacol. 2006 Dec 15;217(3):235–44.
3. Varga T, Czimmerer Z, Nagy L. PPARs are a unique set of fatty acid regulated transcription factors controlling both lipid metabolism and inflammation. Biochim Biophys Acta. 2011 Aug;1812(8):1007–22.
4. Mandard S, Muller M, Kersten S. Peroxisome proliferator-activated receptor a target genes. Cell Mol Life Sci. 2004 Feb 1;61(4):393–416.
5. Kersten S. Integrated physiology and systems biology of PPARα. Vol. 3, Molecular Metabolism. Elsevier GmbH; 2014. p. 354–71.
6. Janssen AWF, Betzel B, Stoopen G, Berends FJ, Janssen IM, Peijnenburg AA, et al. The impact of PPARα activation on whole genome gene expression in human precision cut liver slices. BMC Genomics. 2015;16.
7. Leone TC, Weinheimer CJ, Kelly DP. A critical role for the peroxisome proliferator-activated receptor (PPAR) in the cellular fasting response: The PPAR -null mouse as a model of fatty acid oxidation disorders. Proc Natl Acad Sci. 1999 Jun 22;96(13):7473–8.
8. Kersten S, Seydoux J, Peters JM, Gonzalez FJ, Desvergne B, Wahli W. Peroxisome proliferator-activated receptor alpha mediates the adaptive response to fasting. J Clin Invest. 1999 Jun;103(11):1489–98.
9. Mandard S, Müller M, Kersten S. Peroxisome proliferator-activated receptor α target genes. Vol. 61, Cellular and Molecular Life Sciences. Springer; 2004. p. 393–416.
10. Gariot P, Barrat E, Mejean L, Pointel JP, Drouin P, Debry G. Fenofibrate and human liver - Lack of proliferation of peroxisomes. Arch Toxicol. 1983 Jun;53(2):151–63.
11. Morimura K, Cheung C, Ward JM, Reddy JK, Gonzalez FJ. Differential susceptibility of mice humanized for peroxisome proliferator-activated receptor α to Wy-14,643-induced liver tumorigenesis. Carcinogenesis. 2006 May;27(5):1074–80.
12. Willson TM, Brown PJ, Sternbach DD, Henke BR. The PPARs: From orphan receptors to drug discovery. Vol. 43, Journal of Medicinal Chemistry. American Chemical Society ; 2000. p. 527–50.
13. Rakhshandehroo M, Hooiveld G, M?ller M, Kersten S. Comparative Analysis of Gene Regulation by the Transcription Factor PPARalpha between Mouse and Human. Laudet V, editor. PLoS One. 2009 Aug 27;4(8):e6796.
14. Kersten S. Integrated physiology and systems biology of PPARα. Mol Metab. 2014 Jul;3(4):354–71.
15. Gibney ER, Nolan CM. Epigenetics and gene expression. Vol. 105, Heredity. Nature Publishing Group; 2010. p. 4–13.
16. Peters JM, Aoyama T, Cattley RC, Nobumitsu U, Hashimoto T, Gonzalez FJ. Role of peroxisome proliferator-activated receptor α in altered cell cycle regulation in mouse liver. Carcinogenesis. 1998 Nov;19(11):1989–94.
17. Corton JC, Cunningham ML, Hummer BT, Lau C, Meek B, Peters JM, et al. Mode of action framework analysis for receptor-mediated toxicity: The peroxisome proliferator-activated receptor alpha (PPARα) as a case study. Vol. 44, Critical Reviews in Toxicology. Informa Healthcare; 2014. p. 1–49.
18. Stark GR, Kerr IM, Williams BRG, Silverman RH, Schreiber RD. How cells respond to interferons. Vol. 67, Annual Review of Biochemistry. Annu Rev Biochem; 1998. p. 227–64.
19. Horras CJ, Lamb CL, Mitchell KA. Regulation of hepatocyte fate by interferon-γ. Vol. 22, Cytokine and Growth Factor Reviews. NIH Public Access; 2011. p. 35–43.

20. Li SF, Gong MJ, Zhao FR, Shao JJ, Xie YL, Zhang YG, et al. Type i interferons: Distinct biological activities and current applications for viral infection. Vol. 51, Cellular Physiology and Biochemistry. S. Karger AG; 2018. p. 2377–96.

21. Jensen-Cody SO, Potthoff MJ. Hepatokines and metabolism: Deciphering communication from the liver. Vol. 44, Molecular Metabolism. Elsevier GmbH; 2021. p. 101138.

22. Masumoto N, Tateno C, Tachibana A, Utoh R, Morikawa Y, Shimada T, et al. GH enhances proliferation of human hepatocytes grafted into immunodeficient mice with damaged liver. J Endocrinol. 2007 Sep;194(3):529–37.

23. Sutti S, Albano E. Adaptive immunity: an emerging player in the progression of NAFLD. Vol. 17, Nature Reviews Gastroenterology and Hepatology. Nature Research; 2020. p. 81–92.

24. Defour M, Hooiveld GJEJ, Van Weeghel M, Kersten S. Probing metabolic memory in the hepatic response to fasting. Physiol Genomics. 2020 Dec 1;52(12):602–17.

25. Bissig-Choisat B, Wang L, Legras X, Saha PK, Chen L, Bell P, et al. Development and rescue of human familial hypercholesterolaemia in a xenograft mouse model. Nat Commun. 2015 Jun 17;6.

26. Zabulica M, Srinivasan RC, Akcakaya P, Allegri G, Bestas B, Firth M, et al. Correction of a urea cycle defect after ex vivo gene editing of human hepatocytes. Mol Ther. 2021;

27. Lagrutta LC, Montero-Villegas S, Layerenza JP, Sisti MS, García de Bravo MM, Ves-Losada A. Reversible Nuclear-Lipid-Droplet Morphology Induced by Oleic Acid: A Link to Cellular-Lipid Metabolism. Aspichueta P, editor. PLoS One. 2017 Jan 26;12(1):e0170608.

28. Layerenza JP, González P, García De Bravo MM, Polo MP, Sisti MS, Ves-Losada A. Nuclear lipid droplets: A novel nuclear domain. Biochim Biophys Acta - Mol Cell Biol Lipids. 2013 Feb 1;1831(2):327–40.

29. Lagrutta LC, Montero-Villegas S, Layerenza JP, Sisti MS, García De Bravo MM, Ves-Losada A. Reversible nuclear-lipid-droplet morphology induced by oleic acid: A link to cellular-lipid metabolism. PLoS One. 2017 Jan 1;12(1).

30. Barbosa AD, Siniossoglou S. New kid on the block: lipid droplets in the nucleus. FEBS J. 2020 Nov 17;287(22):4838–43.

31. Romanauska A, Köhler A. The Inner Nuclear Membrane Is a Metabolically Active Territory that Generates Nuclear Lipid Droplets. Cell. 2018 Jul 26;174(3):700-715.e18.

32. Sołtysik K, Ohsaki Y, Tatematsu T, Cheng J, Fujimoto T. Nuclear lipid droplets derive from a lipoprotein precursor and regulate phosphatidylcholine synthesis. Nat Commun. 2019 Dec 1;10(1):1–12.

33. Maier A, Wu H, Cordasic N, Oefner P, Dietel B, Thiele C, et al. Hypoxia-inducible protein 2 Hig2/Hilpda mediates neutral lipid accumulation in macrophages and contributes to atherosclerosis in apolipoprotein E-deficient mice. FASEB J. 2017 Nov 1;31(11):4971–84.

34. de la Rosa Rodriguez MA, Deng L, Gemmink A, van Weeghel M, Aoun ML, Warnecke C, et al. Hypoxia-inducible lipid droplet-associated induces DGAT1 and promotes lipid storage in hepatocytes. Mol Metab. 2021 Jan 1;47:101168.

35. den Brok MH, Raaijmakers TK, Collado-Camps E, Adema GJ. Lipid Droplets as Immune Modulators in Myeloid Cells. Trends Immunol. 2018 May 1;39(5):380–92.

36. Melo RCN, D'Avila H, Wan H-C, Bozza PT, Dvorak AM, Weller PF. Lipid Bodies in Inflammatory Cells: Structure, Function, and Current Imaging Techniques. J Histochem Cytochem. 2011;59(5):540.

37. McPherson S, Hardy T, Henderson E, Burt AD, Day CP, Anstee QM. Evidence of NAFLD progression from steatosis to fibrosing-steatohepatitis using paired biopsies: Implications for prognosis and clinical management. J Hepatol. 2015 May 1;62(5):1148–55.

38. Adams LA, Ratziu V. Non-alcoholic fatty liver - Perhaps not so benign. Vol. 62, Journal of Hepatology. Elsevier B.V.; 2015. p. 1002–4.

39. Castoldi A, Monteiro LB, van Teijlingen Bakker N, Sanin DE, Rana N, Corrado M, et al. Triacylglycerol synthesis enhances macrophage inflammatory function. Nat Commun. 2020 Dec 1;11(1):1–11.

40. Boutens L, Stienstra R. Adipose tissue macrophages: going off track during obesity. Diabetologia. 2016 May 3;59(5):879–94.

41. Weisberg SP, McCann D, Desai M, Rosenbaum M, Leibel RL, Ferrante AW. Obesity is associated with macrophage accumulation in adipose tissue. J Clin Invest. 2003 Dec 15;112(12):1796–808.

42. Lumeng CN, Delproposto JB, Westcott DJ, Saltiel AR. Phenotypic switching of adipose tissue macrophages with obesity is generated by spatiotemporal differences in macrophage subtypes. Diabetes. 2008 Dec 1;57(12):3239–46.

43. Prieur X, Mok CYL, Velagapudi VR, Núñez V, Fuentes L, Montaner D, et al. Differential lipid partitioning between adipocytes and tissue macrophages modulates macrophage lipotoxicity and M2/M1 polarization in obese mice. Diabetes. 2011 Mar;60(3):797–809.

44. Shapiro H, Pecht T, Shaco-Levy R, Harman-Boehm I, Kirshtein B, Kuperman Y, et al. Adipose Tissue Foam Cells Are Present in Human Obesity. J Clin Endocrinol Metab. 2013 Mar 1;98(3):1173–81.

45. Robblee MM, Kim CC, Abate JP, Valdearcos M, Sandlund KLM, Shenoy MK, et al. Saturated Fatty Acids Engage an IRE1α-Dependent Pathway to Activate the NLRP3 Inflammasome in Myeloid Cells. Cell Rep. 2016 Mar 22;14(11):2611–23.

46. Jaitin DA, Adlung L, Thaiss CA, Weiner A, Li B, Descamps H, et al. Lipid-Associated Macrophages Control Metabolic Homeostasis in a Trem2-Dependent Manner. Cell. 2019 Jul 25;178(3):686-698.e14.

47. Sullivan TJ, Miao Z, Zhao BN, Ertl LS, Wang Y, Krasinski A, et al. Experimental evidence for the use of CCR2 antagonists in the treatment of type 2 diabetes. Metabolism. 2013 Nov 1;62(11):1623–32.

48. Kraakman MJ, Kammoun HL, Allen TL, Deswaerte V, Henstridge DC, Estevez E, et al. Blocking IL-6 trans-signaling prevents high-fat diet-induced adipose tissue macrophage recruitment but does not improve insulin resistance. Cell Metab. 2015 Mar 3;21(3):403–16.

49. Matsumoto M, Hada N, Sakamaki Y, Uno A, Shiga T, Tanaka C, et al. An improved mouse model that rapidly develops fibrosis in non-alcoholic steatohepatitis. 2013;

50. Mattijssen F, Georgiadi A, Andasarie T, Szalowska E, Zota A, Krones-Herzig A, et al. Hypoxia-inducible lipid droplet-associated (HILPDA) is a novel peroxisome proliferator-activated receptor (PPAR) target involved in hepatic triglyceride secretion. J Biol Chem. 2014 Jul 11;289(28):19279–93.

51. van Dierendonck XAMH, de la Rosa Rodriguez MA, Georgiadi A, Mattijssen F, Dijk W, van Weeghel M, et al. HILPDA Uncouples Lipid Droplet Accumulation in Adipose Tissue Macrophages from Inflammation and Metabolic Dysregulation. Cell Rep. 2020 Feb 11;30(6):1811-1822.e6.

52. Bilzer M, Roggel F, Gerbes AL. Role of Kupffer cells in host defense and liver disease. Liver Int. 2006 Dec 1;26(10):1175–86.

53. Kazankov K, Jørgensen SMD, Thomsen KL, Møller HJ, Vilstrup H, George J, et al. The role of macrophages in nonalcoholic fatty liver disease and nonalcoholic steatohepatitis. Vol. 16, Nature Reviews Gastroenterology and Hepatology. Nature Publishing Group; 2019. p. 145–59.

54. Wouters K, van Gorp PJ, Bieghs V, Gijbels MJ, Duimel H, Lütjohann D, et al. Dietary cholesterol, rather than liver steatosis, leads to hepatic inflammation in hyperlipidemic mouse models of nonalcoholic steatohepatitis. Hepatology. 2008 Aug;48(2):474–86.

55. DiStefano MT, Roth Flach RJ, Senol-Cosar O, Danai L V., Virbasius J V., Nicoloro SM, et al. Adipocyte-specific Hypoxia-inducible gene 2 promotes fat deposition and diet-induced insulin resistance. Mol Metab. 2016 Dec;5(12):1149–61.

56. Gimm T, Wiese M, Teschemacher B, Deggerich A, Schodel J, Knaup KX, et al. Hypoxia-inducible protein 2 is a novel lipid droplet protein and a specific target gene of hypoxia-inducible factor-1. FASEB J. 2010 Nov 1;24(11):4443–58.

57. Dijk W, Mattijssen F, De La Rosa Rodriguez M, Valdes AL, Loft A, Mandrup S, et al. Hypoxia-inducible lipid droplet-associated is not a direct physiological regulator of lipolysis in adipose tissue. Endocrinology. 2017 May 1;158(5):1231–51.

58. Wolins NE, Brasaemle DL, Bickel PE. A proposed model of fat packaging by exchangeable lipid droplet proteins. Vol. 580, FEBS Letters. John Wiley & Sons, Ltd; 2006. p. 5484–91.

59. Padmanabha Das KM, Wechselberger L, Liziczai M, De La Rosa Rodriguez M, Grabner GF, Heier C, et al. Hypoxia-inducible lipid droplet-associated protein inhibits adipose triglyceride lipase. J Lipid Res. 2018;59(3).

60. Zhang X, Saarinen AM, Hitosugi T, Wang Z, Wang L, Ho TH, et al. Inhibition of intracellular lipolysis promotes human cancer cell adaptation to hypoxia. Elife. 2017 Dec 19;6.

61. Mayer N, Schweiger M, Romauch M, Grabner GF, Eichmann TO, Fuchs E, et al. Development of small-molecule inhibitors targeting adipose triglyceride lipase. Nat Chem Biol. 2013 Dec 6;9(12):785–7.

62. Bhatt-Wessel B, Jordan TW, Miller JH, Peng L. Role of DGAT enzymes in triacylglycerol metabolism. Arch Biochem Biophys. 2018 Oct 1;655:1–11.

63. Qi J, Lang W, Geisler JG, Wang P, Petrounia I, Mai S, et al. The use of stable isotope-labeled glycerol and oleic acid to differentiate the hepatic functions of DGAT1 and -2. J Lipid Res. 2012 Jun 1;53(6):1106–16.

64. Wurie HR, Buckett L, Zammit VA. Diacylglycerol acyltransferase 2 acts upstream of diacylglycerol acyltransferase 1 and utilizes nascent diglycerides and de novo synthesized fatty acids in HepG2 cells.

65. Villanueva CJ, Monetti M, Shih M, Zhou P, Watkins SM, Bhanot S, et al. Specific role for acyl CoA:diacylglycerol acyltransferase 1 (Dgat1) in hepatic steatosis due to exogenous fatty acids. Hepatology. 2009 Aug 1;50(2):434–42.

66. Itabe H, Yamaguchi T, Nimura S, Sasabe N. Perilipins: a diversity of intracellular lipid droplet proteins. Lipids Health Dis. 2017 Apr 28;16(1):83.

67. Zhang X, Saarinen AM, Hitosugi T, Wang Z, Wang L, Ho TH, et al. Inhibition of intracellular lipolysis promotes human cancer cell adaptation to hypoxia. Elife. 2017 Dec 19;6:e31132.

68. Caldo KMP, Acedo JZ, Panigrahi R, Vederas JC, Weselake RJ, Lemieux MJ. Diacylglycerol acyltransferase 1 is regulated by its N-terminal domain in response to allosteric effectors. Plant Physiol. 2017;175(2):667–80.

69. Sui X, Wang K, Gluchowski NL, Elliott SD, Liao M, Walther TC, et al. Structure and catalytic mechanism of a human triacylglycerol-synthesis enzyme. Nature. 2020 May 21;581(7808):323–8.

70. Zechner R, Kienesberger PC, Haemmerle G, Zimmermann R, Lass A. Adipose triglyceride lipase and the lipolytic catabolism of cellular fat stores. J Lipid Res. 2009 Jan 1;50(1):3–21.

71. Hofer P, Taschler U, Schreiber R, Kotzbeck P, Schoiswohl G. The lipolysome—a highly complex and dynamic protein network orchestrating cytoplasmic triacylglycerol degradation. Vol. 10, Metabolites. MDPI AG; 2020.

72. Guan C, Niu Y, Chen SC, Kang Y, Wu JX, Nishi K, et al. Structural insights into the inhibition mechanism of human sterol O-acyltransferase 1 by a competitive inhibitor. Nat Commun. 2020 Dec 1;11(1):1–11.

Summary

Abnormal lipid metabolism has been associated with a wide range of chronic and infectious diseases including non-alcoholic fatty liver disease, viral hepatitis C infection, atherosclerosis, diabetes, and cancer. Peroxisomal proliferator activator receptor alpha (PPARα) is a ligand-activated transcription factor that plays a major role in the regulation of lipid metabolism. Gene expression studies performed on PPARα null mice have shed light into a variety of genes regulated by PPARα. A comprehensive understanding of the physiological and molecular function of PPARα target genes is needed for the accurate development of therapeutical strategies.

The research contained in this thesis first sought to improve our current knowledge on the transcriptional regulation by peroxisome proliferator-activated receptors (PPAR)-α activation on human liver *in vivo* using a novel humanized-liver mouse model. Then, we pursued to expand our understanding on the physiological and molecular function of two PPARα target genes, Hilpda and Slc25a47. We studied the function of HILDPA in adipose tissue macrophages (ATM) in the context of obesity-induced inflammation and in hepatocytes during non-alcoholic steatohepatitis (NASH). Ultimately, we sought to identify the physiological function of the liver-specific mitochondrial carrier Slc25a47 in liver lipid metabolism and energy expenditure.

The role of PPARα in gene regulation in mouse liver is well characterized. However, less is known about the effect of PPARα activation in human liver *in vivo*. Model systems to study PPARα in human liver vary from hepatoma cell lines, human primary hepatocytes, human precision cut liver slices, and mice expressing human PPARα. A novel model to study *in vivo* PPARα activation in human liver is a chimeric mouse carrying human liver cells. These mice are generated by transplanting human hepatocytes into albumin enhancer–driven urokinase-type plasminogen activator transgenic/severe combined immunodeficiency (uPA/SCID) mice, leading to replacement of the host hepatocytes. In this research, we performed transcriptomics analysis on the effect of fenofibrate in mice with hepatocyte-humanized livers and compared the results with other relevant transcriptomics datasets. We observed that human hepatocytes exhibited excessive lipid accumulation. Fenofibrate increased the size of the mouse but not human hepatocytes and tended to reduce steatosis in the human hepatocytes. Quantitative PCR indicated that induction of PPARα targets by fenofibrate was less pronounced in the human hepatocytes than in the residual mouse hepatocytes. Comparison with other transcriptomics datasets indicated that hepatocyte humanized livers recapitulate the principal effects of PPARα activation on lipid metabolism as revealed by other model systems of human liver. In contrast, pathways connected to DNA synthesis were downregulated by fenofibrate in chimeric mice with hepatocyte humanized livers yet upregulated by fenofibrate in normal mouse livers. Our results support the major role of PPARα in regulating hepatic lipid metabolism, highlight the more modest

effect of PPARα activation on gene regulation in human liver compared to mouse liver, and indicate that PPARα may have a suppressive effect on DNA synthesis in human liver.

In the second part of this thesis, we characterized the physiological and molecular function of HILDPA in ATM in the context of obesity-induced inflammation and in hepatocytes during NASH. To this end we used a HILPDA tissue-specific knockout mice model in macrophages and hepatocytes generated by using *LysM*-Cre and *Alb*-Cre transgenic mice, respectively. In diet-induced obese mice, HILPDA deficiency in macrophages markedly reduced lipid accumulation in macrophages yet it did not alter any measured inflammatory or metabolic parameters. Mechanistically, HILPDA acts an inhibitor of ATGL-mediated lipolysis in macrophages. Treatment with the ATGL inhibitor Atglistatin rescued lipid accumulation inside lipid droplets in HILPDA-deficient macrophages. This research questions the contribution of lipid droplet accumulation in adipose tissue macrophages in obesity-induced inflammation and metabolic disfunction. Similarly, in diet-induced NASH mice, HILPDA hepatocyte deficiency modestly yet significantly reduced liver triglyceride accumulation and plasma ALT levels. However, expression of macrophage/inflammatory markers and fibrosis were not different between HILPDA knockout and floxed mice. In hepatoma cell lines, fatty acids increase *Hilpda* expression and protein levels. *Hilpda* overexpression in turn induces triglyceride accumulation inside lipid droplets. Mechanistically, HILPDA interacts and increases DGAT1 protein level and activity as indicated by FRET-FLIM analysis, western blot and Dgat1 activity assay. These findings propose a novel regulatory mechanism by which fatty acids promote triglyceride synthesis and storage.

In the last part of this thesis, we sought to characterize the liver-specific mitochondrial carrier SLC25A47. We identified *Slc25a47* from a transcriptome data analysis of three independent studies in which human primary hepatocytes were treated with the PPARα agonist Wy14643 or GW7647 for 24 hours. *Slc25s47* was consistently induced by PPARα agonists in the three datasets. To study the functional role of SLC25A47 in mouse liver, we overexpressed *Slc25a47* in liver using adeno-associated virus. We first studied the effect of *Slc25a47* overexpression in fed and fasted mice. No significant effects were observed on liver triglyceride levels, nor on plasma glucose, triglyceride, cholesterol, glycerol, non-esterified fatty acids and β-hydroxybutyrate levels. Similarly, after feeding mice a high fat diet for 8 weeks, we did not observe any effect of *Slc25a47* overexpression in any of the beforementioned parameters. However, transcriptome analysis at the pathway level showed that several gene sets related to cholesterol synthesis were significantly enriched among the upregulated genes, suggesting that SLC25A47 might stimulate cholesterol synthesis. Next, we reasoned a knockout model would provide a clearer phenotype than the overexpression given that Slc25a47 is already expressed at high levels in liver. We next performed indirect calorimetry in wildtype and *Slc25a47* knockout mice in the fed and

fasted state yet there was no difference in energy expenditure, activity level nor respiratory exchange ratio between genotypes. We subsequently placed the WT and *Slc25a47*-/- mice on a high fat diet for 20 weeks to induce obesity and insulin resistance and another cohort of WT and *Slc25a47*-/- mice on a low fat diet for the same duration. No significant differences were observed in body weight gain, food intake, liver or white adipose tissue weight, either on the low fat diet or the high fat diet. By contrast, glucose tolerance was significantly improved in the *Slc25a47*-/- mice compared to the WT mice. Similarly, no significant differences were observed between WT and *Slc25a47-/-* mice in hepatic triglyceride nor in plasma glucose, cholesterol, triglycerides, glycerol and non-esterified fatty acids in either condition. At the molecular level, we explored if SLC25A47 might led to mitochondria uncoupling as previously reported. However, we did not observe and change in mitochondria respiration in mice liver overexpressing Slc25a47, nor in transiently transfected Hepa 1-6 cells as measured by high-resolution respirometry with Oroboros. However, image intensity analysis showed a significant decrease on the intensity of Mitrotrack Red, a membrane-potential dependent dye, on Slc25a47 overexpressing mitochondria. This research does not support an uncoupling role of SLC25A47 yet it identifies SLC25A47 as novel PPARα-regulated gene in human and mouse hepatocytes. Further studies are needed to identify SLC25A47 function in liver metabolism.

Acknowledgements

As I start writing this meaningful section of my thesis book, thousands of memories of the past years come to my mind. Undoubtfully, I share the merit of accomplising this educational degree with many people.

To my academic mentors, **Sander** and **Jan Willem,** thank you for trusting my capabilities. Thank you for the freedom you gave me to perform my research. Thank you for your incredible guidance. I greatly enjoyed having you as my mentors.

Shohreh, words are not enough to express how much I treasure your support inside and outside the lab. Thank you for the love, support, and all the laughs.

The **"Corner Office"**, **Sophie**, **Merel**, **Mieke**, **Caroline**, **Lisa**, **Tessa**, **Wout**. Thank you for the fantastic working environment, the chats, and happy mornings. It was great sharing office with you. **Merel**, thank you for your moral support and all the frustrated experiment relief talks.

Jenny, **Mechteld**, **Mieke**, **Caroline**, **Karin**, **Shohreh**, thank you for keeping the lab up and running.

Sander's group, **Rinke, Xanthe**, **Lisa**, **Danny**, **Brecht**, **Frank**, **Merel**, **Philip**, and **Antwi**, it has been great learning with and from you. To my master's thesis supervisor, **Frits**, thank you for encouraging my self-confidence in the lab. **Antwi**, we started our PhD together, you guided me through my first assays, great company in scientific meetings and courses, not to mention how recomforting it was to walk by your desk and exchange a few motivational words after difficult days. **Danny**, thank you for your great cooking and friendship.

My master students **Venetia**, **Christy**, **Nienke**, **Eva**, **Marielena**, **Samira**, **Kaja**, **Anneke** and **Fabian**. I learned a lot from each of you. All of you have made valuable contributions to this thesis. Thank you for all your effort.

Human Nutrition Group, thank you for an amazing working environment. I really felt at home. It has been great doing research with you. **Rieneke**, **Benthe**, **Mara**, thank you for sharing your positive energy in our corridor short talks. **Jasmijn Mater**, thank you for your great assistance, always helping me out.

Guido, thank you for your support on transcriptomic analysis and the enjoyable bike rides from the Dreijen to Bennekom. **Rajat Singh**, thank you for your valuable advice and help with autophagy analysis. **Michel Van Veeghel**, thank you for your support with lipidomics analysis. **Geert Stoopen**, thank you for your assistance with mice liver slices. **Anne Gemmik**, thank you for your assistance with STED imaging and the amazing trips to the Lipid Droplet meetings in Colorado together with **Nyenke van Polanen**. Great company.

Nhien Ly, thank you for your advice and support with the TLC plates. **Bert** and **Wilma**, thank you for the thousand of mice you cared for and all your support with the mice experiments.

Dr. Gerardo Gamba, **Dr. Jorge Eugenio Valdez García**, **Dra. Elizabeth Tejero**, **Dra. Leticia Elizondo Montemayor**, **Dr. Gregorio Martínez-Ozuna, Lic. Nut. Luz Pérez-Ávila**: I greatly appreciate your support on my grant application process from CONACYT. It has been fundamental for the realization of this research. Thank you for encouraging my academic development.

Family and friends

Papá Norberto y **mamá Diana**, thank you for your example of hard work and dedication, for always providing me with the best education, and for encouraging me to follow my passion for health and nutrition. But overall, thank you for all the happy moments that make life meaningful.

My husband, friend, cook, entertainer, illustrator, **Eduardo**, thank you for sharing your dreams with me. It all started with you pursuing a master's degree. Thank you for making every day special. Thank you for your fantastic cooking, except when you made me gain 5kg. Thank you for bringing joy to our lives, you are a spark. Home will always be where you are. **Dudu** and **Caterina** the joy of my life.

Papá Chito (†), I inherit from you my passion for health. Always strong, consistently exercising, never missed your supplements, always healthy, always reading. I miss you every day. **Mamá Blanca** (†), thank you for your example of independence and strength. **Abuelita Mayita,** the personification of kindness, peace, and will power. I'm fortunate to be your granddaughter.

Dianita y **Arturo**, you are an example of strength and kindness. **Norbert**, thank you for all the holidays you spent with us. I cherish every memory, except that New Year's Eve, you had me eating kebabs outside the train station in Rotterdam. **Lau**, sis, you are wonderful.

Ber and **Ana**, creative souls, I greatly appreciate all your support in caring for Dudu and Caterina. Thank you for sharing all your playful joy and creativity with them. **Gus** and **Ale**, thank you for joining us in this life experience of living abroad in The Netherlands. We hope it will happen again.

Tio Joao and **Tia Le,** all this work would not have been possible without you. Thank you for all the trips you made from Brazil to the Netherlands to support us by taking care of Dudu and Caterina. I cherish every moment spent with you.

Becky, **Almita**, **Adri**, **Nats**, **Anishky** my sisters of life. Thank you for always being there despite the distance.

Primos a todo dar, you are a happiness pill. **Tíos-compadres**, thank you for all the love and encouragement.

Marce, Rafa, Jose and **Ele**, thank you for the amazing company during this journey, the happy moments, the encouragement and the fun family time together.

Simon, thank you for all your French-Brazilian dancing moves, fancy dinners and French wines. By the way, Duda is not allowed to go out to café Daniels. As meninas **Maira** and **Thais**, **Iame** and **Fran**, thank you for the great feasts, for more to come.

Mama **Ana**, Papa **Michiel,** sweet **Julia**, and **Amelia,** thank you for your amazing friendship. It is great seeing our kids grow together.

The **Roze kamer** (Pipeloi) and **Bellefleur**, **Bloesem**, **Stampertjes** and **Sterappeltjes** (het Klokhuis): Having you cared and care for Dudu and Caterina gave me the calm and confidence I needed to do this research. Your work is fantastic.

For all of you that already left Wageningen but have made this experience unforgettable: **Marcell** and **Lisiane**, **Loïc**, **Mimiri**, **Marcos, Thalita**, **Chela**, **Margarita** and **Marek**, **Polinho**, **Danito**, **Mosen** and **Paulien**, **Rafa** and **Cynara**, **Thiago** and **Andrielli**. I am always looking forward to seeing you again.

My **patients** from eQüi, you were the inspiration that encouraged me to start this journey.

Finally, my paranymphs, **Philip-Felipe**: your perseverance is admirable. I enjoyed our everyday lunch and coffees, all your fasting talks, and not to mention all your grumpiness. Thank you for your help formatting this thesis. I miss having you around. Compadre **Bjorn**, thank you for always being there for us. I deeply appreciate all your love, caring and friendship during all these years.

Thank you all.

About the author

Montserrat Alejandra De la Rosa Rodríguez was born in Monterrey, México on December 30, 1985. Since a young age, she showed a great passion for nutrition and health. Therefore, she decided to enroll in the School of Medicine of Tecnológico de Monterrey, pursuing clinical nutrition studies. During her undergrad education, she gained practical experience in nutritional therapy in health and disease. She performed clinical rotations in various hospitals such as MD Anderson Cancer Center (Houston, USA), Memorial Hermann Hospital (Houston, USA), Hospital Sao Lucas (Porto Alegre, Brazil), and Hospital San José Tec de Monterrey (Monterrey, México). After receiving her bachelor's degree in Clinical Nutrition and Wellness in 2009, she founded eQüi Wellness Center, where she worked as a clinical nutrition practitioner. Inspired by her patients, Montserrat decided to pursue a Master of Science in Nutrition and Health at Wageningen University in 2012. During her master's studies, she became fascinated with Nutrigenomics; therefore, she specialized in Molecular Nutrition. Montserrat wrote her master thesis on the characterization of PPAR target protein HILPDA in the group of Nutrition, Metabolism, and Genomics. After completing her master's in science, she continued her research on the characterization of PPAR target proteins guided by her promotor Prof. Dr. Sander Kersten and co-promotor Dr. Ing. Jan Willem Borst. During her doctoral research, she became acquainted with mice experimentation and diverse molecular biology and confocal microscopy techniques to identify the physiological and molecular function of proteins.

List of publications

de la Rosa Rodriguez MA, Kersten S. Regulation of lipid droplet-associated proteins by peroxisome proliferator-activated receptors. Biochim Biophys Acta - Mol Cell Biol Lipids. 2017;1862(10).

Dijk W, Mattijssen F, **de la Rosa Rodriguez M**, Loza Valdes A, Loft A, Mandrup S, et al. Hypoxia-Inducible Lipid Droplet–Associated Is Not a Direct Physiological Regulator of Lipolysis in Adipose Tissue. Endocrinology. 2017 May 1;158(5):1231–51.

de la Rosa Rodriguez MA, Sugahara G, Hooiveld GJEJ, Ishida Y, Tateno C, Kersten S. The whole transcriptome effects of the PPARα agonist fenofibrate on livers of hepatocyte humanized mice. BMC Genomics. 2018 Jun 7;19(1):443.

Padmanabha Das KM, Wechselberger L, Liziczai M, **De La Rosa Rodriguez M**, Grabner GF, Heier C, et al. Hypoxia-inducible lipid droplet-associated protein inhibits adipose triglyceride lipase. J Lipid Res. 2018;59(3).

de la Rosa Rodriguez MA, Kersten S. Regulation of lipid droplet homeostasis by hypoxia inducible lipid droplet associated HILPDA. Biochim Biophys acta Mol cell Biol lipids. 2020 Sep 1;1865(9):158738.

van Dierendonck XAMH, **de la Rosa Rodriguez MA**, Georgiadi A, Mattijssen F, Dijk W, van Weeghel M, et al. HILPDA Uncouples Lipid Droplet Accumulation in Adipose Tissue Macrophages from Inflammation and Metabolic Dysregulation. Cell Rep. 2020;30(6).

de la Rosa Rodriguez MA, Deng L, Gemmink A, van Weeghel M, Aoun ML, Warnecke C, et al. Hypoxia-inducible lipid droplet-associated induces DGAT1 and promotes lipid storage in hepatocytes. Mol Metab. 2021 Jan 1;47:101168.

Overview of completed training activities

Discipline specific activities

NutriScience 15, VLAG (Wageningen, the Netherlands, 2015).

Advanced imaging of molecular complexes inside living cells, FEBS (Amsterdam, the Netherlands, 2015).

Annual Dutch Diabetes Research Meeting, NVDO (Oosterbeek, the Netherlands, 2015).

Lipid Droplet Meeting "Lipid Droplets: Dynamic Organelles in Metabolism and Beyond", FASEB (Snowmass, USA, 2016).

Microscopic Image Analysis: From Theory to Practice, Erasmus MC, (Rotterdam, the Netherlands, 2016).

Animal Handling course, Utrecht University (Utrecht, the Netherlands, 2016).

Energise Meeting, CVON (Leiden, the Netherlands, 2016).

Energise Meeting, CVON (Maastricht, the Netherlands, 2017).

Energise Meeting, CVON (Leiden, the Netherlands, 2018).

Lipid Droplet Meeting "Lipid Droplets on the Move from Health to Disease", FASEB (Springs, USA, 2018).

Functional Imaging course, LCAM (Amsterdam, the Netherlands, 2018).

Healthy Food Design, VLAG (Wageningen, the Netherlands, 2018).

Energise Meeting, CVON (Wageningen, the Netherlands, 2019).

Lipid Droplet Meeting "(VIRTUAL) Lipid Droplet Conference", FASEB (remotely, 2020).

General courses

Phd workshop Carousel, WGS (Wageningen, the Netherlands, 2015).

Reviewing a Scientific Paper, WGS (Wageningen, the Netherlands, 2015).

Brain Training, WGS (Wageningen, the Netherlands, 2015).

Phd Week, VLAG (Baarlo, the Netherlands, 2015).

Scientific Writing, WGS (Wageningen, the Netherlands, 2015).

Pitch Perfect, WGS (Wageningen, the Netherlands, 2015).

Bridging across cultural differences, WGS (Wageningen, the Netherlands, 2016).

Techniques for Writing and Presenting Scientific Papers, WGS (Wageningen, the Netherlands, 2016).

Adobe inDesign, WUR Library (Wageningen, the Netherlands, 2016).

Project and Time Management, WGS (Wageningen, the Netherlands, 2017).

Optional courses/activities

Preparation of Research Proposal, HNH (Wageningen, the Netherlands, 2015).

Journal Club, HNH (Wageningen, the Netherlands, 2015-2020).

NMG lab meetings, HNH (Wageningen, the Netherlands, 2015-2020).

The research contained in this thesis was financially supported by the Netherlands Organisation for Scientific Research (2014/12392/ALW), Consejo Nacional de Ciencia y Tecnologia de México (CONACYT-455071) and by the Netherlands Cardiovascular Research Initiative (CVON2014-02 ENERGISE), an initiative with support of the Dutch Heart Foundation.

I gratefully acknowledge the financial support by Wageningen University and the Graduate School VLAG for the printing and publishing of this thesis.

Cover: Eva Maria Salazar

Layout: Philip Ruppert

Printed by: Digiforce || proefschriftmaken.nl